



**This electronic thesis or dissertation has been  
downloaded from Explore Bristol Research,  
<http://research-information.bristol.ac.uk>**

*Author:*

**Lopez Filun, Pablo**

*Title:*

**Integrated modelling of slope hydrology and stability hazards to explore the potential effects of land use and climate change on dynamic multi-hazard interactions**

**General rights**

Access to the thesis is subject to the Creative Commons Attribution - NonCommercial-No Derivatives 4.0 International Public License. A copy of this may be found at <https://creativecommons.org/licenses/by-nc-nd/4.0/legalcode> This license sets out your rights and the restrictions that apply to your access to the thesis so it is important you read this before proceeding.

**Take down policy**

Some pages of this thesis may have been removed for copyright restrictions prior to having it been deposited in Explore Bristol Research. However, if you have discovered material within the thesis that you consider to be unlawful e.g. breaches of copyright (either yours or that of a third party) or any other law, including but not limited to those relating to patent, trademark, confidentiality, data protection, obscenity, defamation, libel, then please contact [collections-metadata@bristol.ac.uk](mailto:collections-metadata@bristol.ac.uk) and include the following information in your message:

- Your contact details
- Bibliographic details for the item, including a URL
- An outline nature of the complaint

Your claim will be investigated and, where appropriate, the item in question will be removed from public view as soon as possible.

---

---

**Integrated modelling of slope hydrology and stability hazards  
to explore the potential effects of land use and climate change  
on dynamic multi-hazard interactions**

---

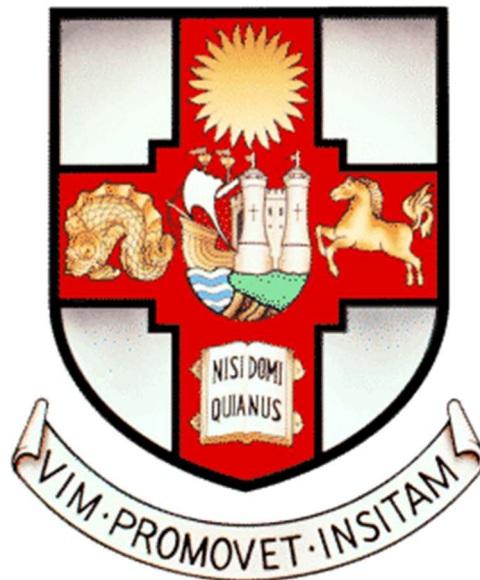
---

By

**Pablo López Filun**

Department of Civil Engineering

University of Bristol



A dissertation submitted to the University of Bristol in accordance with the requirements for  
award of the degree of Doctor of Philosophy in the Faculty of Engineering.

September 2022

Word count: 76,146



## **Abstract**

The impacts of climate and land use change are increasing the frequency and magnitude of rainfall-triggered landslides, debris flows, and hillslope erosion hazards in regions of the world that have already experienced increasing levels of impact and disaster risk. Understanding these hazards and their interactions requires recognizing the interrelationships of the catchment's physical characteristics such as topography, hydrology, soil properties, and land with climate variables. Physically-based distributed multi-hazard models integrate these relationships; however, these models require a large number of input parameters that are challenging to obtain in catchments where no data are available to represent all relevant catchment physical characteristics. For regions with the highest levels of hazards and disaster risks, this type of model is associated with significant challenges related to data scarcity, uncertainty, model complexity, and possible over-parameterisation. Uncertainties arise due to the quality of the available data and the accessibility of different spatial resolution data to accurately represent these hazards within different catchment scales. This thesis addresses such uncertainties by developing a new modelling workflow that enables physically-based distributed multi-hazard models to be applied in data-scarce regions. Using this workflow, model parameterisation and uncertainty management were addressed to explore climate and land use scenarios in the two case study sites proposed in this thesis (Soufriere catchment, Saint Lucia, and The Maipo sub-catchment, Chile) to demonstrate the utility of this approach for informing resilient land use planning and policy. Applying the workflow to the two selected study sites identified the parameter-set values for land use and soil types that best approximated the spatial representation of rainfall-triggered landslides, debris flows, and hillslope erosion hazards for registered rainfall events, allowing the exploration of climate and land use scenarios at both study sites. This thesis has contributed by introducing a systematic modelling workflow that addresses the uncertainties in multi-hazard modelling, thereby improving the representation of hillslope hydrological hazard interactions for catchments with data scarcity.

## **Acknowledgments**

First of all, my biggest thanks go to my supervisor Liz Holcombe who has guided me and showed her support when most I needed it through this PhD. I would like to thank also to my supervisors Katerina Michaelides and Jeremy Philips who guided me on the relevant topics to complete my PhD research. Together with Liz, they have supported me to develop all the necessary skills to be a good researcher.

I would like to thank professors Carolina Martinez, Jorge Quense and Cristian Henriquez from the Institute of Geography of the Pontifical Catholic of Chile for supporting me and encouraging me to pursue a PhD. Thanks to the people of Woodland Road, especially my officemates Shaini and Elisa to share good talks and biscuits. Also, to Giuseppe, Ke He (Klaus), Yong Shin and Lina to share good moments with me. To my friend Leo to share all those talks about politics and academic life, dinners, beers, and trips. A special thanks go to Claudio who has been my support in sharing moments of talks, trips night outs and dinners. I would like to extend my thanks to Ray, Richard, Gino, Jeevantha, Mary, and Cristina for sharing good moments in Bristol.

Most important I want to thank my parents and my sister who have been my greatest support during this process.

This PhD thesis was funded by the National Agency for Research and Development (ANID) Chile 2017.

## **Authors declaration**

I declare that the work in this dissertation was carried out in accordance with the requirements of the University's Regulations and Code of Practice for Research Degree Programmes and that it has not been submitted for any other academic award. Except where indicated by specific reference in the text, the work is the candidate's own work. Work done in collaboration with, or with the assistance of, others, is indicated as such. Any views expressed in the dissertation are those of the author.

**Signed:**

**Date:** 02/09/2022

# Table of contents

<b>Chapter 1</b>	<b>Introduction</b>	<b>1</b>
1.1	Introduction	2
1.1.1	Background and motivation	2
1.1.2	The importance for accounting catchment physical characteristics	5
1.1.3	Understanding hillslope hydrological hazard interactions under land use and climate change	8
1.2	Hillslope hydrological multi-hazard modelling approaches	11
1.2.1	Assessment of hillslope hydrological hazard interactions	13
1.2.2	Challenges and gaps in hillslope-hydrological hazard interaction modelling	16
1.3	Research aims and objectives	21
1.4	Thesis outline	24
<b>Chapter 2</b>	<b>Hillslope hydrological hazard interaction: in search of an integrated hazard modelling approach</b>	<b>26</b>
	Introduction	27
2.1	Integrated physically-based multi-hazard modelling	28
2.1.1	The multi-hazard approach in hydrological and stability hazards	28
2.1.2	Understanding hazard interactions between hillslope hydrological hazards	30
2.1.3	Frequency-magnitude relationships of interacting hazards	34
2.2	Identifying a suitable method for hillslope-hydrological hazard interaction modelling	35
2.2.1	Multi-hazard modelling approaches for hillslope hydrological hazards	35
2.2.2	Model selection: The OpenLISEM Hazard model	39
2.3	Defining a modelling workflow for multi-hazard interaction modelling	42
2.3.1	Stage 1: Model parameterisation	43
2.3.1.1	Defining a parameterisation method	44
2.3.2	Stage 2: Model verification and sensitivity analysis (SA)	45
2.3.2.1	Model internal verification	46
2.3.2.2	Model accuracy	47
2.3.2.3	Criteria for parameter-set selection	50
2.3.2.4	Sensitivity analysis (SA)	51
2.3.3	Stage 3: Model application for climate and land use scenarios	52
2.4	Chapter summary	53
<b>Chapter 3</b>	<b>Developing the workflow for parameter exploration and experimental design</b>	<b>56</b>
3.1	Introduction	57
3.2	Methodology	58
3.2.1	Soufriere catchment: Rainfall event selection and hazard inventory	60
3.2.2	Definition of catchment physical characteristics for multi-hazard modelling	62
3.2.3	Setting OpenLISEM hazard model input parameters	62
3.2.4	Define input parameter value ranges	65
3.2.5	Designing parametric simulations	67
3.2.6	Hazard representation	68

3.3	Results.....	69
3.3.1	Responsiveness parametric simulations.....	69
3.3.2	Hazard representation.....	71
3.4	Discussion.....	74
3.4.1	Responses of parametric simulations.....	74
3.4.2	Parameters affecting hazard representations.....	76
3.5	Conclusions.....	77
<b>Chapter 4 Developing the workflow for model verification and investigation of catchment response to climate and land use change.....</b>		<b>79</b>
4.1	Introduction.....	80
4.2	Methodology.....	81
4.2.1	Spatial similarity assessment.....	83
4.2.2	Spatial accuracy assessment.....	84
4.2.3	Simulation parameter-set selection criteria.....	85
4.2.4	Sensitivity Analysis (SA).....	85
4.2.5	Sensitivity to land use and soil types variation.....	86
4.2.6	Explore land use and climate change scenarios.....	86
4.3	Results.....	88
4.3.1	Spatial similarity ranking.....	88
4.3.2	Area distribution comparison.....	88
4.3.3	Accuracy assessment.....	89
4.3.4	Behavioural simulation selection.....	90
4.3.5	Sensitivity Analysis (SA).....	91
4.3.6	Parameter set confirmation: sensitivity to land use and soil type variations.....	92
4.3.7	Responsiveness of the Soufriere catchment to land use and rainfall change.....	95
4.4	Discussion.....	98
4.4.1	Behavioural simulation selection.....	98
4.4.2	Sensitivity Analysis (SA) and parameter set confirmation.....	99
4.4.3	Responsiveness of the catchment to land use and rainfall change scenarios..	100
4.5	Conclusions.....	101
<b>Chapter 5 Assessing hillslope hydrological hazards and interactions under changing climate and land use in Maipo, Chile.....</b>		<b>103</b>
5.1	Introduction.....	104
5.2	Applying the modelling workflow.....	106
5.3	Multi-hazard assessment of Maipo sub-catchment case study.....	108
5.3.1	Step 1: assembling data for the Maipo sub-catchment.....	108
5.3.2	Step 2: defining model input parameter ranges.....	110
5.3.3	Steps 3 & 4: Running parametric simulations and verifying catchment-scale hazard representation.....	114
5.3.4	Steps 5 & 6: Sub-catchment scale verification of parameter-sets and simulations.....	114
5.3.5	Steps 7 & 8: Sensitivity Analysis (SA) and sensitivity to land use and soil type variations.....	116
5.3.6	Step 9: Explore land use and climate change scenarios.....	116



5.4	Results.....	117
5.4.1	Behavioural simulation selection.....	117
5.4.2	Sensitivity Analysis (SA).....	118
5.4.3	Hazard magnitudes evolution.....	119
5.4.4	Sensitivity to land use and soil type variation.....	121
5.4.5	Responsiveness of the Maipo sub-catchment to land use and rainfall change.....	124
5.5	Discussion.....	126
5.5.1	Applicability of the modelling workflow for the Maipo sub-catchment.....	126
5.5.2	Representation of hillslope hydrological multi-hazard interactions.....	127
5.5.3	Responsiveness to land use and rainfall change scenarios.....	128
5.6	Conclusions.....	129
<b>Chapter 6</b>	<b>Summary and conclusions.....</b>	<b>131</b>
6.1	Research summary.....	132
6.1.1	A modelling workflow to assess hillslope hydrological hazard interactions for land use and rainfall change.....	132
6.1.2	Identification parameter variations and uncertainties in multi-hazard assessment.....	133
6.1.3	Single hazard vs multi-hazard for the Soufriere catchment and Maipo sub-catchment.....	134
6.1.4	An end-to-end methodology to explore climate and land use scenarios for different catchment environments.....	141
6.2	Overall thesis conclusions.....	142
6.2.1	Direction for future works.....	142
6.2.2	A modelling workflow methodology to improve confidence in multi-hazard modelling.....	143
6.2.3	Improving the understanding of multi-hazards and their interactions: Future outlook.....	144
6.3	Concluding remarks.....	147
<b>References</b>	<b>.....</b>	<b>148</b>
<b>Appendix A</b>	<b>- Supporting information for Chapter 2.....</b>	<b>172</b>
	A.1 The OpenLISEM modelling approach.....	172
<b>Appendix B</b>	<b>- Supporting information for Chapter 3.....</b>	<b>178</b>
	B.1 Hurricane Tomas rainfall event intensity-duration estimation.....	178
	B.2 Landslide inventory rectification.....	179
	B.3 Setting the OpenLISEM hazard model input parameters.....	180
	B.4 Parametric simulations.....	182
<b>Appendix C</b>	<b>- Supporting information for Chapter 4.....</b>	<b>186</b>
	C.1 Spatial similarity assessment.....	186
	C.2 Accuracy assessment.....	187
	C.3 Response to land use and rainfall change scenarios.....	188
<b>Appendix D</b>	<b>- Supporting information for Chapter 5.....</b>	<b>186</b>
	D.1 Setting the OpenLISEM hazard model input parameters.....	186
	D.2 Response to land use and rainfall change scenarios.....	189
	D.3 Parametric simulations.....	191

**List of figures**

Figure 1.1 Global zonation of landslides and debris flow hotspots. Very high hazard regions can be found in Central America and the Caribbean, Central Asia, and the Middle East. Medium hazard regions can be found in South America and Central and Eastern Europe (Source: <https://datacatalog.worldbank.org/search/dataset/0037584>). ..... 3

Figure 1.2 Catchment physical characteristics..... 8

Figure 1.3 Effects of Hurricane Tomas in Saint Lucia, Eastern Caribbean, and effects of exceptional rainfall event during summer in Maipo sub-catchment, Santiago metropolitan region, Chile. (a) Fond St. Jacques debris flow (rural settlement) (ECLAC 2011); (b) Melocoton ravine Maipo sub-catchment, Chile (Marín et al. 2017). ..... 10

Figure 1.4 Overview of multi-hazard modelling framework for hillslope-hydrological hazards. .. 15

Figure 2.1 Conceptual framework for hazard interactions. .... 30

Figure 2.2 Conceptual framework for hillslope hydrological hazard interaction modelling. .... 33

Figure 2.3 Spatial similarity approach for model verification..... 47

Figure 2.4 Spatial overlapping method approach. .... 49

Figure 3.1 Study site location: Soufriere catchment, Saint Lucia, Eastern Caribbean. .... 58

Figure 3.2 Hurricane Tomas rainfall event. .... 61

Figure 3.3 Rectified landslide inventory. (a) spatial distribution of landslides areas (b) landslide size distribution ..... 62

Figure 3.4 Spatial distribution of hydrological input parameter values. .... 64

Figure 3.5 Spatial distribution of geotechnical input parameter values..... 64

Figure 3.6 Hydrological and geotechnical input parameter value distributions..... 65

Figure 3.7 Hydrological and geotechnical input parameter value ranges. .... 67

Figure 3.8 Overall responsiveness of the catchment to the simulated ‘Hurricane Tomas’ rainfall forcing for each of the 144 parameter dataset combinations. Hazard magnitudes are indicated in terms of (a) total landslide surface area, (b) total debris flow runout area, (c) total net erosion rates..... 71

Figure 3.9 Hazard representation: (a) total landslide surface area..... 73

Figure 3.10 Hazard representation. (b) total debris flow runout area. .... 73

Figure 3.11 Hazard representation. (c) total net erosion. .... 74

Figure 4.1 Landslide spatial distribution and area comparison: (a) landslide spatial distribution for simulation 22, (b) area distribution for simulation 22, (c) landslide spatial distribution for simulation 25, (d) area distribution for simulation 25..... 89

Figure 4.2 Sensitivity indices (S.I) for key input parameters. The bars correspond to the sensitivity indices mean value estimated with bootstrapping while the vertical lines at the top bar represent the confidence interval for each parameter..... 91

Figure 4.3 Parameter value distribution for land use. (a) Saturated hydraulic conductivity, (b) Saturated moisture content. The symbol (▲) indicates highly sensitive soil type units. ....	92
Figure 4.4 Land use for the Soufriere catchment. ....	93
Figure 4.5 Parameter values for soil types. (c) Saturated hydraulic conductivity, (d) Saturated moisture content, (e) Soil cohesion, (f) Soil internal friction angle. The symbol (▲) indicates highly sensitive soil type units. ....	94
Figure 4.6 Soil types for the Soufriere catchment. ....	95
Figure 4.7 Multi-hazard response of the Soufriere catchment to land use and rainfall change..	97
Figure 5.1 The second study site location: Maipo sub-catchment, central Chile. ....	105
Figure 5.2 25 February 2017 rainfall event. ....	108
Figure 5.3 Hazard inventory. (a) Debris flow inventory (b) debris flow runout area distribution. ....	109
Figure 5.4 Spatial distribution of hydrological input parameter values for the Maipo sub-catchment. ....	111
Figure 5.5 Spatial distribution of geotechnical input parameter values for the Maipo sub-catchment. ....	112
Figure 5.6 Hydrological and geotechnical input parameter value distributions. ....	113
Figure 5.7 Hydrological and geotechnical input parameter value ranges. ....	113
Figure 5.8 Sensitivity indices (S.I) for each input parameter. The bars correspond to the sensitivity indices mean value estimated with bootstrapping while the vertical lines at the top bar represent the confidence intervals for each input. ....	119
Figure 5.9 Hazard magnitude evolution. (a) Rainfall duration and discharge, (b) landslide and debris flow magnitude evolution, (c) net erosion rates. ....	120
Figure 5.10 Parameter values for soil types. (a) Saturated hydraulic conductivity (land use), (b) Saturated moisture content (land use), (c) Saturated hydraulic conductivity (soil types), (d) Saturated moisture content (soil types), (e) Soil cohesion (soil types), (f) Soil internal friction angle (soil types). ....	122
Figure 5.11 (a) Land use and (b) soil types of the Maipo sub-catchment. ....	123
Figure 5.12 Multi-hazard response of the Maipo sub-catchment to land use and rainfall change. ....	125
Figure 6.1 Hillslope hydrological hazard simulated as a multi-hazard event for the Soufriere catchment (Hurricane Tomas): (a) All hazards with location of cascading interactions indicated, (b) Landslides, (c) Debris flows, (d) Hillslope erosion hazards abstracted from the multi-hazard modelling result to indicate their extent more clearly. ....	138
Figure 6.2 Hillslope hydrological hazard representations for the Maipo sub-catchment (25 February 2017 rainfall event): (a) cascading interactions, (b) Landslides, (c) Debris flows, (d) Hillslope erosion. ....	140
Figure A.1: Diagram of forces for infinite slope approach. ....	172
Figure B.1. Hurricane Tomas rainfall cumulative curves. ....	178
Figure B.2: Landslide inventory rectification process. ....	179

Figure B.3: (a) land use categories, (b) soil types units.....	180
Figure B.4: (a) soil depth for soil layer 1, (b) soil depth for soil layer 2.....	181
Figure B.5. Total of parametric simulations for the OpenLISEM model.....	183
Figure C.1 Spatial similarity assessment parametric simulations.....	186
Figure C.2 Fuzzy membership function.....	187
Figure C.3: (a) Euclidean distance for the landslide inventory polygons, (b) fuzzy membership distance.....	187
Figure C.4. Tolerance area and catchment flat areas identification.....	188
Figure C.5. 20-year return period synthetic rainfall intensity-duration: (a) 24-hour rainfall event, (b) 10-hour rainfall event and (c) 5-hoyr rainfall event.....	189
Figure D.1: (a) geological units, (b) soil types.....	186
Figure D.2 Soil depth spatial distribution for the Maipo sub-catchment: (a) soil depth 1, (b) soil depth 2.....	187
Figure D.3. Land use for the Maipo sub-catchment.....	188
Figure D.4. 10-year return period synthetic rainfall intensity-duration: (a) 12-hour rainfall event, (b) 6-hour rainfall event and (c) 4-hour rainfall event.....	190
Figure D.5. Hazard representation: (a) total landslide surface area.....	191
Figure D.6. Hazard representation: (b) total debris flow runout area.....	191
Figure D.7. Hazard representations: (c) total net erosion.....	192

## List of tables

Table 2.1. Overview of hillslope-hydrological hazard modelling approaches.....	38
Table 2.2 Advantages and disadvantages of the OpenLISEM Hazard model.....	41
Table 2.3 Strategies to address uncertainty in multi-hazard modelling.....	43
Table 2.4 Similarity and skill scores coefficients classification.....	50
Table 3.1 Modelling workflow stage 1: model parameterisation.....	58
Table 3.2 OpenLISEM hazard model hydrological and geotechnical input parameter values... ..	63
Table 4.1 Modelling workflow stages 2 and 3: model verification and sensitivity analysis (SA).....	81
Table 4.2 Ranking of parametric simulations with hazard area difference scores in red font.....	88
Table 4.3 Accuracy score values.....	90
Table 5.1 OpenLISEM hazard model hydrological and geotechnical input parameter values.....	110
Table 5.2 Behavioural simulations ranking and accuracy scores.....	118
Table B.1. Soil geotechnical parameters.....	182
Table B.2. Slope stability and flow dynamics numerical settings.....	183
Table B.3. Hydrological input parameter for land use categories.....	184
Table B.4. Hydrological input parameter for soil type units.....	184
Table B.5. Geotechnical input parameters for soil type units.....	185
Table C.1. Spatial similarity ranking.....	186

Table C.2. Template land use change matrix to explore the rate of change of hazard magnitudes for land use change scenarios.....	188
Table D.1. Hydrological input parameter for land use categories and soil type units .....	188
Table D.2. Geotechnical input parameters for soil type units .....	189
Table D.3. Template land use change matrix to explore the rate of change of hazard magnitudes for land use change scenarios.....	189

---

---

# **Chapter 1 Introduction**

---

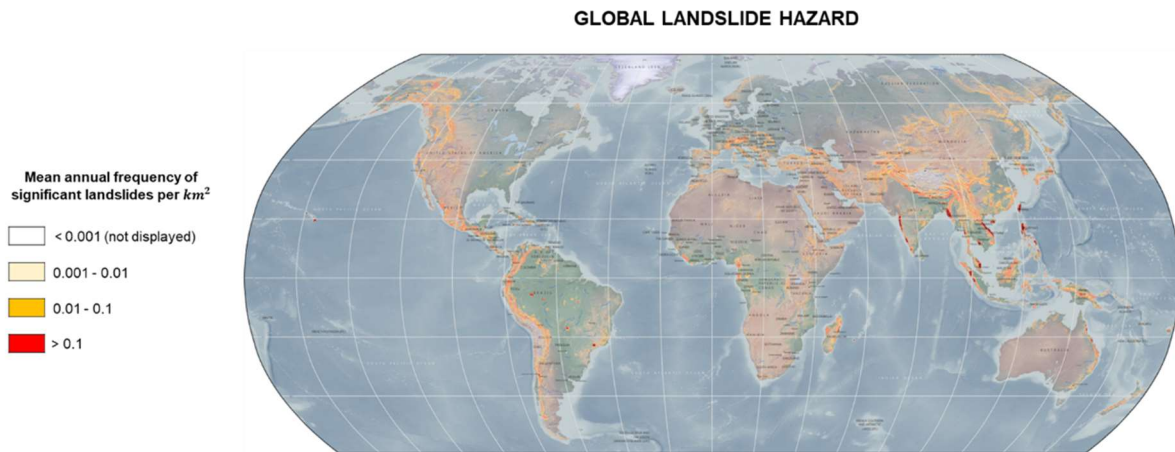
---

## 1.1 Introduction

### 1.1.1 Background and motivation

There is evidence that the frequency and magnitude of rainfall-triggered landslides, debris flows, and hillslope erosion hazards is significantly increased by both land use change and climate change (Stoffel et al. 2014; Borrelli et al. 2020; Moreiras et al. 2021). These hazards are normally referred to as **hillslope hydrological hazards** because their occurrence is related to the interaction of slope surface and sub-surface hydrological and stability processes (Caloiero 2018; Beevers et al. 2022). The occurrence and impacts of these hazards is greater in regions of the world where there is limited capacity to assess hazards under different climate and land use scenarios; or to design and enforce disaster-resilient land use planning and disaster risk reduction policies (Kelman et al. 2016; Rus et al. 2018; Mateos et al. 2020). These regions are already experiencing increasing levels of disaster risk as hazards combine with increasing exposure and vulnerability of populations, economic infrastructure and environmental resources (De Angeli et al. 2022; Cremen et al. 2022). For example, between 2004 and 2016, the number of fatal rainfall-triggered landslide events increased by almost 95% on slopes occupied by informal settlements, especially in the mountainous catchments of China, Southeast Asia, Latin America, and the Caribbean (Sepúlveda and Petley 2015; Froude and Petley 2018). Similarly, between 2005 and 2013, the records of fatalities and socio-economic losses associated with debris flows were higher in mountainous regions in developing countries (Lower and Middle-income Countries, LMICs, as defined by the World Bank, 2022) compared with countries with greater resources for hazard mitigation and risk planning (Turkington et al. 2016; Hirschberg et al. 2021; Moreiras et al. 2021). Likewise, between 2001 and 2015, the impacts of erosion hazards have been more evident in mountain catchments of China, India and some countries in Europe, Africa, and Latin America (Li and Fang 2016), where the hillslopes erosion rates have increased as a consequence of the impacts of land use change for economical purposes or, as a result of the direct effects of climate change such as droughts and wildfires (Anache et al. 2018; Borrelli et al. 2020).

The Intergovernmental Panel on Climate Change (IPCC, 2022) remarks that in developing countries, settlements and infrastructure in mountain regions are already experiencing the impacts of more frequent and intense weather extremes. This coincides with the mountainous regions that are already most prone to rainfall-triggered landslides, debris flows, and hillslope erosion hazards (see Figure 1.1). Additionally, changes in land use within these regions have substantially impacted the frequency and magnitude of these hazards (Siriwardena et al. 2006; Mahat et al. 2016). Urban settlements have experienced the most significant impacts of rainfall-triggered landslides and debris flows due to unplanned urban expansion onto hillslopes and fluvial terraces that have a high degree of exposure to these hazards; and where urbanisation activities that change plant cover, topography and drainage patterns may increase the hazard (Alcántara-Ayala 2002; Johnston et al. 2021).



*Figure 1.1 Global zonation of landslides and debris flow hotspots. Very high hazard regions can be found in Central America and the Caribbean, Central Asia, and the Middle East. Medium hazard regions can be found in South America and Central and Eastern Europe (Source: <https://datacatalog.worldbank.org/search/dataset/0037584>).*

Another important consideration is that **hillslope hazard processes interact with each other** – and these interactions need to be represented under both current and future climate and land use scenarios. It has been demonstrated that rainfall-triggered landslides, debris flows and hillslope erosion hazards do not occur as isolated processes but may be cascading, concurrent or compounding events (de Ruiter et al. 2020). For example, rainfall-triggered landslides and intensive hillslope erosion can influence debris flow magnitude, velocity, and runout (Cascini et al. 2013; Zhang et al. 2019). These hazard interactions are determined by the interrelationship between hydrological and stability processes that in majority are governed by lithological, topographical, and environmental factors (Guzzetti et al. 1996; Sidle and Ochiai 2006; Gill and Malamud 2014). These factors, also known as "**preparatory factors**", configure the hillslope hydrology and stability and its susceptibility to hydrological hazards response to rainfall events (Fell et al. 2008; van Westen et al. 2008; Shano et al. 2020). In this thesis, the term "**catchment physical characteristics**" will be used from now on to refer to the preparatory factors that govern hillslope hydrology and stability and contribute to a hazard-forming environment with societal and environmental risk (Leonard et al. 2014; Liu et al. 2016). Identifying how hazard interactions are affected by climate and land use change is challenging, particularly in assessing their effects on the interrelationships between catchment physical characteristics and climate variables (Gill and Malamud 2014). Physically-based models integrate these interrelationships by incorporating the catchment physical characteristics within their modelling structures through the integration of the physical and mechanical laws of hillslope hydrology and stability (Terlien et al. 1995; Herrera et al. 2022). These models allow for simulating the interrelationships between catchment properties and climate variables, thus enabling the modelling of hydrological and stability processes that influence the interaction of hillslope hydrological hazards (Van den Bout et al. 2018).

Assessing these interactions requires the characterisation of the hazard location, frequency, and magnitude (van Westen et al. 2006; Van den Bout et al. 2021). Therefore, modelling hillslope hydrological hazard interactions must be performed using models that consider both time and space



(De Angeli et al. 2022). Physically-based *distributed models* integrate these two approaches to model the temporal and spatial probability of occurrence of hillslope hydrological hazards (Terlien et al. 1995; van Westen et al. 2006). In this type of models, the spatial representation of these hazards introduces several issues that need to be addressed (Beven and Binley 1992; Pogson and Smith 2015). These issues can be grouped into model complexities, over-parameterisation, input uncertainties and data quality (Koo et al. 2020). Model complexities refer to the effects of model structures in relation to the number of parameters required to represent the catchment's physical processes and hillslope hydrology and stability (Uusitalo et al. 2015; Beven et al. 2018). Model complexities results from the inability of the model structure to mimic the real world (Yen et al. 2014). Whereas, input uncertainty is associated with the quality of the input data and model parameters (Pogson and Smith 2015). The input uncertainty, also known as "**epistemic uncertainty**," stems from the lack of knowledge and information available in input datasets to characterised the model parameters (Almeida et al. 2017; Herrera et al. 2022).

Uncertainties regarding input datasets and model parameters are manageable by implementing conceptual frameworks that evaluate the available information in input datasets, identify sources of uncertainty by adjusting input parameters around their nominal values, and establish workflows to assess the impact of uncertainty on model outcomes, ensuring the appropriate application of the model (Walker et al. 2003; Refsgaard et al. 2007; Uusitalo et al. 2015; Beven et al. 2018). When physically-based models are applied as a tool to forecast or support decision-making processes at regional or local scales, it is important to quantify and reduce uncertainty and their results (Matott et al. 2009; Beven et al. 2018; Herrera et al. 2022). Managing these uncertainties is considered a "*good practice*" in hillslope hydrological hazard modelling, particularly in the context of climate and land use change (Beven et al. 2018; Wagener and Pianosi 2019). It involves evaluating multiple model configurations that reasonably fit observed hazards, improving the modelling of hillslope hydrological hazards through ex-ante evaluations (Walker et al. 2003; Williams et al. 2020). This approach enables modellers to make consistent and justifiable decisions, selecting model outcomes that best fit the requirements to support decision-makers in formulating **more effective disaster risk reduction** policies and adaptation strategies for settlements and infrastructures in urban and rural areas, incorporating the representation and assessment of rainfall-triggered landslides, debris flows, and hillslope erosion hazards under different land use and climate scenarios (Schmidt et al. 2011; de Ruiter et al. 2020). Addressing the potential impacts of interacting hazards must be conducted in a multidisciplinary framework between researchers, policymakers, governmental institutions, and private organizations to provide better insights into understanding these hazards from their perspective and reduce their impacts under future climate extremes (Gallina et al. 2016; De Angeli et al. 2022).

**The overall aim of this thesis** is to elaborate a modelling workflow that handles issues in parameterisation and uncertainties arising in hillslope hydrological hazard interaction modelling to investigate their potential effects on climate and land use change in two multi-hazard-prone catchments in Saint Lucia and Chile. This requires the development of a new modelling workflow that enables physically-based distributed multi-hazard models to be applied in data-scarce regions, transparently accounting for issues such as parameter uncertainties and equifinality. Using this workflow, hazard

scenarios will be explored in the two case study locations to demonstrate the utility of this approach for informing resilient planning and policy. The rest of this introductory section outlines the importance of accounting for catchment physical characteristics that drive hillslope hydrological hazard interactions (section 1.1.2) and the impacts of climate and land use change in the occurrence of these hazards (section 1.1.3). Section 1.2 provides a brief overview of current approaches to hillslope hazard assessment and outlines the need for new approaches to applying hillslope hydrological multi-hazard models. To address these challenges, the detailed research aims, and objectives of this thesis are introduced (section 1.3) and an overview of the thesis structure is provided (section 1.4).

### 1.1.2 The importance for accounting catchment physical characteristics

**Rainfall-triggered landslides** and **debris flows** are classified as mass movement processes. According to Selby (1993), **mass movements** correspond to the movement of soil and/or rock down the slope under the influence of gravity and water. Various classifications of mass movement processes exist, with the most well-known being those of Varnes (1978); and Hungr et al. (2001). These classifications categorize mass movements based on the involved materials (e.g., mud, soil, rock and debris) and the type of movement (e.g., falls, topples, slides (rotational and translational), lateral spreads and flows) (Varnes 1978; Cruden and Varnes 1996). In the context of **rainfall-triggered landslides**, they can be defined as the displacement of soil and rock down hillslopes due to the combined forces of gravity and water. This encompasses various types of slope movements, such as topples, rotational slides, and translational slides (Korup 2012). These types of movements can be classified as **shallow and deep-seated** (Hungr et al. 2014). Shallow landslides occur within approximately three meters or less from the ground surface, while deep-seated landslides occur at significant depths within the slope, ranging from about three meters to several hundred meters deep (Guerra et al. 2017; Shou and Chen 2021). While landslides can also be triggered by earthquakes (Hungr et al. 2014), rainfall-triggered landslides are the most common globally, particularly in humid tropics and mountainous regions with high-intensity rainfall events (Aleotti 2004; Guzzetti et al. 2007). **Debris flows**, on the other hand, are a specific type of mass movement characterised by the movement of water-saturated mixtures of soil and sediment of varying sizes, ranging from clay to boulders (Varnes 1978; Sidle et al. 1985). These mixtures move downhill under the influence of gravity until reaching a point where the transported material is deposited (Montgomery and Dietrich 1994; Hungr et al. 2001; Iverson et al. 2002). Debris flows can be initiated by hillslope runoff, the transformation of landslides, or the gradual entrainment of material into the flow from the surface, leading to a significant increase in volume (Takahashi 1978; Chen and Zhang 2015).

**Hillslope erosion** occurs when water detaches, transports, and deposits particles of soil and rock material from the hillslope surface under similar condition (Aksoy and Kavvas 2005; Meng et al. 2021). According to Ellison (1948); Govers et al. (1990) and Cuomo et al. (2015), the process of hillslope erosion is initiated by the detachment of soil surface particles, either through runoff erosion caused by hillslope runoff or rainsplash erosion caused by rainfall characteristics. **Runoff erosion** is particularly significant on hillslopes with rainfall rates that exceed the soil's infiltration capacity, especially when the soil is thin and unconsolidated (Michaelides and Martin 2012). The consequences of runoff erosion

include **sheet erosion**, which involves the uniform removal of a thin layer of soil over the slope, as well as **rill and interrill erosion** caused by the flow of water across the soil surface. Additionally, **gully erosion** occurs when surface runoff removes soil along drainage lines, forming deep channels or trenches (Merritt et al. 2003; Li et al. 2017). **Rainsplash erosion**, on the other hand, correspond to the detachment and mobilisation of soil particles resulting from raindrop impact (Aksoy and Kavvas 2005). This type of erosion depends on the impact forces such as rainfall intensity and soil mechanical properties (Guerra et al. 2017). Hillslopes are subject to erosion through various dominant mechanisms, including surface-water runoff and mass movement processes (van Beek et al. 2008). Landslides, such as debris flows, can act as agents of erosion, facilitating the movement and transport of material toward channels and alluvial fans (van Beek et al. 2008). As a result, rainfall-triggered landslides and debris flows are natural components of the hillslope erosion process (Korup 2009; Larsen et al. 2010).

The occurrence of rainfall-triggered landslides, debris flows, and hillslope erosion hazards is governed by the interrelationship between the catchment physical characteristics, such as topography, soil properties and surface cover, and triggering factors, such as rainfall (Coe and Godt 2012; Pardeshi et al. 2013). According to Montgomery and Dietrich (1994) and Bogaard and Greco (2014), to identify these interrelationships, it is necessary to understand their roles in hillslope hydrology and stability. Figure 1.2 illustrates the catchment's physical characteristics including soil types and their properties such as soil depths, hydrological and geomechanically properties, topography comprising slope angles and drainage patterns, and land use/land cover. The interplay between these catchment physical characteristic and rainfall determines the frequency and magnitude of hillslope hydrological hazards. Hillslope hydrological hazards are typically observed in unsaturated and saturated soils (Figure 1.2) (Cuomo and Della Sala 2015; Sidle et al. 2019). In these soils, hydrological and stability processes initiated by rainfall on hillslope surfaces and subsurfaces depend on the soil structure in terms of grain, porosity, and depth variability of hillslope soil deposits (Bogaard and Greco 2016; Rahardjo et al. 2019). These soil characteristics determine hydrological and geomechanically properties such as moisture content, matric potential, hydraulic properties, cohesion, and angle of friction (Townsend 1985; Fan et al. 2016). For example, saturated hydraulic conductivity determines infiltration rates, soils with higher porosity influence greater infiltration rates than soils with lower porosities (Farrell and Larson 1972; Muntohar and Liao 2010). In addition, pore size influences the soil saturated moisture content, which is the maximum amount of water contained in the pore space, and soil water-holding capacity, which is a key aspect for partitioning rainfall into infiltration and runoff in unsaturated soils (Kirkby 1988; Bogaard and Greco 2016). As rainfall infiltrates, the soil matric suction is reduced due to an increase in moisture content as the soil becomes saturated by the advance of wetting front (Muntohar and Liao 2010; Zhang et al. 2011). The preceding, results in positive pore water pressures that affect the strength and stability of the soil (Bogaard and Greco 2016). Slope failure occurs when the weight of the saturated soil increases the slope shear forces, which reach a limit because of the reduction in the slope shear strength (Montgomery and Dietrich 1994).

Moreover, as the soil becomes saturated, rainfall intensity surpasses the soil infiltration capacity accumulating water in the soil surface micro-depressions and initiating runoff by the action of gravity (Lu

and Godt 2013). The term **hillslope runoff** will be used to denote surface water flow on hillslopes (Michaelides and Martin 2012). Hillslope runoff can also originate from infiltration excess which occurs when the rainfall intensity exceeds the soil infiltration capacity (Aksoy and Kavvas 2005). Soil depth (Figure 1.2) plays an important factor in hillslope runoff, especially in hillslope hydrology because it determines the subsurface flow processes that control the connectivity of saturated areas at the soil-bedrock interface, thereby determining landslide failure depth surfaces and surface flow generation (Lanni et al. 2013; Kim et al. 2016). Hillslope runoff is also one of the main initiation mechanisms of debris flows and hillslope erosion (Liu et al. 2021). The effects of hillslope runoff on debris flow motion are expressed by the entrainment of both landslide material and bed erosion according to the magnitude of the surface flow generated in terms of depth and velocity (Hutter et al. 1994; Iverson 1997). In the case of hillslope erosion, the erosion rates depend on the flow velocity and soil properties such as depth, cohesion, and vegetation (Michaelides and Martin 2012; Cuomo and Della Sala 2015).

Topography also plays an important role in controlling hydrology and slope stability (Figure 1.2), particularly slope gradient influences the concentration of subsurface flow and the routing of surface flow into channels (Kiani-Harchegani et al. 2022). The slope geometry and its length are key influential topographic factors that affect the runoff initiation, volume and intensity of the flow, and travel distance of the landslide and debris flows as steeper slopes promotes more gravitational energy of the flowing mass (Gao 1993; Gao et al. 2021). For example, steep slopes increase the surface flow velocity and demand forces that move soil material down the slope (Montgomery and Dietrich 1994). The calculation of slope stability relies on the infinite slope model, which assumes that slope failure occurs along a sliding surface parallel to the ground surface (Mergili et al. 2014). The fraction of forces acting on the failure plane is expressed in terms of the Factor of Safety (FoS) which under an infinite slope approach can be assessed as the ratio of shear strength forces (force capacity) to shear forces (force demand) (Van den Bout et al. 2021). The travel distance of rainfall-triggered landslides and debris flows is governed by the properties of the soil materials and movement paths (e.g., drainage direction paths) (Takahashi 1978; Miller and Burnett 2007). Therefore, topography and lithological conditions have direct impacts on landslide and debris flows runout distances (Gao et al. 2021). Additionally, land use (Figure 1.2) affects the physical properties of soil (Giertz et al. 2005). The impacts are evidenced in the reduction and modification of natural land cover, which has a role in controlling hydrology and stability (Sidle et al. 1985; Persichillo et al. 2017).

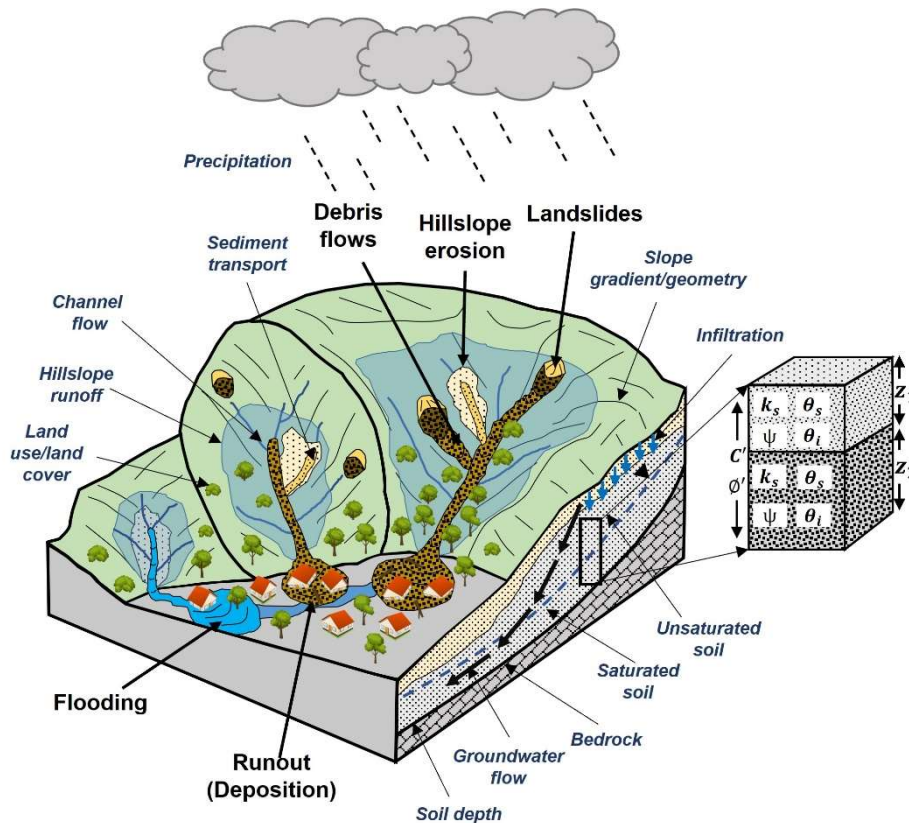


Figure 1.2 Catchment physical characteristics.

### 1.1.3 Understanding hillslope hydrological hazard interactions under land use and climate change

The impacts of climate and land use change on hillslope hydrological hazards are not isolated phenomena (Van Beek and Van Asch 2004; Caloiero 2018). These hazards occur across a range of geological, environmental, and climatic conditions, which constantly change because of climate and land use changes (Dai et al. 2001; Guzzetti et al. 2007). Consequently, the occurrence of these hazards is highly variable and complex at all scales, especially when the catchment is highly sensitive to changes in its hydrological and stability conditions because of the impacts of climate and land use change (Beven 2001; Sivakumar and Singh 2012). In other words, hillslope hydrological hazards are stochastic because their occurrence is dynamic and varies over time making it difficult to predict when and where they will occur as a consequence of these impacts (Montgomery and Dietrich 1994; Beven 2021). To understand the influence of these changes on the occurrence of rainfall-triggered landslides, debris flows, and hillslope erosion hazards across different magnitudes, it is necessary to assess the response of hydrological and stability processes to various climate and land use scenarios. This assessment helps identify how hillslope hydrological and stability characteristics respond to the occurrence and interaction of one or more hazards (Van Beek and Van Asch 2004; Van den Bout et al. 2018).

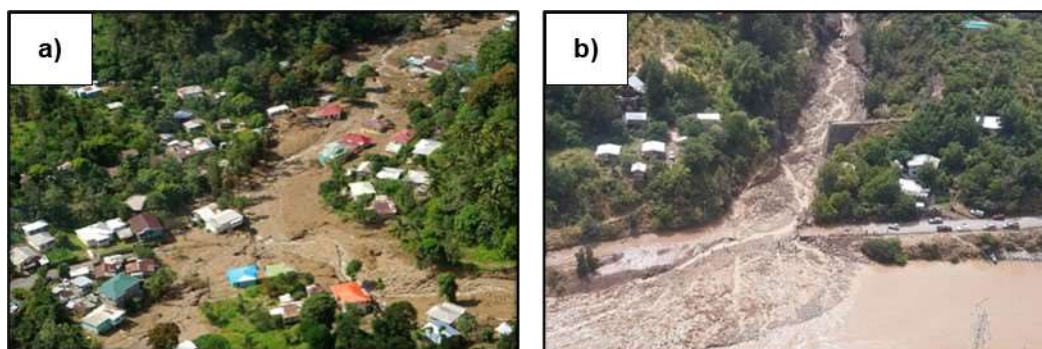
## Impact of climate change on hillslope hydrological hazards

Rainfall-triggered landslides, debris flows, and hillslope erosion share the same trigger and all three occur predominantly during extreme rainfall events (Larsen and Simon 1993; Shen et al. 2018). Climate change-induced variations in rainfall patterns, such as intensity, duration, and total volume, affect hillslope hydrological and stability processes differently (Huggel et al. 2012). Short and intense rainstorms are commonly observed as significant triggers for debris flows and shallow landslides (Martelloni et al. 2011; Turkington et al. 2016). Similarly, high-intensity storm events are associated with the severity of hillslope erosion, resulting in rapid hillslope runoff generation and increased detachment, transport, and deposition of sediment material (Li and Fang 2016; Meng et al. 2021). The response to hillslope hydrological hazards is particularly evident in mountainous regions, where spatiotemporal rainfall patterns have become more extreme in terms of intensity and duration (Caloiero 2018; Vergara et al. 2020). For instance, humid tropical catchments in the Caribbean, India, and South Asia have experienced increased rainfall intensities during hurricanes, cyclones, and typhoons (Reed et al. 2022). In contrast, Mediterranean regions are projected to face more extreme events, including heatwaves and prolonged drought periods, accompanied by a significant reduction in annual precipitation (Giorgi and Lionello 2008; Zittis et al. 2019). However, in these regions, heavy rainfall can still occur in short time periods following extended dry periods due to interannual variability associated with the El Niño–Southern Oscillation (ENSO) (Lionello et al. 2014; Vergara et al. 2020; Moreiras and Sepúlveda 2022). These short and intensive rainfall events after extended dry or drought periods lead to increased infiltration-excess runoff by altering soil properties, such as reducing pore spaces (Luterbacher et al. 2006; Soto et al. 2017).

The impacts of rainfall variability on hillslope hydrological hazards are closely related to the response of the lithological setting in different environments (Guzzetti et al. 1996; Rahardjo et al. 2019). In humid-tropic environments, the lithological setting is characterised by residual soils with varying textural characteristics, ranging from clay to gravel (Townsend 1985). These soils result from the accumulation of weathered material on top of the bedrock, which occurs through mechanical, chemical, and biological weathering processes (Bicocchi et al. 2019). On the other hand, Mediterranean environments have sedimentary soils that form from shallow colluvial and alluvial deposits of different sizes (Yaalon 1997). These deposits originate from weathering, fluvial, and gravitational processes (Townsend 1985). The response of both lithological settings to spatiotemporal rainfall variability depends on the type of soil and its hydrological and geotechnical properties, including soil water content, infiltration rates, soil cohesion, and internal friction angle. These properties vary according to the climatic characteristics of the respective environments (Wohl et al. 2012; Vereecken et al. 2015).

The soil water content in humid-tropic regions increases during extended rainfall periods and wet seasons, leading to elevated pore water pressures (Wohl et al. 2012). This increase in pressure can induce slope instability and trigger various processes, including hillslope runoff, debris flow generation, and hillslope erosion (Reading 1991; Garland and Olivier 1993). Conversely, Mediterranean regions experience seasonal and annual rainfall variability, resulting in reduced soil moisture. Extended dry periods in these regions can cause soil desiccation, leading to reduced soil cohesion and strength (Ruiz

Sinoga et al. 2010; Moreiras and Sepúlveda 2022). Consequently, during short and intense rainfall events, rapid soil saturation occurs, leading to increased surface runoff and influencing the generation of debris flows, hillslope erosion, and the initiation of shallow landslides (Sillero-Medina et al. 2020). In particular, mountainous catchments within these regions have exhibited different slope hydrological and stability response to changes in rainfall intensity and duration that has been translated into more frequent shallow landslides, extensive debris flows, and severe hillslope erosion (see Figure 1.3) (Leonard et al. 2014; Moreiras et al. 2021).



*Figure 1.3 Effects of Hurricane Tomas in Saint Lucia, Eastern Caribbean, and effects of exceptional rainfall event during summer in Maipo sub-catchment, Santiago metropolitan region, Chile. (a) Fond St. Jacques debris flow (rural settlement) (ECLAC 2011); (b) Melocoton ravine Maipo sub-catchment, Chile (Marín et al. 2017).*

### **Impact of land use change on hillslope hydrological hazards**

Land use change (LUC) represents the second dynamic influence on hillslope hydrological hazards (Persichillo et al. 2017; Johnston et al. 2021). Anthropogenic activities, including urbanization, agriculture, and deforestation, exert growing pressure on hillslopes, leading to the loss of natural land cover that impacts the hillslope soil properties (Ávila et al. 2020; Moreiras et al. 2021). For example, informal urban expansion into slopes prone to landslides influences deforestation and hillslope cutting, leading to negative consequences for slope stability (Dai et al. 2001; Dai et al. 2002). This was highlighted by Bozzolan et al. (2020), who studied the effects of informal housing on slope stability, identifying that the presence of informal housing modifies the natural slope angle, soil cohesion, and soil thickness modifying the natural role of the slope in maintaining stability. Moreover, the expansion of farmlands into hillslopes also has essential effects on hydrological processes and soil mechanical structures (Persichillo et al. 2017). Natural land covers, such as scrubs and forests are the most sensitive to the effects of urbanisation and deforestation, as they play a crucial role in enhancing soil stability and hydrology (Sidle et al. 1985; Schmaltz et al. 2017). Their role in stability is the aggregates of soil particles, increasing the shear strength and bonding of soil particles, particularly in the upper few centimetres of the soil layers, which helps prevent surface erosion (Masi et al. 2021; Murgia et al. 2022). Moreover, natural land cover regulates the hydrological regime of slopes by influencing moisture content, infiltration, and rainfall-runoff dynamics (Wohl et al. 2012; Zhang et al. 2022). Additionally, it

adds roughness and friction to flow propagation, thereby reducing flow velocity and energy (Nepf and Koch 1999). Therefore, the response of hydrological and stability processes to changes in rainfall intensity and duration is associated with the impact of land use changes on soil properties (Vanacker et al. 2003; Giertz et al. 2005).

According to Marhaento et al. (2018), humid tropical regions are more susceptible to the impacts of land use change. Deforestation for agriculture and urbanisation are the main drivers of land use change in these regions (Foley et al. 2005; Wu et al. 2011). However, according to Guns and Vanacker (2013), changes in land cover from forest to pasture on steep slopes (e.g., crop rotation) have been the main drivers of changes in soil properties and hydrology, reducing slope stability. Moreover, soil erosion in humid tropics is dramatically concentrated over deforested hillslopes where bare soil and agricultural landscapes are predominant (Labrière et al. 2015). Alternatively, in Mediterranean regions land use change is highly dominated by the direct impacts of climate change due to extended drought periods and more intense wildfires (Parise and Cannon 2012). For example, in mountainous catchments, the severity of drought periods reduces the covered-trees areas in favour of scrubs or grasslands (Akinyemi 2021). Whereas wildfires remove all types of natural land cover, creating water-repellent soils that increase surface runoff and hillslope erosion (Fraser et al. 2022). These factors increase the severity of shallow landslides and debris flow activity (Glade and Crozier 2010; Moreiras et al. 2021). However, agriculture for economic purposes is also a driver of land use change in the Mediterranean regions. According to Schulz et al. (2010), in the last decade, the major trends in landscape changes were due to the reduction of forests and conversion of shrublands to intensive land uses such as farmlands, increasing erosion, and impacting the hydrological regimes of these environments.

## 1.2 Hillslope hydrological multi-hazard modelling approaches

According to Malamud et al. (2004); Fell et al. (2008) and Corominas et al. (2014), rainfall-triggered landslides, debris flows, and hillslope erosion hazards can be defined as potentially damaging physical events that may negatively impact society and the natural environment. These impacts are assessed by calculating the “**Risk ( $R_s$ )**” (Equation 1.1) that measures the probability of potential consequences of these hazards over the population (life expected losses), infrastructure and economic activities in areas highly exposed to hillslope hydrological hazards (van Westen et al. 2006; Corominas and Moya 2008). The risk is often estimated by calculating the “**Hazard (H)**” which corresponds to the probability of occurrence of a landslide, debris flow or hillslope erosion hazard within a determined area and period (e.g., hours, days, months). The “**Vulnerability (V)**” which is the degree of physical, social, economic and environmental factors that increase the susceptibility of a community to the impacts of these hazards and the “**Exposure (E)**” which is the set of elements (e.g., population, buildings, public services such as hospitals and schools) or any other critical infrastructure potentially affected by the hazard (Fell et al. 2008; UNDDR 2020; De Angeli et al. 2022).

$$\text{Risk } (R_s) = H * V * E \quad \text{Equation 1.1}$$



The assessment of hillslope hydrological hazard interactions requires models that can integrate catchment physical characteristics and climatic variables to analyse their spatiotemporal interrelationships (van den Bout 2020; van Westen et al. 2021). According to Gill and Malamud (2014), the impacts of natural hazards on the natural environment cover different temporal and spatial scales. The first one corresponds to the duration in which the hazard acts and the second one is the area in which the hazard impacts (Corominas et al. 2014). Physically-based models are capable of evaluating these interrelationships by incorporating relevant physical and climatic variables and processes, such as slope hydrology, stability, and rainfall characteristics (Terlien et al. 1995; Herrera et al. 2022). These models can represent the drivers of landslides or debris flows and their responses to historical, current, and potential climate scenarios. However, describing hazard interactions within these models becomes challenging at different spatial scales, especially at the catchment level (Van den Bout et al. 2018). For example, hydrological or slope stability process representation requires catchment physical characteristics, such as soil depth, cohesion, and angle of friction, which are site-specific and can only be modelled properly using site-specific mechanistic models (van Westen et al. 2006). These characteristics make these models more suitable for assessing the temporal probability of landslides or debris flows on individual slopes by relating the slope hydrology and stability to triggering factors such as rainfall (Von Ruetten et al. 2013; Van den Bout et al. 2021).

GIS-based models, instead, can be used to identify the spatial distribution of hazards at different scales (van Westen et al. 2006). These models use various approaches, including qualitative methods like field geomorphological analysis and heuristic methods that rely on expert opinions (Pardeshi et al. 2013; Shano et al. 2020). In geomorphological methods, experts create detailed maps of landslide sizes and debris flow runout areas while identifying the factors responsible for these hazards (Aleotti and Chowdhury 1999). Heuristic methods involve mapping and weighting factors based on experts' personal experiences and their expected contributions to landslides or debris flows (Dragičević et al. 2015). Quantitative methods, such as statistically-based approaches, predict the probability of landslide, debris flow, or hillslope erosion occurrence based on the relationship between spatially distributed factors such as topography, geology, soil types, and land use/land cover, considering past observed hazards (Guzzetti et al. 1999; Reichenbach et al. 2018). These approaches offer the advantage of cost-effectively assessing the susceptibility of different areas at various spatial scales, especially for land use planning purposes (Fell et al. 2008). However, when it comes to landslides and debris flows, these models are limited to susceptibility analysis and do not incorporate physical and climatic properties or hazard drivers (Guzzetti et al. 1999; van Westen et al. 2006). As a result, they cannot quantify the frequency and magnitude of these events under different triggering conditions, which is crucial for a comprehensive hazard assessment (Van den Bout et al. 2021).

Physically-based methods can be integrated into GIS environments to create physically-based distributed hazard models, allowing the spatiotemporal representation of rainfall triggered, landslides, debris flows and hillslope erosion hazards (Aleotti and Chowdhury 1999; Aksoy and Kavvas 2005). These models offer the advantage of incorporating the spatial variability of topography, geology, environment, land use, and other drivers to simulate hillslope hydrology and stability at different

catchment scales (van den Bout 2020). They can provide information on landslide locations, areas, depths, debris flow runout areas, and erosion and deposition volumes (Crosta and Frattini 2003; Starkloff et al. 2018). However, a well-known challenge with these models is the need for a substantial amount of data to represent hydrological and stability processes (Fisher 1986; Almeida et al. 2017; Beven et al. 2018). The complexity of simulating real hazards e.g., landslides, debris flows, and hillslope erosion requires extensive data to set model parameters (van den Bout 2020). Collecting or estimating such data is particularly difficult, especially over large spatial scales and in data-scarce environments (Lilburne and Tarantola 2009; Herrera et al. 2022). Furthermore, the spatial representation of these hazards depends on the catchment scale and the resolution of the input data (van Westen et al. 2008). When dealing with large areas, high-resolution data and simulations can be computationally expensive in these models, and coarse-resolution simulations may not accurately identify specific slope failures or debris flow runout areas (Van den Bout et al. 2021; Mead et al. 2021).

### 1.2.1 Assessment of hillslope hydrological hazard interactions

According to van Westen et al. (2006); Cascini et al. (2011); Mergili et al. (2012) and Pudasaini and Fischer (2020), physically-based models provide a better understanding of the physical and climatic interrelationships that contribute to multi-hazard interactions compared to empirical-statistical models. Recent advancements in physically-based distributed modelling have focused on climate, hydrological, and stability-related hazards (van den Bout 2020). The work of Godt et al. (2008); Chen and Zhang (2015); He et al.(2016); Mergili et al. (2017); Salvatici et al. (2018) and van den Bout (2020), introduced new improvements to assess the initiation of rainfall-triggered landslides and their interactions with debris flows, as well as the occurrence of debris flows and their impacts on erosion at regional and catchment scales. These advancements involve the coupling of hydrological and stability models, which refers to the exchange of information between models to address complex interrelationships among climatic, hydrological, and stability processes (Panday and Huyakorn 2004; Flato 2011). The coupling of models includes catchment-scale infiltration and rainfall-runoff models, differential and kinematic wave equations for flow simulation and routing, sediment equations for detachment, transport capacity and deposition, regional slope failure models for assessing potential slip surfaces on a regional scale, and numerical runout models for simulating solid and fluid interactions on larger spatial scales (Van Beek and Van Asch 2004; von Ruetten et al. 2016; Baumann et al. 2020; Cuomo et al. 2021). As a result, physically-based distributed models can be regarded as "**multi-hazard models**" since they enable the integrated modelling of two or more hazards providing a comprehensive framework for studying and understanding the complex interactions between various hazards in an integrated manner (van den Bout 2020).

In the case of hillslope hydrological hazards, the assessment of interactions involves identifying the key interrelationships between hydrological and stability processes that contribute to the transition of rainfall-triggered landslides into debris flows and their combined impact on hillslope erosion (Cascini et al. 2013; Fan et al. 2017; Van den Bout et al. 2018) (Figure 1.4). It provides valuable insights into the catchment sensitivity to land use and climate change on hydrological and stability interrelationships driving multi-hazard interactions (Van Beek and Van Asch 2004; Malet et al. 2005). To evaluate these

interrelationships, it is necessary to couple regional- or catchment-scale models for hillslope hydrology and stability. For catchment scales, slope stability assessment involves integrating physically-based distributed slope stability models with spatially distributed hydrological and infiltration models (Wilkinson et al. 2002; Muntohar and Liao 2010). The integration of the infinite slope method into GIS raster formats has facilitated slope stability calculations for large scales in one- or two-dimensional space (Terlien et al. 1995; Guzzetti et al. 1999; Corominas et al. 2014). This coupling enables the incorporation of slope stability models with infiltration models for vertical water flow and hydrological models for surface flow, thereby improving the quantification of interrelationships between slope stability and catchment hydrological surface and subsurface processes (Muntohar and Liao 2010; Arnone et al. 2011).

Establishing the link between rainfall-triggered landslides and debris flows requires coupling distributed slope failure models to search for potential slip surfaces with numerical runout models (von Ruetten et al. 2016; Fan et al. 2017; Cuomo et al. 2021). Current slope failure methods, such as iterative failure methods, random ellipsoids method, and random sampling methods, provide detailed information about the Factor of Safety (FoS), potential failure surfaces, and associated volumes (Michel et al. 2020; Van den Bout et al. 2021). The coupling of slope failure methods to estimate failure depths and volumes can easily be coupled with physically-based numerical models (Figure 1.4) capable of describing the competitive fluid and solid forces that influence the transition from failure volumes to debris flow. These models incorporate entrainment and rheological parameters to assess motion, magnitudes, and their impacts on erosion and deposition rates (Chen and Zhang 2015; Pudasaini 2019; Pudasaini and Fischer 2020). However, the transition from rainfall-triggered landslides to debris flows and their impact on erosion depend on the volumetric sediment concentrations, flow depth, and velocity (Takahashi 1978; Iverson 1997; Liu et al. 2021). Therefore, the coupling of rainfall-runoff models is required to assess the effects of surface flow on the entrainment of bed material (surface erosion) and slope failure volumes on flow volumetric sediment concentrations (Mergili et al. 2017; Liu and He 2020). This is essential for assessing the flow mixture composition in terms of fluid phases (flow frictional forces) and solid phases (basal resistance forces), which determine the entrainment rates (erosion) and debris flow runout (deposition) (Pudasaini and Fischer 2020).

Incorporating characteristics into regional- or catchment-scale physically-based distributed multi-hazard models faces several issues that must be addressed. The large number of hydrological and geotechnical parameters used to represent all relevant catchment processes for hydrology and stability requires a substantial amount of data, making multi-hazard modelling more complex in terms of process representation (Beven and O'Connell 1982; Von Ruetten et al. 2013; Liu et al. 2020). This complexity can degrade the applicability of multi-hazard models and increase uncertainty in their outcomes (van den Bout 2020). Furthermore, these models require proper spatial resolution to accurately represent the temporal frequency and spatial location of rainfall-triggered landslides, debris flows, and hillslope erosion hazards by incorporating all the hydrological and stability processes (Zhang et al. 2013; Fuchs et al. 2014). However, in regions, where the data accessibility or information available to estimate hydrological and geotechnical parameters for process modelling is scarce or limited, the modelling of hillslope hydrological hazards and quantifying their interactions poses a disadvantage in properly

assessing the impacts of climate and land use change on their frequency, magnitude, and location (van Westen et al. 2008; Kuriakose et al. 2009; Gorgoglione et al. 2020).

Implementing workflows to parameterise complex multi-hazard models for modelling hillslope hydrological hazards requires considering the number of input parameters necessary to model hazard interactions and handle uncertainties arising from data representation. This is particularly important for countries with limited data accessibility, which hampers the spatial representation and quantification of these hazards and their interactions. To achieve this, it is crucial to identify a suitable multi-hazard model that incorporates various methods and techniques to model hydrological and stability interrelationships leading to hazard interactions. This enables the assessment of feedback mechanisms that define the type interaction and magnitude of hazards like rainfall-triggered landslides, debris flows, and hillslope erosion caused by climate and land use change (Figure 1.4). Therefore, according to Figure 1.4, regional- or catchment-scale physically-based distributed multi-hazard models are more suitable for assessing the impacts of climate and land use change on hillslope hydrological hazard interactions, as they can model the temporal frequency of these hazards, as well as their spatial location, allowing the quantification of their magnitudes and impacts for different scenarios.

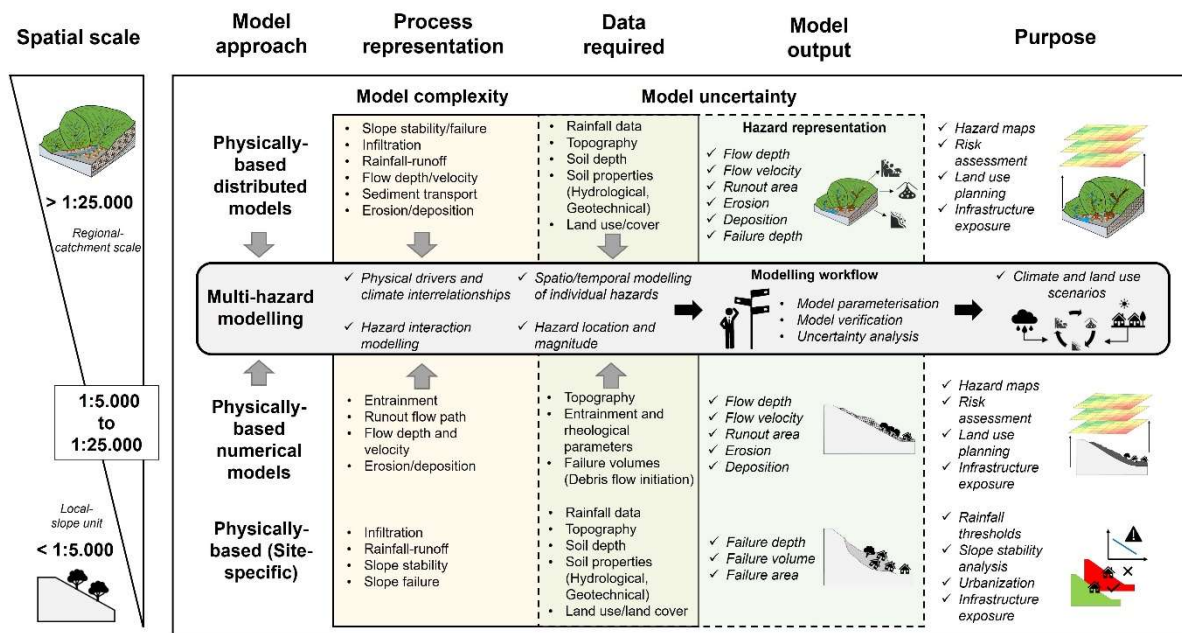


Figure 1.4 Overview of multi-hazard modelling framework for hillslope-hydrological hazards.

### 1.2.2 Challenges and gaps in hillslope-hydrological hazard interaction modelling

In the previous section, it was proposed that assessing the impacts of climate and land use change on hillslope hydrological hazard interactions requires physically-based distributed multi-hazard modelling approach at catchment scales. In Chapter 2, the precise model selected for the task is discussed in detail. However, as discussed in section 1.2.1, the selection of a catchment-scale multi-hazard model to assess hillslope hydrological hazard interactions driven by climate and land use change faces several challenges that must be addressed. These challenges can be classified as, (i) model complexity: the coupling between models and methods for process representation increases the number of parameters required to model multi-hazard interactions (over-parameterisation); (ii) model parameterisation: the definition of values for the set of parameters of the chosen multi-hazard model to represent hydrological and stability processes that lead to hazard interaction; and (iii) the management of uncertainty that arises owing to the quality of the available data to estimate the required hydrological and geotechnical parameters for the chosen multi-hazard model, which impacts the representation of multiple-hazard interactions.

One of the initial steps in addressing these challenges involves considering a methodology that helps bridge gaps in handling parameterisation of multi-hazard models and uncertainties arising from data quality. When assessing interactions between hillslope hydrological hazards, the objective is to quantify the influences between hazards resulting from climate and land use changes. For instance, this includes measuring the increase in debris flow runout areas due to heightened landslide activity during extreme rainfall events or the rise in hillslope erosion rates in deforested areas, leading to more landslides and debris flow during short and intense rainfall events. To accomplish this objective, it is necessary to frame the analysis of hillslope hydrological hazard interactions based on the desired outcomes for potential users such as researchers, modellers, decision-makers, and stakeholders (Refsgaard et al. 2007; van Vliet et al. 2016; Beven et al. 2018; Williams et al. 2020). This entails analysing the interactions within the catchment where they occur by examining the spatial distribution of rainfall-triggered landslides, debris flows, and hillslope erosion, and quantifying their magnitudes resulting from the interactions. Therefore, the parameterisation of the multi-hazard model should primarily focus on identifying the appropriate set of parameter values that accurately represent multiple hazard interactions under different climate and land use scenarios, while also identifying sources of uncertainty that may impact the representation of these interactions, such as inaccuracies in hazard locations and magnitudes compared to historical observations.

According to Refsgaard (1997); Wooldridge et al. (2001) and Malone et al. (2015), the parameterisation and uncertainty of a model affect the model outcomes and are influenced by the quality of input data. To accurately represent interactions between hillslope hydrological hazards, detailed data on physical site characteristics is necessary. This data is typically obtained from field measurements and is used to estimate the physical properties of the catchment (van Westen et al. 2008; Kuriakose et al. 2009; Tofani et al. 2017). However, data scarcity is a limitation in certain regions, particularly in the Global South (Gentile et al. 2022). In these regions, information is often derived from literature reviews, existing databases, or published data due to the high cost of accessing field-measured data for estimating

hydrological and geotechnical parameters in large catchments (Pellicani et al. 2013; Biccocchi et al. 2019). Therefore, it is crucial to design a modelling workflow that guides the parameterisation of complex multi-hazard models and helps identify and control sources of uncertainty arising from the quality of input data. This approach contributes to improving the modelling of multiple hazard interactions in data-poor regions under different climate and land use scenarios. Consequently, any analysis and decisions regarding the impacts of potential climate and land use changes on hillslope hydrological hazard interactions rely on both parameterisation and uncertainty control (Uusitalo et al. 2015; Williams et al. 2020). The recommendations for disaster-risk policies are dependent on how these processes are handled in multi-hazard modelling (Beven et al. 2018; van den Bout 2020). The design of a modelling workflow for multi-hazard interactions should consider methodological steps encompassing parameterisation, uncertainty analysis, and model application for climate and land use scenarios. It should also address challenges related to data gathering in data-poor contexts, as well as parsimony, equifinality, and model verification. In the subsequent paragraphs, these challenges will be explored in more detail.

**Data assembling and spatial distribution of input parameter values:** According to Beven (2001); Fan et al. (2016) and Herrera et al. (2022), understanding the physical boundaries of a catchment is essential for determining the spatial distribution of hydrological and geotechnical parameter values. These boundaries can be defined by encompassing the entire catchment area or dividing it into sub-catchments (Summerell et al. 2005). Within the catchment boundaries, the distribution of parameter values can be estimated using representative data for catchment soil types, geological/geomorphological features, and land cover/use using literature reviews or various sources of data (Refsgaard 1997; Feyen et al. 2000; Wooldridge et al. 2001). The collected information is associated with possible values for hydrological and geotechnical parameters based on their spatial distribution, such as soil texture classes and land use categories (Burton et al. 1998; Feyen et al. 2000). When estimating spatially distributed values for different soil type features or land use classes, certain factors need to be considered. The first factor is **uniqueness**. According to Beven (2000), each catchment's hydrological system is unique due to its physical characteristics, including soil type, geology, topography, and vegetation. These characteristics influence how the catchment responds to rainfall, such as infiltration and surface runoff generation. As a result, catchments with different characteristics may exhibit diverse responses to rainfall events in terms of hydrological processes and stability (Beven 2001). Considering these factors is crucial, particularly when assessing the catchment's hydrological response to various climate and land use scenarios.

The second concept is **nonlinearity**. This concept refers to the fact that the relationship between input parameters and model outcomes is not proportional (Beven and Binley 1992). This means that changes in certain input parameters can cause significant variations in the model results, affecting the catchment's hydrological and stability responses (Sivakumar and Singh 2012). To account for nonlinearity, input parameter value estimation should consider a range of values for a specific parameter, such as saturated hydraulic conductivity or soil cohesion for a particular soil type (Herrera et al. 2022). This allows to understand how the catchment responds to different parameter values,

especially to identify the most sensitive values that influence the hydrological and stability responses to rainfall-triggered landslides, debris flows, and hillslope erosion (Song et al. 2015). The influence of **spatial scale and resolution of data** is the third concept to consider. Estimating parameter values at different spatial scales can lead to distortions in the heterogeneity and variability of soil properties and vegetation within the catchment, affecting the modelled hydrological and stability processes (Leavesley et al. 2002; White et al. 2003; Brunner et al. 2012). At smaller scales, more detail and variability can be captured, providing a better representation of processes like infiltration. However, at larger scales, these processes are simplified and represented as a single unit of homogeneous properties (Beven 2001). This simplification hinders the modelling process as it fails to capture the spatial variability of infiltration rates over large areas, limiting the accuracy of the modelled process (Beven 2000; Zhang et al. 2013). On the other hand, obtaining a detailed representation of hydrological processes at higher resolutions can be computationally demanding, requiring more significant computational resources (van Westen et al. 2008). According to Hessel (2005) and van den Bout and Jetten (2020), one of the limitations of physically-based distributed modelling is that the results obtained depend on the spatial resolution of the input data and timestep length. Higher-resolution input data over large areas will require a longer simulation time, limiting the usability of this type of model when computer resources are not available (Vázquez et al. 2002; De Sy et al. 2013). Conversely, lower-resolution data may not adequately represent individual hazards and their interactions since the resolution of input parameters extends beyond the process domain (Beven 2001; Claessens et al. 2005).

**Model parameterisation and equifinality:** **Parameterisation** refers to the process of selecting parameter values for a model to simulate the catchment hydrological system based on available data (Refsgaard 1997; Cullmann et al. 2011). Physically-based distributed models offer the flexibility to vary the values of initial parameters, allowing exploration of the parameter space to find the optimal values that yield high consistency between model outcomes and observations (Beven and Binley 1992; Oreskes et al. 1994; Herrera et al. 2022). Estimating parameter values is a standard procedure, especially in data-scarce environments where measured data to characterised the spatial variability of hydrological and geotechnical soil properties are lacking (Almeida et al. 2017; Beven et al. 2018). The assessment of parameter value variation requires methodologies that quantify the range of values within which initial parameter values can vary to best represent hillslope hydrological hazards (Guinot and Gourbesville 2003). However, it is neither feasible nor desirable to allow parameter values to vary freely (Refsgaard 1997). Inaccurate variation of parameter values can constrain the modelling of catchment hydrology and stability, leading to unrealistic hazard representations that do not align with observations (Malone et al. 2015). To assess the variation of input parameter values, several methodologies exist, such as sensitivity analysis techniques (Wagener and Pianosi 2019). One approach is the One-At-a-Time (OAT) method, which varies one input parameter value at a time while keeping other parameter values fixed to observe the effects on model outputs. Another method is the All-At-a-Time (ATT) method, where all parameter values vary simultaneously to evaluate the relative importance of each parameter in influencing model outputs (Song et al. 2015; Pianosi et al. 2016). Additional methods include Latin Hypercube Sampling (LHS) and Monte Carlo simulation, which generate random sampling parameter values covering a range of possibilities (Douglas-Smith et al. 2020).

When assessing variations in input parameter values during the parameterisation process, it is important to consider equifinality. **Equifinality** suggests that different combinations of parameter values can lead to similar model outputs and predictions (Beven 2001; Herrera et al. 2022). Therefore, there won't be a single representation of catchment hydrological and stability processes, but rather an ensemble of parameter-set values that are considered acceptable for predicting rainfall-triggered landslides, debris flows, and hillslope erosion hazards (Beven 2019). As new information becomes available over time, the ensemble of acceptable parameter-set values may evolve. Considering equifinality in the parameterisation process goes beyond fitting model results to observations. It aims to identify parameter-set values that not only align with observations but also provide meaningful and accurate representations of the modelled hazard (Refsgaard 1997; Beven 2006). This approach enhances the robustness of the model outputs by accounting for the uncertainty introduced by the model's input parameters (Uusitalo et al. 2015). Furthermore, incorporating equifinality improves the accuracy and reliability of the model's predictions, making them valuable for decision-making and risk assessment (Oreskes et al. 1994; van Vliet et al. 2016). By acknowledging the concept of equifinality and selecting parameter-set values that capture the inherent uncertainty in the system, the parameterisation process becomes more robust, and the model's predictions become more trustworthy and useful (Malone et al. 2015).

**Model verification and sensitivity analysis (SA):** During the model parameterisation process, verification is essential for selecting parameter-set values that accurately represent hazards in relation to observations (Oreskes et al. 1994; Beven 2019). This process is particularly important when selecting hydrological and geotechnical parameter-set values for different soil types and land use categories. Model verification can be divided into two procedures. The first is model internal verification, which evaluates the consistency and accuracy of a model's internal logic and calculations (Fawcett et al. 1995). This step helps identify parameter sets that provide an acceptable representation of observed hazards, considering the uncertainty and equifinality in the model results (Hofmann 2005; Beven 2019). The second procedure is model verification, which assesses the accuracy, consistency, and reliability of model outcomes (Guzzetti et al. 1999; Chung and Fabbri 2003). This involves applying verification techniques and analysing the agreement between model results and observed data using accuracy statistics (Guzzetti et al. 2006; Frattini et al. 2010). Both verification procedures are crucial for the parameterisation process as they establish criteria for selecting the parameter set that best represents observations. Assessing the sensitivities of the selected parameter set is also important because it identifies the input parameters that have the greatest impact on the model outcome (Crosetto et al. 2000; Đukić and Radić 2016). According to Refsgaard et al. (2007); Lilburne and Tarantola (2009) and Beven et al. (2018), parameter sets should properly reflect the uncertainties that arise from the estimation of their values, especially in data-scarce environments. To address uncertainties and improve accuracy, sensitivity analysis (SA) techniques can be integrated. **Sensitivity analysis (SA)** evaluates the sensitivity of model outputs to changes in input parameters, providing a means to identify uncertainties and reduce uncertainty in the model results (Pianosi et al. 2016; Wagener and Pianosi 2019; Douglas-Smith et al. 2020). By combining model verification and sensitivity analysis, the



parameterisation process becomes more robust, ensuring that the selected parameter-set accurately represents hazards and reduces uncertainties.

**Model application for climate and land use change scenarios:** This process involves the selection of parameter-set values for soil types and land use categories in various catchment settings. This selection provides valuable insights into the effects of climate and land use change on hillslope hydrological hazards under different scenarios. Changes in land use and projected climate can modify the response of catchments to rainfall-triggered landslides, debris flows, and hillslope erosion, either at the scale of a single slope or the entire catchment (Van Beek and Van Asch 2004; Merritt et al. 2006; Crozier 2010). To assess the impacts of climate change, one approach is to create synthetic rainfall events of varying intensities and durations based on historical observations that triggered hillslope hydrological hazards in the past (Gariano and Guzzetti 2016; Alvioli et al. 2018). Another approach involves developing hypothetical land use scenarios based on the documented impacts of land use change, such as urbanization, agriculture, and deforestation (Van Beek and Van Asch 2004; Persichillo et al. 2017). Land use change is a dynamic anthropogenic process that varies over time (Reichenbach et al. 2014). Quantifying its impact on a catchment's physical characteristics is crucial for understanding how the catchment responds to different rainfall events and the subsequent occurrence of hillslope hydrological hazards. By identifying and selecting hydrological and geotechnical parameter set values, it is possible to assess the physical characteristics of a catchment that influence the occurrence of rainfall-triggered landslides, debris flows, and hillslope erosion under various sets of rainfall events and hypothetical land use scenarios. These findings contribute to the development of disaster risk reduction policies, infrastructure resilience, and decision-making processes aimed at effective land use planning and adaptation to climate change (Uusitalo et al. 2015; van Westen et al. 2021).

### 1.3 Research aims and objectives

The overall aim of this thesis is to investigate the potential effects of land use and climate change on the occurrence and interactions of the rainfall-triggered landslide, debris flow and hillslope erosion hazards in two multi-hazard-prone and data-scarce catchments. Specifically, to achieve this aim, a new modelling workflow will be developed that enables physically-based distributed multi-hazard model to be selected and applied in such regions whilst accounting for issues of parameterisation, uncertainty and equifinality. The aim will be addressed through the following research objectives:

***RQ1: What are the physical characteristics of catchments that drive hillslope hydrological multi-hazards and their interactions?***

***RQ2: What is the influence of catchment parameter variations and uncertainties on multi-hazard assessments?***

***RQ3: How do hillslope hydrological multi-hazards and their interactions respond to changes in land use and rainfall characteristics?***

Two study sites are selected to address these research questions as typical multi-hazard forming environments and data-scarce contexts: the Soufriere catchment in Saint Lucia, Eastern Caribbean, and a sub-catchment corresponding to the Maipo basin in central Chile. The Soufriere catchment has a humid tropical climate that has experienced a considerable increase in extreme rainfall events, such as hurricanes and tropical storms, because of the effects of climate change (Anderson et al. 2011; Bozzolan et al. 2020). Moreover, anthropogenic processes such as land use change have increased the deforestation of natural tropical forests for agricultural and urbanisation purposes (Bégin et al. 2014). In recent decades, both climate and land use changes have increased the frequency of hillslope hydrological hazards within the Soufriere catchment area (Anderson et al. 2008; Walters 2016). In October 2010, Hurricane Tomas triggered shallow landslides, debris flows, flooding, and erosion with significant impacts on urban and rural settlements (ECLAC 2011).

The Maipo sub-catchment has a Mediterranean climate with dry summers and rainy periods during winter; however, the impacts of climate change on the fluctuations of the El Niño–Southern Oscillation (ENSO) in central Chile have affected the variability of rainfall, increasing the occurrence of short and intense rainfall events (Vergara et al. 2020; Moreiras et al. 2021). In February 2017, an extraordinary rainfall event during the summer caused multiple shallow landslides and debris flow, resulting in multiple fatalities and infrastructure damage, particularly to houses, roads, and bridges (Marín et al. 2017). In addition, land use changes in recent decades have replaced the natural land cover, such as scrubs and natural forests, with intensive agricultural systems and urbanisation of rural areas (Schulz et al. 2010; Benavidez-Silva et al. 2021). These changes, along with the direct impacts of climate change expressed in extensive drought periods have increased the occurrence of wildfires in the area, reducing the slope vegetation and increasing the impact on hillslope erosion rates and the magnitude of the observed shallow landslides and debris flows (Garreaud et al. 2017; Moreiras et al. 2021; Vergara et al. 2022).

In the two study sites, the research questions will be addressed through the setting of specific objectives for each question. To address research question 1 (RQ1), the following objectives were proposed:

**Obj. 1.1:** *Choose a physics-based multi-hazard model with an appropriate level of process-representation.*

**Obj. 1.2:** *Define and apply a modelling workflow for experimental design and parameter exploration in data-scarce locations.*

The purpose of objective 1.1 (obj. 1.1) is to select a physically-based multi-hazard model that can represent individual hazards at the catchment scale, the mechanisms that influence multi-hazard interactions, and the magnitude and impact of each hazard to simulate hillslope hydrological hazard interactions for climate and land use scenarios in the two selected study sites. The purpose of objective 1.2 (obj. 1.2) is to design a modelling workflow to parameterise the selected physically-based multi-hazard model. The aim is to explore the variation in the model's initial parameter values by running parametric simulations with different parameter-set values combinations to identify the catchment's physical characteristics that drive hillslope hydrological hazard interactions. The modelling workflow will allow the identification of the parametric simulations with the best approximation in the representation of the rainfall-triggered landslides, debris flows, and hillslope erosion hazards observed during the rainfall events of October 2010 and February 2017 in the two study sites. Once applied the modelling workflow, the parametric simulations with the best proximity to observed hazards will be selected to address research question 2 (RQ2). To address research question 2 (RQ2), the following objectives were proposed:

**Obj. 2.1:** *Define and apply a modelling workflow for model verification and parameter-set selection.*

**Obj. 2.2:** *Assess catchment sensitivities to parameter value variations for soil types and land use.*

The purpose of objective 2.1 (obj. 2.1) is to continue applying the modelling workflow by establishing a sequence of verification steps to select the parametric simulation with the best parameter-set values to represent hillslope hydrological hazard interactions. The foregoing will allow the identification of the spatial distribution of hydrological and geotechnical parameter values for different land use classes and soil types for the two study sites. The purpose of objective 2.2 (obj. 2.2) is to assess the sensitivities introduced by the variation of initial values of the selected parameter-set to quantify its impacts on the representation of the interaction and magnitude of hillslope hydrological hazards. This will allow the identification of the most sensitive parameters for land use classes and soil types. Once applied the modelling workflow, the selected parameter-set can then be used to address research question 3 (RQ3). To address research question 3 (RQ3), the following objectives were proposed:

**Obj. 3.1:** *For the selected and verified model parameter-set, investigate the catchment response to different land use and rainfall scenarios.*

**Obj. 3.2:** *Compare multi-hazard interactions and responses for catchments and demonstrate applicability of modelling workflow.*

The purpose of objective 3.1 (obj. 3.1) is to investigate the potential effects of different climate and land use change scenarios on hillslope hydrological hazard interactions using the selected parameter-set for the two study sites. This will allow the assessment of the potential magnitudes of rainfall-triggered landslides, debris flows and hillslope erosion hazards according to hypothetical climate and land use scenarios. The purpose of objective 3.2 (obj. 3.2) is to compare the responses to hillslope hydrological hazard interactions of the two selected study sites and demonstrate the applicability of the modelling workflow to assess its effectiveness in two study sites with poor data accessibility.

The two study sites represent two different climatic and lithological environments where the physical properties of the catchment may respond differently to different climate and land use scenarios. Therefore, the application of a modelling workflow to parameterise and handle uncertainties in multi-hazard modelling, and thus identify appropriate parameters for soil types and land use categories to represent individual hazards and their interactions, can introduce better practices in disaster risk reduction policies and decision-making to reduce the impacts of hillslope hydrological hazards under potential climate and land use change scenarios. Addressing the research questions with their respective objectives will be done according to the following thesis structure, which is outlined in the next section.

## 1.4 Thesis outline

The thesis outline is structured according to research question and objectives as follows:

### ***Chapter 2: Hillslope hydrological hazard interactions: in search of an integrated hazard modelling approach***

Multi-hazard interaction types and feedback mechanisms that influence hazard interactions are reviewed. Current hazard modelling methods are also reviewed, and a suitable physically based multi-hazard model, the OpenLISEM Hazard model, is selected to assess hillslope hydrological hazard interactions.

A modelling workflow is proposed to address the parameterisation and uncertainties that arise in complex multi-hazard models, which limits the assessment of hillslope hydrological hazard interactions for land use and climate change scenarios.

[This chapter addresses RQ1, Objective 1.1]

### ***Chapter 3: Developing the workflow for parameter exploration and experimental design***

A modelling workflow for experimental design is developed and implemented to explore parametric simulations using the OpenLISEM hazard model to identify the input parameter value ranges that influence the spatial representation and interactions of rainfall-triggered landslides, debris flows, and hillslope erosion hazards at the catchment scale.

[This chapter addresses RQ1, Objective 1.2]

### ***Chapter 4: Developing the workflow for model verification and investigation of catchment response to climate and land use change***

A modelling workflow for model verification and sensitivity analysis (SA) and for climate and land use scenarios is implemented and applied to select and verify the behavioural simulations with the parameter-set that provides the best representation and similarity of rainfall-triggered landslides, debris flows, and hillslope erosion to observed hazards.

The most sensitive input parameters for land use categories and soil types units are identified to assess their responsiveness to different land use and rainfall scenarios.

[This chapter addresses RQ2, Objective 2.1 and Objective 2.2]

### ***Chapter 5: Assessing hillslope hydrological hazards and interactions under changing climate and land use in Maipo, Chile***

Apply the full extent of the modelling workflow for experimental design and model verification in a data scarce catchment to assess how landslides, debris flows, and erosion hazard interact and respond to different land use and rainfall scenarios.

[This chapter addresses RQ3, Objective 3.1]

***Chapter VI: Summary and conclusions***

The modelling workflow developed and applied for both study sites selected in this thesis is discussed, and recommendations and future outlooks are discussed for the implemented modelling workflow.

[This chapter addresses RQ3, Objective 3.2]

---

---

**Chapter 2 Hillslope hydrological hazard interaction: in  
search of an integrated hazard modelling approach**

---

---

## Introduction

This chapter aims to identify and select a physically-based distributed multi-hazard modelling method to represent hillslope hydrological hazard interactions according to different climate and land use change scenarios and propose a modelling workflow to address issues of parameterisation and uncertainty of the selected model. To achieve this aim, it is first necessary to determine the type of hazard interaction to be modelled to identify a proper multi-hazard modelling approach. Hillslope hydrological hazards can interact in unidirectional and bidirectional relationships that determine the compounding, cascading, concurrent or coincidence of two or more hazards (Gill and Malamud 2016; Pescaroli and Alexander 2018). Therefore, it is necessary to identify the interrelationships and feedback between hydrological and stability processes that influence this type of interactions between hillslope hydrological hazards, and how these interrelationships are integrated into different multi-hazard modelling approaches. This chapter focuses on reviewing the multi-hazard interactions in hydrological and stability hazards. In particular, it will focus on reviewing the interconnection between hydrological and stability processes that determine different types of interactions between these hazards and review the most suitable current multi-hazard models available to assess and quantify these interactions.

As discussed in Chapter 1, assessing the impacts of climate and land use change on the interaction between rainfall-triggered landslides, debris flows, and hillslope erosion hazards requires multi-hazard modelling approaches capable of assessing the interrelationships between the catchment's physical properties and climatic factors that influence the interaction of these hazards (Delmonaco et al. 2006). Catchment-scale multi-hazard models assess these interrelationships by coupling slope stability and failure models, numerical runout models, and rainfall-runoff models to assess, for example, the influence of landslide mobilization and volume on debris flow magnitude and runout and their impacts on hillslope erosion (van den Bout 2020). However, the coupling of diverse hydrological and stability models makes current multi-hazard models highly complex in terms of the number of input parameters and data required for hydrological and stability process representations (Hofmann 2005; Beven et al. 2018). Moreover, the estimation of input parameter values for these types of models in data-scarce contexts increases the uncertainty in model outcomes, impacting the representation of hillslope hydrological hazards for different climate and land use scenarios. Therefore, in addition to selecting a multi-hazard model to represent hazard interactions, a modelling workflow that guides the parameterisation of multi-hazard models is necessary to identify and select parameter-set values suitable for catchments with different climatic and lithological settings, and to handle the uncertainties that arise in input parameters owing to data scarcity. Using this modelling workflow, climate and land use scenarios will be explored to assess the impacts of hillslope hydrological hazards in the two selected study sites (Soufriere catchment and Maipo sub-catchment) to demonstrate the utility of this workflow in developing disaster-risk reduction policies and resilient land use planning to reduce the impacts of these hazards due to climate change.



## 2.1 Integrated physically-based multi-hazard modelling

### 2.1.1 The multi-hazard approach in hydrological and stability hazards

In general terms "**multi-hazard**" refers to the totality of relevant hazards and their potential interactions in a determined region (Kappes et al. 2012; Gill and Malamud 2014). However, no single unified definition has been established to refer to the multi-hazard concept (Pescaroli and Alexander 2018). For instance, UNDDR (2020) defines **multi-hazard** as the simultaneous, cascading, or compounding occurrence of multiple major hazards in a particular area, considering their interrelated effects. Delmonaco et al. (2006), defined **multi-hazard** as the utilization of various modelling methods to assess and map the potential occurrence of different types of natural hazards and quantify their interactions in a specific spatial and temporal context. The common aspect among these definitions is the recognition of interactions between individual hazards (Cutter 2018; De Angeli et al. 2022). The available literature on multi-hazard assessments is extensive, with a focus on hydrological, geological, and climate hazards (Tilloy et al. 2019). The work of van Westen et al. (2014); Zhang et al. (2014); de Brito (2021); McNamee et al. (2022); Ming et al. (2022) and Sharma et al. (2022) have employed various multi-hazard modelling methods to assess the compounding and cascading interactions among hazards, for instance, earthquakes, flooding, landslides, debris flows, wildfires, and droughts for multi-hazard risk assessment and climate change scenarios. However, one of the main challenges in multi-hazard assessment is the establishment of clear frameworks and guidelines for comprehensive multi-hazard modelling, which is essential for risk assessment and disaster risk reduction (DDR) policies (de Ruiter et al. 2020; Ward et al. 2022).

The term **multi-hazard interaction** refers to the interrelationships that arise from a combination of multiple drivers, including physical processes and climate variables, which determine the type of interaction between multiple hazards (Gill and Malamud 2017; de Ruiter et al. 2020). According to Kappes et al. (2012); Terzi et al. (2019) and van Westen et al. (2021) the potential interaction of multiple hazard events can significantly influence the behaviour of other hazards in terms of magnitude. These hazards can interact in various ways, including one hazard event triggering another, two hazard events occurring independently but in close spatial and temporal proximity, or two hazards overlapping during the same period (Marzocchi et al. 2012; Liu et al. 2016). Therefore, multi-hazard models should ideally consider all relevant individual hazards to characterise the possible interrelationships that influence the type of interactions that increase their magnitude and impact when combined (Sadegh et al. 2018; Raymond et al. 2020). Consequently, for the purpose of this thesis multi-hazard interactions will be classified according to their interaction type, as follows:

**Cascading hazards:** This type of interaction, also known as 'coupled hazards' or 'triggering hazards,' involve a sequential process in which a primary hazard triggers a secondary hazard, which in turn triggers a tertiary hazard (Kappes et al. 2010; Marzocchi et al. 2012; Tilloy et al. 2019). This process is often referred to as the domino effect because the occurrence of multiple hazards is interconnected in a cause-and-effect chain, where the magnitude of one hazard influences the magnitude of another hazard (Delmonaco et al. 2006; Pescaroli and Alexander 2018). The characteristic of cascading hazards

is their close proximity in both time and space, indicating that the primary hazard possesses enough energy to trigger subsequent events (Cutter 2018). For instance, in the context of hillslope hydrological hazards, the occurrence of rainfall-triggered landslides during a rainfall event increases the likelihood of triggering debris flows and hillslope erosion (Korup 2009; van Westen et al. 2014). In some cases, hillslope erosion can also initiate debris flows by contributing eroded material, resulting in increased erosion rates and deposition (van Beek et al. 2008; Chen and Zhang 2015).

**Concurrent hazards:** This type of hazard involves the simultaneous occurrence of two or more unrelated hazards in close proximity during the same time period without necessarily amplifying their magnitudes and impacts (Hillier et al. 2020; Wang et al. 2020). These hazards can have the same or different triggers and do not depend on each other for occurrence (Raymond et al. 2020).

**Compounding hazards:** This type of interaction arises when two or more hazards originating from the same or different triggers occur simultaneously or successively in a specific area (Leonard et al. 2014; Pescaroli and Alexander 2018). While compounding hazards do not necessarily occur in the same time period, they amplified their magnitude and impact when combined or overlapped (Cutter 2018; Zscheischler et al. 2018). For example, within a catchment, an extreme rainfall event can trigger landslides, and if flash floods are also triggered in specific zones of the catchment where landslides occurred, the two hazards can spatially overlap, potentially initiating debris flows (van Westen et al. 2014).

**Coincident hazards:** This type of hazard also known as “independent hazards” occur when two or more hazards without a common cause occur simultaneously in close spatial proximity or overlap temporarily during the same time period (Liu et al. 2016; Gentile et al. 2022). These hazardous events do not influence each other and differ in terms of their origin and trigger. However, when they coincidence, their magnitude and impact increase (van Westen et al. 2021). For instance, an extreme rainfall event can trigger the simultaneous occurrence of flash floods and landslides that might lead to significant impacts if these two hazards occur in close spatial proximity (Ming et al. 2022).

**Conditional hazards:** This type of hazards are related to the susceptibility or likelihood of increasing the intensity and magnitude of other hazards by changes in the underlying conditions such as topography and vegetation modified by the primary hazard (van Westen et al. 2021). This means that when a hazard occurs of geophysical, hydrological or climatic origin, it can alter the environmental parameters of a given area and determine the occurrence of another hazard through different triggering mechanisms (e.g., earthquakes and storms) (Wu et al. 2015). For example, wildfires reduce the vegetation on slopes, creating conditions that increase surface runoff and trigger debris flows during rainfall events (Parise and Cannon 2012; Fraser et al. 2022).

The occurrence of rainfall-triggered landslides, debris flows, and hillslope erosion hazards is determined by the same trigger, which corresponds to rainfall events of different intensities and durations (Larsen and Simon 1993; Saito et al. 2010). While these hazards can happen independently during the same rainfall event, their occurrence can lead to cascading, concurrent, and compounding interactions (Figure 2.1). The specific type of interaction depends on the hydrological and stability conditions when these

hazards take place. When these hazards happen in close proximity during the same rainfall event, they can result in concurrent events or can create compounding interactions when spatially overlap (Figure 2.1). In addition, landslide occurrences can initiate cascading interactions, triggering secondary hazards e.g., debris flows and tertiary hazards such as hillslope erosion (Figure 2.1). The feedback mechanisms that influence these types of interactions is reviewed in the next section.

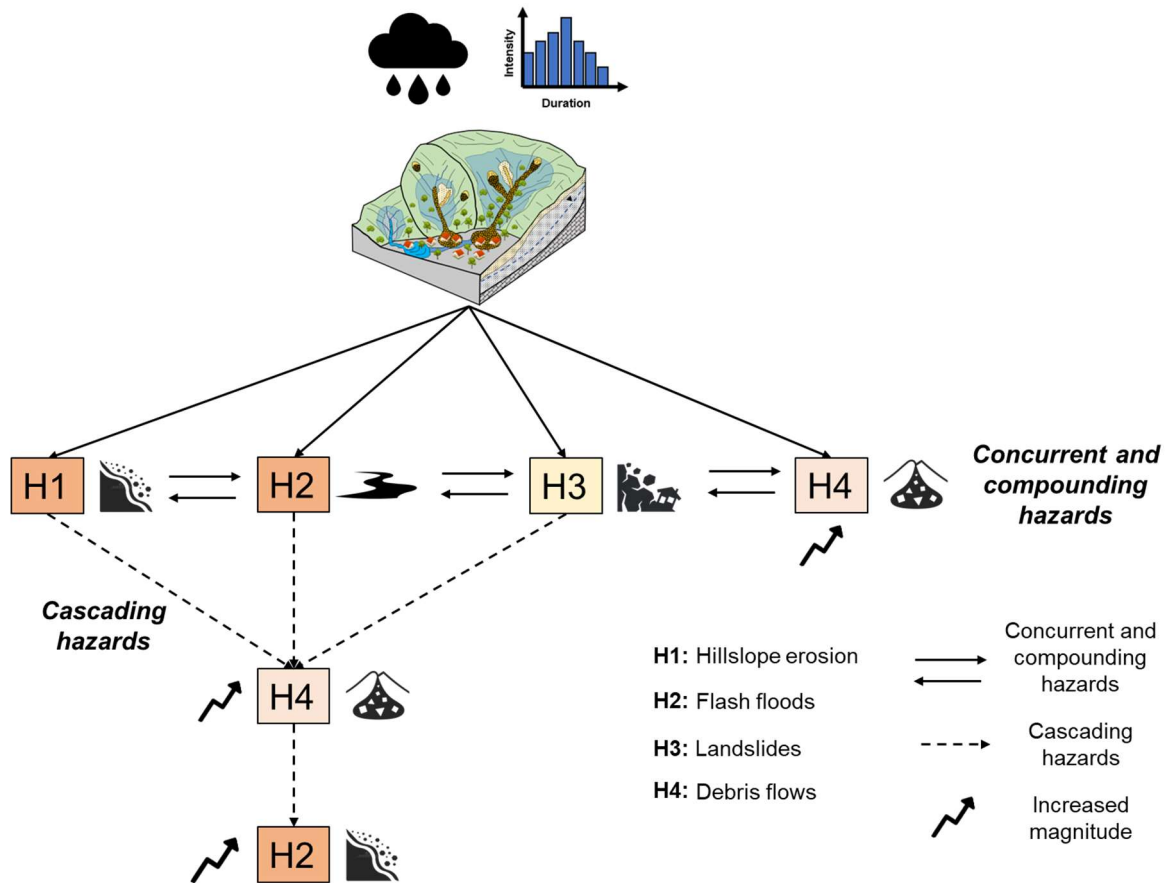


Figure 2.1 Conceptual framework for hazard interactions.

### 2.1.2 Understanding hazard interactions between hillslope hydrological hazards

As identified in the previous section, **hillslope hydrological hazard interactions** can be defined as the cascading, concurrent and compounding of rainfall-triggered landslides, debris flows, and hillslope erosion. Therefore, for the purpose of this thesis, the term hillslope hydrological hazard interactions will be used from now on to refer to these types of interactions between these hazards. Hydrology plays an important role in this type of interactions between hillslope hydrological hazards (Bogaard and Greco 2016; Sidle et al. 2019). To assess these types of interactions, first, it is necessary to identify the role of hydrology in the interconnection or feedback between the hydrological and stability processes (Ciabatta et al. 2016; Liu et al. 2016). As discussed in Chapter 1, section 1.1.2, hydrological and stability process representations are governed by the interrelationships between catchment physical characteristics

including soil types and their hydrological and geotechnical properties, vegetation, topography with climate variables. These characteristics determine the feedback mechanisms that influence the initiation of different types of hazard interactions (Gill et al. 2020; van Westen et al. 2021). To understand how the feedback mechanisms that lead to hazard interactions between hillslope hydrological hazards occur, different stages are proposed to describe their initiation. These are described as follows:

At the beginning of a rainfall event of specific intensity and duration (Figure 2.2a), rainfall infiltrates the hillslope soil based on its physical characteristics such as hydraulic conductivity and initial moisture content (Muntohar and Liao 2010; Lu and Godt 2013). As rainfall intensity increases, rainsplash erosion occurs by detaching soil particles due to raindrop impacts (Cuomo et al. 2015). In unsaturated soils, the infiltration rates depend on the initial moisture content (Rahardjo et al. 2019). Soils having low initial moisture content shows low infiltration rates compared to those with high initial moisture content (Hino et al. 1988; Wei et al. 2022). Consequently, the different initial moisture content percentages on hillslopes within the catchment determine the time it takes for rainfall to infiltrate and become soil-saturated (Lee et al. 2020). This affects the time in which hillslope runoff is generated by infiltration or saturation excess depending on the initial moisture content distributed within the catchment at the moment the rainfall occurs (Lu and Godt 2013).

As rainfall increases in intensity and duration (Figure 2.2b), in some parts of the catchment with low initial moisture content, hillslope runoff is initiated by infiltration excess, leading to a flow discharge generated by Horton overland flow (Kirkby 1988; Bogaard and Greco 2016). In addition, in other parts of the catchment, hillslope runoff is initiated by saturation excess, especially in hillslopes with high initial moisture content (Lee and Kim 2021). When hillslope runoff is generated by both mechanisms in different parts of the catchment, the flow is routed into channels to initiate channel flow (Kirkby 1988; Liu et al. 2004). The presence of hillslope runoff results in hillslope erosion in different parts of the catchment (Wang et al. 2019). The erosion starts when the generated hillslope runoff begins to detach and transport poorly sorted sediment material from the hillslope bed (Ellison 1948; Hessel and Jetten 2007; Cuomo et al. 2015). **Detachment** occurs when the hydraulic shear stress, exerted by the flow on the hillslope surface, exceeds the cohesive strength of the surface material (De Roo and Offermans 1995; Xiao et al. 2017). The detached material is loaded by the flow, influenced by the characteristics of the sediment particles such as grain sizes, density, and settling velocity (Goossens and Buck 2011; Nguyen et al. 2016). The transport of sediment material depends on the sediment concentration, which is determined by the flow's transport capacity (Julien and Simons 1985; Aksoy and Kavvas 2005). The **transport capacity** refers to the maximum equilibrium sediment load that a flow can transport (Govers et al. 1990). The foregoing is determined by the flow stream power and density of sediment particles (De Roo et al. 1994; van den Bout et al. 2018). According to this approach, soil erosion (detachment) occurs only when the sediment concentration is less than the hillslope runoff transport capacity, and deposition occurs when the sediment concentration exceeds this transport capacity (De Roo et al. 1996; Zhang et al. 2011). Therefore, at this stage, hillslope erosion is determined by the hillslope runoff transport capacity, which influences the rates of detachment and deposition that increases as rainfall increment in intensity and duration.

At the same time, in different zones of the catchment (Figure 2.2c), flash floods are generated as rainfall intensity and hillslope runoff increase into the channels. **Flash floods** correspond to the overflow of hillslope channels caused by the coupling of the hillslope runoff and channel flow (van den Bout and Jetten 2018). Moreover, the hillslope reaches saturation levels that increase the pore water pressure which initiates slope failure in some parts of the catchment as a consequence of the reduction in soil shear strength (Figure 2.2d) (Lanni et al. 2012; Bordoni et al. 2015). After the slope failure occurs, the rapid generation of plastic strains influences the deformation and rapid acceleration of the saturated failure mass volume, which increases the landslide mobility and magnitude (Figure 2.2d) (Sassa and Wang 2007; Cascini et al. 2013). Simultaneously, flash floods increase their volume and discharge towards the channels, increasing the channel flow velocity and depth (De Roo and Offermans 1995; Van den Bout et al. 2018). In zones of the catchment in which both processes occur in close spatial proximity (Figure 2.2d), the concurrence or compounding of triggered hazards is initiated. In the first case, both hazards can increase the impacts in the area in which they occur by the magnitude of the flooded area and landslide runout area. In the second case, these hazards can produce compounding events when they overlap (van Westen et al. 2014). The spatial overlapping between these hazards can influence the formation of debris flows and subsequent compounding with hillslope erosion, amplifying their overall impacts (Figure 2.2e).

In addition, when the magnitude of flash floods increases in zones of the catchment where landslides are triggered or in zones where the hillslope is highly eroded cascading interactions begin to reproduce (Figure 2.2f). These feedback mechanisms are provided by the interaction between the solid and fluid forces influenced by the saturated failure mass volumes, bed eroded material and flash floods (Iverson et al. 2002; Liu et al. 2020). The interaction mechanism between these two forces is determined by the force exerted by the flash floods down the slope in terms of its velocity and depth, and the force exerted by the hillslope surface opposite to the flow direction (Pudasaini 2012; Meng and Wang 2016). Both forces apply net shear stresses along the flow interface, which influence the entrainment rates of the saturated failure mass volumes (Takahashi 1978; Iverson 1997). **Entrainment** occurs when the erodible substrate is mechanically weaker than the flowing material (Iverson and Ouyang 2015; Liu et al. 2021). The antecedent temporarily and spatially changes the fluid properties (e.g., viscosity, volume, and density) by adding the saturated failure mass volumes, as well as the eroded bed material by transport capacity at the beginning of the rainfall event (Shen et al. 2020). The deposition process begins as soon as the bed starts to decelerate the frontal part of the debris flow because of the higher frictional resistance of the bed than that of the flowing material (Pudasaini and Fischer 2020). During deposition, the basal surface begins to gain sediment material, which increases the volume of sediment in the deposited area (Prancevic et al. 2020).

Cascading interactions can also occur in some parts of the catchment where the landslide failure volume displacement is influenced by the amount of eroded bed material. According to Pudasaini and Krautblatter (2021), the influence of hillslope erosion on landslide failure volume mobility is associated with the excessive volume of eroded material, which influences the momentum exchange mechanisms between the eroded basal substrate and the velocity of the mobilised volumes. This effectively reduces

frictional stresses in the erodible substrate by adding sediment material (entraining) that immediately accelerates and influences landslide surface area and distance (Pudasaini and Fischer 2020). Hillslope erosion can significantly increase the destructive power of landslides by amplifying their volume, mobility, and impact force (Cuomo and Della Sala 2015; Pudasaini and Krautblatter 2021). The magnitude of these hazard interactions is evident at the end of the rainfall event by the cumulative magnitude resulting from the interactions. **The cumulative magnitude** can be expressed as the total landslide surface area, including mobilized failure volumes, debris flow runout areas, and volumes of eroded and deposited sediment material influenced by cascading interactions. Finally, at this stage, the cumulative hillslope erosion rates are determined by rainfall-triggered landslides, debris flows, and transport capacity (Korup et al. 2007; Larsen et al. 2010). Cumulative erosion is caused by an increase in the volume of eroded material where landslides and debris flows occur (Korup 2009).

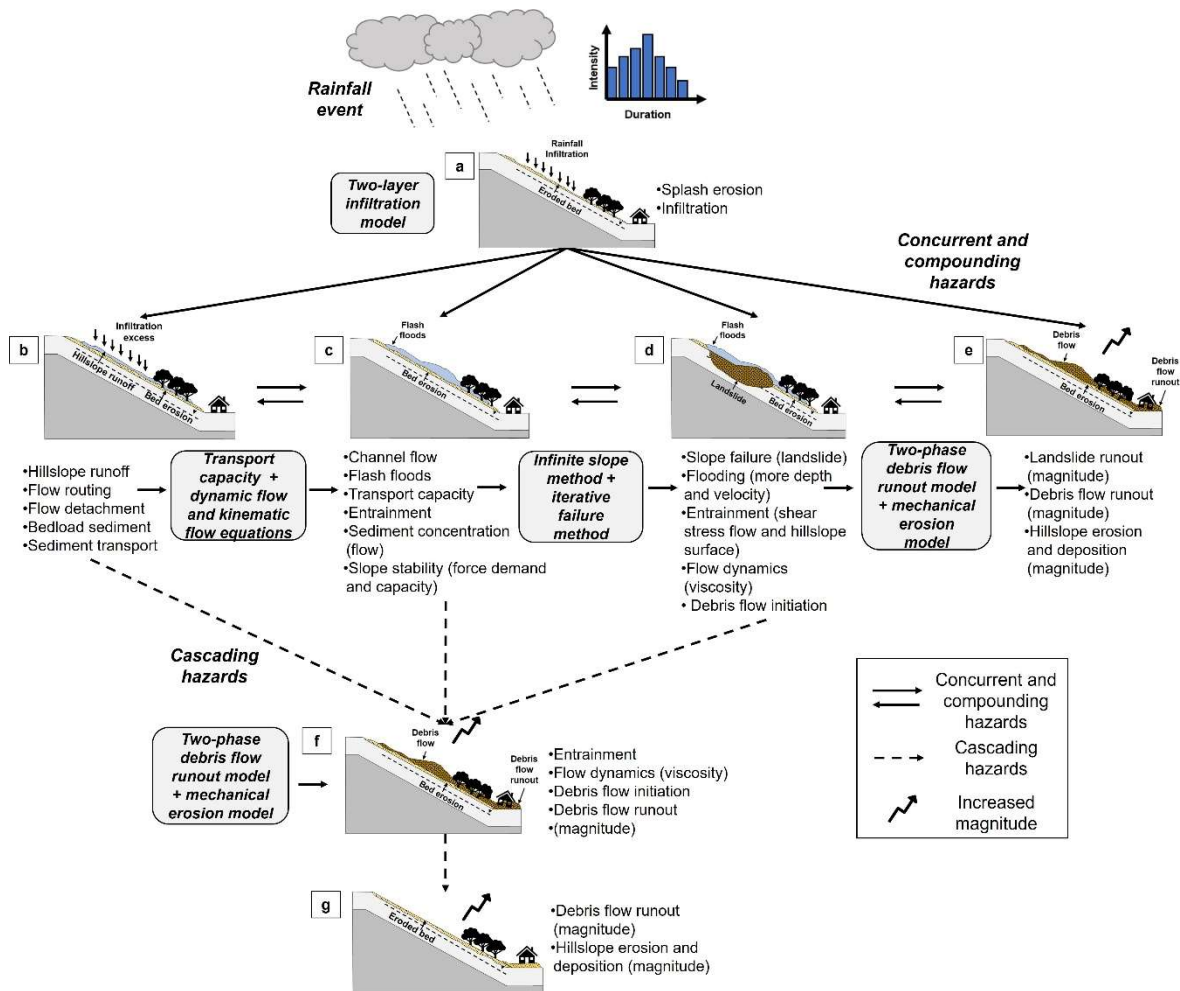


Figure 2.2 Conceptual framework for hillslope hydrological hazard interaction modelling.

### 2.1.3 Frequency-magnitude relationships of interacting hazards

The measurement of hazard magnitudes allows for assessing the cumulative effect of interacting hazards, enabling the identification of the frequency-magnitude relationship for each hazard. The **frequency-magnitude** relationship describes the correlation between the frequency of hazard events and their magnitudes (Malamud et al. 2004; Guthrie and Evans 2005). **Frequency** refers to the number of times a hazard occurs within a specific interval, while hazard **magnitude** is related to the energy released during the event (Guzzetti et al. 2002; Guthrie et al. 2008). Studying the frequency-magnitude relationship of rainfall-triggered landslides, debris flows, and hillslope erosion provides valuable information about the factors and triggers influencing their occurrence and the conditions leading to larger or more frequent magnitudes (Hurst et al. 2013; Tanyaş et al. 2019). Rainfall-triggered landslides can be measured in terms of surface area and failure volumes (Galli et al. 2008; Santangelo et al. 2015). Failure volumes play a critical role in determining the distance and propagation of landslides and debris flows, the extent of eroded areas, and the potential impacts and damages (Corominas 2011; Michel et al. 2020). However, determining failure volumes is a more difficult task because it requires information about the slope failure geometry (e.g., depth, length, width, and area) (Guzzetti et al. 2009; Lombardo et al. 2021). On the other hand, estimating the **surface area** of landslides is more accessible as it encompasses the failure area, propagation distance, and deposition (runout) (Taylor et al. 2018).

The impact of debris flows can be measured by assessing the **runout area**, which represents the maximum distance travelled by the debris flow from its source to the deposition zone (De Haas et al. 2015; Nishiguchi and Uchida 2022). Similarly, for rainfall-triggered landslides, the runout area of debris flows can be determined by considering the surface area of the runout (Van den Bout et al. 2021). The size and shape of the runout surface area provide valuable information about the initiation and deposition areas of debris flows (Mead et al. 2021). The magnitude of hillslope erosion can be evaluated based on the rates of detachment and deposition of sediment material within a specific surface area (De Roo et al. 1996; Jetten et al. 2003). This can be estimated using **total net erosion**, which is a measure that takes into account the amount of soil or sediment material eroded from a surface, considering both erosion and deposition processes (Xiao et al. 2017). Net erosion is calculated by subtracting the sum of particles arriving at the surface from the sum of particles leaving the surface (Goossens and Buck 2011). The magnitude of erosion can be quantified using various units depending on the type of erosion under investigation. For example, surface erosion is often measured by the volume of soil losses in kilograms or tonnes per square meter (kg/tonnes per square meter) (Aksoy and Kavvas 2005). These magnitudes can be assessed using hazard metrics to measure the shape and form of the topographic surface modified by landslides, debris flows, and hillslope erosion volumes at a particular point in time (Taylor et al. 2018). Different approaches and metrics have been proposed to determine the "magnitude" of a single landslide, debris flow, or erosion volume within a specific area resulting from a single event or multiple events over a certain period (Lombardo et al. 2021). In this thesis, a **hazard metric** is defined as the quantification of the landslide surface area, debris flow runout area and hillslope net erosion rates resulting from a rainfall event.

## 2.2 Identifying a suitable method for hillslope-hydrological hazard interaction modelling

### 2.2.1 Multi-hazard modelling approaches for hillslope hydrological hazards

Table 2.1 summarizes a number of available models for hillslope hydrological hazard modelling. Most available physically-based models to assess rainfall-triggered landslides, debris flows, and hillslope erosion hazards have advantages in simulating and representing a single hazard or more than one hazard at a time incorporating temporal and spatial approaches. For landslide hazard modelling, CHASM is a model that couples hydrological and geomechanically models to simulate landslide initiation and propagation at the hillslope scale, considering dynamic slope hydrology and soil properties. However, its analysis is limited to local scales  $< 1:5.000$  (Bozzolan et al. 2023). On the other hand, physically-based distributed models like STARWARS, TRIGRS 2.0, SCOOP3D, OpenLISEM hazard, r.rotstab, r.slope.stability, Landslide Hydro-mechanical Triggering (LHT), and Step-Tramm are more suitable for regional or catchment scales. These models incorporate spatiotemporal modelling of hydrological and stability processes to assess slope stability and failure (Baum et al. 2008; Mergili et al. 2014; Reid et al. 2015; Fan et al. 2017; van den Bout et al. 2018). The models differ in how they calculate slope stability and failure. For example, STARWARS uses a finite element method to assess slope stability and predict slope failure by analysing the mechanical behaviour of the slope during a landslide event, simulating the location and magnitude of shallow and deep-seated landslides (Malet et al. 2005; Von Ruetten et al. 2013). In the TRIGRS 2.0 model, the Factor of Safety (FoS) is calculated using a grid-based slope stability analysis method based on slope geometry, soil properties, and rainfall intensity and duration. Slope failure is determined by employing a block sliding and continuum method to calculate the displacement and deformation of the sliding mass (Salciarini et al. 2006; Baum et al. 2008). Models like SCOOP-3D utilize a three-dimensional limit equilibrium method to evaluate slope stability. They employ spheres as potential slip surfaces to estimate landslide material volumes (Reid et al. 2015; Van den Bout et al. 2021). Furthermore, models such as Landslide Hydro-mechanical Triggering (LHT) and Step-Tramm adopt hydro-mechanical methods to assess landslide initiation and propagation under hydrological conditions (Fan et al. 2017; van Westen et al. 2021).

Alternatively, models such as OpenLISEM hazard, r.rotstab, and its extension *r.slope.stability* calculate the slope stability Factor of Safety (FoS) using an infinite slope method integrated into a GIS environment (Mergili et al. 2014; van den Bout et al. 2018). OpenLISEM Hazard integrates an iterative failure method to estimate failure volumes by assessing the progressive failure of soil materials down the slope (Van den Bout et al. 2021). In this method, the failure volume is calculated using several primary steps. First, slope stability is calculated to identify all raster grid cells with an FoS lower than 1; then, unstable pixels are removed by assuming stability can be achieved by decreasing elevations (removing failure depths) of those pixels. This is done by defining a slope between unstable and surrounding stable pixels to identify force demand and capacity of the slope. The process continues until the FoS for unstable cells exceeds 1. For r.rotstab and r.slope.stability, both models calculate the



probability of slope failure using randomly selected ellipsoidal or truncated slip surfaces, predicting areas with a greater potential for slope failure (Mergili et al. 2014; Van den Bout et al. 2021).

Although the aforementioned models have the potential to calculate slope stability and failure, gaps remain in how slope failure is calculated to estimate failure depths and volumes to link with runoff models for assessing motion and behaviour down the slope (Mergili et al. 2017; Van den Bout et al. 2018). The assessment of failure surface and volume is important to analyse their behaviour, motion, routing, impact areas, and potential impacts on the population and infrastructure (Iverson et al. 2002; Gabet and Mudd 2006; Michel et al. 2020). Debris flow runoff models like RAMMS 2-D, Flow-R, LaharFlow, r.avaflow, FLO-2D, and EDDA 1.0/2.0 directly incorporate slope failure volumes as key input parameters to determine debris flow behaviour (Mergili et al. 2017; Stancanelli et al. 2017; Shen et al. 2018). Some of these models also assess the impacts of debris flow on hillslope erosion. RAMMS 2-D, Flow-R, and LaharFlow focus on the motion and deposition of debris flow and lahars, indirectly helping estimate erosion rates through the path and deposition of debris flows, which can lead to changes in topography (Chen and Zhang 2015; Tang et al. 2019; Pudasaini and Krautblatter 2021). However, these models do not explicitly simulate hydrological processes such as infiltration, runoff, or surface and subsurface flow, limiting their usability in assessing the impact of landslides or debris flow on hillslope erosion.

Models such as OpenLISEM hazard, r.avaflow, FLO-2D, and EDDA 1.0/2.0 can simulate the effects of landslide volumes on debris flow and their impacts on hillslope erosion. These models integrate catchment-scale hydrology to simulate infiltration and surface flow, allowing them to simulate erosion, sediment transport, and deposition (Mergili et al. 2017; Shen et al. 2018; van den Bout 2020). The integration of numerical solutions, such as two-phase equations describing fluid and solid interactions, mass and momentum exchange, Mohr-Coulomb plasticity, and non-Newtonian viscous stress, enables these models to simulate the entrainment of landslide volumes and bed erosion into surface flow, assessing their impacts on debris flow and hillslope erosion (Pudasaini 2012; Chen and Zhang 2015). However, although these models incorporate catchment-scale hydrology and failure volumes to assess their impacts on debris flow and hillslope erosion, they have the disadvantage (except for the OpenLISEM hazard model) of not being coupled with slope stability methods to estimate failure volumes during the modelling process (van den Bout 2020). This limitation arises because the incorporation of failure volumes in these models depends on simplified failure volume estimation from different sources, such as field observations and landslide inventories, which may not accurately reflect the identification of failure volumes (Blahut et al. 2010). Moreover, the spatial resolution and lack of validation of these sources may introduce uncertainty into model results, affecting their accuracy.

Erosion models such as EUROSEM, EROSION 3-D, KINEROS, and LISEM (Table 2.1) assess temporal and spatial erosion through the transport and deposition of sediment according to the generation of surface flow (Aksoy and Kavvas 2005). Compared with slope stability and debris runoff flow models, erosion models have the advantage of being spatially distributed and include catchment hydrology to assess the temporal impacts of rainfall on surface erosion (Merritt et al. 2003). Moreover, these models have the advantage of including land use or vegetation cover to determine the effects of land use change

on erosion (Baartman et al. 2013). However, these models do not consider the effects of landslides and debris flows on hillslope erosion within their modelling approach, limiting the assessment of these impacts on erosion and deposition rates within the catchment (Chen and Zhang 2015).

From the models mentioned in Table 2.1, models such as OpenLISEM hazard, r.avafLOW, FLO-2D, and EDDA 1.0/2.0 can be classified as multi-hazard models because they can simulate the interaction between rainfall-triggered landslides, debris flows, and hillslope erosion to some extent. However, the effectiveness of these models in assessing hazard interactions may vary due to the specific process representations in their modelling structures. Therefore, accurately representing the physical processes of each hazard is crucial for assessing their potential interactions. This requires models capable of simulating various physical processes, such as landslide initiation and propagation, sediment and debris transport by flows, sediment erosion and deposition, and catchment hydrological response. While r.avafLOW, FLO-2D, and EDDA 1.0/2.0 are useful for simulating individual hazards, the OpenLISEM hazard model is better suited for assessing the complex interactions between multiple hazards and their impacts on landscapes and communities at different catchment scales.

Table 2.1. Overview of hillslope-hydrological hazard modelling approaches.

Model	Source	Hazard modelling				Spatial	Temporal	Catchment scale
		LS		DF	ER			
		ST	SF					
<b>CHASM+</b>	Anderson et al (2008)	✓	x	x	x	x	✓	x
<b>STARWARS</b>	Van Beek (2002)	✓	x	x	x	x	✓	x
<b>SCOOP3D</b>	Reid et al. (2015)	✓	✓	x	x	✓	✓	✓
<b>TRIGRS 2.0</b>	Baum et al. (2008)	✓	x	x	x	✓	✓	✓
<b>r.rotstab</b>	Mergili et al. (2014)	✓	x	x	x	✓	x	x
<b>r.slope.stability</b>		✓	x	x	x	✓	x	✓
<b>RAMMS 2-D</b>	Christen et al. (2010)	x	x	✓	x	✓	x	x
<b>Flow-R</b>	Horton et al. (2013)	x	x	✓	x	✓	x	✓
<b>LaharFlow</b>	Woodhouse et al. (2021)	x	x	✓	x	✓	x	x
<b>EUROSEM</b>	Morgan et al. (1993)	x	x	x	✓	✓	✓	✓
<b>EROSION-3D</b>	Schmidt (1991); Werner (1995)	x	x	x	✓	✓	✓	✓
<b>KINEROS</b>	Woolhiser et al. (1990)	x	x	x	✓	✓	✓	✓
<b>LISEM</b>	De Roo et al. (1996)	x	x	x	✓	✓	✓	✓
<b>OpenLISEM (Hazard)</b>	(Van den Bout et al. 2018)	✓	✓	✓	✓	✓	✓	✓
<b>r.avaflow</b>	Mergili et al. (2017)	x	x	✓	✓	✓	x	x
<b>FLO-2D</b>	O'Brien et al. (1993)	x	x	✓	x	✓	✓	✓
<b>EDDA 1.0/2.0</b>	(Shen et al. 2018)	✓	x	✓	✓	✓	✓	✓
<b>Landslide Hydro-mechanical Triggering (LHT)</b>	Lehmann and Or (2012)	✓	x	✓	x	✓	x	✓
<b>Step-Tramm</b>	Von Ruetten et al. (2017)	✓	✓	✓	x	✓	✓	✓

\* LS = Landslides, ST = Slope stability (landslide initiation), LR = Landslide runout, DF = Debris flow, ER = erosion

### 2.2.2 Model selection: The OpenLISEM Hazard model

The previous section identified the OpenLISEM hazard model as a comprehensive multi-hazard modelling approach for integrating hydrological and stability processes and representing hazards. The OpenLISEM hazard model is a Multi-hazard Land Surface Process Model developed by the International Institute for Geo-Information Science and Earth Observation (ITC) (van den Bout et al. 2018). This physically-based distributed multi-hazard model aims to simulate individual hazards and their interactions, including flooding, rainfall- and earthquake-triggered landslides, debris flows, and hillslope erosion. These hazards are simulated by integrating spatially distributed infiltration models, such as Green and Ampt (1911), Smith and Parlange (1978), and the SWATRE multi-layered soil water model (Bastiaanssen et al. 1996) which employ the empirical Darcy equation for vertical soil water movement. Overland flow and channel flow are simulated by incorporating kinematic flow, diffusive flow, and Saint-Venant flow (van den Bout and Jetten 2018). The model also integrates a catchment-scale infinite slope approach to assess slope stability and an iterative slope failure method to estimate landslide failure depths and volumes (Van den Bout et al. 2021). A two-phase model by Pudasaini (2012) is coupled with this method, considering competitive forces to simulate the effects of landslide volumes and bed erosion on debris flow behaviour and magnitude, as well as their impacts on erosion and deposition rates. Hillslope erosion modelling is incorporated by integrating the transport capacity equation developed by Govers et al. (1990) to simulate the sediment load in overland flow. Erosion is modelled through splash and flow detachment that incorporate sediment into the flow through different bedload equations such as Van Rijn (1984a), Van Rijn (1984b) and Wu, Wang, and Jia (2000). The advantage of the OpenLISEM hazard model over other multi-hazard modelling approaches is its consideration of the spatial variability of soil types and land use, enabling the spatial distribution and variation of hydrological and geotechnical parameter values, as well as land use categories within the catchment. This feature makes the OpenLISEM hazard model highly suitable for assessing the impacts of climate and land use change on the occurrence and interaction of rainfall-triggered landslides, debris flow, and hillslope erosion at the catchment scale.

Based on the above, the OpenLISEM hazard model was selected as the most appropriate model to simulate the hazard interaction between rainfall-triggered landslides, debris flows, and hillslope erosion hazards according to the level of representation of hydrological and stability processes for different catchment scales, and its ability to assess the effects of rainfall extremes and land use on the occurrence of these hazards. The main modelling approaches for three mentioned hazards are described as follows:

**Slope stability and slope failure:** In the OpenLISEM hazard model, the slope stability estimation method is based on the infinite slope approach. This method assumes slope failure occurs along a failure surface parallel to the ground (Van Westen and Terlien 1996). The OpenLISEM hazard model assumes the slope consists of two layers: a bedrock material with high cohesion, considered a boundary condition for calculations, and a top layer of loose material (Van den Bout et al. 2021). Under this assumption, by considering a homogeneous slope and material across the entire catchment area, the expression for calculating both the local downslope (shear forces) and local resisting forces (strength forces) can be simplified (see Appendix A.1 ). Therefore, a fraction of forces acting on the failure plane

is expressed in terms of the Factor of Safety (FoS), which, under an infinite slope approach, can be assessed as the ratio of shear strength forces (force capacity) to shear forces (force demand) (Van den Bout et al. 2021). Once the slope stability is calculated over the entire catchment area, the slope failure is estimated according to the iterative slope failure method (see Appendix A.1 ) (Van den Bout et al. 2018). This method was developed to calculate the progressive slope failure within a raster element that was determined to be unstable (Van den Bout et al. 2021).

**Debris flow modelling:** In the OpenLISEM hazard model, the debris flow modelling approach consists of a fluid and solid phase modelled through a set of two-phase equations estimated by Pudasaini (2012). The fluid phase consists of a fluid volume fraction derived from the Saint-Venant equations for shallow water flow based on depth averaging, which includes mass conservation for flow velocity components and momentum balance for slope friction (see Appendix A.1 ). The solid phase consists of a solid volume fraction (see Appendix A.1 ) derived from the volume of soil resulting from slope failure and entrained by the surface flow (Liu et al. 2020). The solid volume fraction also includes the volume of sediment concentrated within the flow due to bed erosion (Pudasaini and Fischer 2020). Additional forces within the solid phase, such as the Mohr-Coulomb plasticity criteria, are considered to account for the reaction of the surface to the weight of the flow material (Van Den Bout et al. 2021).

**Hillslope erosion modelling:** In OpenLISEM hazard model the erosion modelling is given under two approaches. The first one is according to sediment load in overland flow and channel flow using the transport capacity ( $T_c$ ) given by (Govers et al. 1990) (see Appendix A.1 ). From the transport capacity ( $T_c$ ), the sediment load in overland flow and channel flow will determine the detachment and deposition of the soil. The sediment is loaded into the flow according to a set of sediment load equations for bed and suspended sediment load for overland and channel flow from Van Rijn (1984a) and Van Rijn (1984b). The user chooses the most suitable equation for sediment load. It was used Van Rijn (1984a and 1984b) bed and suspended load full equations. Once the sediment is loaded into the flow, the sediment concentration will determine the flow transport capacity ( $T_c$ ), in which for sediment concentrations  $C_v$  less than  $T_c$  ( $kg.m^{-3}$ ), flow detachment will take place (erosion), and for sediment concentrations,  $C_v$  larger than  $T_c$  ( $kg.m^{-3}$ ) deposition will take place.




However, some advantages and disadvantages must be considered for the use of this model (Table 2.2). These are described as follows:

**Advantages:** As shown in Table 2.2, in the OpenLISEM hazard model, rainfall-triggered landslides, debris flows, and hillslope erosion hazards are represented by coupling catchment-scale slope stability and failure methods, two-phase debris flow equations to simulate debris flow initiation and runout, and transport capacity equations to simulate erosion and deposition. The advantage of these methods is the low cost of their implementation in catchments of different sizes and scales. Moreover, these methods are coupled with catchment-scale hydrology, improving the representation and locations of these hazards for individual slopes and catchment scales. Another advantage is that the OpenLISEM hazard model is spatially distributed and integrated with GIS allowing the assessment of the spatial distribution and magnitude of the simulated hazards. Nevertheless, its major advantage over other multi-hazard

models is that it simulates the impacts of climate and land use change by including rainfall events of different intensities and durations and land use within its modelling structure.

**Disadvantages:** According to Table 2.2, the representation of rainfall-triggered landslides, debris flows, and hillslope erosion hazards require the integration of multiple processes, such as hydrological, sediment, and stability processes that require extensive amounts of input parameters and data. This increases the model complexity in terms of the number of model parameters and the amount of data required to characterise these parameters. Therefore, the use of this type of model requires parameterisation guidelines to reach a proper representation of hazards, owing to the number of parameters to be calibrated. Moreover, as the OpenLISEM hazard model is spatially distributed, it introduces great spatial variability in the input parameter values. This introduces levels of uncertainty that are increased by data scarcity to characterise the input parameter values. In addition, the model is computationally expensive for high-resolution data, increasing the simulation time for large catchments and long-duration rainfall events.

Table 2.2 Advantages and disadvantages of the OpenLISEM Hazard model.

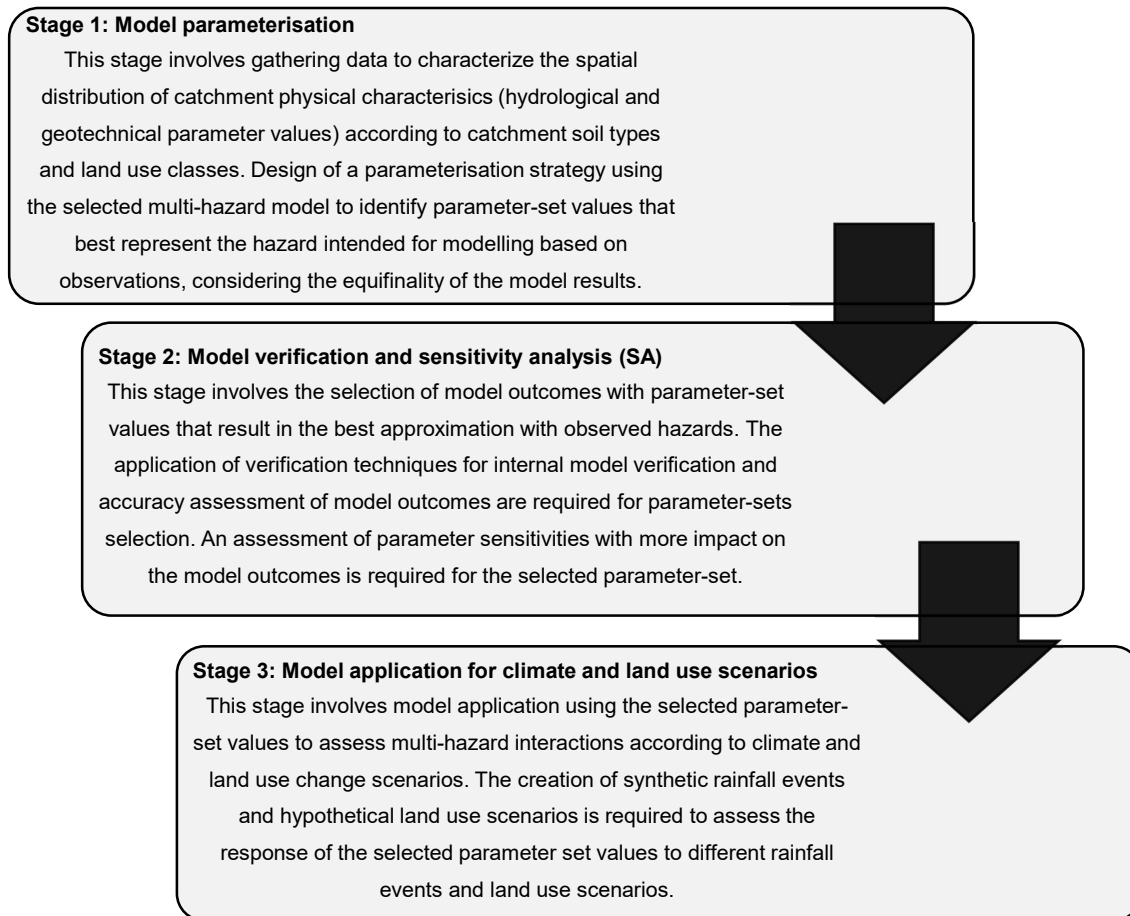
Hazard representation	Process integration	Data required	Advantages	Disadvantages
<b>Rainfall-triggered landslides</b> 	<b>Hydrological processes:</b> <ul style="list-style-type: none"> <li>• Infiltration</li> <li>• Hillslope runoff</li> <li>• Channel flow</li> <li>• Channel flooding</li> </ul>	Rainfall data (intensity and duration)  Land use/cover	Catchment-scale hydrology, stability methods and two-phase debris flow model (low simulation cost for catchments with different sizes).	Model complexity: a large number of input parameters (gaps in parameterisation).  Requires a lot of input data, which can be time-consuming and expensive to obtain.
<b>Debris flows</b> 	<b>Sediment processes:</b> <ul style="list-style-type: none"> <li>• Flow detachment (erosion)</li> <li>• Sediment transport</li> <li>• Entrainment</li> <li>• Deposition</li> </ul>	Topography (Digital elevation model DEM)  Drainage network (width and depth)  Soil depths	Model results for individual slopes and different catchment scales.  Can simulate the impacts of climate and land use change.	Spatial data variability: uncertainty propagation in inputs parameters and model outputs (effects on data-scarce environments).
<b>Hillslope erosion</b> 	<b>Stability processes:</b> <ul style="list-style-type: none"> <li>• Slope stability</li> <li>• Slope failure</li> <li>• Solid-fluid phase</li> <li>• Runout (landslides and debris flows)</li> </ul>	Soil types (hydrological and geotechnical properties)  Rheological parameters	Spatially distributed integrated with GIS able to use different resolution data.  Spatial location of hazard magnitudes.	High-resolution data is computationally expensive for large catchments (longer simulation times)

## 2.3 Defining a modelling workflow for multi-hazard interaction modelling

As discussed in Chapter 1, section 1.2.1 one of the most challenging aspects of multi-hazard modelling is addressing gaps in parameterisation and uncertainty caused by model complexities, such as the extensive number of parameters needed for representing hydrological and stability processes, and the quality of available data for estimating the required hydrological and geotechnical parameter values. Addressing these gaps in multi-hazard modelling is considered good practice, particularly when forecasting the impacts of climate and land use change on hillslope hydrological hazards. Managing complex models through an ex-ante evaluation improves the modelling of hillslope hydrological hazards by ensuring accurate hazard representations and assisting modellers in making consistent and justifiable decisions regarding model outputs for addressing research, practice, or policy questions of interest (van Vliet et al. 2016; Kremmydas et al. 2018). Several studies have addressed parameterisation, uncertainty, and equifinality Wooldridge et al. (2001); Walker et al. (2003); Aumann (2007); Tolson and Shoemaker (2008); Yen et al. (2014); Malone et al. (2015); Uusitalo et al. (2015); van Vliet et al. (2016); Koo et al. (2020) and Williams et al. (2020) have defined methodological workflows to guide the modelling of complex models to support the calibration and validation of hydrological models, decision-making in land use planning, and socio-environmental and agricultural policies.

According to Beven et al. (2018) and Koo et al. (2020), **workflows** consist of sequential methodological steps that guide modellers in applying the method accurately and effectively for decision support. This section defines methodological steps as a modelling workflow to address parameterisation and uncertainty gaps in multi-hazard modelling. The proposed modelling workflow outlines the necessary steps for guiding model parameterisation and uncertainty analysis when assessing hillslope hydrological hazards under climate and land use scenarios. The development of a modelling workflow (Table 2.3) involves key strategies, including selecting a model with appropriate process representation for the problem of interest (the OpenLISEM hazard model selected in section 2.2.2), acquiring and estimating model parameter values, configuring and executing the model, verifying the model through equifinality analysis, identifying sensitive parameter values for uncertainty assessment, and applying the model to climate and land use scenarios. The key strategy steps are as follows:

Table 2.3 Strategies to address uncertainty in multi-hazard modelling.



### 2.3.1 Stage 1: Model parameterisation

The design of a modelling workflow for multi-hazard modelling involves developing strategies that cover data acquisition for estimating model parameter values and designing parameterisation methods to accurately represent the intended hazard while considering uncertainties in input parameters. However, estimating input parameter values for multi-hazard models can be impractical in many cases, particularly in large catchments and regions with limited data accessibility regarding catchment characteristics such as hydrological and geotechnical properties, soil depths, topography, and land cover (Tilloy et al. 2019; Neal 2022). This data limitation introduces uncertainties in input parameter estimation, leading to a cascade of epistemic uncertainties throughout the modelling process due to information gaps (White et al. 2003; Yen et al. 2014). These uncertainties affect the model outputs, including spatial distribution of landslides, failure depths, shape, and surface area, which restrict the representation of hazards and constrain the assessment of their magnitudes and potential impacts under different climate and land use change scenarios (Crossley et al. 2000; Marshall and Randhir 2008; Sadegh et al. 2018). Researchers have made significant contributions to improve the characterization of soil physical properties for hydrological hazard modelling. Notably, Iwashita et al. (2012); Fan et al. (2016); Tofani et al. (2017); Bicocchi et al. (2019) and Shephard et al. (2019) have expanded methodologies and



databases for estimating soil parameters in physically-based landslide and debris flow modelling, particularly in data-scarce environments where direct measurements and laboratory testing for hydrological and geotechnical information are limited and costly.

One of the strategies to address input parameter uncertainty is to assess their value distribution through the definition of the minimum and maximum value ranges (Beven and Binley 1992; Refsgaard 1997). Statistical techniques such as Monte Carlo simulations, Latin Hypercube Sampling (LHS), Bayesian approaches, and random sampling methods can be used to explore parameter value distributions (Francos et al. 2003; Song et al. 2015; Wagener and Pianosi 2019). Physically-based distributed models offer the flexibility to define scaling factors that determine the range of variation for parameter values (Beven 2001; Guinot and Gourbesville 2003; Refsgaard et al. 2007). **Scaling factors** are multiplication factors used to adjust the initial value distribution of input parameters and define their minimum and maximum ranges (Brown et al. 2012). In developing a modelling workflow to address parameterisation, the first step is to identify the parameter sets in the selected multi-hazard model that influence the intended hazard representation. The second step involves estimating their values based on different soil types and land use classes, utilizing data from various sources such as literature reviews, published databases, and open-source information. Finally, the minimum and maximum distribution ranges for the estimated values of each input parameter are defined, allowing exploration of different parameter values until the model outputs align with observation (Guinot and Gourbesville 2003; Malone et al. 2015).

#### 2.3.1.1 Defining a parameterisation method

One of the strategies in designing a modelling workflow involves defining a parameterisation methodology to ensure the multi-hazard models represents the physical and climatic factors governing hydrological and stability processes in a specific catchment environment (Wagener and Wheeler 2006; Lane et al. 2021). **Model parameterisation**, as described by Refsgaard (1997) and Malone et al. (2015), determines suitable parameter values for the model in a specific catchment area, considering representative values for soil types, vegetation types, and geological layers. Proper parameterisation is crucial to avoid issues in model calibration and verification (Refsgaard and Storm 1996). **Model calibration** refers to the procedure of adjusting or optimize model parameter values until the model outputs fit with observations (Beven and Binley 1992; Guinot and Gourbesville 2003). Therefore, the parameterisation process is focused on identifying the values of a set of input parameters for different catchment physical characteristics considered acceptable in reproducing an observed behaviour of the catchment system (Beven and Freer 2001). The parameterisation process should properly account for uncertainties arising from data scarcity and model complexities. This means accepting the possibility that multiple sets of parameter values can be considered acceptable in representing the behaviour of the hydrological and stability catchment (Beven 2001). This concept is known as "**Equifinality**," which suggests that there is no unique representation of the catchment system behaviour, but rather a range of parameter values that are deemed acceptable as data quality improves over time (Beven 2006; Beven 2019). Equifinality allows for the identification of behavioural and non-behavioural simulations based on their similarity to observations. A **behavioural simulation** is defined as one in which the parameter sets are considered acceptable for representing observed hazards such as rainfall-triggered landslides,

debris flows, and hillslope erosion. On the other hand, **non-behavioural simulations** are those that fail to predict or accurately represent observed hazards (Beven and Binley 1992; Beven 2019). To achieve this, the parameterisation process involves designing **parametric simulations**, which entail searching for model parameter values by modifying their initial values (Lee et al. 2019). Parametric simulations allow for the combination of different parameter sets with varying value ranges, considering soil types and land use classes. This approach enables the selection of parameter values that are considered acceptable in representing hillslope hydrological hazards (Refsgaard 1997; Yen et al. 2014).

One approach for designing parametric simulations to identify behavioural and non-behavioural simulations involves using a Global Sensitivity Analysis (GSA) method (Wagener et al. 2001; Song et al. 2015). GSA assesses how variations in parameter values affect the variability of model outputs, allowing for the combination of multiple parameter sets (Pianosi et al. 2016; Wagener and Pianosi 2019). This method offers the advantage of identifying parameter sets that are consistent with observations while considering the uncertainties propagated during the modelling process (Beven 2019). The All-Factors-At-a-Time (AAT) method, a GSA sampling strategy, enables the simultaneous variation of input parameter values, providing insights into the sensitivity of each parameter within the set and its contribution to model output variability (Pianosi et al. 2016; Douglas-Smith et al. 2020). However, using this method, several to hundreds of simulations has to be performed until find acceptable parameter-set values (Herrera et al. 2022). Physically-based distributed multi-hazard models, such as the OpenLISEM hazard model selected in section 2.2.2, present challenges due to the number of required input parameters, data resolution, and catchment area extension, which make the simulation process time-consuming (Hessel 2005; Lilburne and Tarantola 2009; Pogson and Smith 2015). In the modelling workflow, the parameterisation method is designed following a GSA approach, which involves developing an experimental design that includes parametric simulations with different combinations of parameter-set values.

### 2.3.2 Stage 2: Model verification and sensitivity analysis (SA)

**Model verification** is commonly used to assess a modelling structure's capability to reproduce observations or true values based on available data (Oreskes et al. 1994; Beven 2019). According to Oberkampf (2019), defines model verification as the process of confirming that an observation or true value corresponds to the exact solution of the model. However, this procedure does not focus on determining the modelling structure's ability to replicate a specific process of interest. Instead, it aims to estimate the numerical accuracy of the model structure given specific input data (Oberkampf and Barone 2006). **Model validation** involves the assessment of the model performance by measuring the consistency of their outputs with observations through different statistical accuracy metric (Oreskes et al. 1994; Frattini et al. 2010). **Model accuracy** is a performance metric used to evaluate the goodness of fit (GOF) by assessing the agreement between model outputs and observed data (Frattini et al. 2010; Formetta et al. 2016). When observations are available, they can be used to assess the accuracy of the model structure by comparing the model outputs to the observed data (Formetta et al. 2016).

Elaborating hazard inventories is a crucial stage before model verification (Guzzetti et al. 1999; Beguería 2006). The inventory provides insights into the triggered hazard's type, location, magnitude, volumes, and date of occurrence (Guzzetti et al. 2012). According to Blahut et al. (2010), most rainfall-triggered occur during rainfall events with varying distributions, intensities, and durations. Therefore, the landslide or debris flow recorded in a hazard inventory should align with the rainfall event that generated these hazards (van Westen et al. 2008). Landslide inventories aim to furnish databases with crucial information about past landslide activity and its primary triggers (Pellicani et al. 2013). These inventories are compiled at different scales using techniques e.g., geomorphological analysis, Geographic Information Systems (GIS), aerial photographs, and satellite imagery (Galli et al. 2008; van Westen et al. 2008). However, constructing landslide inventories often requires the use of multi-temporal information, which can be challenging to obtain (van Westen et al. 2008). The mapping resolution depends on the available imagery, which can limit the identification of landslide boundaries, impact areas, debris flow sources, and runout areas (Ardizzone et al. 2002). This limitation restricts the understanding of landslide shapes, sizes, and frequency distribution (Malamud et al. 2004; Taylor et al. 2018). Mapping errors in the construction of landslide inventories introduce uncertainty in terms of landslide locations and boundaries, impacting the quality of the inventory map (Mead et al. 2021). These errors affect the agreement between simulated and observed landslides, thereby influencing the calculation of accuracy scores (Hagen-Zanker and Martens 2008). Consequently, tolerance levels should be considered within the mapped landslides (Sterlacchini et al. 2011; Mead et al. 2021).

Nonetheless, assessing the accuracy of the modelling structures using observed data is challenging. As was mentioned in section 2.3.1, the model complexity, the uncertainty introduced in the input parameters and the effects of data resolution might impact the internal process representation of the model (Fawcett et al. 1995). To address the impacts of uncertainty in model results, model verification should be approached through two strategic approaches. The first one corresponds to the model internal verification (equifinality) and the second one to the accuracy of the modelling structures. The approaches are described in the following sub-sections.

### **2.3.2.1 Model internal verification**

Within the modelling workflow, this procedure is crucial for model verification, as it helps identify parameter sets that can represent observed hazards adequately while considering uncertainty and equifinality in the model outputs (Hofmann 2005; Beven 2019). This procedure involves the evaluation of the model's internal logic and calculations (Fawcett et al. 1995), to ensure that the model accurately represents hazard locations and magnitudes based on its internal structure. Verification in this process focuses on assessing whether the model outcomes, such as landslide areas or debris flow runout areas, exhibit the same characteristics as observed hazards, including area difference, distribution, and spatial location. To facilitate this procedure, the development of inventories for landslides, debris flows, and erosion rate records is important as they provide a reference point for comparing the model outputs (van Westen et al. 2008; Blahut et al. 2010; Guzzetti et al. 2012). Additionally, it is essential to define **hazard metrics** that quantify the magnitude of the modelled hazards, such as surface areas or volumes, for comparison with the magnitude distribution of observed hazards. Considering uncertainty and

equifinality in the model outputs, it is recommended to perform additional procedures for model verification, as it is considered good practice (Beven 2019; Herrera et al. 2022).

Equifinality is directly linked to the parameterisation and verification processes in the modelling process (Oreskes et al. 1994). Figure 2.3 illustrates a spatial similarity approach used to address model equifinality during the verification process. Incorporating equifinality in physically-based distributed multi-hazard models helps identify the parameter sets that produce an observed hazard by considering the uncertainty derived from measurement limitations (Beven and Freer 2001). The internal verification process involves comparing the simulated and observed hazards in terms of spatial distribution patterns, magnitudes, and sizes to assess equifinality (Malamud et al. 2004). Within the modelling workflow, equifinality is considered by incorporating a spatial similarity approach as an additional model verification procedure. This approach focuses on assessing the similarity between a hazard simulated using different parameter sets and an observed hazard (Figure 2.3). The spatial similarity approach selects criteria based on area differences and frequency area distributions to determine the parameter set that best approximates an observation.

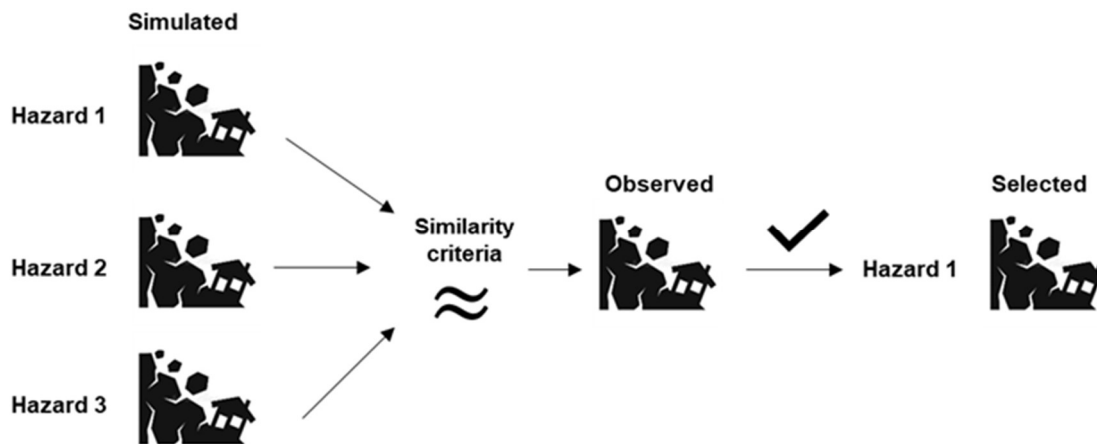


Figure 2.3 Spatial similarity approach for model verification.

### 2.3.2.2 Model accuracy

As mentioned in Section 2.3.2, the model accuracy was assessed by comparing the model outputs with observed data. Various techniques are available to evaluate this agreement, but the choice of technique depends on the modelling approach and its results (Beguería 2006; Frattini et al. 2010). For instance, in statistical susceptibility models for landslides or debris flows, verification involves comparing the prediction of terrain units (susceptibility zoning) with the distribution of past landslides or debris flows (landslide inventory) within each zoning unit (Guzzetti et al. 1999; Beguería et al. 2009). In physically-based distributed multi-hazard models like OpenLISEM, verification is based on the spatial agreement between the simulated runout areas of landslides or debris flows and the observed inventory areas (van Westen et al. 2006; Corominas et al. 2014). In erosion modelling approaches, verification focuses on assessing the simulation of spatial patterns of erosion and deposition (Van Oost et al. 2005). While

hydrographs and sediment graphs measured at the catchment outlet have traditionally been used to verify erosion models, it is important to spatially verify distributed models as well, not solely relying on catchment-outlet comparisons (Batista et al. 2019). While hydrographs and sediment graphs measured at the catchment outlet have traditionally been used to verify erosion models, it is important to spatially verify distributed models as well, not solely relying on catchment-outlet comparisons (Takken et al. 1999). For physically-based distributed multi-hazard models, the most suitable observational data for verification purposes come from landslides and debris flow runout areas, requiring techniques to assess the spatial agreement between simulated and observed hazards, which will be discussed in the following sections.

### **Spatial overlapping method**

This method, introduced by Hagen-Zanker and Martens (2008) and Brown et al. (2012) serves as a map comparison method for physically-based models. The same approach has been utilized by Carrara et al. (1991) and subsequently by Ardizzone et al. (2002); Galli et al. (2008); Santangelo et al. (2015), to evaluate the reliability of landslide inventory maps through a "map overlay" approach between different sources of inventory areas. The method aims to estimate the discrepancy or similarity between corresponding polygons in two maps (Santangelo et al. 2015). Over time, this approach has become suitable for verifying physically-based distributed models by assessing the spatial agreement between simulation results and observations (Hagen-Zanker and Martens 2008). The overlap agreement, such as between two debris runout polygons, within this method measures the uncertainty associated with landslide simulation results by calculating various accuracy metrics (Mead et al. 2021). The spatial agreement estimation involves calculating the intersection between the simulated and observed hazards, which can represent either landslides or debris flow runout polygons (Figure 2.4). In catchment scale models like the OpenLISEM hazard model, the intersection corresponds to the True Positive (TP) value, which is the intersection area between two polygons. The False Negative (FN) value is obtained by subtracting the intersected area (TP) from the observed polygon area, while the False Positive (FP) value is obtained by subtracting the TP area from the simulated polygon area. The True Negative (TN) values are calculated by subtracting the union of the simulated and observed polygons from the catchment area. It is important to consider additional criteria when using the catchment area, such as excluding flat areas from the TN value estimation.

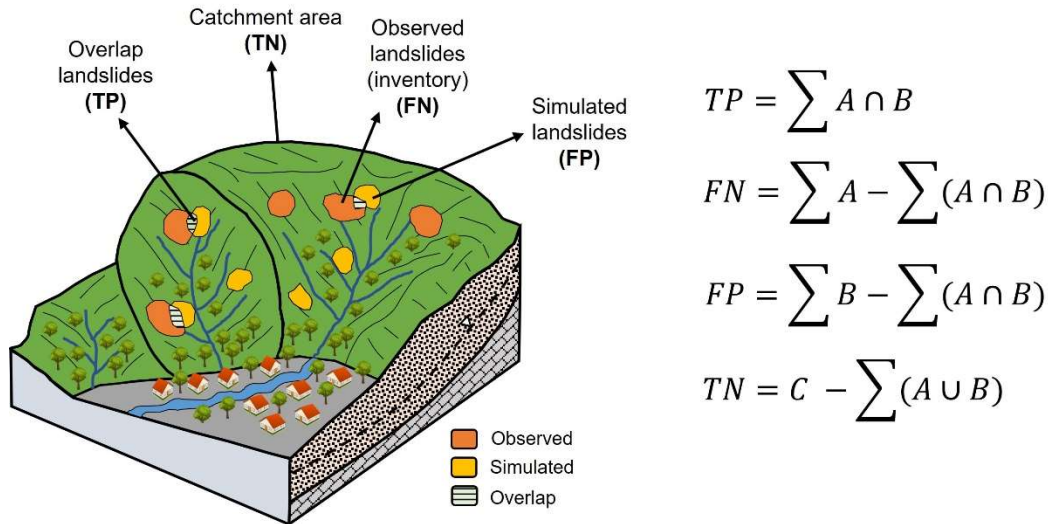


Figure 2.4 Spatial overlapping method approach.

### Accuracy metrics

The common approach to defining an accuracy metric involves testing the hypothesis that the model's prediction aligns with empirical observation (Oberkampff 2019). The consistency between the model results and observations is represented by a range of values that span from low to high, indicating the level of agreement between the model and experimental measurements (Landis and Koch 1977). Accuracy metrics are typically derived from a confusion matrix that quantifies the number of correctly and incorrectly simulated observations (Beguería 2006). Accuracy metrics can be categorized into similarity and skill score coefficients (Liu et al. 2007). Similarity coefficients assess the resemblance between two sets and yield scores ranging from 0 to 1. A score close to 1 indicates a higher similarity between the two sets (Hagen-Zanker and Martens 2008). Among the available similarity coefficients (Table 2.4), Jaccard (1901), Sorensen-Dice (1948), Anderberg (1973), Ochiai (1957), and the Fowlkes-Mallows index are commonly used for accuracy assessment. These coefficients, however, overlook the True Negative (TN) values when calculating accuracy scores (Briggs and Ruppert 2005).

Neglecting TN values in the accuracy assessment of models like OpenLISEM hazard can lead to accuracy score values that do not adequately represent the scale-dependent distribution of predicted and observed fields (Brown et al. 2012). The accuracy score for similarity indices is determined by the ratio of TP values to the combined areas of simulated and observed hazards. However, similarity coefficients are most appropriate for evaluating models that do not follow a catchment-scale approach. For instance, in the case of debris-flow runout path models, similarity indices such as the Jaccard Index are commonly employed to evaluate the spatial agreement between debris flow deposition and runout areas (Mead et al. 2021). Skill score coefficients, on the other hand, incorporate TN values in the accuracy metrics, offering a better understanding of the scale-dependent factor in accuracy scores (Brown et al. 2012; Wheatcroft 2019). Various skill score coefficients are available (see Table 2.4), with one of the most commonly used being the Heidke skill score (Cohen's kappa) (Landis and Koch 1977). This coefficient provides insight into the scale dependency of distributed hazards within the catchment

by quantifying the degree of spatial agreement or consistency between simulated and observed hazards.

Table 2.4 Similarity and skill scores coefficients classification.

Similarity coefficients	Formula	Range	Optimal value	
Jaccard (1901)	$\frac{TP}{TP + FN + FP}$	[0, 1]	1	<b>Similarity coefficients or Jaccardian coefficients</b> (measures the level of matches between two samples)
Dice (1945); Sorensen (1948)	$\frac{2TP}{2TP + FN + FP}$	[0, 1]	1	
Anderberg (1973)	$\frac{TP}{TP + 2 * (FN + FP)}$	[0, 1]	1	
Ochiai (1957)	$\frac{TP}{\sqrt{(TP + FN) + (TP + FP)}}$	[0, 1]	1	
Fowlkes–Mallows index	$\sqrt{\frac{TP}{TP + FP} * \frac{TP}{TP + FN}}$	[0, 1]	1	
Skill score coefficients	Formula	Range	Optimal value	
Success index (SI)	$\frac{1}{2} * \left( \frac{TP}{TP + FN} + \frac{TN}{FP + FN} \right)$	[0, 1]	1	<b>Skill scores</b> (measures the relative accuracy of a model by demonstration the level of agreement between observation and prediction)
True skill statistics (TSS)	$\frac{(TP * TN) - (FP * FN)}{(TP + TN) * (FP + FN)}$	[-1, 1]	1	
Simple matching (SM) Sokal and Michener (1958)	$\frac{TP + TN}{TP + FN + FP + TN}$	[0, 1]	1	
Rogers and Tanimoto (1960) (RT)	$\frac{TP + TN}{TP + 2FN + 2FP + TN}$	[0, 1]	1	
Russel and Rao (1940) (RR)	$\frac{TP}{TP + FN + FP + TN}$	[0, 1]	1	
Heidke skill score (Cohen's kappa)	$k = \frac{P_0 - P_e}{1 - P_e}$ , where $P_0 = \frac{TP + TN}{\text{Catchment area}}$ and $P_e = \frac{[(TP + FN) * (TP + FP) + (TN + FN) * (TN + FP)]}{(\text{Catchment area})^2}$	$[-\infty, 1]$	1	
Phi coefficient (mean square contingency coefficient)	$MCC = \frac{(TP * TN) - (FP * FN)}{\sqrt{(TP + FP) * (TP + FN) * (TN + FP) * (TN + FN)}}$	[0, 1]	1	

### 2.3.2.3 Criteria for parameter-set selection

The strategies in the modelling workflow for parameter-set selection are based on the equifinality approach and model accuracy, as defined in sections 2.3.2.1 and 2.3.2.2. The equifinality approach guides the selection of parameter sets by considering the difference and distribution of hazard magnitudes between the modelled and observed data. Various techniques can be used to evaluate the area difference, such as comparing the total area of modelled hazards with observed hazard areas, and analysing the area distribution through methods like histograms (Xiaolong et al. 2017; Lombardo et al. 2021). It is crucial to have access to observed hazards in order to perform this procedure effectively. Developing a hazard inventory that includes observed landslides and debris flow runout polygons is essential for determining the total area and distribution of individual hazards (Guzzetti et al. 2002; Malamud et al. 2004). In this approach, parameter-sets that yield model outputs with minimal area differences and area distributions that best match the observed hazards are typically preferred. In addition to the equifinality approach, the accuracy approach can be applied by employing spatial overlapping methods to calculate different accuracy metrics that assess the spatial agreement between

the modelled and observed hazards (van den Bout 2020). The selection of an appropriate accuracy metric is crucial as it provides a score to determine the model outputs with the best spatial agreement (Beguería 2006; Frattini et al. 2010). By combining internal verification techniques based on the equifinality approach and model verification using accuracy metrics, valuable information is obtained to establish criteria for selecting parameter-sets..

#### **2.3.2.4 Sensitivity analysis (SA)**

**Sensitivity Analysis (SA)** assesses how the variability of model outputs relates to changes in input parameter values (Lilburne and Tarantola 2009; Pianosi et al. 2016). It quantifies the resulting uncertainty in model outputs caused by uncertainties in input parameters (Crosetto et al. 2000; Douglas-Smith et al. 2020). This analysis is a crucial step in the modelling workflow as it identifies sensitive parameters that significantly influence hazard representations within selected parameter values (Pianosi et al. 2016; Wagener and Pianosi 2019). Two commonly used techniques for sensitivity analysis are local and global sensitivity analysis (SA) (Song et al. 2015). Local sensitivity analysis examines the variability of model outputs when an input parameter varies around a specific value, while global sensitivity analysis considers variations across the entire range of input parameter variability (Pianosi et al. 2016). The choice of sensitivity analysis (SA) method depends on the analysis's purpose. In the context of the modelling workflow, the objective is to identify and select parameter values that effectively reproduce observed hazards. Thus, the aim of this study is to identify the most sensitive parameters that influence the spatial representations of rainfall-triggered landslides, debris flow, and hillslope erosion rates. This can be achieved by ranking the input parameters based on their contributions to model output variability, screening out parameters with negligible influence, or mapping the input parameter value space that yields extreme output results (Sarrazin et al. 2016; Noacco et al. 2019). Considering the mentioned methods, the chosen SA method for this study aims to identify the most sensitive parameters. Therefore, the SA method chosen for this is described as follows:

#### **Regional Sensitivity Analysis (RSA)**

Regional Sensitivity Analysis (RSA) (Spear and Hornberger 1980) aims to identify regions of input parameter values used for Factor *Ranking* or *Mapping* (Pianosi et al. 2016). This method, also known as Monte Carlo filtering, divides parameter sets into "behavioural" and "non-behavioural" groups based on a prescribed threshold value (Noacco et al. 2019). The choice of threshold value is crucial in RSA, as it separates the "behavioural" parameter set, which approximates or is consistent with observations, from the "non-behavioural" set with no approximation to the observed hazard (Pianosi et al. 2016). For physically-based distributed multi-hazard models such as the OpenLISEM hazard model, the threshold is associated with the magnitude of the hazard representation obtained from the model output, as the magnitude depends on variations within the parameter set values. Therefore, the threshold choice has to be related to an equifinality principle described in section 2.3.1 to select the hazard representation with more proximity to an observed hazard.

The distinction between "behavioural" and "non-behavioural" parameter set is performed by the calculation of two Cumulative Distribution Functions (CDF) which describe the separation between the



two curves (Equation 2.1). The separation between the curves is computed using the Kolmogorov-Smirnov (KS) statistic, which can be used to rank the (Bozzolan et al. 2020). The larger the distance between the CDFs curves, the more influential the factor. The sensitivity index is expressed as follows:

$$s_i = \max_{x_i} |F_i^B(x_i) - F_i^{\bar{B}}(x_i)| \quad \text{Equation 2.1}$$

Where  $s_i$  correspond to the sensitivity index,  $F_i^B(x_i)$  correspond to the behavioural CDF, and  $F_i^{\bar{B}}(x_i)$  correspond to the non-behavioural CDF. The sensitivity index ( $s_i$ ) varies from 0 to 1, a high value indicates that the variation of the input factors significantly influences the hazard spatial.

### 2.3.3 Stage 3: Model application for climate and land use scenarios

The identification of parameter-set values in **Stage 1**, section 2.3.1, and the selection of the best parameter-set value representing an observed hazard in **Stage 2**, section 2.3.2, allow the exploration of interactions between rainfall-triggered landslides, debris flows, and hillslope erosion hazards. This exploration is conducted under different climate and land use scenarios using the OpenLISEM hazard model selected in section 2.2.2. This represents the final stage of the modelling workflow, where various scenarios are examined using the chosen parameter-set. The sensitivity analysis of the selected parameter-set values helps identify the most sensitive parameters that have a significant influence on the magnitude of rainfall-triggered landslides, debris flows, and hillslope erosion hazards. These parameters include landslide area, debris flow runout area, and volumes of eroded and deposited sediment material (net erosion). By determining the most influential parameters based on soil types and land use categories, it becomes possible to assess their responses to different climate and land use scenarios.

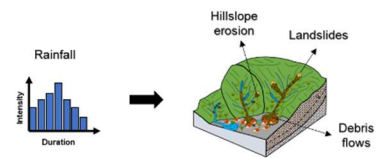

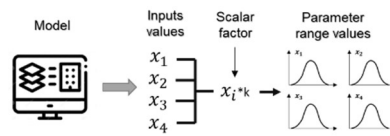
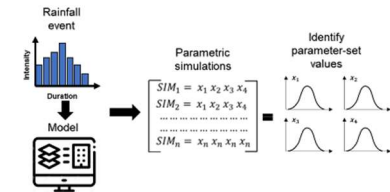
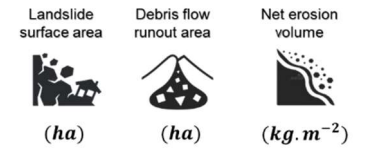
To evaluate these responses, sets of synthetic rainfall events with different intensities and durations are created, along with hypothetical land use scenarios reflecting the impacts of land use change such as urbanization, agriculture, and deforestation. The parameter value of the most influential parameter for land use categories is modified for the land use category intended to change (e.g., natural forest). Subsequently, a specified number of simulations is performed to assess the response of the selected parameter set to varying rainfall intensities, durations, and changes in land use values. Finally, the response of each scenario is evaluated by quantifying the magnitude of each hazard and comparing the rate of change between scenarios. This assessment determines whether the hazard magnitudes increase or decrease under different rainfall intensities and durations, and land use scenarios. It enables the identification of the specific conditions under which the interactions of rainfall-triggered landslides, debris flows, and hillslope erosion hazards intensify and have greater impacts.

## 2.4 Chapter summary

Based on the challenges of dealing with uncertainty in multi-hazard modelling. A modelling workflow is proposed that addresses the key aspects according to the literature review discussed in section 2.3. The proposed modelling workflow includes three stages related to model parameterisation, model verification and model application. The three phases are proposed as follows:

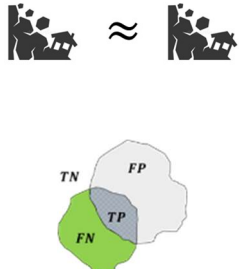

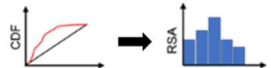
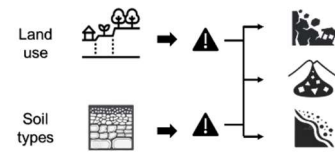
**Modelling workflow stage 1:** This stage presents the steps necessary to assess the design of parametric simulations with different parameter value ranges to identify the appropriate parameter set that reproduces the interactions between hillslope hydrology and hazards. This stage includes the necessary steps to assess the uncertainties introduced by the lack of information describing the physical characteristics of the catchment that provide the data required to set the model input parameters. This stage of the modelling workflow is fully developed and applied to the first case study catchment in Chapter 3.

### Stage 1: Model parameterisation

<p><b>1. Assemble available data for selected catchment</b></p>	<p>Select a catchment, define an inventory with observed hazards, and identify their spatial distribution and magnitude. Estimate the intensity and duration of the rainfall event that triggered the observed hazards within the catchment.</p>	
	<p>Identify model input parameters, gather data for parameter value estimation according to catchment physical characteristics, and define the spatial resolution and extent of the catchment scale.</p>	
<p><b>2. Define parameters value ranges</b></p>	<p>Define input parameter value ranges through a scalar factor to identify minimum and maximum values for each input parameter. Define parameter value statistical distributions to identify possible values for each parameter.</p>	
<p><b>3. Define parametric simulation</b></p>	<p>Design and run an ensemble of parametric simulations by setting different parameter-set value combinations to explore the likely parameter value space for physical catchment characteristics.</p>	
<p><b>4. Verify hazard representation at the catchment level</b></p>	<p>Assess the behavioural performance of parameter-set combinations in response to a rainfall event to assess their ability to replicate an observed hazard event within the catchment (total area of landslides and debris flows, and net erosion).</p>	

**Modelling workflow stage 2:** This stage presents the necessary steps to select parametric simulations with the parameter set that gives the best approximation to the observed hazards. A verification method is proposed using an equifinality approach that considers the uncertainties in the hazard representations. This approach is valid for both landslide and debris flow observations. A spatial similarity criterion is defined to select simulated hazards based on their similarity to the spatial attributes of the observed hazards. In addition, a spatial accuracy metric is selected using a spatial overlap method to assess model performance with respect to hazard locations. The application of these two approaches will allow the verification and selection of the parameter set with greater accuracy in reproducing an observation. In the final step, a sensitivity analysis is considered to identify the influential parameters and explore their impact on the hazard representations. In addition to this step, the most influential parameter values will be identified according to their spatial distribution in land use categories and soil types.

**Stage 2: Model verification and sensitivity analysis**

<p><b>5. Model verification (sub-catchment and catchment scale)</b></p>	<p>Define and apply a suitable spatial similarity assessment method for internal model verification (e.g., 'total area difference' and 'area distribution'). Identify the parameter-sets and associated simulations with the highest similarity scores with respect to observed hazard.</p> <hr/> <p>Define and apply a spatial accuracy metric to the simulations with parameter-sets with the highest similarity scores (e.g., Cohen's kappa coefficient to measure the spatial agreement between simulated and observed hazard locations).</p>	
<p><b>6. Parameter-set selection</b></p>	<p>Select the parameter-set and associated simulation that meet the criteria for spatial similarity and accuracy.</p>	
<p><b>7. Sensitivity analysis (SA)</b></p>	<p>For the selected model parameter-set, undertake sensitivity analysis to identify influential parameters and the impact of uncertainty on hazard representations.</p>	
<p><b>8. Sensitivity to soil types and land use variations</b></p>	<p>For the selected parameter-set, explore the influence of variations in the parameters characterising different soil types and land use categories in terms of their spatial distributions within the catchment. Look for soils and land use (and associated subdomain areas) in which the hazard magnitude is most responsive to these parameter variations.</p>	

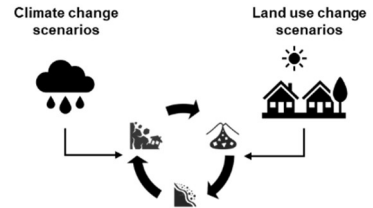
**Modelling workflow stage 3:** This stage corresponds to the application of the model. Having verified the model outputs and selected the behavioural parameter set, the final step in the modelling workflow is to explore the catchment response to different land use and rainfall scenarios. Having confirmed the distribution of parameter set values for land use units and soil types for the selected catchment, it is now possible to explore land use change scenarios and their response to different rainfall events.

**Stage 3. Model application for climate and land use scenarios**

---

**9. Explore climate and land use change scenarios**

This is the final stage, and it is now possible to define climate and land use change scenarios according to the confirmed parameter-set values for the catchment land use categories.



---

---

## **Chapter 3 Developing the workflow for parameter exploration and experimental design**

---

---

### 3.1 Introduction

This chapter develops and applies the first stage of the modelling workflow proposed in Chapter 2, section 2.3.1. The aim is to address issues in parameterisation, input parameter uncertainty and model equifinality for the application of the OpenLISEM hazard model selected in Chapter 2, section 2.2.2. The design of the first stage of the modelling workflow is developed following the key strategies proposed in Chapter 2, section 2.3.1 for data gathering to define the catchment physical characteristics, parameterisation strategy (experimental design) and parameter-set identification (equifinality). The application of the stage one of the modelling workflow will allow the addressing of the first research question of this thesis:

**RQ1: What are the physical characteristics of catchments that drive hillslope hydrological multi-hazards and their interactions?**

Addressing this research question involved the selection of an appropriate physically-based distributed multi-hazard model (Obj. 1.1) (OpenLISEM hazard model) and the definition and application of a modelling workflow to address gaps in parameterisation and uncertainty in multi-hazard models in the context of data scarcity (Obj. 1.2). Therefore, the Soufriere catchment in Saint Lucia is one of the study sites selected for developing, evaluating, and applying the first stage of the modelling workflow to represent and identify the catchment physical characteristics that drive hillslope hydrological hazards registered as a consequence of Hurricane Tomas. On October 31, 2010, the island of Saint Lucia suffered the devastating effects of Hurricane Tomas (Figure 3.1). Observations of the damage sustained over the island indicated that the Soufriere catchment recorded the areas with the most significant impacts produced by rainfall-triggered landslides and debris flows, particularly in the communities of Fond St. Jacques, Ravine Claire, and Toraille (APSL 2010). The Soufriere catchment is characterised by a tropical climate classified as *Aw* according to the Köppen-Geiger climate classification (ECLAC 2011). This type of climate is highly susceptible to hurricane seasons, producing heavy rainfall over short and long periods (Reed et al. 2022). However, the effects of climate change have increased the frequency and duration of hurricane rainfall intensity (He et al. 2016). According to rainfall-triggered landslides are the most common and dominant hazard in Saint Lucia. In the Soufriere catchment, the lithological structure set by colluvial, and alluvial tropical soils derived from volcanic rocks that go from completely decomposed rock (Grade V) to entirely residual soil (grade VI) (Shepherd et al. 2019), renders the Soufriere catchment into the highly susceptible landslide-prone catchment. However, the increase in extreme rainfall events due to hurricane intensification and land use change processes, such as the increase of farmlands and urban settlements on steep slopes, have increased landslide activity and the frequency of debris flows in the Soufriere catchment (Walters 2016). Moreover, there is evidence that agriculture, as an economic activity, has increased catchment sediment yield during the last few decades (Bégin et al. 2014). Therefore, the physical characteristics of the Soufriere catchment and the intensification of the extreme rainfall events and the accelerated land use change processes observed in the last decades make the Soufriere catchment in a highly susceptible multi-hazard forming environment.

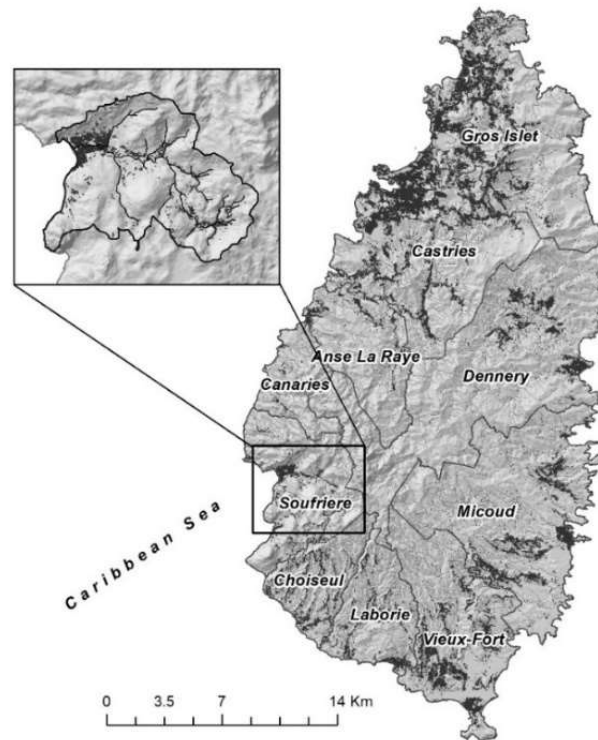


Figure 3.1 Study site location: Soufriere catchment, Saint Lucia, Eastern Caribbean.

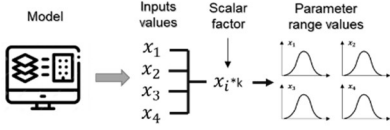
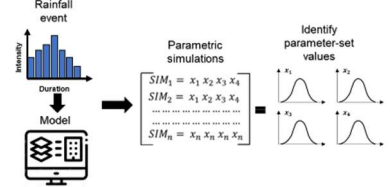

### 3.2 Methodology

The following workflow (Table 3.1) describes the methodological steps corresponding to the first stage of the modelling workflow to parameterise the OpenLISEM Hazard model or similar physically-based distributed multi-hazard models. The first stage of the modelling workflow will be applied through the development of an experimental design that addresses issues such as data gathering, parameter value estimation, parameterisation, and model equifinality for different catchment environments.

Table 3.1 Modelling workflow stage 1: model parameterisation.

#### Stage 1: Model parameterisation

<p><b>1. Assemble available data for selected catchment</b></p>	<p>Select a catchment, define an inventory with observed hazards, and identify their spatial distribution and magnitude. Estimate the intensity and duration of the rainfall event that triggered the observed hazards within the catchment.</p>	
	<p>Identify model input parameters, gather data for parameter value estimation according to catchment physical characteristics, and define the spatial resolution and extent of the catchment scale.</p>	

<p><b>2. Define parameters value ranges</b></p>	<p>Define input parameter value ranges through a scalar factor to identify minimum and maximum values for each input parameter. Define parameter value statistical distributions to identify possible values for each parameter.</p>	
<p><b>3. Define parametric simulation</b></p>	<p>Design and run an ensemble of parametric simulations by setting different parameter-set value combinations to explore the likely parameter value space for physical catchment characteristics.</p>	
<p><b>4. Verify hazard representation at the catchment level</b></p>	<p>Assess the behavioural performance of parameter-set combinations in response to a rainfall event to assess their ability to replicate an observed hazard event within the catchment (total area of landslides and debris flows, and net erosion).</p>	

Based on the modelling workflow steps described in Table 3.1, the key methodological steps are described as follows:

**Step 1: Assemble available data for the selected catchment**

This step comprises the selection of catchments highly sensitive to the impacts of climate and land use change. The assembling of information available on a selected catchment is required to identify past-triggered hillslope hydrological hazards and to define the physical characteristics of the selected catchment. Hazard identification is performed through elaboration of a hazard inventory that identifies rainfall-triggered landslides, debris flows, or hillslope erosion rates by characterising their spatial location and magnitudes. This step also involves the identification of the rainfall event that triggered the identified hazards by determining its intensity and duration. The defined hazard inventory and identified rainfall event are described in Section 3.2.1. The catchment's physical characteristics are defined by acquiring spatial data corresponding to the catchment land use, soil types, topography, and soil depths. These characteristics are the basis to define the model input parameter values. Hydrological and geotechnical parameter values are estimated according to catchment soil types and land use based on a literature review or other sources of information. The spatial distribution of the estimated values is defined according to catchment soil types and land use. The catchment hydrological and geotechnical parameter values spatial distribution is defined in Section 3.2.3.

**Step 2. Define input parameters value ranges**

Assess the distribution of the estimated input hydrological and geotechnical parameter values for soil types and land use using statistical methods such as histograms, boxplots, or probability distributions to identify the minimum and maximum value ranges for each input parameter. Explore the variability of the input parameter value ranges by defining scaling factors to decrease or increase the minimum and



maximum value ranges of each input parameter value. This allows an assessment of how the variability of the input parameter value ranges affects the model outputs in terms of the representation of rainfall-triggered landslides, debris flows, and hillslope erosion hazards. This is an important procedure to evaluate the level of uncertainty introduced by input parameters in the model outputs that are expressed in hazards representations of different orders of magnitude. The input parameter value distribution method and the definition of scale factors for each input parameter are described in section 3.2.4.

### **Step 3. Define parametric simulations**

Define parametric simulations by determining a total number of parameter-set combinations with different value ranges determined by the proposed scale factor to decrease or increase the minimum and maximum value ranges of each input parameter value. The aim is to create a number of parameter-set combinations that might be behavioural or non-behavioural in representing the observed hazard in the hazard inventory for the selected catchment. The foregoing allows for identifying parameter-set values deemed suitable for representing the observed hazard according to representative hydrological and geotechnical values for the catchment soil types and land use. The procedure to define the elaboration of parametric simulations is described in Section 3.2.5.

### **Step 4. Verify hazard representations**

Assess the hazard representation resulting from the total of parametric simulations by implementing hazard metrics that quantify the total magnitude of the simulated rainfall-triggered landslides, debris flows and hillslope erosion hazards within the catchment. The aim is to identify the parametric simulations that resulted in a behavioural or non-behavioural representation of the observed hazards in the inventory by comparing their total magnitudes with the total magnitude observed in the hazard inventory. The procedure to quantify the hazard representations and their magnitudes is described in Section 3.2.6.

In the following subsections, is describe in detail the modelling workflow steps to implement the experimental design.

#### **3.2.1 Soufriere catchment: Rainfall event selection and hazard inventory**

As mentioned in Section 3.1, the Hurricane Tomas rainfall event was selected to assess the response of parametric simulations in reproducing the rainfall-triggered landslides and debris flows observed in the Soufriere catchment during the passage of the hurricane. Therefore, it is necessary to estimate the rainfall duration and intensity registered by Hurricane Tomas and their impacts on rainfall-triggered landslides, debris flows, and erosion. The procedures to estimate the hurricane rainfall event in terms of intensity and duration and the spatial distribution and magnitude of the observed hazards are described as follows:

### Hurricane Tomas 2010 rainfall event

The Hurricane Tomas rainfall event corresponded to a 27-hour rainfall duration with a total volume of 662 mm (Figure 3.2). The ranges of rainfall intensity were estimated by creating a synthetic rainfall event from the total rainfall volume registered for the Soufriere catchment obtained from the Desraches station near the Soufriere catchment. The procedure for the synthetic rainfall estimation is performed in Appendix B.1 The rainfall intensity duration was discretized in time intervals of 10 min, giving a total of 1620 min for a 27-hour rainfall duration (Figure 3.2).

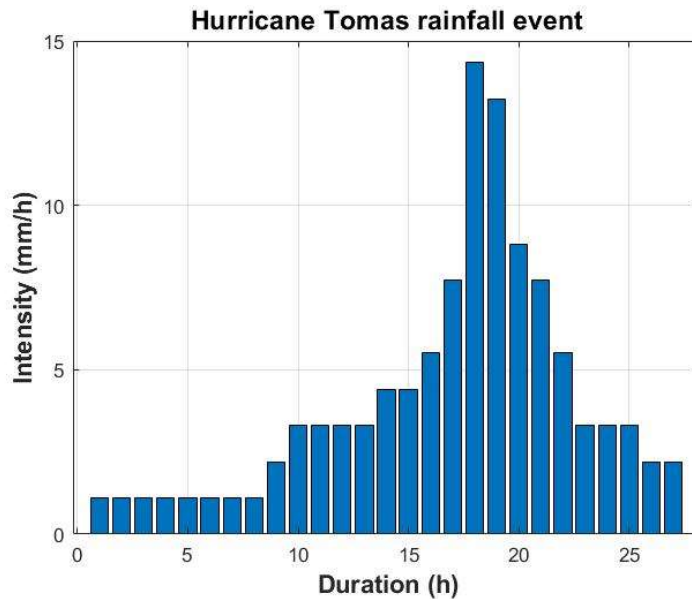


Figure 3.2 Hurricane Tomas rainfall event.

### Hazard inventory

The spatial distribution of landslides and debris flows triggered by Hurricane Tomas within the Soufriere catchment was obtained from the landslide inventory of the British Geological Survey (2014). The landslide inventory was conducted by capturing polygons of the landslides and debris flows from a RapidEye image from 03/01/2011. The landslide inventory and the RapidEye image are available from the CHARIM GeoNode platform: <http://charim-geonode.net/>. However, it was observed that the attributes related to these polygons did not contain any information about the process type, such as landslides or debris flows. Moreover, a disagreement was identified between the spatial projections of the landslide inventory and RapidEye image. The spatial disagreement was overcome by rectifying the landslide inventory corresponding to the British Geological Survey (2014) with the available RapidEye image (Figure B.2). The rectification identified 69 landslides polygons with a total area of 23.58 (ha) and 11 debris flow polygons with a total area of 6.02 (ha) (Figure 3.3)

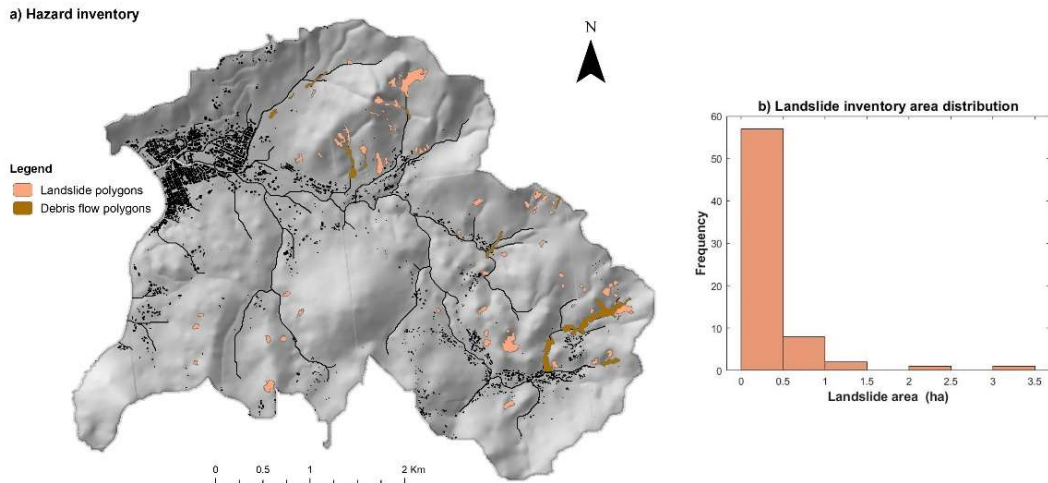


Figure 3.3 Rectified landslide inventory. (a) spatial distribution of landslides areas (b) landslide size distribution.

### 3.2.2 Definition of catchment physical characteristics for multi-hazard modelling

The physical characteristics of the Soufriere catchment were defined according to the datasets available for the OpenLISEM hazard model at: <https://sourceforge.net/projects/lisem/files/Example%20Datasets/>. These open-source spatial datasets contain all the necessary information to define the physical characteristics of the Soufriere catchment and set up OpenLISEM hazard model input parameters related to land use, topography (DEM SRTM), soil type, and soil depth. The dataset is available at a 10 × 10 metres spatial resolution and is spatially referenced in the projected UTM coordinates system WGS84 zone 20N. Based on these datasets, the OpenLISEM hazard model input parameters were defined and grouped into hydrological and geotechnical input parameters (Table 3.2). These are the most relevant input parameters in the OpenLISEM hazard model related to hydrology and slope stability (van den Bout et al. 2018). A characteristic of these input parameters is the variability of their initial values by different multiplication factors set in the OpenLISEM hazard model. Other input parameters exist related to catchment topography (e.g., slope gradient, LDD (local surface drainage direction), channels, catchment boundaries, and surface (roughness and Manning's coefficient)).

### 3.2.3 Setting OpenLISEM hazard model input parameters

The values of the hydrological input parameters corresponded to the original initial values in the available datasets (Table 3.2). However, for the geotechnical input parameters, the value distribution for these input factors was uniform for the entire catchment, without considering their value variability according to the catchment soil types. Therefore, the spatial distribution of the soil cohesion and internal friction angle values was identified according to the geotechnical properties of the soil types in the Soufriere catchment (Appendix B.3). The geotechnical properties were assessed according to Regional Research Laboratory (RRL) (1966) and Shepherd et al. (2019) (Appendix B.3). Other input factors,

such as soil density and grain size, corresponded to the values established in the original datasets. The hydrological and geotechnical input parameter values are summarised as follows:

Table 3.2 OpenLISEM hazard model hydrological and geotechnical input parameter values.

Input factors	Symbol/Unit	Range values			
		Soil layer 1		Soil layer 2	
		min	max	min	max
Soil depth*	(m)	0.05	0.15	0.1	3.6
<b>Hydrological</b>					
Saturated hydraulic conductivity*	$k_s (mm \cdot s^{-1})$	$2.7 \times 10^{-4}$	$4.3 \times 10^{-2}$	$2.4 \times 10^{-4}$	$2.01 \times 10^{-2}$
Suction at the wetting front	$\Psi (kPa)$	40	50	40	50
Saturated moisture content*	$\theta_s (cm^3 \cdot cm^{-3})$	0.2	0.64	0.17	0.55
Initial moisture content	$\theta_i (cm^3 \cdot cm^{-3})$	0.17	0.54	0.14	0.56
<b>Geotechnical</b>					
Soil density	$\rho (kN \cdot cm^{-3})$	2100			
Soil cohesion*	$c' (kPa)$	8 – 80			
Internal friction angle*	$\phi' (^{\circ})$	24 – 60			
Soil grain size*	(m)	0 - 0.0000156			

\*Initial parameter values subject to variation within the OpenLISEM model.

The hydrological input parameter values were spatially distributed according to land use categories (Figure B.3a) and soil types in the Soufriere catchment (Figure B.3b). These input parameters correspond to the saturated hydraulic conductivity ( $k_s$ ) and the saturated moisture content ( $\theta_s$ ) (Figure 3.4). This distribution was derived from the OpenLISEM hazard modelling approach for infiltration, which is based on the Green and Ampt (1911) method for two soil layers (van den Bout et al. 2018). The input parameter value distribution for land use categories was defined for soil layer 1, which corresponds to soil depth 1 (Figure B.4a), and the parameter value distribution for soil types was set for soil layer 2, which corresponds to soil depth 2 (Figure B.4b). Geotechnical parameters such as soil cohesion ( $c'$ ) and soil internal friction angle ( $\phi'$ ) (Figure 3.5), were spatially distributed according to the total soil depth (Table 3.2). This value distribution was derived from the slope stability modelling approach in the OpenLISEM hazard model based on the infinite slope method (van den Bout et al. 2018).

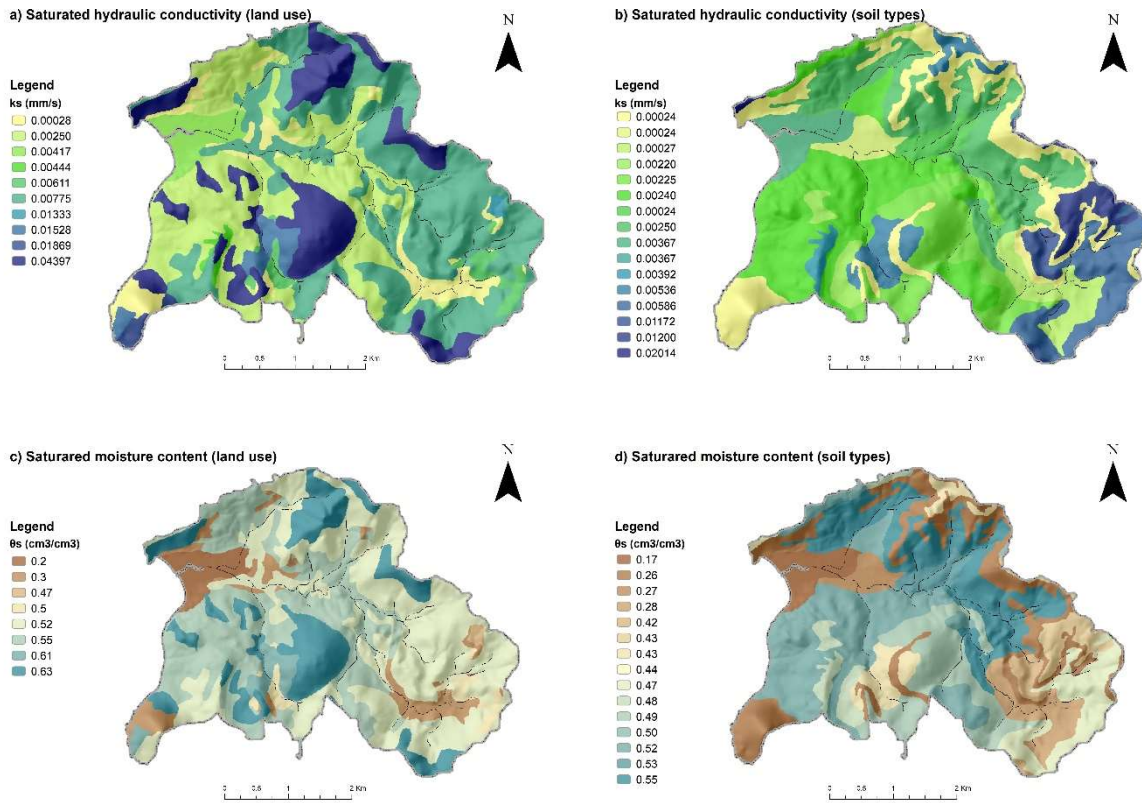


Figure 3.4 Spatial distribution of hydrological input parameter values.

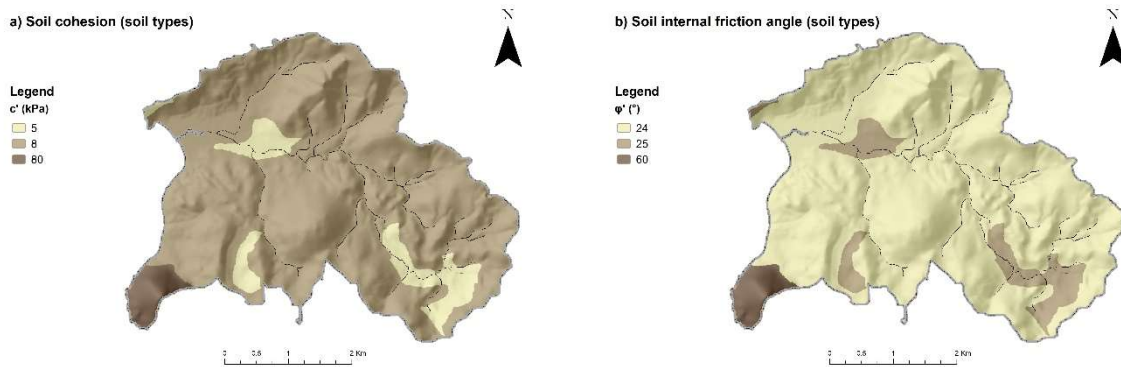


Figure 3.5 Spatial distribution of geotechnical input parameter values.

### 3.2.4 Define input parameter value ranges

The definition of input parameter value ranges was performed by identifying the value distribution of the hydrological and geotechnical input parameters for the Soufriere catchment soil types and land use. The distribution of the input parameter values was estimated using histograms to assess the frequency and identify the minimum and maximum value ranges for saturated hydraulic conductivity ( $k_s$ ), saturated moisture content ( $\theta_s$ ), for land use and soil types and soil cohesion ( $c'$ ) and soil internal friction angle ( $\phi'$ ) for soil types (Figure 3.5). The identified distributions were used to explore the variability in the value distribution ranges of each parameter to assess their sensitivity in the spatial representation of rainfall-triggered landslides, debris flows, and hillslope erosion hazards. The preceding allows for identifying the regions of the value space that might introduce sources of uncertainty in the model outputs, which are expressed in hazard representations of different orders of magnitude.

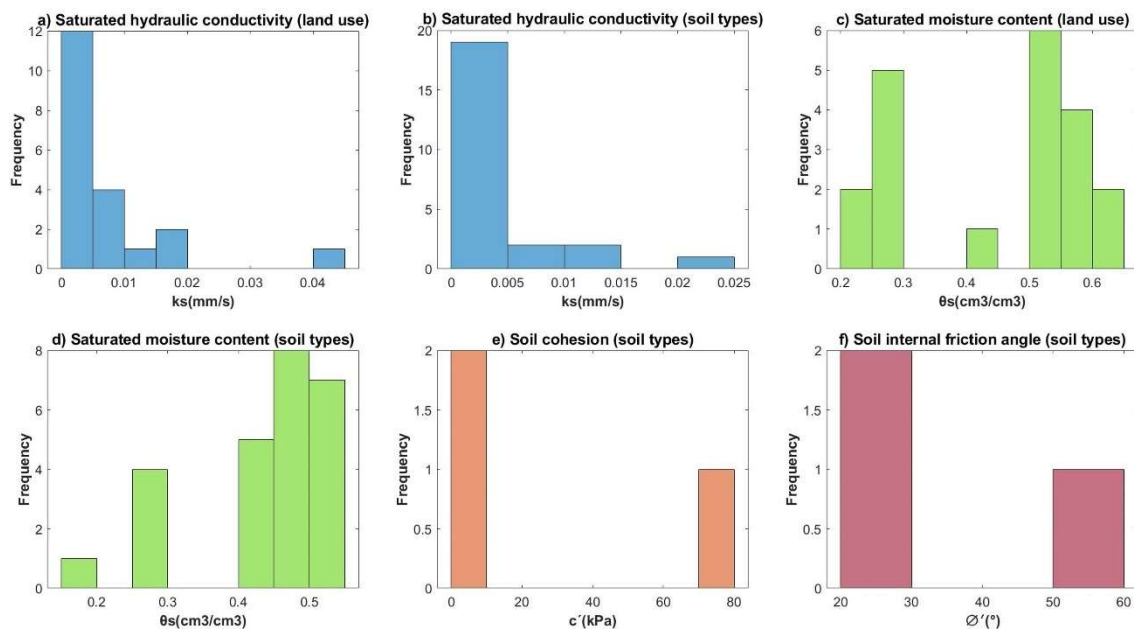


Figure 3.6 Hydrological and geotechnical input parameter value distributions.

To explore the variability in the input parameter value ranges, a scale factor was established to decrease, maintain, and increase the minimum and maximum value ranges of each parameter. The scale factor was defined by setting different multiplication factors for each input parameter. The setting of the multiplication factors is based on the OpenLISEM hazard model structure, which allows the modification of their initial parameter values through multiplication factors (van den Bout et al. 2018). Each multiplication factor modifies the initial hydrological and geotechnical parameter values by changing their values for the soil types and land use in the Soufriere catchment. The foregoing allows the OpenLISEM hazard model setting of the catchment's physical characteristics to identify the most sensitive input parameters that influence the occurrence of hillslope hydrological hazards. The choice of multiplication factors for each input parameter is based on their influence on hillslope hydrology and stability and their maximum variability. A high multiplication factor can increase the initial value of the

parameter, leading to extreme variability in the model outputs. Therefore, the multiplication factors chosen for each input parameter maintained a degree of variability in their initial values that do not lead to extreme model outputs. The scale factors for each input parameter are described as follows:

**Saturated hydraulic conductivity ( $k_s$ ):** The initial value distribution for land use and soil types was maintained by a multiplication factor of (x1.0), decreased by (x0.4), and increased by (x1.2) (Figure 3.6). The decrease in the initial values of ( $ksat$ ) recreates hillslopes that can result in reduced rainfall infiltration rates that can lead to increased hillslope runoff, more channel discharge and increased hillslope erosion and sedimentation in areas with poor soil structure or excessive soil compaction (Usowicz and Lipiec 2021). Instead, an increase in ( $ksat$ ) values implies hillslopes with higher infiltration rates, which can result in lower hillslope runoff generation and increased soil saturation (García-Gutiérrez et al. 2018). When soil becomes saturated the slope stability is reduced, thus, the hillslope becomes more prone to landslides and debris flows (Muntohar and Liao 2010; Yang et al. 2019).

**Saturated moisture content ( $\theta_s$ ):** The initial value distribution for land use and soil types was maintained by a multiplication factor of (x1.0), decreased by (x0.8) and increased by (x1.1) (Figure 3.6). The decrease in the initial values recreates hillslopes with less saturated moisture content, which implies positive pore-water pressures in hillslopes with unsaturated soils that increase soil shear strength and slope stability (Lee and Kim 2021). On the other hand, an increase in recreates saturated hillslopes that influence negative pore-water pressures that reduce soil shear strength and slope stability (Marhaento et al. 2017)

**Soil cohesion ( $c'$ ):** The initial values were maintained by a multiplication factor of (x1.0), decreased by a multiplication factor of (x0.3) and (x0.5) and increased by (x1.2) (Figure 3.6). The decrease in the initial values recreates hillslopes with soils with less shear strength, influencing the reduction in slope stability, and an increase will recreate hillslopes with soils with higher shear strength and stability.

**Soil internal friction angle ( $\phi'$ ):** The initial values were maintained by a multiplication factor of (x1.0), decreased by a multiplication factor of (x0.4) and (x0.6) and increased by (x1.2) (Figure 3.6). The decrease in the initial values recreates hillslopes with soils with less shear resistance to internal stresses, thus reducing slope stability. On the other hand, an increase in recreates hillslopes with soils with higher shear resistance, increasing slope stability (Zhang et al. 2020)

According to Figure 3.7, outliers were identified in the in both saturated hydraulic conductivity values for land use and soil types, and saturated moisture content for soil types. The distribution of outliers is associated with the initial values assigned for soil types and land use in the available dataset for the OpenLISEM hazard model. These values are outside of the overall distribution of the parameter value ranges and that might come from measurement errors and value assignment for each soil type unit and land use category.

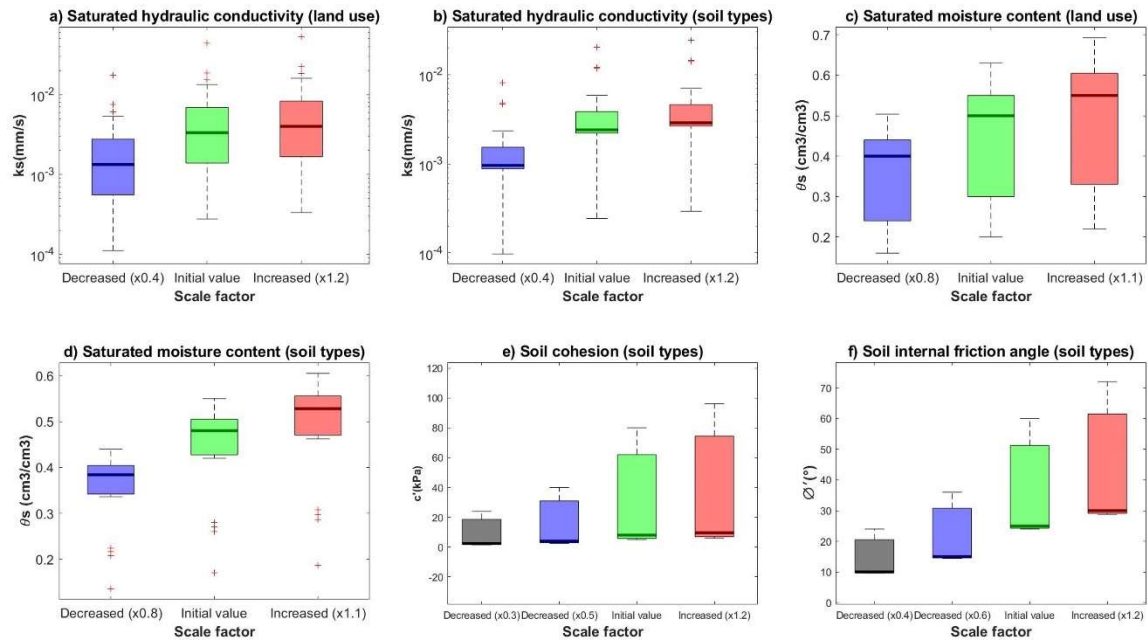


Figure 3.7 Hydrological and geotechnical input parameter value ranges.

### 3.2.5 Designing parametric simulations

The parametric simulations were designed according to the Global Sensitivity Analysis (GSA) method. In this method, uncertainties in the model outputs are influenced by simultaneously varying the values of the model input parameters (Pianosi et al. 2016; Douglas-Smith et al. 2020). Therefore, an ensemble of parametric simulations was designed by creating different parameter-set combinations with different value ranges. The parameter-set combination was performed according to parameter value ranges established by the scale factors defined in Section 3.2.4 for saturated hydraulic conductivity ( $k_s$ ), saturated moisture content ( $\theta_s$ ), for land use and soil types and soil cohesion ( $c'$ ) and soil internal friction angle ( $\phi'$ ) for soil types. The design of parametric simulations allows the identification of parameter-set values that might be behavioural or non-behavioural in reproducing rainfall-triggered landslides, debris flows, and hillslope erosion hazards observed in the Soufriere catchment during Hurricane Tomas. The combination of parameter sets yielded 144 parametric simulations for the OpenLISEM hazard model (Figure B.5). Different user-defined numerical settings were established for slope stability and flow dynamics modelling for the run of the total parametric simulations in the OpenLISEM hazard model (Table B.2). The numerical settings for slope stability are related to the Factor of Safety (FoS) thresholds for slope failure initiation and failure depths (m), and the flow dynamics settings are related to viscosity parameters, entrainment coefficients, and volumetric sediment concentrations for debris flow behaviour in terms of velocity (m/s) and depths (m), and total soil losses (ton).

In the OpenLISEM hazard model, the running of parametric simulations depends on the spatial resolution of the input parameters and duration of the rainfall event. Therefore, according to the duration (1620 min) of the Hurricane Tomas rainfall event defined in Section 3.2.1 and the spatial resolution of the input parameters defined in Section 3.2.2 ( $10 \times 10$  m) for the Soufriere catchment. The simulations



of rainfall-triggered landslides, debris flows, and hillslope erosion hazards were computed in time steps of 10 seconds within the total simulation time. The timestep size should be identical to the data resolution to maintain numerical stability and to model the underlying hydrological and slope stability processes.

### 3.2.6 Hazard representation

The parametric simulations were verified by first identifying the simulations that resulted in the simultaneous simulation of rainfall-triggered landslides, debris flows, and hillslope erosion. Simulations with two or one simulated hazard were discarded from the verification process. The identified parametric simulations were classified into behavioural and non-behavioural, according to the magnitude estimated for each of the simulated hazards. Behavioural simulations were identified by screening the parametric simulations that resulted in the best spatial approximation according to the magnitude estimated for the observed rainfall-triggered landslides and debris flows in the hazard inventory in Section 3.2.1. Therefore, a set of hazard metrics is proposed to screen the parametric simulations whose parameter-set provides the best proximity to the rainfall-triggered landslides and debris flows observed during Hurricane Tomas. These hazard metrics allow an initial assessment of the model's ability to simulate hazard processes and a comparison with the observed hazard magnitude. This is the first step in model verification (internal verification steps using spatial similarity scores, for example, are detailed in Chapter 4).

The proposed hazard metrics were related to the cumulative magnitude of each hazard at the catchment scale in every parametric simulation. In the OpenLISEM hazard model, the magnitude of the simulated hazards corresponds to the cumulative magnitude simulated for every timestep during the total simulation time (van den Bout et al. 2018). For rainfall-triggered landslides, the total landslide surface area ( $A_L$ ) is proposed (Equation 3.1). This equation provides the sum of the landslide surface areas (ha) resulting from the simulation of failure depths (m) within the catchment. The landslide surface area was estimated by selecting pixels with failure depths of greater than 0 metres. For debris flows, the total debris flow runout area ( $A_D$ ) was proposed (Equation 3.2). This equation provides the sum of the simulated debris flow runout areas (ha) within the catchment. The runout area was estimated by selecting pixels in which the debris flow depth was equal to or greater than 0.5 meters. For hillslope erosion, total net erosion ( $Net_E$ ) was proposed (Equation 3.3). This equation provides the net erosion rates ( $ton.m^{-2}$ ). Net erosion was estimated by subtracting the total detached sediment ( $ton.m^{-2}$ ) minus the total amount of deposited sediment ( $ton.m^{-2}$ ) within the catchment. From this equation, a positive value indicates a predominance of erosion, and a negative value indicates a predominance of deposition.

$$A_L = \frac{\sum_{l>1}^N N_A}{100000} \quad \text{Equation 3.1}$$

Where  $N$  are the pixels with failure depths  $> 0$  and  $N_A$  is the pixel area ( $m^2$ )

$$A_D = \frac{\sum_{i \geq 0.5}^N N_A}{100000} \quad \text{Equation 3.2}$$

Where  $N$  are the pixels re the pixels with flood height  $\geq 0.5 m$  and  $N_A$  is the pixel area ( $m^2$ )

$$Net_E = E_T - D_T \quad \text{Equation 3.3}$$

Where  $E_T$  correspond to the total detached soil ( $ton$ ) and  $D_T$  correspond to the total deposited soil ( $ton$ ).

### 3.3 Results

#### 3.3.1 Responsiveness parametric simulations

According to the total parametric simulations (144 simulations), only 54 resulted in the simultaneous simulation of rainfall-triggered landslides, debris flows, and hillslope erosion hazards. These simulations were concentrated from simulations 1 to 54 (Figure 3.8). On the other hand, 90 simulations resulted only in debris flow and hillslope erosion simulations, with no landslide simulations. These simulations were concentrated from simulations 55 to 144 (Figure 3.8). Therefore, these simulations were screened out from the process of identifying and selecting parametric simulations that obtained the closest representation to the observed hazards identified in the hazard inventory. The parametric simulations that resulted in the simultaneous simulation of these three hazards, that is, simulations 1–54, were classified as behavioural and non-behavioural according to the total magnitude result for each hazard within the Soufriere catchment. The total magnitude was estimated by assessing the total landslide surface area ( $A_L$ ), debris flow runout area ( $A_D$ ), and net erosion ( $Net_E$ ) according to the hazard metrics proposed in Section 3.2.6.

According to the magnitude results, non-behavioural simulations were identified according to the total landslide surface area ( $A_L$ ), this metric was chosen as allows the comparison with the total landslide surface area ( $A_{INV}$ ) observed in the hazard inventory. Therefore, parametric simulations with total landslide surface area ( $A_L$ )  $\geq 1000 ha$  and ( $A_L$ )  $\geq 100 < 1000 ha$  were identified as non-behavioural as their total magnitude do not approach the total landslide surface area ( $A_{INV}$ ) (23.6 ha) observed for Hurricane Tomas. From these results, 27 parametric simulations were identified as non-behavioural, 9 with total landslide surface area ( $A_L$ )  $\geq 1000 ha$  and 18 with total surface areas ( $A_L$ )  $\geq 100 < 1000 ha$ . From these simulations, it was possible to observe the impacts of the debris flow runout area ( $A_D$ ), and total net erosion ( $Net_E$ ). For example, simulation 3 registered the highest landslide surface area ( $A_L$ ) with (1275.3 ha), for the same simulation the total debris flow runout area ( $A_D$ ) reached (1190.6 ha) and the net erosion ( $Net_E$ ) the (-165605  $ton.m^{-2}$ ). From these results, the magnitude of rainfall-triggered landslides clearly impacted the magnitude of the simulated debris flow and, thus, the magnitude of hillslope erosion rates. This indicates that the landslide volume material and the debris flow runout deposition material increase the net erosion rates when these hazards occur simultaneously.

This trend was observed for all the identified non-behavioural simulations. For example, for simulations with total landslide surface areas ( $A_L$ )  $\geq 100$  and  $< 1000$  ha, the lowest surface area was identified in simulation number 36, with a total area ( $A_L$ ) of 112.8 ha. Within this simulation, the debris flow runoff area ( $A_D$ ) and net erosion ( $Net_E$ ) were reduced to 36.8 ha and  $-6298.2 \text{ ton.m}^{-2}$  respectively. The parameter-set value combination for the total identified non-behavioural simulations provided model outputs that were far from representing the rainfall-triggered landslides and debris flows registered for the hazard inventory. Therefore, the parameter value ranges determined for these sets of parameters introduced the biggest source of uncertainty in the model outputs expressed in unrealistic hazard magnitudes.

From the total of parametric simulations, 27 simulations were identified as behavioural. This corresponds to simulations whose total landslide surface areas ( $A_L$ ) were between  $> 1$  and  $\leq 100$  ha, as their total magnitudes are close to the total landslide surface area ( $A_{INV}$ ) (23.6 ha) identified for Hurricane Tomas. From the total behavioural simulations, six simulations were screened out as their total surface areas were between 0 and 1 ha. Therefore, their magnitudes were too small for comparison and verification. The total landslide surface areas ( $A_L$ ) of the identified behavioural simulations were compared with the total areas ( $A_{INV}$ ) of rainfall-triggered landslides (23.6 ha) estimated for the hazard inventory to identify proximities between simulated and observed magnitudes. From this comparison, it was determined that the closest proximities resulted in six parametric simulations. These corresponded in order from less to the closest proximity to simulation numbers 29, 19, 35, 32, and 25 y 22 (Figure 3.8). For the rest of behavioural simulations, the resulting total landslide surface area ( $A_L$ ) was below the observed total landslide inventory surface area ( $A_{INV}$ ). For simulations 29, 19, 35, and 32 the total landslide surface areas ( $A_L$ ) were overpredicted in magnitude by almost 50 ha in relation to the 23.6 ha observed in the hazard inventory ( $A_{INV}$ ). However, only simulations 22 and 25 resulted in the closest proximity to the total landslide inventory surface area ( $A_{INV}$ ), registering 23.1 and 23.2 ha, respectively.

In relation to the total debris flow runoff area ( $A_D$ ), the identified behavioural simulations were also compared with the observed total runoff area estimated from the hazard inventory (Figure 3.8). For simulations 29, 19, 35, and 32, the resulting total debris flow runoff area ( $A_D$ ) was overpredicted by almost 20 ha compared to the 6.02 ha registered in the hazard inventory ( $A_{INV}$ ). However, only simulations 22 and 25 registered total debris flow runoff area ( $A_D$ ) below to the estimated in the hazard inventory with 3.8 and 0.4 ha, respectively. From these simulations, simulation 22 registered the closest proximity to the debris flow runoff area for the hazard inventory. According to total net erosion ( $Net_E$ ) registered for the identified behavioural simulations, simulation numbers 29, 19, 35, 32 obtained total net erosion rates ( $Net_E$ )  $\geq -792.1 \text{ (ton.m}^{-2}\text{)}$  with simulation 29, 32 and 35 with the highest values. In relation to simulation 22 and 25, their result showed total net erosion ( $Net_E$ ) of  $-240.4$  and  $-197.7 \text{ (ton.m}^{-2}\text{)}$  respectively.

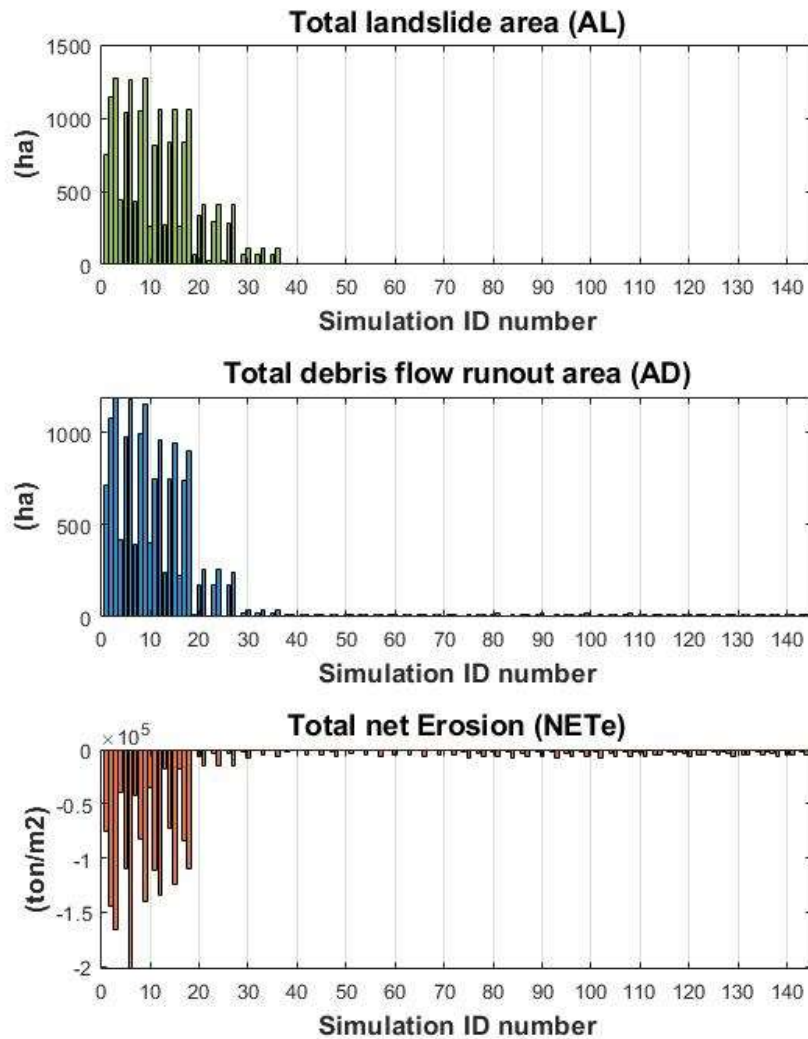


Figure 3.8 Overall responsiveness of the catchment to the simulated 'Hurricane Tomas' rainfall forcing for each of the 144 parameter dataset combinations. Hazard magnitudes are indicated in terms of (a) total landslide surface area, (b) total debris flow runout area, (c) total net erosion rates.

### 3.3.2 Hazard representation

Figure 3.9 illustrates the total landslide surface areas ( $A_L$ ) resulting from the total parametric simulations performed. The behavioural simulations identified in Section 3.4.1 are highlighted in greyscale to identify their parameter-set combinations and their resulting magnitudes. The most significant landslide surface areas ( $A_L \geq 100$  and  $< 1200$  ha) were registered in simulations in which the saturated moisture content values were reduced by multiplication factors by (x0.8), maintained by (x1.0) and increased by (x1.1) and the saturated hydraulic conductivity values were reduced by (x0.4), maintained by (x1.0) and increased by (x1.2) (see Table B.3 and Table B.4 for values for land use categories and soil types). The magnitude of these areas also resulted from a reduction of the soil cohesion values by (x0.3) and a reduction of the soil internal friction angle values by (x0.4) and (x0.6), respectively (see Table B.5).

However, according to the estimation of the total landslide surface area ( $A_L$ ), these results do not look realistic as the landslide areas were overpredicted in size regarding to the total landslide surface area ( $A_{INV}$ ) (23.6 ha) identified for Hurricane Tomas. It was observed that total landslide surface areas ( $A_L$ )  $> 10$  and  $< 100$  ha on simulations in which the saturated moisture content and the saturated hydraulic conductivity values were also reduced, maintained, and increased by the mentioned multiplication factor (see Figure 3.4). However, unlike the results above, these landslide surface areas were simulated with a reduction of the soil cohesion values by (x0.3) but maintaining the soil internal friction angle values by (x1.0) and increasing its values by (x1.2) (see Table B.5 and Figure 3.7).

A significant reduction in the total landslide areas ( $A_L$ )  $< 10$  ha was observed in simulations that reduced the saturated moisture content values by (x0.8) (see Table B.3 and Table B.4). These landslide surface areas ( $A_L$ ) were also simulated with reduced, maintained, and increased saturated hydraulic conductivity values. These landslide areas were reduced in simulations in which the soil cohesion values were reduced, and the soil internal friction angle was increased by (x1.2) (see Table B.5). Finally, the landslide areas ( $A_L$ )  $< 10$  ha were also observed in simulations in which the saturated moisture content and saturated hydraulic conductivity reduced, maintained, and increased their initial values but in which the soil cohesion was reduced by (x0.5) and the soil internal friction angle was reduced by (x0.4) and (x0.6) (see Table B.5 and Figure 3.7). No simulated landslides were obtained when the soil cohesion values were maintained by (x1.0) and increased by (x1.2) (see Table B.5 and Figure 3.7).

Figure 3.10 shows the total debris flow runout areas ( $A_D$ ) estimated for the total behavioural simulations. It was identified that the more significant debris flow flooded areas ( $A_D$ )  $\geq 100$  and  $< 1200$  ha were registered within the same simulations in which the landslide surface areas ( $A_L$ ) were overestimated. On the other hand, total debris flow runout areas ( $A_D$ )  $> 20$  and  $< 100$  ha were identified in simulations in which the landslide surface area ( $A_L$ ) was  $> 10$  and  $< 100$  ha. For the case of simulations with no landslide simulation, the total debris flow runout areas ( $A_D$ ) were  $< 20$  ha. According to this, the magnitude of the debris flows was influenced by the erosional material entrained by the flow. Under this condition, the extensive total debris flow runout areas ( $A_D$ ) between 15 and 16 ha were registered in simulations in which the saturated moisture content was increased by (x1.1) (see Table B.3 and Table B.4). In simulations in which the saturated moisture content maintained its values by (x1.0), the total debris flow runout areas ( $A_D$ ) was between 6 and 11 ha and in simulations in which the saturated moisture content values were decreased total debris flow runout areas ( $A_D$ ) was between 5 and 1 ha. These debris flow flooded areas ( $A_D$ ) were simulated with reduced, maintained, and increased saturated moisture content and saturated hydraulic conductivity values.

Figure 3.11 illustrates the total net erosion ( $Net_E$ ) for the total behavioural simulations. The most extensive rates were also registered in simulations with large total landslide surface areas ( $A_L$ ) total debris flow runout areas ( $A_D$ ). Within these simulations, the results indicate mostly high deposition rates  $> -17673.62$  ( $ton.m^{-2}$ ). It was observing a reduction in the net erosion rates with deposition values  $< -14708.88$  ( $ton.m^{-2}$ ). These values were reduced in simulations in which the total landslide surface areas ( $A_L$ ) and total debris flow runout areas ( $A_D$ ) reduced their areas. In simulations in which no landslides were simulated, the net erosion rates were maintained steady, especially in simulations in

which the soil cohesion was maintained by (x1.0) and increased by (x1.2) in its values (see Table B.5 and Figure 3.7), and the soil internal friction angle values were decreased, maintained, and increased. The higher deposition rates were registered in simulations in which saturated moisture content values were increased by (x1.1), and the lowest was registered in simulations that maintained the saturated moisture content by (x1.0) and decreased by (x0.8) (see Table B.3 and Table B.4)

**a) Total landslide surface area ( $A_L$ ) (ha)**

		Slope hydrology									
		$k_s$ (mm. h <sup>-1</sup> )			$k_s$ (mm. h <sup>-1</sup> )			$k_s$ (mm. h <sup>-1</sup> )			
		(x0.4)			(x1.0)			(x1.2)			
		$\theta_s$ (cm <sup>3</sup> . cm <sup>-3</sup> )			$\theta_s$ (cm <sup>3</sup> . cm <sup>-3</sup> )			$\theta_s$ (cm <sup>3</sup> . cm <sup>-3</sup> )			
Slope stability	$c'$ (kPa)	$\phi'$ (°)	(x0.8)	(x1.0)	(x1.1)	(x0.8)	(x1.0)	(x1.1)	(x0.8)	(x1.0)	(x1.1)
	(x0.3)	(x0.4)	754.7	1139.3	1275.3	445.2	1039.3	1259.4	430.6	1044.7	1273.6
		(x0.6)	258.4	818.2	1055.7	270.1	830.3	1053.8	263.3	832.9	1054.4
		(x1.0)	69.3	330.2	410.3	23.1	287.6	410.0	23.2	285.8	410.2
		(x1.2)	4.1	74.0	115.0	1.7	65.2	113.7	1.8	66.6	112.8
	(x0.5)	(x0.4)	1.9	7.3	9.2	1.4	6.1	9.6	1.3	6.3	9.7
		(x0.6)	0.0	0.4	1.1	0.0	0.1	1.0	0.0	0.2	1.1
		(x1.0)	0.0	0.0	0.0	0.0	0.0	0.0	0.0	0.0	0.0
		(x1.2)	0.0	0.0	0.0	0.0	0.0	0.0	0.0	0.0	0.0
	(x1.0)	(x0.4)	0.0	0.0	0.0	0.0	0.0	0.0	0.0	0.0	0.0
		(x0.6)	0.0	0.0	0.0	0.0	0.0	0.0	0.0	0.0	0.0
		(x1.0)	0.0	0.0	0.0	0.0	0.0	0.0	0.0	0.0	0.0
		(x1.2)	0.0	0.0	0.0	0.0	0.0	0.0	0.0	0.0	0.0
	(x1.2)	(x0.4)	0.0	0.0	0.0	0.0	0.0	0.0	0.0	0.0	0.0
		(x0.6)	0.0	0.0	0.0	0.0	0.0	0.0	0.0	0.0	0.0
		(x1.0)	0.0	0.0	0.0	0.0	0.0	0.0	0.0	0.0	0.0
		(x1.2)	0.0	0.0	0.0	0.0	0.0	0.0	0.0	0.0	0.0

**Simulations**

- N°19
- N°22
- N°25
- N°29
- N°32
- N°35

Figure 3.9 Hazard representation: (a) total landslide surface area.

**b) Total debris flow runout area ( $A_D$ ) (ha)**

		Slope hydrology									
		$k_s$ (mm. h <sup>-1</sup> )			$k_s$ (mm. h <sup>-1</sup> )			$k_s$ (mm. h <sup>-1</sup> )			
		(x0.4)			(x1.0)			(x1.2)			
		$\theta_s$ (cm <sup>3</sup> . cm <sup>-3</sup> )			$\theta_s$ (cm <sup>3</sup> . cm <sup>-3</sup> )			$\theta_s$ (cm <sup>3</sup> . cm <sup>-3</sup> )			
Slope stability	$c'$ (kPa)	$\phi'$ (°)	(x0.8)	(x1.0)	(x1.1)	(x0.8)	(x1.0)	(x1.1)	(x0.8)	(x1.0)	(x1.1)
	(x0.3)	(x0.4)	712.1	1077.5	1190.6	419.8	976.1	1178.2	390.2	992.1	1151.6
		(x0.6)	403.8	749.0	955.8	237.9	744.0	938.4	227.5	741.2	902.5
		(x1.0)	9.4	173.8	257.4	3.8	170.4	257.4	0.4	170.5	237.9
		(x1.2)	1.4	21.1	39.6	0.1	22.3	41.3	0.2	24.2	36.8
	(x0.5)	(x0.4)	1.1	10.9	16.1	0.1	11.5	16.1	0.0	10.7	15.9
		(x0.6)	0.9	10.9	16.1	0.1	10.7	15.9	0.0	10.2	16.0
		(x1.0)	0.9	10.1	16.0	0.1	10.8	16.1	0.0	9.8	16.1
		(x1.2)	0.9	10.1	16.0	0.1	10.8	16.1	0.0	9.8	16.1
	(x1.0)	(x0.4)	0.9	6.8	15.8	0.1	11.1	15.4	0.1	10.0	16.9
		(x0.6)	0.9	6.8	15.8	0.1	11.1	15.4	0.1	10.0	16.9
		(x1.0)	0.9	6.8	15.8	0.1	11.1	15.4	0.1	10.0	16.9
		(x1.2)	0.9	6.8	15.8	0.1	11.1	15.4	0.0	10.0	16.9
	(x1.2)	(x0.4)	1.2	9.4	15.7	0.3	8.8	14.8	0.2	10.2	15.3
		(x0.6)	1.2	9.4	15.7	0.3	8.8	14.8	0.2	10.2	15.3
		(x1.0)	1.2	9.4	15.7	0.3	8.8	14.8	0.2	10.2	15.3
		(x1.2)	1.2	9.4	15.7	0.3	8.8	14.8	0.2	10.2	15.3

**Simulations**

- N°19
- N°22
- N°25
- N°29
- N°32
- N°35

Figure 3.10 Hazard representation. (b) total debris flow runout area.

**c) Total net erosion ( $Net_E$ ) ( $ton \cdot m^{-2}$ )**

		Slope hydrology									
		$k_s$ ( $mm \cdot h^{-1}$ )			$k_s$ ( $mm \cdot h^{-1}$ )			$k_s$ ( $mm \cdot h^{-1}$ )			
		(x0.4)	(x1.0)	(x1.1)	(x0.8)	(x1.0)	(x1.1)	(x0.8)	(x1.0)	(x1.1)	
		$\theta_s$ ( $cm^3 \cdot cm^{-3}$ )			$\theta_s$ ( $cm^3 \cdot cm^{-3}$ )			$\theta_s$ ( $cm^3 \cdot cm^{-3}$ )			
Slope stability	$c'$ (kPa)	$\phi'$ (°)	(x0.8)	(x1.0)	(x1.1)	(x0.8)	(x1.0)	(x1.1)	(x0.8)	(x1.0)	(x1.1)
	(x0.3)	(x0.4)	-75737.7	-143614.3	-165695.4	-39538.9	-109119.4	-202430.1	-41788.6	-83084.6	-140053.0
		(x0.6)	-35278.4	-110855.3	-134338.4	-17673.6	-73193.3	-123881.4	-17979.4	-84245.6	-110526.5
		(x1.0)	-792.1	-6971.8	-14679.7	-240.4	-3812.3	-14679.7	-197.7	-4177.9	-14708.9
	(x0.5)	(x1.2)	-491.1	-1600.4	-7341.9	-213.1	-1306.2	-5337.6	-253.5	-1193.9	-6298.2
		(x0.4)	-343.1	-1540.8	-1037.9	-190.1	-1037.9	-5487.5	-161.6	-1001.9	-4366.7
		(x0.6)	-406.3	-1442.6	-6493.7	-126.2	-831.1	-4285.0	-127.9	-976.5	-4386.6
	(x1.0)	(x1.0)	-378.9	-1372.6	-6123.8	-128.1	-936.8	-4850.3	-116.1	-850.1	-5113.4
		(x1.2)	-378.9	-1372.6	-6123.8	-128.1	-936.8	-4850.3	-116.1	-850.1	-5113.4
		(x0.4)	-326.5	-2860.8	-8207.9	-144.7	-2953.2	-7091.0	-136.2	-2812.8	-6718.4
	(x1.2)	(x0.6)	-326.5	-2860.8	-8207.9	-144.7	-2953.2	-7091.0	-136.2	-2812.8	-6718.4
		(x1.0)	-326.5	-2860.8	-8207.9	-144.7	-2953.2	-7091.0	-136.2	-2812.8	-6718.4
		(x1.2)	-326.5	-2860.8	-8207.9	-144.7	-2953.2	-7091.0	-136.2	-2812.8	-6718.4
	(x1.2)	(x0.4)	-1890.6	-3689.4	-5997.9	-995.3	-5300.3	-4311.8	-995.3	-2271.4	-4391.2
		(x0.6)	-1890.6	-3689.4	-5997.9	-995.3	-5300.3	-4311.8	-995.6	-2271.4	-4391.2
		(x1.0)	-1890.6	-3689.4	-5861.0	-995.3	-5300.3	-4311.8	-995.3	-2271.4	-4391.2
		(x1.2)	-1873.2	-3689.4	-5997.9	-995.3	-5300.3	-4311.8	-995.3	-2271.4	-4391.2

**Simulations**

Figure 3.11 Hazard representation. (c) total net erosion.

## 3.4 Discussion

### 3.4.1 Responses of parametric simulations

The quantification of the landslide surface area ( $A_L$ ), total debris flow runout area ( $A_D$ ) and the total net erosion rates ( $Net_E$ ) through the established hazard metrics allowed to screen 54 behavioural with the three simultaneous hazards representation and 90 non-behavioural simulations with only debris flows and hillslope erosion with no landslide representation. Identifying these simulations is essential because it identifies the parameter-set that resulted in a close approximation to the hazards registered during Hurricane Tomas. The foregoing allowed the assessment of the impacts of uncertainty within the parameter-set for the total of parametric simulations, allowing to screen out the parameter-set that does not reproduce rainfall-triggered landslides, debris flows and hillslope erosion hazards. The designing of the total of parametric simulations following a Global Sensitivity Analysis (GSA) approach was essential to identify the parameter-set combinations with more proximity to the hazard in the inventory. For example, from the results, parametric simulations with total landslide surface area ( $A_L$ )  $\geq 1000$  ha and ( $A_L$ )  $\geq 100 < 1000$  ha were identified as non-behavioural as their total magnitude do not approach the total landslide surface area ( $A_{INV}$ ) (23.6 ha) estimated in the hazard inventory. Therefore, Global Sensitivity Analysis (GSA) provides a comprehensive view of the sensitivity and influence of changes in the input parameter values on the model outputs expressed in the magnitude resulting for each hazard (Almeida et al. 2017; Yildiz et al. 2023). According to Lari et al. (2014) by quantifying these sensitivities in terms of hazard magnitudes, global sensitivity analysis can help researchers and practitioners better understand the uncertainties and variability in model outputs.

This is essential in multi-hazard modelling because uncertainty can affect the accuracy of hazard predictions, the understanding of hazard interrelationships, and the identification of potential vulnerabilities in the face of multiple hazards (Almeida et al. 2017; Tilloy et al. 2019; Visser-Quinn et al.

2019). The first stage of the modelling workflow adequately addressed and quantified these uncertainties to ensure that the selected multi-hazard model (The OpenLISEM hazard model) provided robust and reliable results in the representation and interaction of rainfall-triggered landslides, debris flows, and hillslope erosion hazards. Consequently, the comparison of the hazard magnitudes related to total landslide surface area ( $A_L$ ) and debris flow runout area ( $A_D$ ) with the total inventory area ( $A_{INV}$ ) estimated for the rainfall-triggered landslides and debris flow registered from Hurricane Tomas allowed the identification of behavioural simulations with closer proximity to the observed hazards. The identification of simulations 29, 19, 35, 32, and 25 y 22 as “behavioural” as their results in terms of hazard magnitudes were within the equifinality criteria to identify behavioural simulations.

The behavioural simulations with more proximity to the hazard inventory was detected in simulations 22 and 25. For these simulations, the total landslide surface area ( $A_L$ ), corresponded to 23.08 ha and 23.02 ha respectively, which is proximate to the 23.58 ha ( $A_{INV}$ ) estimated in the landslide areas registered in the hazard inventory. The same approximation was observed for the total debris flow runout area ( $A_D$ ), in which simulation 22 obtained the most proximate area to the 60.2 ha ( $A_{INV}$ ) estimated to the debris flow area in the hazard inventory with 3.77 ha, respectively. Regarding the total net erosion rates ( $Net_E$ ), simulations 22 and 25 obtained -240.4 and -197.7 ( $ton.m^{-2}$ ) respectively, which mainly correspond to deposition rates. However, no information was available in the hazard inventory. Studies such as Bégin et al. (2014), have identified that, as a consequence of Hurricane Tomas, the Soufriere catchment has increased sediment deposition rates by 35 %.

According to Beven and Freer (2001) and Khatami et al. (2019) the incorporation of the equifinality principle implies the development of methods to identify the set of parameters that can reproduce or explain observed data, considering the uncertainty in input parameters. For example, this suggests that multi-hazard models such the OpenLISEM hazard model can be parameterized in a variety of ways while still yielding results that are equivalent in terms of predictions or probability measures (Refsgaard 1997; van den Bout 2020). By considering equifinality, multi-hazard models can be parameterised in accordance with various procedures, enabling a more varied and thorough investigation of potential model representations (Fan et al. 2021). The development and application of the first stage of the modelling workflow contributed to exploring the parameter-set combinations that resulted in behavioural and non-behavioural representations of the hazards observed during Hurricane Tomas. According to Beven et al. (2018); Tilloy et al. (2019) and Gill et al. (2020), the development of strategies that handle the uncertainties that arise from the complexities in multi-hazard modelling related to the number of input parameters and data quality, multi-hazard models can better capture the inherent uncertainties and complexities of hazard interactions acknowledging that hazards do not operate in isolation and that their interactions can be complex and dynamic. By parameterizing multi-hazard models such as the OpenLISEM hazard model, researchers and policymakers can better quantify and analyse the combined effects from multiple hazards, which can help in making informed decisions for disaster risk reduction policies and land use planning to mitigate the impacts of these hazards for different climate and land use scenarios (van Vliet et al. 2016; Williams et al. 2020).



### 3.4.2 Parameters affecting hazard representations

The setting of parametric simulations highlighted the effect of the data quality on the results of hazard representations. The variety of rainfall-triggered landslides, debris flows, and hillslope erosion magnitudes obtained within the first 54 simulations indicated the manifestation of the uncertainties in the input parameters values. According to Mergili et al. (2017) and Van den Bout et al. (2021), the spatial representation of landslides and debris flows is highly influenced by the uncertainty introduced by the spatial resolution and hydrological and geotechnical input parameter values. For the case of the Soufriere catchment, the spatial resolution of the hydrological and geotechnical input parameters (10 x 10 metres) allowed a good response of the OpenLISEM hazard model to represent these hazards considering the catchment scale and the Hurricane Tomas rainfall duration (27-hours). On the other hand, setting scaling factors for each input parameter to vary their initial values to recreate the slope hydrological and geotechnical conditions of the Soufriere catchment allowed the identification of the input parameters value ranges that influenced the representation of the hazard registered during Hurricane Tomas. The mentioned above reduced the effects of uncertainty which according to Beven and Binley (1992) and Refsgaard (1997) is a characteristic within spatially distributed modelling due to their ability to vary the number of parameter values within the model domain.

Hence, the setting of scaling factors within the first stage of the modelling workflow is essential to manage the maximum variation of input parameter value ranges. A method that establishes the limits of the input parameter value range variability helps to identify the variation space for each input parameter that influences the representation and magnitude of landslides, debris flows and hillslope erosion. Under this approach, it was identified that the landslide surface areas > 1000 ha were influenced by the reduction of soil cohesion values by (x0.3) (see Table B.5), the reduction of soil internal friction angle by (x0.4) (see Table B.5), and the initial saturated moisture content values by (x1.0) and increased by (x1.1) (see Table B.3). On the other hand, it was observed that the landslide surface areas < 10 ha were influenced by the reduction of soil cohesion by (x0.3) and (x0.5) and the initial soil internal friction angle by (x1.0) and increased by (x1.1) (see Table B.5). No landslides were simulated with the reduction of soil cohesion by (x0.5) and with the initial soil internal friction angle by (x1.0) and increased by (x1.2) (see Table B.5). Nevertheless, the landslide area increased with increased saturated moisture content values by (x1.1), and it was reduced with reduced values by (x0.8) (see Table B.3). Concerning the saturated hydraulic conductivity values, the landslide magnitude showed the same pattern for reduced, initial, and increased values.

The response of the OpenLISEM hazard model to the simulated landslides clearly influenced the debris flow magnitude and erosion rates. Studies such as von Ruetten et al. (2016); Fan et al. (2017) and Van den Bout et al. (2018) have identified that landslides location and volumes influence debris flow runout distances increasing the hillslope entrainment (erosion) and deposition of material in runout pathways. For the case of the Soufriere catchment, it was identified the same pattern, especially in parametric simulations with the simultaneous representation of rainfall-triggered landslides, debris flows and hillslope erosion.

Identifying the input parameter value ranges resulting from the scaling factors helps us understand under which parameter value combination of the parameter set for every behavioural simulation will reproduce realistic or unrealistic results. This is an important step within the model parameterisation in which recognising the suitable parameter value combination that is in some sense optimal to represent rainfall-triggered landslides, debris flows, and hillslope erosion could improve the representation of any of these hazards and provide a good fit with observations. This improves not only the individual representation of these hazards but also the assessment of their interactions (Gill and Malamud 2014; Van den Bout et al. 2018). Overall, these findings demonstrate that the response of the OpenLISEM hazard model in representing these hazards is not only influenced by the parameter-set established for every behavioural simulation but also by the quality and resolution of input parameters.

### 3.5 Conclusions

The application of the first stage of the modelling workflow developed in this chapter addresses and answers the first research question of this thesis (RQ1: *What are the physical characteristics of catchments that drive hillslope hydrological multi-hazards and their interactions?*). The design of parametric simulations following a Global Sensitivity Analysis (GSA) approach allowed the exploration of parameter-set combinations that provided behavioural and non-behavioural representations of rainfall-triggered landslides and debris flows that occurred during Hurricane Tomas. A total of 54 parametric simulations with simultaneous representations of rainfall-triggered landslides, debris flows, and hillslope erosion and another 90 with only debris flows and hillslope erosion representations with no landslide simulation were conducted. Simulations 19, 22, 25, 29, 32, and 35 were identified as behavioural simulations, which resulted in closer proximity to the magnitudes of the rainfall-triggered landslides and debris flows registered from Hurricane Tomas.

The application of hazards metrics such as the total landslide surface area ( $A_L$ ), debris flow runout area ( $A_D$ ), and net erosion ( $Net_E$ ) quantified the magnitude of each hazard for every parametric simulation. The foregoing contributed to screen out the parametric simulation with biggest uncertainties in their outputs, this is total landslide surface area ( $A_L$ ) was  $\geq 1000 \text{ ha}$ , total debris flow runout area ( $A_D$ )  $\geq 9000 \text{ ha}$  and total net erosion ( $Net_E$ )  $\geq -100000 \text{ ton.m}^{-2}$ . The hazard metrics identified parametric simulations that reflected more uncertainty in their results, as their hazard magnitudes did not represent the magnitude of the rainfall-triggered landslides and debris flows registered in the hazard inventory. In addition, it contributed to identifying the behavioural simulations that resulted in the best approximation of the observed hazards in the inventory. The application of an equifinality approach to identify behavioural simulations allowed identify spatial patters related to area difference and surface area between the simulated and observed hazards.

Behavioural simulations 22 and 25 were identified with the closest proximity to rainfall-triggered landslides and debris flows registered in Hurricane Tomas. Both simulations obtained a total landslide surface area ( $A_L$ ) of 23.08 ha and 23.02 ha (23.58 ha in the hazard inventory) and a total debris flow runout area ( $A_D$ ) of 3.8 and 0.4 ha (6.02 ha in the hazard inventory). Regarding the total net erosion

rates ( $Net_E$ ), simulations 22 and 25 obtained -240.4 and -197.7 ( $ton.m^{-2}$ ) respectively. Therefore, the initial and increased by (x1.2) parameter value range of saturated hydraulic conductivity values for land use and soil type, the reduced saturated moisture content values by (x0.8) for land use and soil types, the reduced soil cohesion values by (x0.3) for soil types, and the initial soil internal friction angle values represented the physical characteristics of Soufriere catchment that drove hillslope hydrological hazard interactions during Hurricane Tomas.

After the results obtained from the application of the first stage of the modelling workflow for this chapter. The next stage is to verify and select the identified behavioural simulations with the best proximity to the hazard observed for Hurricane Tomas. This will be addressed in chapter IV where an internal verification and parameter-set selection based on spatial similarity scores and sensitivity analysis will carry out. The aim is to select the parameter-set that will be applied in the forward exploration of climate and land use change scenarios in the Soufriere catchment.

---

---

**Chapter 4 Developing the workflow for model  
verification and investigation of catchment response to  
climate and land use change**

---

---

## 4.1 Introduction

This chapter develops and applies the second and third stages of the modelling workflow proposed in Chapter 2, sections 2.3.2 and 2.3.3 respectively. The aim of the second stage of the modelling workflow is to verify the parametric simulations performed in Chapter 3 and select the parameter-set considered “behavioural” in representing the hazards triggered by Hurricane Tomas in the Soufriere catchment under an equifinality approach. According to the selected parameter-set, the most sensitive hydrological and geotechnical input parameters for soil type units and land use categories were assessed to identify the most influential input parameter value ranges in the representation of the modelled hazards for the Soufriere catchment. Then, the third stage of the modelling workflow is applied to explore climate and land use scenarios according to the identified sensitive input parameter values of the selected parameter-set in order to assess their response in hazard representation and magnitudes according to different rainfall events. Therefore, the application of the second and third stages of the modelling workflow will allow the addressing of the second research question of this thesis:

### **RQ2 What is the influence of catchment parameter variations and uncertainties on multi-hazard assessments?**

The verification and selection of the behavioural simulations with the parameter-set that best represents the rainfall-triggered landslides and debris flow from the hazard inventory (3.2.1) is a crucial step in assessing the reliability and robustness of the input parameter values estimated from different data sources, especially when applying physically based multi-hazard models in data-limited locations. The preceding reduces the impacts of uncertainty in the model outputs normally expressed in hazard representations of different orders of magnitude, as identified in section 3.3.1, Chapter 3. Verifying the model outputs under an equifinality approach allows for the selection of parameter-set values with less uncertainty in the representation of hillslope hydrological hazards. This process enables the application of highly complex multi-hazard models such as the OpenLISEM hazard model, whose outputs can be used for various purposes such as risk assessment, development of disaster risk reduction policies, and assessment of climate and land use scenarios. According to van Vliet et al. (2016) and Williams et al. (2020), policy recommendations derived from the outputs of highly complex models depend on how parameterisation and uncertainty are handled in their results because any output with high uncertainty can lead to biased policy recommendations.




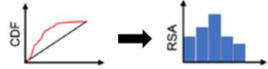
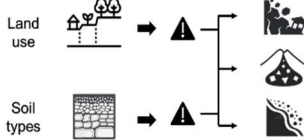
In the case of the Soufriere catchment, land use change (LUC) dynamics over the last few decades have intensified farming practices on steep slopes, leading to increased deforestation and transformation of the landscape into a predominantly agricultural-export region (Foley et al. 2005; Walters 2016). This has reduced the natural land cover of the catchment related to tropical forests and shrublands, which play a role in hillslope hydrology and stability that control processes such as infiltration, hillslope runoff, and slope stability (Wohl et al. 2012; Marhaento et al. 2018). Unplanned housing on steep hillsides in existing urban areas has further contributed to the reduction of hillslope vegetation and alterations in slope geomechanics and hydrology (Holcombe 2006; Anderson et al. 2011; Bozzolan et al. 2023). These changes in land use within the Soufriere catchment, coupled with projected

climate predictions indicating an increase in hurricane activity like Hurricane Tomas, are likely to result in an increase in the frequency and magnitude of rainfall-triggered landslides, debris flows, and hillslope erosion. It is important to assess these impacts under different climate and land use scenarios to provide necessary outputs for researchers, planners, and policymakers (Uusitalo et al. 2015; van Westen et al. 2021). These outputs can be used to develop policy recommendations aimed at mitigating and reducing the impacts of these hazards based on projected climate and land use change trends. Such assessments are especially crucial for decision-making processes, as they aim to reduce the risk faced by communities that are already socioeconomically vulnerable to the impacts of climate change (Holcombe 2006; Anderson et al. 2007).

## 4.2 Methodology

The following (Table 4.1) describes the second and final stages of the modelling workflow. The second stage describes the methodological steps for model verification, parameter-set selection procedures, and subsequent sensitivity analysis (SA) of the hydrological and geotechnical input parameters of the behavioural simulations identified according to the experimental design described in Chapter 3. The final stage (stage 3) describes the methodological steps to explore climate and land use change scenarios according to the parameter-set selected in stage two.

Table 4.1 Modelling workflow stages 2 and 3: model verification and sensitivity analysis (SA).

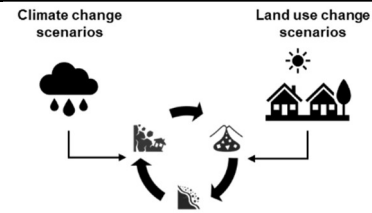
Stage 2: Model verification and sensitivity analysis (SA)		
<b>5. Model verification (sub-catchment and catchment scale)</b>	<p>Define and apply a suitable spatial similarity assessment method for internal model verification (e.g., 'total area difference' and 'area distribution'). Identify the parameter-sets and associated simulations with the highest similarity scores with respect to observed hazard.</p>	
	<p>Define and apply a spatial accuracy metric to the simulations with parameter-sets with the highest similarity scores (e.g., Cohen's kappa coefficient to measure the spatial agreement between simulated and observed hazard locations).</p>	
<b>6. Parameter-set selection</b>	<p>Select the parameter-set and associated simulation that meet the criteria for spatial similarity and accuracy.</p>	
<b>7. Sensitivity analysis (SA)</b>	<p>For the selected model parameter-set, undertake sensitivity analysis to identify influential parameters and the impact of uncertainty on hazard representations.</p>	
<b>8. Sensitivity to soil types and land use variations</b>	<p>For the selected parameter-set, explore the influence of variations in the parameters characterising different soil types and land use categories in terms of their spatial distributions within the catchment. Look for soils and land use (and associated subdomain areas) in which the hazard magnitude is most responsive to these parameter variations (identify the most sensitive land use categories for land use change scenarios).</p>	

### Stage 3. Model application for climate and land use scenarios

---

#### 9. Explore climate and land use change scenarios

This is the final stage, and it is now possible to define climate and land use change scenarios according to the confirmed parameter-set values for the catchment land use categories.



The modelling workflow for stage two entails the following steps (the numbering follows on from stage one, steps 1-4, outlined in Table 3.1):

#### Step 5. Model verification

Model verification is performed on the top five 'behavioural simulations' previously identified in step 4 (Chapter 3). These were the simulations that best replicated the total magnitude of the hazards at the catchment scale: the total landslide surface area ( $A_L$ ), total debris flow runout area ( $A_D$ ), and total net erosion ( $Net_E$ ). In Step 5, the first level of model verification (assessing the performance within the catchment domain) is a spatial similarity assessment. This ranks the top five behavioural simulations that resulted in hazard representations according to the spatial similarity with the observed hazards. In this case, the verification is with respect to the post-Hurricane Tomas landslide and debris flow inventory polygons identified for the Soufriere catchment. The spatial similarity assessment method is described in section 4.2.1. The second level of verification is an accuracy assessment. This is the assessment of the spatial agreement between the landslide polygons estimated by the simulations with the landslide polygons observed in the hazard inventory. An accuracy metric is selected to calculate the accuracy score for the ranked simulations based on the spatial agreement between the simulated and observed landslides. The accuracy assessment is described in more detail in section 4.2.2.

#### Step 6. Simulation parameter-set selection

Define criteria to select one of the top five parametric simulations with the best proximity to the observed landslides in the hazards inventory. The criteria are based on the area difference between the simulated and observed landslides and the area distribution of the landslide sizes. The accuracy score based on the spatial agreement between the simulated and observed landslides was also considered as a criterion. It was defined the parametric simulation selection based on the mentioned criteria. The procedure to define the simulation selection criteria is described in section 4.2.3.

#### Step 7. Sensitivity Analysis (SA)

A Regional Sensitivity Analysis (RSA) technique was performed on the behavioural simulation selected according to the established criteria. The aim is to identify how the spatial representation of rainfall-triggered landslides, debris flows and hillslope erosion rates resulting from the selected behavioural simulation can be attributed to the scaling of the input parameter values established for the parametric simulations in Chapter 3, section 3.2.4. The goal is to identify which hydrological and geotechnical input parameters within the parameter-set of the selected behavioural simulation are the most sensitive in

representing these hazards. The method for performing Regional Sensitivity Analysis (RSA) is described in section 4.2.4.

### **Step 8. Sensitivity to land use and soil type variations**

Sensitivity to land use and soil type parameter value variations was established in two stages. The first stage is parameter-set confirmation for the behavioural simulation, selected according to the criteria specified in section 4.2.3. The aim is to identify the hydrological and geotechnical parameter values from the parameter-set according to the land use categories and soil types that have influenced the spatial representation of rainfall-triggered landslides and their accuracy scores at the sub-catchment level. The second stage is the confirmation of the hydrological and geotechnical parameters by identifying their values according to the spatial distribution of the simulated rainfall-triggered landslides for each land use category and soil type in each sub-catchment. The method used to perform the parameter-set confirmation is described in section 4.2.5.

### **Step 9. Explore land use and climate change scenarios**

This corresponds to the final stage of the modelling workflow. The aim is to verify that the confirmed parameter-set values for the catchment land use and soil types of the selected behavioural simulation will respond and provide different hazard patterns for different land use and rainfall scenarios. The procedure to perform the response to land use and rainfall change is described in section 4.2.6.

#### **4.2.1 Spatial similarity assessment**

Spatial similarity assessment methods assess the equifinality (similitude) of the resulting rainfall-triggered landslides and debris flows resulting from the parametric simulations according to their "approximation" to the magnitude and size distribution of the observed landslides and debris flow in the hazard inventory. In Chapter 2, section 2.3.2, these methods are reviewed. In stage two of the modelling workflow, two spatial similarity approaches were selected: calculation of the total area difference ( $\Delta A_T$ ) (Equation 4.1) and assessment of the area distribution. The area difference method was used to estimate the difference between the total hazard magnitude (e.g., total landslide surface area ( $A_L$ )) and total magnitude ( $A_{INV}$ ) of rainfall-triggered landslides and debris flows estimated from the hazard inventory. The area difference method ( $\Delta A_L$ ) is performed to the total landslide surface area ( $A_L$ ) of the parametric simulations identified as "behavioural" in Chapter 3, section 3.3.1 since the landslides observed in the hazard inventory contain a greater number of observations than debris flows.

Three classes of equifinality approaches were defined to rank the identified behavioural simulations according to their spatial similarity. The criteria to define these classes were based according to the total landslide surface area estimated in the hazard inventory. Therefore, a threshold of simulated total landslide surface area ( $A_L$ )  $\leq 50$  ha will be considered acceptable in proximity to the ( $A_{INV}$ ) (23.6 ha) of the hazard inventory. This criterion considers the uncertainty in the model outputs as well as the spatial resolution chosen for the distribution of the input parameter values.



The first class included behavioural simulations with a total area difference  $\Delta A_T \geq 50 \text{ ha}$ ; simulations with this level of difference in total landslide surface area ( $A_L$ ) were considered to have no approximation to the total landslide inventory area ( $A_{INV}$ ). The second class corresponded to the area difference  $\Delta A_T \geq -1 \text{ and } \leq 50 \text{ ha}$ ; this difference was considered proximate to the total landslide inventory area ( $A_{INV}$ ). The third class corresponded to an area difference  $\Delta A_T \leq -1 \text{ ha}$ ; simulations with this difference were considered to be underestimates of the total landslide inventory area ( $A_{INV}$ ). Parametric simulations with area differences  $\Delta A_T \geq -1 \text{ and } \leq 50 \text{ ha}$  were ranked from lowest to highest difference. The total area difference  $\Delta A_L$  is described as follows:

$$\Delta A_T = A_{SIM} - A_{INV} \quad \text{Equation 4.1}$$

Where  $\Delta_T$  is the total area difference,  $A_{SIM}$  is the total simulated landslide surface area ( $A_L$ ) *ha* and  $A_{INV}$  is the total landslide surface area (*ha*) estimated from the hazard inventory. The advantage of this method is that also can calculate the area difference  $\Delta A_D$  for debris flow areas in case of using this hazard for verification purposes.

The second spatial similarity assessment approach considered the statistical distributions of individual landslide sizes. This was achieved by comparing histograms of simulated versus observed landslide sizes. The aim is to identify simulations that resulted in an approximate estimation of landslide size distribution observed in the hazard inventory.

#### 4.2.2 Spatial accuracy assessment

The spatial accuracy assessment was performed using the spatial overlapping method described in Chapter 2, section 2.3.2.2. The aim is to calculate the spatial agreement between the simulated and observed landslide polygons that were distributed within the catchment. Cohen's kappa coefficient ( $\kappa$ ) (Equation 4.2) was selected as an accuracy metric to assess the degree of spatial agreement between simulated and observed landslide polygons. This coefficient corresponds to a skill score coefficient that measures the inter-rater reliability of categorical data (Landis & Koch, 1977). The Cohen's kappa coefficient ( $\kappa$ ) scores can be interpreted as poor agreement with scores  $\leq 0.2$ , fair agreement with scores between 0.21 to 0.4, moderate agreement with scores between 0.41 to 0.6, good agreement with scores between 0.61 to 0.8, and very good agreement with scores between 0.81 to 1.0. Cohen's kappa coefficient ( $\kappa$ ) is described as follows:

$$\kappa = \frac{P_0 - P_e}{1 - P_e} \quad \text{Equation 4.2}$$

where  $P_0 = \frac{TP + TN}{\text{Catchment area}}$  and  $P_e = \frac{[(TP + TN)(TP + FP)(TN + FN)(TN + FP)]}{(\text{Catchment area})^2}$

Where  $P_0$  is the proportion of observed agreements and  $P_e$  is the proportion of expected agreements by random chance. The proportions of the observed and expected agreements were derived according to a confusion matrix (Appendix B.2). True Positive (TP), False Positive (FP), and False Negative (FN) values were derived according to the spatial overlapping method, and True Negative (TN) values were

established according to the tolerance level (Figure C.2). Agreement scores were assessed according to the strength of the agreement categories for Cohen's kappa coefficient ( $\kappa$ ).

The uncertainty introduced in the OpenLISEM hazard model input parameters affected the location and spatial distribution of the simulated rainfall-triggered landslides in the resulting behavioural parametric simulations. This produces a mismatch in the spatial overlap between the simulated and inventory landslide polygons, which affects the calculation of accuracy metrics. Therefore, a tolerance level was necessary to assess the spatial overlap between the simulated and observed landslide polygons. The tolerance level was defined according to two main criteria. The first corresponds to establishing a tolerance area around the landslide polygons from the hazard inventory, and the second involves excluding the flat areas within the catchment (where landslide source areas would not be expected). The tolerance area was defined as the buffer or influence area of the landslide polygons identified from the hazard inventory. The calculation of the tolerance area was performed using a fuzzy membership function that assesses the neighbouring cells with more membership to the landslide inventory polygon boundary through a distance decay function (Mead et al. 2021). (Figure C.2). Neighbouring cells > 0.6 meters were selected from the landslide inventory polygon boundary as tolerance areas. Flat catchment areas were excluded if they were below hillslopes of 15 degrees. The areas that met this condition were set as the True Negative (TN) values (Figure C.4).

#### 4.2.3 Simulation parameter-set selection criteria

Based on the spatial similarity scores (section 4.2.1) and accuracy assessment scores (section 4.2.2), the next step was to select the simulation that provided the most similar hazard prediction to those observed in the hazard inventory. In the Soufriere catchment, model verification and parameter-set selection were performed with respect to the landslide polygons available in the hazard inventory. Three selection criteria were used:

- lowest total area difference  $\Delta A_T$
- best area distribution fit between simulated and observed hazard
- Cohen's kappa coefficient ( $\kappa$ ) agreement scores  $\geq 0.21$  (fair agreement)

The parametric simulation that meets these three criteria will be selected as a behavioural simulation as its parameter-set provides the best spatial representation of the rainfall-triggered landslides observed in the Soufriere catchment during Hurricane Tomas, and the observed debris flows, and hillslope erosion rates are within reasonable representation bounds (as established in step 4).

#### 4.2.4 Sensitivity Analysis (SA)

Regional Sensitivity Analysis (RSA) was performed for the selected behavioural simulation. The aim is to calculate sensitivity indices to determine the most sensitive hydrological and geotechnical input parameters from the selected behavioural simulation. The input parameters were divided into two categories: 'Behavioural' and 'Non-behavioural.' In RSA, 'Behavioural' (acceptable) and 'non-

behavioural' (poor) parameters are derived from Cumulative Density Functions (CDFs) (Equation 4.3) according to a prescribed threshold (Sarrazin et al. 2016).

The threshold was set according to the values of the total landslide surface area ( $A_L$ ), total debris flow runout area ( $A_D$ ), and total net erosion ( $Net_E$ ) resulting from the selected behavioural simulation. From the CDFs, a sensitivity index was estimated by measuring the difference between the behavioural and non-behavioural CDFs curves. This difference is calculated by measuring the maximum vertical distance between the CDFs curves using the Kolmogorov-Smirnov (KS) statistic, which can be used to rank the input parameters (Bozzolan et al. 2020). The larger the distance between the CDFs curves, the more influential the factor. The sensitivity index is expressed as follows:

$$s_i = \max_{x_i} |F_i^B(x_i) - F_i^{\bar{B}}(x_i)| \quad \text{Equation 4.3}$$

Where  $s_i$  is the sensitivity index,  $F_i^B(x_i)$  is the behavioural CDF, and  $F_i^{\bar{B}}(x_i)$  is the non-behavioural CDF.

The sensitivity index ( $s_i$ ) varies from 0 to 1; a high value indicates that the variation input parameters significantly influence the spatial representation of landslides, debris flows, and net erosion rates. The robustness of the sensitivity index was assessed using the bootstrap technique. The robustness analysis estimates whether the sensitivity indices are independent of the specific input-output sample (Pianosi and Wagener 2018). The bootstrapping randomly draws N samples from the available data to compute the K-S statistics for each input parameter. The bootstrap was performed using the Sensitivity Analysis For Everybody (SAFE) toolbox (Pianosi et al. 2015) in MATLAB with N = 100 and using a confidence interval of 95%, as established in the code.

#### 4.2.5 Sensitivity to land use and soil types variation

The sensitivity to soil type units and land use category value variation was determined by assessing the spatial distribution of rainfall-triggered landslides resulting from the selected behavioural simulation for each soil type unit and land use category. The sensitivity to soil type units and land use category value variation was determined by assessing the spatial distribution of rainfall-triggered landslides resulting from the selected behavioural simulation for each soil type unit and land use category. Units and categories with a large number of landslide spatial distributions were established as soil type units and land use categories sensitive to the influence of rainfall-triggered landslides, debris flows, and hillslope erosion hazards. The values of the hydrological and geotechnical input parameters were identified for each sensitive unit and category, and the most influential soil type unit and land use categories were identified according to the RSA results.

#### 4.2.6 Explore land use and climate change scenarios

The final step in the modelling workflow is to explore the catchment response to different climate and land use scenarios using the parameter-set of the selected behavioural simulation. Once the parameter-set value distribution for soil type units and land use categories of the Soufriere catchment was determined, the response of the catchment to different rainfall events and land use scenarios was

assessed by elaborating a matrix that incorporated hypothetical land-use scenarios combined with rainfall events of different intensities and durations (Table C.2). Within the matrix, the response to land use change scenarios was assessed through the calculation of the percentage of change (Equation 4.4) which estimates the increase or decrease of the total landslide surface area ( $A_L$ ), total debris flow runoff area ( $A_D$ ), and total net erosion ( $Net_E$ ) for each scenario.

$$\Delta\% = \frac{(V_1 - V_2)}{|V_1|} * 100 \quad \text{Equation 4.4}$$

Where  $\Delta\%$  is the percentage of change,  $V_1$  is the hazard magnitude under current land use and  $V_2$  is the hazard magnitude for each defined land use change scenario. The magnitude of each hazard was estimated according to the hazard metrics proposed in Chapter 3, section 3.2.6.

According to the current land use of the Soufriere catchment, i.e., the land use layer used to distribute hydrological input parameters in the OpenLISEM hazard model, two land use change scenarios were proposed. The first corresponds to the change in the categories from *natural tropical forest* to *mixed farming and forest*. This scenario was proposed assuming that deforestation of *natural tropical forests* by the expansion of agriculture is susceptible to increase the frequency and magnitude of rainfall-triggered landslides, debris flows, and hillslope erosion observed under current land use. This hypothesis is based on studies by Cox et al. (2006) and Walters (2016), which showed evidence that the decrease in natural forests to the detriment of agriculture has increased the hillslope erosion rates of the Soufriere catchment. The second scenario corresponded to a change in the units of *mixed farming and forests* to *natural tropical forests*. This scenario suggests that the forestation of degraded hillslopes by agriculture will reduce the frequency and magnitude of rainfall-triggered landslides, debris flows, and hillslope erosion (Persichillo et al. 2017) observed under the current land use of the Soufriere catchment. The change in land use units implies a change in the values of the hydrological input parameter values for the mentioned land use categories. For the proposed scenarios, it was only modified the most sensitive input parameter values identified for land use categories according to the Regional Sensitivity Analysis (RSA) performed to the selected parameter-set.

The response of the proposed land use change scenarios to rainfall change was assessed according to the Hurricane Tomas rainfall event and rainfall events derived from an intensity–duration–frequency relationship (IDFs) obtained from Klohn–Crippen (1995) (Figure C.5). The selected rainfall events correspond to a 24-hour rainfall with a total volume of 252 mm, a 10-hour rainfall with a total volume of 200 mm and a 5-hour rainfall with a total volume of 160 mm. Synthetic rainfall events were performed to recreate the selected events (Figure C.5). Hence, eight scenarios were proposed to assess the response of land use change to the selected rainfall events (Table C.2).

## 4.3 Results

### 4.3.1 Spatial similarity ranking

Five parametric simulations resulted within the criteria of area difference  $\Delta A_T$  determined as proximate to the total landslide inventory area ( $A_{INV}$ ) (Table 4.2).

Table 4.2 Ranking of parametric simulations with hazard area difference scores in red font.

Parametric simulations	Catchment discharge ( $m^3$ )	Landslide surface area	Landslide inventory area	$\Delta A_T$ (ha)	Debris flow runout area (ha)	Debris flow inventory area (ha)	$\Delta A_T$ (ha)	Net erosion ( $ton.m^{-2}$ )
		$A_{SIM}$ (ha)	$A_{INV}$ (ha)					
<b>SIM22</b>	<b>76059.2</b>	<b>23.1</b>	<b>23.6</b>	<b>-0.5</b>	<b>3.8</b>	<b>6.02</b>	<b>2.3</b>	<b>-240.4</b>
SIM25	<b>76059.2</b>	<b>23.2</b>	<b>23.6</b>	<b>-0.4</b>	<b>0.4</b>	<b>6.02</b>	<b>5.6</b>	<b>-197.7</b>
SIM32	2678279.4	65.2	23.6	41.6	22.3	6.02	16.3	-1306.2
SIM35	2757857.9	66.6	23.6	43.0	24.2	6.02	17.2	-1193.9
SIM19	1646415.9	69.3	23.6	45.7	9.4	6.02	3.4	-792.1

The parametric simulations with the lowest area difference  $\Delta A_T$  corresponded to simulations 22 and 25. These simulations obtained an area difference  $\Delta A_T$  of -0.5 and -0.4 ha for total landslide surface areas and an area difference  $\Delta A_T$  of -2.2 and -5.6 ha for total debris flow runout areas (Table 4.2). Negative values indicate that the total landslide surface areas and total debris flow runout areas were underpredicted and below the total area estimated for both hazards in the inventory. Similarly, both simulations obtained the same results for catchment discharge (Table 4.2). In relation to the total net erosion rates ( $Net_E$ ), simulation 22 obtained -240.4 ( $ton.m^{-2}$ ) which are mainly deposition values. Instead, simulation 25 obtained the lowest values of -197.7 ( $ton.m^{-2}$ ) (Table 4.2). Regarding the rest of the ranked parametric simulations (Table 4.2), despite being within the criteria of area difference  $\Delta A_T$  the area difference for landslide areas  $\Delta A_L$  and debris flows  $\Delta A_D$  was too broad to obtain a similarity with the landslides and debris flows registered within the hazard inventory.

### 4.3.2 Area distribution comparison

Figure 4.1 compares the area distribution between the simulated landslide sizes from simulations 22 and 25 with the observed landslide sizes in the hazard inventory. The comparison indicates that the landslide sizes from simulation 22 obtained almost the same size distribution pattern as the landslides observed in the hazard inventory. Most simulated landslides were between 0 and 0.5 ha, between 0.5 and 1 ha, and  $\geq 1$  and  $\leq 3.5$  ha, which is the same as the landslide inventory area distribution. However, in simulation 22, an under-prediction was observed for sizes between 0 and 0.5 ha. Regarding simulation 25, the same size distribution pattern was observed – the only difference was an overprediction of the simulated landslides for sizes between 0 and 0.5 ha and between 0.5 and 1 ha. For areas  $\geq 1$  ha the simulated landslide sizes followed the same pattern as in simulation 22.

These results indicate that simulations 22 and 25 obtained the most proximate area distribution with landslides triggered by Hurricane Tomas. However, despite obtaining the best fit between the area distributions, the spatial distribution of the landslides resulting from simulations 22 and 25 did not follow

the same spatial location as the landslides observed in the hazard inventory. Within the Soufriere catchment, simulated landslide locations were close to, but not overlapping with, the observed landslides; or in catchment areas where no landslides were observed during Hurricane Tomas. These differences might be due to uncertainties in the topography (DEM) or hydrological and geotechnical input parameter value spatial distribution for soil types unit and land use categories.

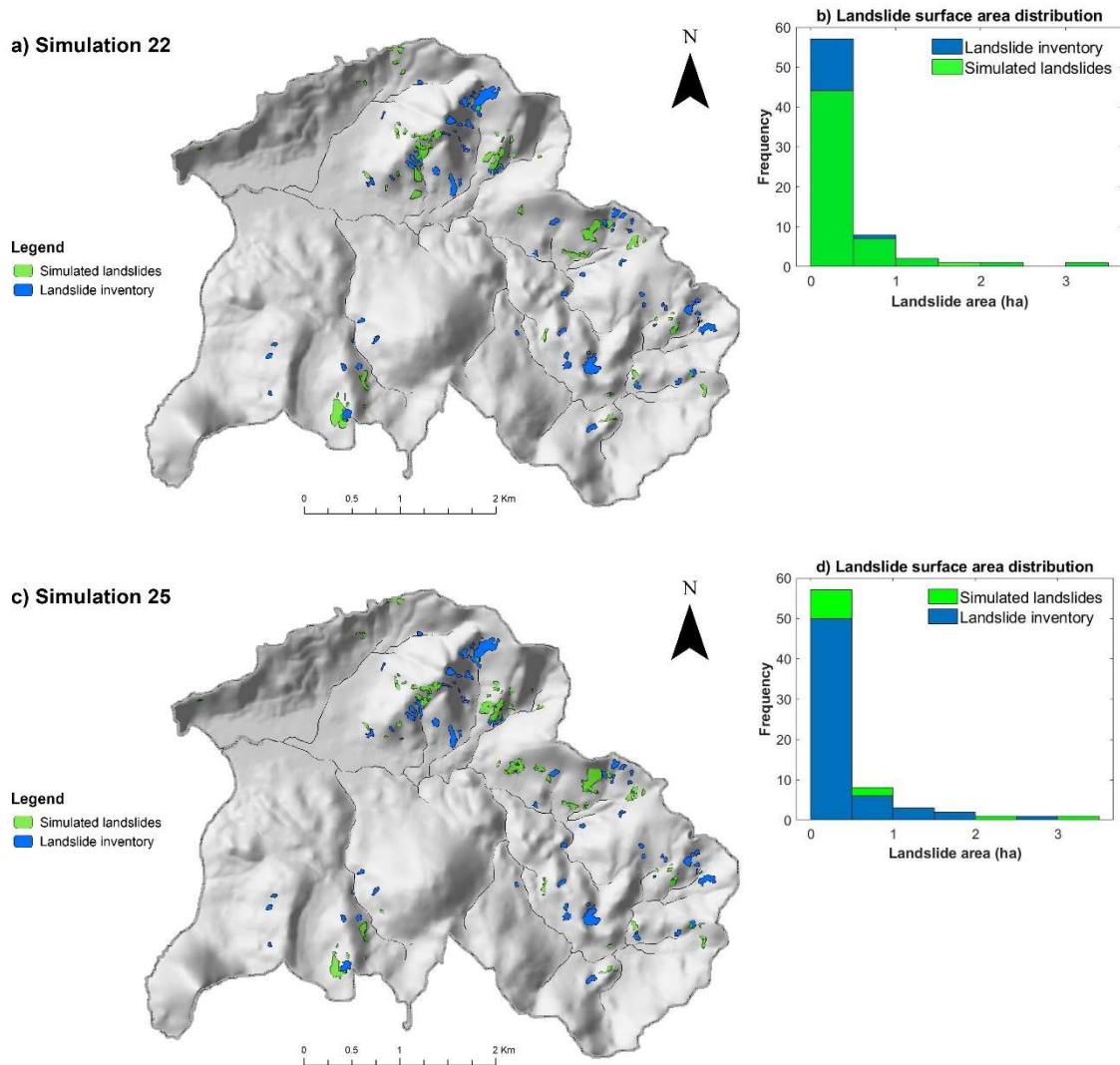


Figure 4.1 Landslide spatial distribution and area comparison: (a) landslide spatial distribution for simulation 22, (b) area distribution for simulation 22, (c) landslide spatial distribution for simulation 25, (d) area distribution for simulation 25.

### 4.3.3 Accuracy assessment

Table 4.3 illustrates the Cohen's kappa coefficient ( $\kappa$ ) scores for the ranked simulations. In section 4.3.2, it was shown that simulations 22 and 25 obtained the most proximate area distribution for the landslides observed in the hazard inventory. However, the spatial location of the landslides from these simulations did not follow the same pattern as the observed landslides resulted from Hurricane Tomas within the

catchment. In these simulations, the landslide locations were sometimes very close to the observed landslides, without overlapping. The introduction of tolerance levels to account for uncertainty in the landslide inventory mapping process (buffer zones around the observed landslides polygons) increased the overlap for these landslide locations and improved the accuracy scores for simulations in which modelled slope failures were close to an observed landslide. This is the case for simulation 22, which achieved a fair agreement score of 0.21 and simulation 25 achieved a poor agreement score of 0.16.

For parametric simulations with broad area difference  $\Delta A_L \geq 41.6$  ha. Accuracy scores with fair agreement between 0.21 and 0.23 were identified. These corresponded to simulations 32, 35 and 19. However, these accuracy scores do not specify whether the simulated landslides are similar to the landslides observed in the hazard inventory, such as those identified in simulations 22 and 25. For these simulations (Table 4.3), the accuracy scores were highly influenced by the uncertainties introduced in their parameter-sets, resulting in overestimation of the landslide sizes across the Soufriere catchment. The estimation of the total landslide surface area ( $A_L$ ) for these simulations (Table 4.3) indicates that the simulation of failure depths within the catchment was translated into large landslide surfaces that easily overlapped with the landslide polygons estimated from the hazard inventory. This influenced the spatial overlap between these polygons increasing the accuracy score for these simulations.

Table 4.3 Accuracy score values.

Parametric simulations	TP (True Positive) (ha)	FN (False Negative) (ha)	FP (False Positive) (ha)	TN (True Negative) (ha)	Landslide area $A_L$ (ha)	Area difference $\Delta A_T$	Kappa coefficient (k)
<b>SIM22</b>	<b>4.43</b>	<b>26.06</b>	<b>8.3</b>	<b>1343.16</b>	<b>23.1</b>	<b>-0.4</b>	<b>0.21</b>
<b>SIM25</b>	<b>3.09</b>	<b>25.71</b>	<b>8.03</b>	<b>1345.12</b>	<b>23.2</b>	<b>-0.5</b>	<b>0.16</b>
SIM32	6.64	43.17	10.88	1321.26	65.2	41.6	0.21
SIM35	6.21	41.87	9.73	1324.14	66.6	43.0	0.21
SIM19	6.05	33.06	12.22	1330.62	69.3	45.7	0.23

#### 4.3.4 Behavioural simulation selection

Regarding the criteria for parameter-set selection defined in section 4.2.3. Simulation 22 was identified as "behavioural" as it meets all the criteria for parameter-set selection. The selection was based on the total area difference criteria ( $\Delta A_T$ ), even though simulation 22 obtained a similar area difference  $\Delta A_T$  ( $-0.5$  ha) with respect to simulation 25  $\Delta A_T$  ( $-0.4$  ha). Simulation 22 obtained the lowest area difference  $\Delta A_T$  ( $-2.2$  ha) between the total debris flow runout areas ( $A_D$ ) and the total runout areas estimated from the hazard inventory. Moreover, the best fit was obtained with the landslide area sizes observed in the hazard inventory where most of the rainfall-triggered landslides sizes distributed across the Soufriere catchment were between 0 and 0.5 ha, between 0.5 and 1 ha, and  $\geq 1$  and  $\leq 3.5$  ha, which is the same as the landslide inventory area distribution. Moreover, simulation 22 obtained the highest accuracy score according to Cohen's kappa coefficient ( $\kappa$ ) with a fair agreement score of 0.21 in relation to simulation 25 which obtained a poor agreement score of 0.16. Therefore, parametric simulation 22 was selected as the behavioural simulation that achieved the best spatial representation of the landslides observed in the hazard inventory for the Soufriere catchment.

### 4.3.5 Sensitivity Analysis (SA)

Figure 4.2 illustrates the sensitivity indices (S.I) for the hydrological input parameters for land use and soil types and the geotechnical parameters for soil types corresponding to the parameter-set of the behavioural simulation (simulation 22) selected in the previous section 4.3.4. From this parameter-set, it was identified that the most influential input parameters (highest sensitivity index) in the representation and magnitude of the total landslide surface area ( $A_L$ ), total debris flow runout area ( $A_D$ ), and total net erosion ( $Net_E$ ) estimated in simulation 22 corresponded in order from highest to lowest sensitivity to saturated hydraulic conductivity ( $k_{s1}$ ) for land use; saturated moisture content ( $\theta_{s2}$ ) for soil types and soil internal friction angle ( $\phi'$ ) for soil types. The less influential input parameters (low sensitivity index) corresponded to saturated hydraulic conductivity ( $k_{s2}$ ) for soil types; saturated moisture content ( $\theta_{s1}$ ) for land use and soil cohesion ( $c'$ ) which varies according to soil types. High sensitivity values (S.I) identified for these parameters indicated that within the parameter-set of simulation 22, the initial values of saturated hydraulic conductivity ( $k_{s1}$ ), had the highest importance in determining the magnitude related to landslide surface area ( $A_L$ ), debris flow runout area ( $A_D$ ), and net erosion ( $Net_E$ ) among all the input parameters. This implies that changes in saturated hydraulic conductivity ( $k_{s1}$ ) values are likely to have a more significant impact on the magnitude of these hazards than changes in the other input parameters within the set. On the other hand, soil cohesion ( $c'$ ) values (with a score of 0.21) have the lowest influence among all the input parameters, indicating that it may have a weaker influence on the magnitude of the simulated rainfall-triggered landslides debris flows and net erosion rates within the Soufriere catchment. These parameters are essential for identifying the spatial distribution of sensitive values for land use categories and soil type units. In general, the sensitivity indices (S.I) estimated through the bootstrap method with 95% confidence indicated the robustness of the results. However, as shown in Figure 4.2, the confidence intervals of the sensitivity indices corresponding to the input parameters still overlap despite increasing the sample size to (N=100).

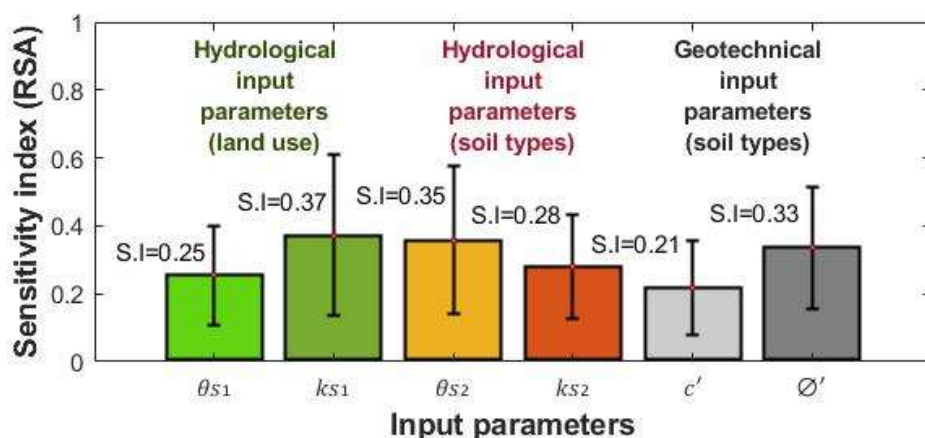


Figure 4.2 Sensitivity indices (S.I) for key input parameters. The bars correspond to the sensitivity indices mean value estimated with bootstrapping while the vertical lines at the top bar represent the confidence interval for each parameter.



### 4.3.6 Parameter set confirmation: sensitivity to land use and soil type variations

In section 4.3.5, the most and least sensitive hydrological and geotechnical input parameters for land use and soil types were identified for the selected behavioural simulation (simulation 22). Therefore, it is important to identify their value distributions according to the soil type units and land use categories of the Soufriere catchment area. Figure 4.3 shows the value distribution for the hydrological input parameters according to land use categories. The most sensitive land use categories were identified according to the spatial distribution of rainfall-triggered landslides resulting from simulation 22 (Figure 4.4). From these results, it was identified that the spatial distribution of the simulated rainfall-triggered landslides was concentrated in land use categories corresponding to natural tropical forests, mixed farming and forest, and densely vegetated farming (Figure 4.4). However, concerning landslide sizes, the largest magnitudes were observed within the natural tropical forest category, and smaller magnitudes were observed in categories such as mixed farming and forest, intensive farming (25%), and densely vegetated farming (Figure 4.4). The differences in landslide magnitude are explained by the high sensitivity of saturated hydraulic conductivity ( $k_{s1}$ ) values for land use according to the Regional Sensitivity Analysis (RSA) results in section 4.2.4. According to the spatial distribution of the  $k_{s1}$  values for each land use category (Figure 4.3), the highest value corresponds to natural tropical forest ( $4.397 \times 10^{-2} \text{ mm} \cdot \text{s}^{-1}$ ). This was related to the distribution of simulated rainfall-triggered landslides within this category, in which the largest landslide magnitudes were observed. Therefore, the saturated hydraulic conductivity ( $k_{s1}$ ) value (Figure 4.3a) for natural tropical forest have significant impacts on the magnitude of rainfall triggered landslides, debris flows and hillslope erosion. In relation to the value distribution of saturated moisture content ( $\theta_{s1}$ ) (Figure 4.3b), it was observed that the values were almost equally distributed within the land use units. However, from the Regional Sensitivity Analysis (RSA) results, this parameter was one of the least influential factors in hazard magnitudes within the parameter set.

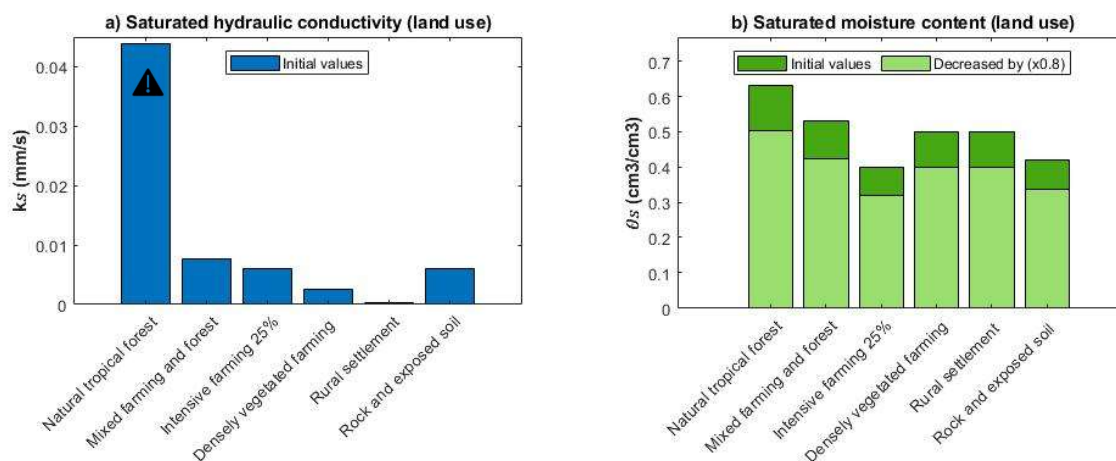


Figure 4.3 Parameter value distribution for land use. (a) Saturated hydraulic conductivity, (b) Saturated moisture content. The symbol ( $\blacktriangle$ ) indicates highly sensitive soil type units.

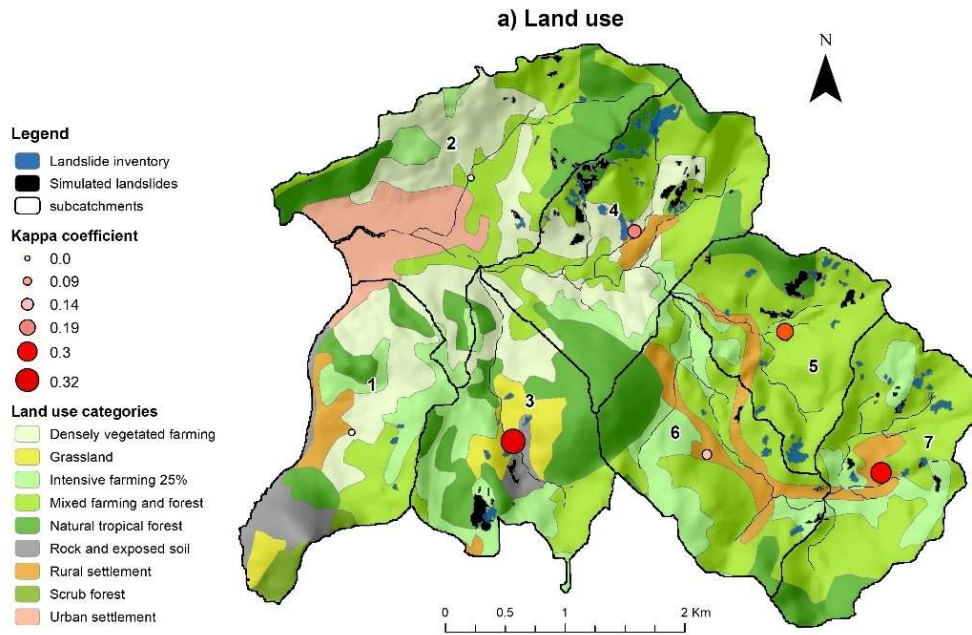


Figure 4.4 Land use for the Soufriere catchment.

For the soil types, Figure 4.5c shows the value distribution of saturated hydraulic conductivity ( $k_{s2}$ ), which indicates that the highest value corresponds to the unit of Calfourc Silty Loam and Panache Silty Clay Loam (Figure 4.6). For the rest of the soil units, the values were equally distributed, except for Casteau gravelly Bouldery, which had the lowest value. From the Regional Sensitivity Analysis (RSA) results, the value distribution of this parameter for soil types was less sensitive within the parameter-set of the simulation 22. Concerning the Saturated moisture content values ( $\theta_{s2}$ ) (Figure 4.5d), the highest values corresponded to the Ivrogne Stony Clay and Rabot Clay. However, within these soil types, the distribution of the largest landslide magnitude was registered within the Ivrogne Stony Clay unit (Figure 4.6). For the rest of the soil type units, the values were distributed equally, except for Casteau gravelly Bouldery, which had the lowest value. The Regional Sensitivity Analysis (RSA) results indicated that this parameter was one of the most sensitive to the influence of rainfall-triggered landslide magnitudes. This suggests that within the value space of this parameter, the value corresponding to Ivrogne Stony Clay was the most sensitive, according to the number of landslides distributed within this unit (Figure 4.6). For the case of soil cohesion ( $c'$ ) and soil internal friction angle ( $\phi'$ ), the value distribution was equally distributed within the total soil type units. Nevertheless, according to the RSA results, the soil internal friction angle ( $\phi'$ ) was the most sensitive, whereas the soil cohesion was less sensitive to the magnitude of the simulated rainfall-triggered landslides.

From the parameter value distribution for the land use categories and soil types units, and the identification of the most and less sensitive parameters for the parameter-set of simulation 22. It was observed that the parameter value combination of saturated hydraulic conductivity ( $k_{s1}$ ) for the natural tropical forest, saturated moisture content ( $\theta_{s2}$ ) and internal friction angle ( $\phi'$ ) for Ivrogne Stony Clay

influenced the spatial distribution of rainfall-triggered landslides of a bigger magnitude and size. Therefore, the simulation of the spatial distribution of landslides is highly sensitive to ( $k_{s1}$ ), ( $\theta_{s2}$ ) and ( $\phi'$ ) ' values assigned to different soil types and land uses - especially combinations such as Ivrogne Stony Clay and Natural Forest in this case.

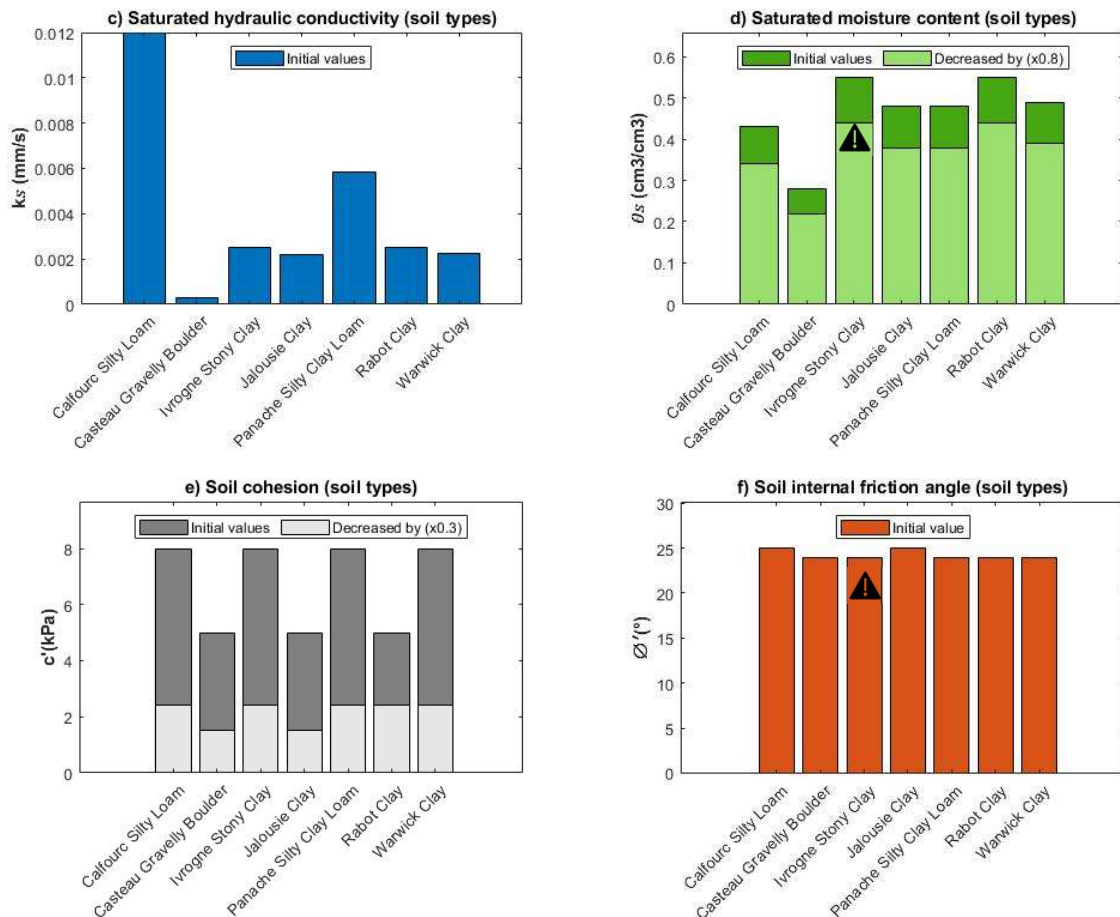


Figure 4.5 Parameter values for soil types. (c) Saturated hydraulic conductivity, (d) Saturated moisture content, (e) Soil cohesion, (f) Soil internal friction angle. The symbol ( $\blacktriangle$ ) indicates highly sensitive soil type units.

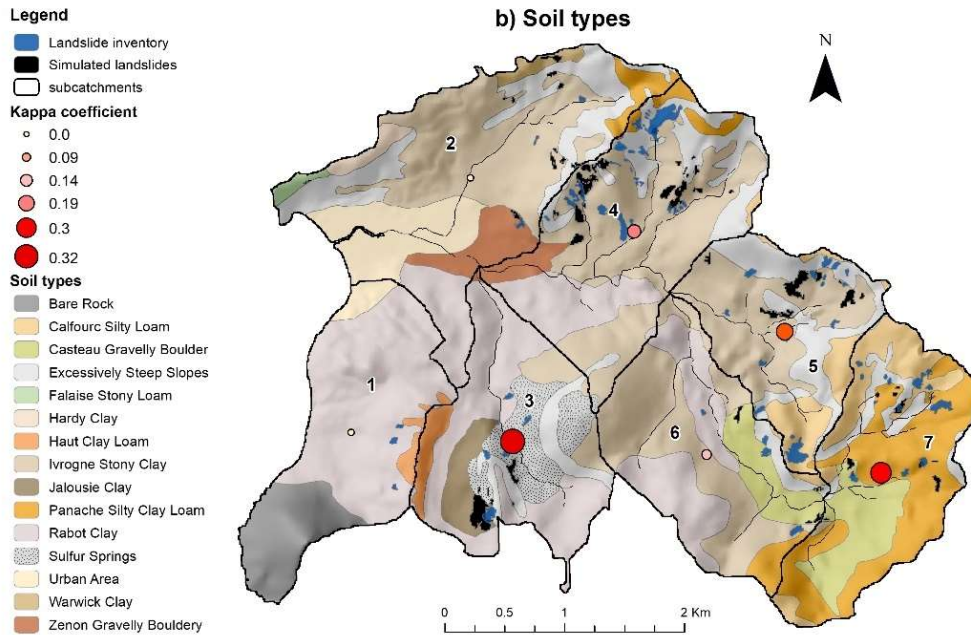


Figure 4.6 Soil types for the Soufriere catchment.

#### 4.3.7 Responsiveness of the Soufriere catchment to land use and rainfall change

Figure 4.7 illustrates the magnitudes and percentage of changes of the total landslide surface area ( $A_L$ ), total debris flow runout area ( $A_D$ ), and total net erosion ( $Net_E$ ) for different land use and rainfall change scenarios modelled for the Soufriere catchment. Simulations relating to the current land use (i.e., the land use layer used to distribute hydrological input parameters in the OpenLISEM hazard model) are in the second row of Figure 4.7, and the rainfall magnitudes decrease from left to right. The hazard magnitudes relating to the Hurricane Tomas rainfall event and Simulation 22, as selected in step 6 of the modelling workflow, are in column 1, row 2.

Concerning the catchment-wide hazard magnitudes estimated from simulation 22, it was observed under the current land use a decrease in the total landslide surface area ( $A_L$ ), total debris flow runout ( $A_D$ ), and total net erosion ( $Net_E$ ) magnitudes for 24, 10 and 5-hour rainfall events (Figure 4.7). For example, for 24-hour rainfall, the simulated total landslide surface area was decreased by -60.6%, the total debris flow runout area by -30.5% and the total net erosion rates by -29.6% in relation to the simulated hazards magnitudes of Hurricane Tomas rainfall event. Despite the reduction in the spatial magnitude of the hazards, the spatial location followed the same spatial distributions simulated for the Hurricane Tomas event. The same pattern was also observed for rainfall events of 10 and 5 hours. For the 10-hour rainfall, the hazard magnitude with respect to the 24-hour rainfall decreased by -42.8% for landslide surface areas, -12.8% for debris flow runout areas, and -25.7% for total net erosion rates. On the other hand, the landslide magnitude for the 5-hour rainfall event increased by +18.3% with respect to the 10-hour rainfall event. However, the debris flow magnitude decreased by -25%, and the net

erosion rates decreased by -11.1%. The previous results indicate that under current land use, the distribution of landslides follows the same distribution pattern as the simulated Hurricane Tomas. The only difference was that the landslide size and magnitude depended on the intensity and duration of the rainfall event, such as in the case of the 5-hour rainfall event.

The second set of scenarios to be explored were cases in which land use was changed. First, natural tropical forests were changed to mixed farming and forests. This change was performed by changing the saturated hydraulic conductivity ( $k_{s1}$ ) values of natural tropical forest by the values of mixed farming and forests. The responsiveness of the Soufriere catchment to rainfall events such as Hurricane Tomas and 24-, 10-, and 5-hour rainfall indicated a change in the spatial distribution of rainfall-triggered landslides and an increase in total landslide surface area ( $A_L$ ), total debris flow runout ( $A_D$ ), and total net erosion ( $Net_E$ ) magnitudes for more extreme rainfall events (higher intensities and durations). For example, when this land use change was imposed and the same Hurricane Tomas rainfall event was applied as before, the simulated total landslide surface area ( $A_L$ ) increased by +256.7%, total debris flows runout area ( $A_D$ ) by +1457%, and total net erosion ( $Net_E$ ) by +371% when compared with the current land use (Figure 4.7 – red arrows). This means that debris flows have a significantly greater increase in magnitude than landslides, and erosion also has a greater magnitude increase than landslides.

Similarly, for the 24-hour rainfall event, the total landslide surface area ( $A_L$ ), increased by +19.7%, the total debris flow runout area ( $A_D$ ) by +9.9%, and the total net erosion ( $Net_E$ ) by +9.3% when compared with the current land use. A similar increase was observed when comparing the imposed land use change with the current land use for the 10-hour rainfall event. Here, the landslide magnitude increased by +6.1%, the debris flow by +6.2%, and the net erosion rate by +7.7%. Again, for the case of a 5-hour rainfall, there is also a simulated increase in the hazard magnitude with +1.7% for landslides, +16.6% for debris flows, and +10.1% for net erosion rates. The most dramatic increase in the simulated hazard magnitudes under land use change occurred with the most extreme rainfall event (Hurricane Tomas), whereas the lower magnitude 5-hour rainfall event saw only modest increases in hazard magnitudes of approximately 6.1% to 7.7%. For Hurricane Tomas and the 24-hour rainfall event, the hazard that was simulated to have the greatest increase in magnitude compared with those simulated under current land use was landslides. For the 10-hour and 5-hour events, erosion had the greatest increase in magnitude. Under this land-use scenario, the spatial distribution of landslides followed the same location pattern as that simulated for current land use. In this scenario, the magnitude of each landslide or debris flow increased considerably compared with those simulated under current land use. This is in line with the hypothesis set for this land use scenario that the loss of natural forest areas and their replacement with farmland increases the magnitude and frequency of rainfall-triggered landslides, debris flows, and hillslope erosion hazards.

The bottom row of Figure 4.7 indicates a scenario in which mixed farming and forests are changed to natural tropical forests. This change was performed by changing the saturated hydraulic conductivity ( $k_{s1}$ ) values of mixed farming and forests by the values of natural tropical forests. The resulting response to rainfall events, such as Hurricane Tomas, showed a decrease in the total landslide surface area ( $A_L$ ),

total debris flow runout area ( $A_D$ ), and total net erosion ( $Net_E$ ) magnitudes (Figure 4.7). For example, in response to Hurricane Tomas, the total landslide surface area ( $A_L$ ) decreased by -16%, and the total debris flow runout area ( $A_D$ ) had a medium increase of +13.1% which is marginal with respect to the debris flow magnitude identified within the current land use (shown in Figure 4.4), and the total net erosion ( $Net_E$ ) decreased by -4%. On the other hand, in response to a 24-hour rainfall event, the landslide magnitude decreased by -2.2%, debris flow by -5.3% and net erosion rates by -4.2% compared with current land use. The catchment responsiveness to 10 and 5-hour rainfall events also showed a decrease in hazard magnitude (Figure 4.7). In response to the 10-hour rainfall event, the landslide magnitude decreased by -44.8%, the debris flow by -25%, and the net erosion rate decreased by -2.7%. Finally, for the 5-hour rainfall event, the landslide magnitude decreased by -15.5%, and the debris flows, and net erosion rates increased by -8.3% and -2.8%, respectively. As observed for current land use and the change from natural tropical forest to mixed farming and forest, the hazards followed the same location, and their magnitude was reduced according to the intensity and duration of the rainfall event. The responsiveness in hazard magnitude for this land use scenario reduced the magnitude of landslides, debris flows, and net erosion rates, indicating that the conservation of natural land cover can be an effective multi-hazard reduction measure for hillslopes that are highly susceptible to these types of hydrological hazards interactions.

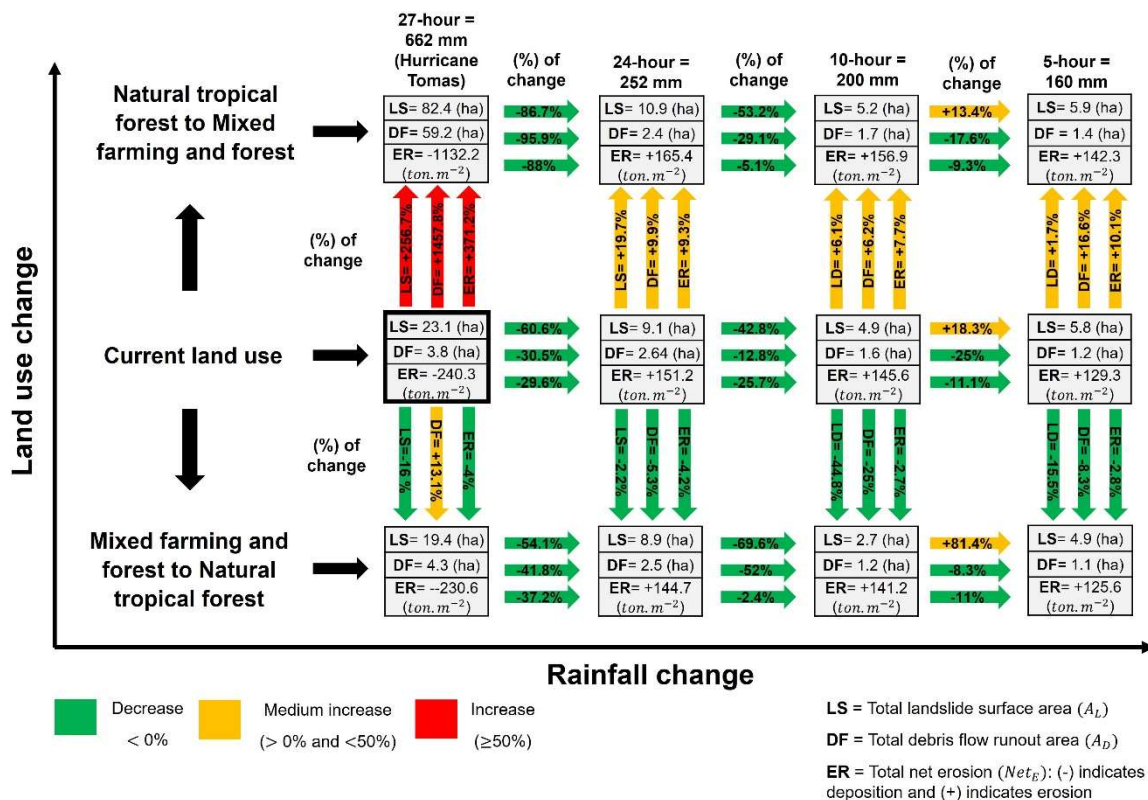


Figure 4.7 Multi-hazard response of the Soufriere catchment to land use and rainfall change.

## 4.4 Discussion

### 4.4.1 Behavioural simulation selection

In the stage two of the modelling workflow, the incorporation of the equifinality criteria through the application of the area difference ( $\Delta A_T$ ) and the spatial similarity method helped to identify the parametric simulations with more proximity to the landslide registered during Hurricane Tomas. Incorporating these criteria is essential to identify the uncertainties propagated in the model results. According to Khatami et al. (2019), the application of the methodologies to assess the model equifinality is based on the realism of the represented hazards according to the response of the model structures to parameter sets. Therefore, there is a problem with decidability in determining which parametric simulations are more feasible to represent observations (Lane et al. 2021). In the spatial similarity method applied in this chapter, the decidability based on the attributes of area difference and area distribution determined the credibility of the landslide representations for the Soufriere catchment. For example, for parametric simulations with area difference  $\Delta A_L \geq 41.6$  ha, it was identified that the simulated landslide sizes were overpredicted concerning the observed landslides. These results helped to identify the parametric simulations with high uncertainties in hazard representations that do not provide realistic results due to (e.g., extreme soil cohesion values, internal friction angle or saturated moisture content). However, for parametric simulations with area difference  $\Delta A_L \leq -0.4$  ha, it was identified that simulated landslides resulted with more similarity to the observed landslides. The area distribution helped to confirm this similitude by identifying the fit of the landslide sizes in which most of them were between 0 and 0.5 ha, between 0.5 and 1 ha and  $\geq 1$  ha, the same as the landslide inventory area distribution. The setting of scaling factors within stage one of the modelling workflow for each input parameter contributed to controlling the maximum and minimum variations for each input parameter value and, therefore, and control the uncertainty in the hazard representation. This is an important consideration when parameter value ranges are explored, as the modification of initial values affects the model outputs, leading to increased uncertainty in the predictions or simulations.

Regarding the accuracy assessment, Cohen's kappa coefficient ( $\kappa$ ) indicated accuracy scores with a fair agreement between 0.21 and 0.23 for the five ranked parametric simulations. Similar score were identified by Van den Bout et al. (2018) who applied the kappa coefficient to assess the overlap between simulated and observed landslides for the Messina catchment in Italy, obtaining kappa scores of 0.22. However, it was identified that some of these accuracy scores were biased by the uncertainties reflected in the hazard representations. This is the case of parametric simulations with area difference  $\Delta A_L \geq 41.6$  ha. For example, for these simulations, the application of the spatial overlapping method to estimate the accuracy scores overlapped overpredicted landslide polygons with observed landslide polygons increasing the values of TP (True Positive) values impacting the accuracy scores. Therefore, high accuracy score values for these simulations do not necessarily reflect their similarity with the observed hazards. For the case of parametric simulations with area difference  $\Delta A_L \leq -0.4$  ha, the accuracy scores were initially low due to low overlap between the simulated and observed landslide polygons. It was identified that this low overlap came from the uncertainties reflected in these simulations that

impacted the landslide spatial distribution and their sizes. It was observed landslide locations very proximate to the observed landslides but with no possibility of overlapping. The application of the tolerance level increased the overlapping of these landslide locations improving the accuracy scores.

The results of the accuracy assessment have indicated how necessarily the incorporation of the equifinality principle is in the model verification process. According to Herrera et al. (2022), considering model equifinality is a crucial stage for model verification because it considers the effects of uncertainty in the model results improving the model calibration and accuracy. The application of the stage two of the modelling workflow for model verification applied in this chapter recognizes this principle by incorporating the spatial similarity method and the criteria to select the parametric simulation with the best similarity with an observed hazard. According to this modelling workflow, it is possible to answer the first question set in section 4.1 by selecting simulation 22 as the behavioural simulation that meets all the requirements in representing the observed landslides during Hurricane Tomas.

#### **4.4.2 Sensitivity Analysis (SA) and parameter set confirmation**

Performing the Regional Sensitivity Analysis (RSA) to selected behavioural simulation allowed the identification of the most influential input parameters that impact the spatial representation of rainfall-triggered landslides, debris flows and hillslope erosion within the Soufriere catchment. Identifying these input parameters is essential to determine the most sensitive values distributed for land use categories and soil types that might affect the spatial representation of these hazards within the catchment. For example, identifying saturated hydraulic conductivity ( $k_{s1}$ ) values for land use, saturated moisture content ( $\theta_{s2}$ ) and internal friction angle ( $\phi'$ ) for soil types as the most influential input parameters might explain the effects on the spatial representation of landslides within the catchment. Studies such as Bozzolan et al. (2020), identified the most influential parameters that affect slope stability in urbanise and non-urbanise slopes using +CHASM model in Saint Lucia, identifying that effective cohesion, soil thickness (layer1), slope angle and rainfall intensity are the main parameters affecting landslides. Other studies, such Bravo-Zapata et al. (2022), have performed Regional Sensitivity Analysis (RSA) to identify the sensitivity of parameters on the occurrence of shallow landslides using the TRIGRS 2.0 model and to assess the set of parameters that influence the geometry and location of landslides, identifying that angle of friction, soil cohesion are the most influential parameters.

According to Francos et al. (2003) and Pianosi et al. (2016), the implementation of sensitivity analysis procedures enhances the calibration and accuracy of the model predictions by "screening" the regions of the parameter range that provide the highest uncertainty. In the case of the Soufriere catchment, those regions were reflected in the spatial distribution of the hydrological and geotechnical input parameters values for the catchment land units and soil types. The assessment of the spatial distribution of the simulated landslides within the soil types and land use units helped to identify the distribution of these values confirming that the categories of natural tropical forest and mixed farming and forest were the most sensitive categories for land use and Ivrogne Stony Clay for soil types. Therefore, the spatial distribution of hydrological and geotechnical parameter values within these sensitive land use categories and soil type units influenced location and landslide sizes within the catchment.



According to van Vliet et al. (2016), the identification of the most sensitive units for land use and soil types implies a “good practice” for physics-based models that assess land use change dynamics. For example, for multi-hazard modelling, the no recognition of the most sensitive parameters for different land use categories might constrain the modelling of events or scenarios in which rainfall-triggered landslides, debris flows, and hillslope erosion hazards occur. Not considering the most influential parameters implies that assessing hydrological multi-hazard interactions will not generate accurate results. The parameter-set confirmation within the stage two of the modelling workflow for model verification identifies how the most sensitive parameter-set values from the selected behavioural simulation are distributed according to the land use units and soil types of the Soufriere catchment. This is an important step in parameterising complex models such as the OpenLISEM hazard model in which the representation of landslides, debris flows, and hillslope erosion depends on the response of the parameter-set values.

#### **4.4.3 Responsiveness of the catchment to land use and rainfall change scenarios**

Having verified and selected a suitable input parameter set, the final step in the workflow was to assess the potential impact of different land use and rainfall scenarios on the multi-hazard profile of the catchment. For the two modelled land use change scenarios and four rainfall scenarios the overall predicted response of the catchment was in line with the conceptual understanding of hydrological multi-hazards outlined in chapters 1 and 2. For example, for the deforestation scenario the magnitude of all three hazards increased; whereas, when farmed land was returned to natural forest, the hazard magnitudes generally decreased. Similarly, for all three land use scenarios a decrease in rainfall magnitude led to a decrease in the simulated hazard magnitude. The modelling workflow thus enabled trust to be built regarding the parameter-set selection and model capability to simulate hazard interactions and magnitudes. Details of the catchment response for these scenarios, and implications for our understanding and management of these multi-hazard interactions, are discussed in the following paragraphs.

The response of the current land use for the 24, 10 and 5-hour rainfall events indicated a decrease of the hazard magnitudes in relation to the magnitudes observed for Hurricane Tomas rainfall event. The application of the percentage of change showed that landslides magnitudes decreased according to the duration of the rainfall events. However, it was observed a medium increase of +18% for landslide magnitudes respect to the 10 to 5-hour rainfall. The increase in the rate of change is explained by the rainfall intensity estimated for the 5-hour rainfall event that was higher concerning to the 10-hour event.

Regarding the spatial distribution of the simulated landslides, these followed the same spatial pattern in terms of location and size concerning the simulated landslides for Hurricane Tomas. The same decrease pattern was observed in the magnitude of debris flows. For example, the percentage of change of the debris flow magnitude observed for Hurricane Tomas decreased by -30.5% with respect to the 24-hour rainfall. The same tendency in reducing magnitude was observed for the 20 and 5-hour rainfall events. Most notably net erosion rates also reported a decrease in their magnitudes. However, it was observed that for Hurricane Tomas rainfall event the net erosion rates were mostly dominated by deposition and

for the case of the 24, 10 and 5-hour rainfall events, erosion was the most dominant process. From these results, it was identified the Soufriere catchment hazard is composed of the predominance of these hazards.

Assuming the scenario in which the natural tropical forest is changed by mixed farming and forest the magnitude of landslides, debris flows, and net erosion rates showed a significant increase with respect to the Hurricane Tomas rainfall and to the 24, 10 and 5-hour rainfall events. The assessment of this scenario confirmed the assumption that changing native forests to detriment of farming areas increases the magnitude of these hazards. For example, assessing the hurricane Tomas rainfall event under this scenario it was identified a significant increase of +256.7% in landslides, +1457.8% in debris flow and +378.2% in net erosion rate magnitudes. These results support the evidence demonstrated for Saint Lucia in which the intensification of land use processes such as farming and urban settlements have increased the landslide activity and the frequency of debris flows and intensified the catchment sediment yield due to agriculture (Bégin et al. 2014; Walters 2016)

The scenario of changing mixed farming and forest to tropical natural forest showed a decrease in the hazard magnitudes. The hazard representations under this scenario confirmed the assumption presented in this chapter that the increase in the natural forest on degraded hillslopes by agriculture reduces the magnitude of landslides, debris flows, and erosion rates observed under the current land use of the Soufriere catchment. These results, therefore, confirm the necessity to assess these hazards under different land use and rainfall change scenarios to formulate mitigation plans to the impacts of these hazard under the current changes in climate.

## 4.5 Conclusions

In this chapter, the application of the stages 2 and 3 of the modelling workflows described in sections 4.2, addressed answer research question 2 of this thesis (RQ2: *what is the influence of catchment parameter variations and uncertainties on multi-hazard assessments?*). the application of the second stage of the modelling workflow allowed to select the behavioural simulations identified in Chapter 3 with the best parameter-set that provided the best approximation to the hazard observed for Hurricane Tomas. The setting of a spatial similarity method identified spatial approximation of the simulated and observed landslides by considering the area difference and the size distribution. The criterion established to rank the behavioural simulations with an area difference  $\Delta A_L \geq -1$  and  $\leq 50$  ha identified simulation 22 with the lowest area difference  $\Delta A_L$  with -0.5 ha. The identified simulation indicated an underprediction of the total landslide areas, especially between 0 and 0.5 ha and 0.5 and 1 ha. However, total simulated landslide areas were between 0 and 3.5 ha the same area range as the observed landslides.

The spatial similarity method indicated the effect of spatial resolution and uncertainty on the simulated landslides. A high accuracy score does not imply a good model response in representing the observed landslides. Behavioural simulations with an overprediction of landslide sizes obtained kappa coefficient scores with fair agreement values, whereas simulations with an underprediction of landslide sizes but

with a similar size distribution with the inventory obtained slight agreement scores. The introduction of a tolerance area to the landslide inventory polygons improved the spatial overlapping between simulated landslides located a few meters from an observed landslide. The tolerance area improved the kappa coefficient of simulation 22 with a fair agreement score of 0.21. Simulation 22 achieve the criteria established to select the behavioural simulation with the parameter set with more proximity to the observed landslides.

The Regional Sensitivity Analysis (RSA) results indicated that no robust conclusion can be made in identifying the most influential parameters as the confidence intervals of the sensitivity indices of the input parameters of behavioural simulation 22 overlap. The sensitivity indices suggested that the totality of parameters has some degree of influence in representing rainfall-triggered landslides, debris flows and hillslope erosion hazards. The most influential parameters by the order are saturated hydraulic conductivity ( $k_{s1}$ ) for land use, internal friction angle ( $\phi'$ ), saturated moisture content ( $\theta_{s2}$ ) and saturated hydraulic conductivity ( $k_{s2}$ ) for soil types. The non-influential corresponded to saturated moisture content ( $\theta_{s1}$ ) for land use and soil cohesion ( $c'$ ) for soil types.

The parameter-set confirmation according to the land use categories and soil types units of the Soufriere catchment improved the parameterisation of the OpenLISEM hazard model by identifying the hydrological and geotechnical parameter values from simulation 22. The confirmation of parameter-set values for each land use categories and soil types units identified the most suitable parameters for each unit to represent hillslope hydrological hazards. Nevertheless, the spatial representation of these hazards is subject to the combination of parameter values for every raster grid cell that can provide different patterns of location and magnitude for each hazard.

The establishment of land-use and rainfall change scenarios allowed the identification of different hazard patterns according to the confirmed parameter values for land-use and soil-type units. In scenarios where the natural tropical forests were changed to mixed farming and forest, the response to Hurricane Tomas rainfall event indicated an increase in the magnitude of landslides, debris flows, and net erosion rates compared to the hazard magnitude estimated in simulation 22. In scenarios where the mixed farming and forest were changed to natural tropical forests, the response to Hurricane Tomas rainfall event indicated higher hazard magnitudes. For scenarios with 24, 10 and 5-hours rainfall the response to the changes of natural tropical forests to mixed farming and forest indicated a decrease in landslides, debris flow and erosion magnitudes. For scenarios in which the mixed farming and forest were changed to natural tropical forests the response to 24, 10 and 5-hour rainfall indicated the same patterns as the previous scenarios but showed that the magnitude of landslides, debris flows, and net erosion rates were higher within natural tropical units. It was identified that the spatial distribution of the simulated hazards followed the same location pattern for the total of scenario

---

---

**Chapter 5 Assessing hillslope hydrological hazards and  
interactions under changing climate and land use in  
Maipo, Chile**

---

---

## 5.1 Introduction

The development and application of stage one of the modelling workflow in Chapter 3 identified behavioural simulations with a parameter-set more suitable for representing rainfall-triggered landslides, debris flows, and hillslope erosion that occurred during Hurricane Tomas. In addition, it helped to identify the physical characteristics of the Soufriere catchment that drove the triggering and interaction of these hazards. On the other hand, the development and application of the second and third stages of the modelling workflow in Chapter 4 helped to select the parameter-set using an equifinality approach and identify the most sensitive input parameters that influenced the representation of these hazards for the subsequent assessment of climate and land use scenarios in the Soufriere catchment.

In the case of the Maipo sub-catchment (Figure 5.1), the impacts of the El Niño–Southern Oscillation (ENSO) have affected the variability of climatic events in Andean catchments in Central Chile (Garreaud et al. 2017; Vergara et al. 2020). These variabilities of events have been expressed in extended drought periods that have increased wildfires, reducing the natural land cover over hillslopes (Garreaud et al. 2017; Soto et al. 2017). In addition, irregular rainfall events of intense and short duration have been recorded that have increased the number of rainfall-triggered landslides and debris flows in different catchments with diverse socioeconomic impacts on the population (Sepúlveda and Petley 2015; Vergara et al. 2020). The latest events recorded on February 25, 2017, influenced by an exceptional rainfall event in the Maipo sub-catchment in the metropolitan region of Santiago, caused multiple landslides and debris flow under the same rainfall event, causing two fatalities and infrastructure damage, especially to houses and roads (Marín et al. 2017). In central Chile, Andean catchments are located in a Mediterranean semi-arid environment, where rainfall occurs seasonally from a short period to hours (Moreiras and Sepúlveda 2022). Most registered extreme rainfall events are related to El Niño events, which have had a substantial impact on the occurrence of landslides and debris flows (Sepúlveda et al. 2006). In semi-arid catchments, hillslope-hydrological hazards are related to runoff triggered by extreme rainfall events that influence the occurrence of rainfall-triggered shallow landslides, debris flows, and hillslope erosion by torrential flows, making Andean catchments a multi-hazard-prone environment (Moreiras et al. 2021). The geological setting of these environments is composed of hillslopes of volcanic soils characterised by materials of various sizes, represented by sediments ranging in size from blocks to gravels, sands, silts, and clays (García et al. 2018). The type of sediment material within semi-arid catchments highly influences debris flow magnitude, sediment transport, and deposition (Mergili et al. 2012; Vergara et al. 2022).

On the other hand, hillslope deforestation due to the direct impacts of climate change expressed in extensive drought periods have increased the occurrence of wildfires in the area, reducing the slope vegetation such as scrubs and natural forests (Demaria et al. 2013; Moreiras et al. 2021). Moreover, the growing pressure of urbanisation of rural areas and intensive agricultural systems have also modified the natural land cover to the detriment of urban expansion, lodging, and industrial agriculture such as vineyards (Schulz et al. 2010; Benavidez-Silva et al. 2021). These impacts have increased the impact

on hillslope erosion rates and the magnitude of the observed shallow landslides and debris flows (Garreaud et al. 2017; Moreiras et al. 2021; Vergara et al. 2022).

In order to investigate the potential impacts of rainfall variability and the effects of land use change in the Maipo sub-catchment in the influence of rainfall-triggered landslides, debris flows and hillslope erosion hazard in a Mediterranean catchment, this chapter applies the complete extension of the modelling workflow developed and applied in Chapter 3 and Chapter 4 respectively. Therefore, this chapter addresses the third research question of this thesis:

**RQ3 How do hillslope hydrological multi-hazards and their interactions respond to changes in land use and rainfall characteristics?**



*Figure 5.1 The second study site location: Maipo sub-catchment, central Chile.*

## 5.2 Applying the modelling workflow

Following the steps of the first stage of the modelling workflow developed and applied in Chapter 3 and the second and third stages developed and applied in Chapter 4, the modelling workflow is now applied to their full extent, including stages one, two, and three for the Maipo sub-catchment. The steps are described as follows:

**Step 1. Assemble available data for selected catchment:** Identify past-triggered hazard events for hazard inventory elaboration. In the case of the Maipo sub-catchment, the debris flows registered for the rainfall event on the 25th of February 2017 were identified by creating a hazard inventory that identified the spatial location and magnitude of the registered debris flows. The February 25 rainfall event was obtained from Marín et al. (2017), where the total rainfall volume and duration were identified. The physical characteristics of the Maipo-sub-catchment were defined by acquiring spatial data related to land use, topography (DEM), soil depths, and soil types based on different open-source databases. For the OpenLISEM hazard model, the hydrological and geotechnical input parameter values for soil type units and land use categories were estimated according to a literature review of soil type characteristics in the Maipo sub-catchment. The procedure to assemble available data is described in section 5.3.1.

**Step 2. Define input parameters value ranges:** The input parameter value ranges for the hydrological and input parameter values established for the Maipo sub-catchment were defined according to the scale factors for each input parameter determined for the OpenLISEM hazard model in the second stage of the modelling workflow in Chapter 3, section 3.2.3. The definition of parameter value ranges will be used to define the parameter-set combinations values for parametric simulations. These are described in section 5.3.3.

**Step 3. Define parametric simulations:** To perform the parametric simulations for the Maipo sub-catchment the procedure elaborated in step 3 of the stage 1 of the modelling workflow was followed. This involved generating an ensemble of 144 different parameter-set combinations – the ‘parametric simulations’ – to explore the parameter space represented by the likely parameter value ranges. The aim is to identify the behavioural simulations capable of reproducing the debris flows registered for the February 25 rainfall event. The procedure to set the parametric simulations is described in section 5.3.3.

**Step 4. Verify hazard representations at the catchment scale:** The hazard spatial representation resulting from the parametric simulations was verified using the hazard metrics proposed in step 4 of stage 1 of the modelling workflow applied in Chapter 3. The aim is to verify the hazard representations resulting from the parametric simulations to assess the behavioural performance in terms of the ability of the parameter set to replicate debris flows observed in the hazard inventory elaborated from the observed debris flows from the 25 February rainfall event. The procedure to quantify the hazard representations and their magnitude is described in section 5.3.3.

**Step 5. Model verification:** For the Maipo sub-catchment, it was applied the spatial similarity method developed for stage 2 of the modelling workflow applied in Chapter 4. The aim is to rank the top five parametric simulations that resulted in debris flow representations with the best spatial similarity with the observed debris flows from the 25 February rainfall event. The procedure for defining the spatial similarity method is described in section 5.3.4. The assessment of the spatial agreement was performed by overlapping the simulated and observed debris flow areas. The Jaccard Index was selected as an accuracy metric to calculate the accuracy score for the ranked parametric simulations, based on the spatial agreement between the simulated and observed landslides. The accuracy assessment is described in more detail in section 5.3.4.

**Step 6. Parameter-set selection:** The criteria defined to select the one of top five parametric simulations with the best proximity to the observed debris flows was based on the area difference between the simulated and observed debris flows and the area distribution of the debris flow sizes. The accuracy score based on the spatial agreement between the simulated and observed landslides was also considered as a criterion. It was defined the parametric simulation selection based on the mentioned criteria. The procedure to define the simulation selection criteria is described in section 5.3.4.

**Step 7. Sensitivity Analysis (SA):** A Regional Sensitivity Analysis (RSA) technique was performed on the behavioural simulation selected according to the criteria established. The aim is to identify how the spatial representation of rainfall-triggered landslides, debris flows and hillslope erosion resulting from the behavioural simulation can be attributed to the scaling of the input parameter values established for the parametric simulations. The goal is to identify which input parameters among hydrological and geotechnical are the most sensitive in representing these hazards. The method to perform the Regional Sensitivity Analysis (RSA) is described in section 5.3.5.

**Step 8. Sensitivity to land use and soil type variations:** It was performed the same procedure established for step 8 of the modelling workflow applied in Chapter 4. It was identified the hydrological and geotechnical parameter values from the selected parameter-set according to the land use categories and soil types units that have influenced the spatial representation of debris flows in the Maipo sub-catchment. The identification of the hydrological and geotechnical parameter values was confirmed according to the spatial distribution of the simulated debris flows for each land use category and soil type. The method to perform the parameter set confirmation is described in section 5.3.5.

**Step 9. Explore climate and land use change scenarios:** Within this step, it was introduced an additional assessment for the selected parameter set. A re-run of the behavioural simulation selected according to the criteria established in section 5.3.4 was performed with a series of map reports to assess the behaviour of landslide surface areas, debris flow runout areas and total net erosion rates during the rainfall duration. The aim is to identify at which moment of the rainfall event the influence of an individual hazard increases the magnitude of another hazard. The procedure to perform the response to land use and rainfall change is described in section 5.3.6.

The responsiveness to land-use and rainfall change was assessed following a land-use change matrix set in section 4.2.5, Chapter 4 that incorporates the response of the land-use units to different rainfall



patterns. The aim is to verify that the confirmed parameter set values will respond and give different hazard patterns for different land use and rainfall scenarios for the Maipo sub-catchment. The procedure to perform the response to land use and rainfall change is described in section 5.3.6.

### 5.3 Multi-hazard assessment of Maipo sub-catchment case study

#### 5.3.1 Step 1: assembling data for the Maipo sub-catchment

**The February 2017 rainfall event** was estimated by creating a synthetic rainfall event from the total rainfall volume registered on the day of the event. The total rainfall volume was obtained from the rain gauge station (Reservoir El Yeso) of the DGA (2017) (General Directorate of Waters). The total rainfall volume corresponded to 20.5 mm of rainfall for an 8-hour duration registered on February 25, 2017. The rainfall event reached a maximum rainfall intensity peak of 5.7 mm/h at the 6-hours from the beginning of rainfall. Once the maximum peak was identified for the Maipo sub-catchment, the rainfall intensities were discretized according to the total rainfall duration (Figure 5.2) The rainfall intensity duration was discretized in time intervals of 10 minutes, giving a total of 480 minutes for an 8-hour rainfall duration.

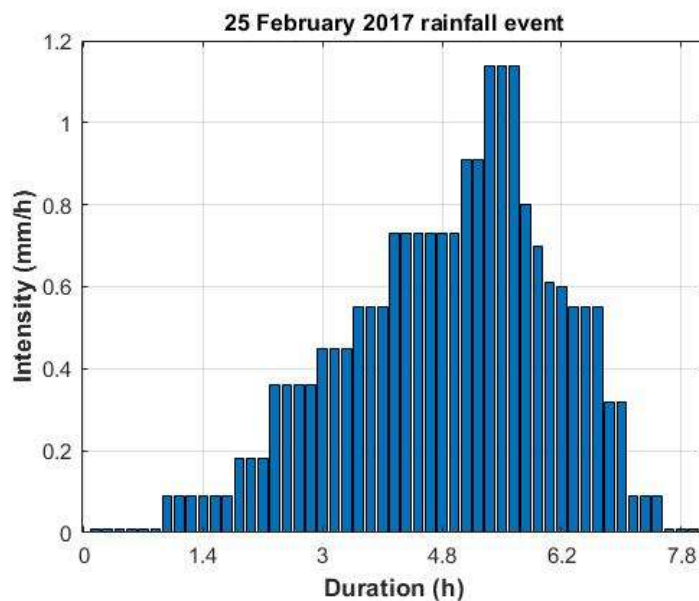


Figure 5.2 25 February 2017 rainfall event.

**The records of the triggered landslides and debris flows** in the Maipo sub-catchment for the February 25, 2017, rainfall event was only available for debris flows. Most of the debris flows that occurred on the day of the event were registered in several ravines within the Maipo sub-catchments. Debris flows impacted the lower parts of the ravines, forming alluvial fans with unconsolidated deposits that reached the Maipo River. The debris flow runout areas were recorded by SERNAGEOMIN (2017) which registered six debris flow events within the Maipo sub-catchment. The location of the registered debris flows was only available as a distribution of points performed using a GPS device (Figure 5.3). Therefore, it was necessary to digitize the debris flow initiation and runout areas. The debris flow polygons were delimited from the available Google Earth images on July 17, 2017 (Figure 5.3). The

advantage of the available images is that they still show the debris flow paths and runout areas of events that occurred on February 25, 2017.

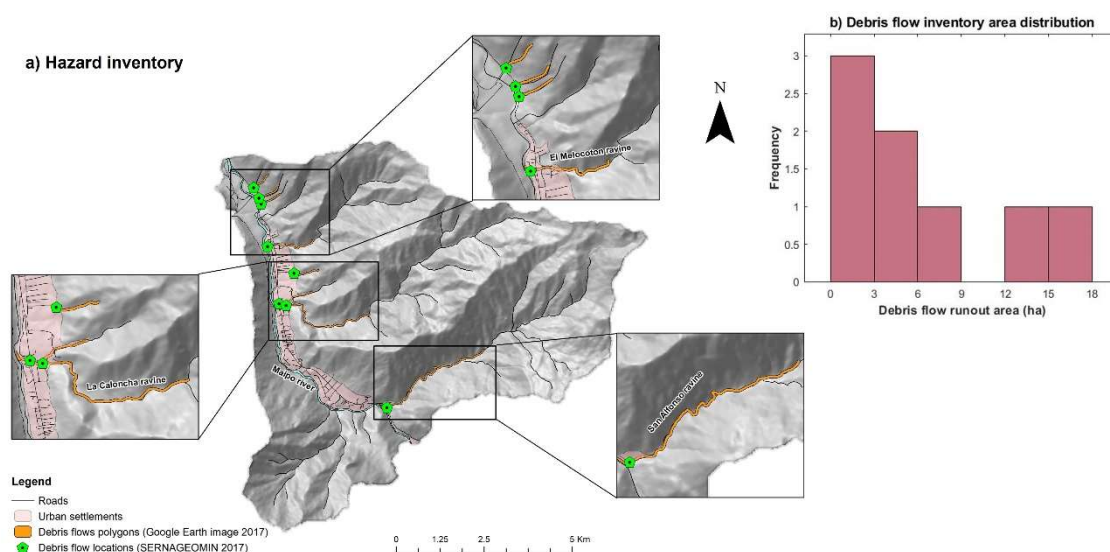


Figure 5.3 Hazard inventory. (a) Debris flow inventory (b) debris flow runout area distribution.

**The Maipo sub-catchment physical characteristics** used to set the OpenLISEM hazard model input parameters were defined according to the information that had been compiled on soil type, soil depth, topography, and land use identified for the study site according to available opensource datasets. The physical characteristics of the Maipo sub-catchment were defined at a spatial resolution of 20 × 20 metres. The selected spatial resolution is suitable for the scale of the Maipo sub-catchment, corresponding to 1:80.000 and an extension of 7753.04 ha. Data resolution below 20 metres will require longer simulation times and a large computer storage capacity for the total model outputs. One of the limitations identified for the Maipo sub-catchment is the lack of available data to estimate the hydrological and geotechnical input parameter values of the OpenLISEM hazard model. These parameters were estimated according to the sub-catchment soil types. However, no spatial data were available to characterise the sub-catchment soil types. Therefore, the sub-catchment soil types were characterised and estimated according to an updated geological map developed by CIGIDEN (2022) (Figure D.1a). From the geological map, the soil types were identified according to each geological unit based on a literature review from Alvarez (2006); Gonzalez (2010) and Luzio (2010) allowing identifying and classifying of the soil types according to the main geological units of the Maipo sub-catchment. The characterisation of the identified soil types was performed by identifying their textural classification according to Luzio (2010) and Casanova et al. (2013) where main textural classes were determined for each identified soil type.

Information regarding to the sub-catchment soil depth was obtained from the SoilGrids global soil map (<https://www.isric.org/explore/soilgrids>), which recently released most detailed global soil dataset, of resolution 250 metres (Batjes et al. 2020). For the Maipo sub-catchment, SoilGrids data were obtained for two soil layers. The first (soil depth 1) corresponds to the depth of the first 200 cm, and the second

(soil depth 2) corresponds to the total depth of the bedrock. Because of the chosen data resolution for the Maipo sub-catchment, the soil depth layers were resampled to a 20 × 20 metres resolution using bilinear interpolation with the *Resample* tool in ArcMap 10.6. Physical characteristics related to topography such as slope gradient and local drainage direction network (LDD) were defined from a corrected Digital Elevation Model (DEM) ALOS-PALSAR of 12.5 metres for the Santiago Metropolitan region obtained from IDE Chile (2021). The DEM was also resampled to 20 × 20 metres using bilinear interpolation with the *Resample* tool in ArcMap 10.6. Information about sub-catchment land use was obtained from CONAF (2013) (Figure D.3). The OpenLISEM hazard model input parameters were defined using the full PCRaster script available from van den Bout et al. (2018) to elaborate and process the base maps required for the model.

### 5.3.2 Step 2: defining model input parameter ranges

The definition of the OpenLISEM hazard model hydrological and geotechnical input parameter values for soil type units and land use categories for the Maipo sub-catchment (Table 5.1) were estimated on the basis of Luzio (2010); Casanova et al. (2013) and Sepúlveda et al. (2016) in which parameter values subject to variation within the OpenLISEM hazard model such as saturated hydraulic conductivity ( $k_s$ ), saturated moisture content ( $\theta_s$ ), soil cohesion ( $c'$ ), and soil internal friction angle ( $\phi'$ ) were estimated according to the textural characteristics of the identified soil types of the Maipo sub-catchment. Table 5.1 summarises the Maipo sub-catchment hydrological and geotechnical input parameter values.

Table 5.1 OpenLISEM hazard model hydrological and geotechnical input parameter values.

Input factors	Source	Symbol/Unit	Parameter value ranges			
			Soil layer 1		Soil layer 2	
			min	max	min	max
Soil depth	SoilGrids (2021)	(m)	0.08	0.21	0.31	5.91
<b>Hydrological</b>						
Saturated hydraulic conductivity*	Casanova et al. (2009)	$k_s(mm.s^{-1})$	$1.61 \times 10^{-3}$	$2.92 \times 10^{-3}$	$2.1 \times 10^{-3}$	$4.2 \times 10^{-3}$
Matric suction		$\Psi(kPa)$	65	75	65	75
Saturated moisture content*	Casanova et al. (2013)	$\theta_s(cm^3.cm^{-3})$	0.01	0.42	0.27	0.44
Initial moisture content		$\theta_i(cm^3.cm^{-3})$	0.25	0.5	0.41	0.47
<b>Geotechnical</b>			<b>Parameter value ranges</b>			
Soil density	Luzio (2010)	$\rho(kN.cm^{-3})$	1400 - 1900			
Soil cohesion*	(Sepúlveda et al. 2016)	$c'(kPa)$	8 – 12.1			
Internal friction angle*		$\phi'(^{\circ})$	24 – 45			
Soil grain size	Luzio (2010)	(m)	$2 \times 10^{-6}$ - $4.2 \times 10^{-4}$			

\*Initial parameter values subject to variation within the OpenLISEM model.

Figure 5.4 and Figure 5.5 illustrates the spatial distribution of the hydrological and geotechnical parameter values for land use categories and soil type units for the Maipo sub-catchment. The spatial distribution of hydrological input parameter values was performed according to the same criteria established for the Soufriere catchment in Chapter 3, section 3.2.2 in which spatial distribution of hydrological input parameter values was performed according to the infiltration modelling method in the OpenLISEM hazard model based on the Green and Ampt (1911) method for two soil layers. Figure 5.4 illustrates the spatial distribution of saturated hydraulic conductivity ( $k_s$ ), and saturated moisture content ( $\theta_s$ ), for the land use categories and soil types of the Maipo sub catchment. The value distribution for land use categories was established for soil layer 1, which corresponds to soil depth 1 (Figure D.2a) and the value distribution for soil types is set for soil layer 2, which corresponds to soil depth 2 (Figure D.2b). Figure 5.5 shows the value distribution for geotechnical input parameter values. These input parameters values were spatially distributed according to the catchment soil types (Figure D.1b) for the whole soil depth layer from topsoil to bedrock. These input parameters correspond to soil cohesion ( $c'$ ), and soil internal friction angle ( $\phi'$ ). The highest cohesion values were distributed within soils forming fluvial terraces and in residual and colluvial soils. The lowest cohesion values were within volcanic soils. In relation to the soil internal friction angle values, the lowest values were distributed within soil forming fluvial terraces and in residual and colluvial soils; and the highest friction angles were found within volcanic soils.

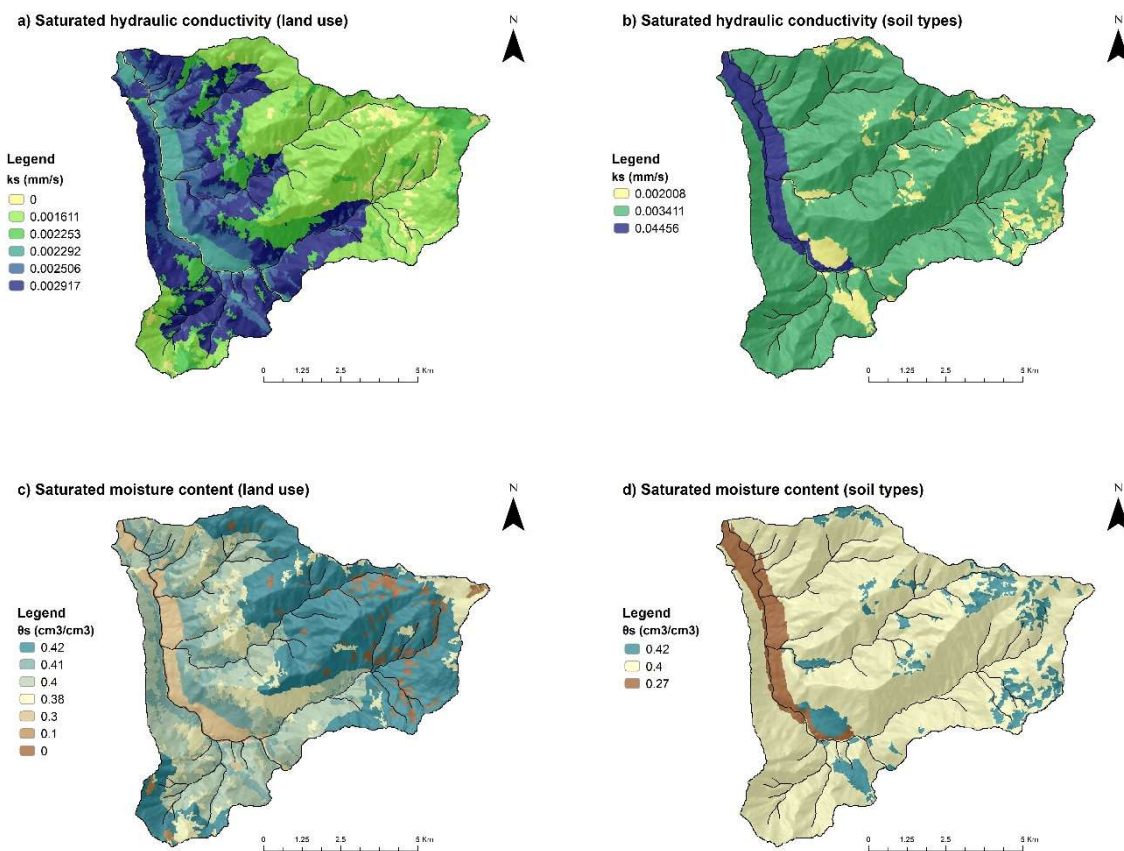


Figure 5.4 Spatial distribution of hydrological input parameter values for the Maipo sub-catchment.

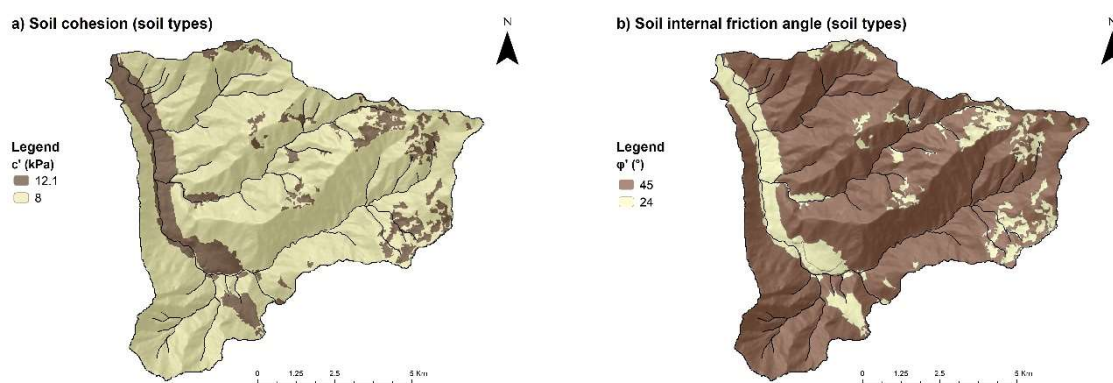


Figure 5.5 Spatial distribution of geotechnical input parameter values for the Maipo sub-catchment.

After identifying the spatial distribution of the hydrological and geotechnical input parameter values for the land use categories and soil types of the Maipo sub-catchment. It was identified the value distributions for hydrological and geotechnical input factors were defined in order to explore the regions of the value space that might introduce sources of uncertainty derived from the value estimations from the literature review. Figure 5.6 shows the value distribution identified for the hydrological and geotechnical input parameter values.

The definition of the distribution of the hydrological and geotechnical input parameter values allows the setting of value ranges to explore their variation in order to identify which value range introduces uncertainty in the spatial representation of rainfall-triggered landslides, debris flows and hillslope erosion hazards (Figure 5.6). To explore the input parameter value regions, the set of scaling factors determined in Chapter 3, section 3.2.4 was applied for each input parameter. The initial saturated hydraulic conductivity values were increased by (x1.2) and decreased by (x0.4) for land use (Figure 5.7a) and for soil types (Figure 5.7b). For the case of saturated moisture content, the initial values were increased by a multiplication factor of (x1.1) and decreased by (x0.8) for value distribution for land use (Figure 5.7c) and for soil types (Figure 5.7d). The initial values for soil cohesion (Figure 5.7e) were increased by (x1.2) and decreased by (x0.5) and (x0.3). Finally, the initial values for soil internal friction angle (Figure 5.7f) were increased by (x1.2) and decreased by (x0.6) and (x0.4). The setting of the multiplication factors to define parameter range values allows the exploring of the input factors value spaces to perform different parameter value combinations to find optimal parameter-set values to represent hillslope hydrological hazards for the Maipo sub-catchment.

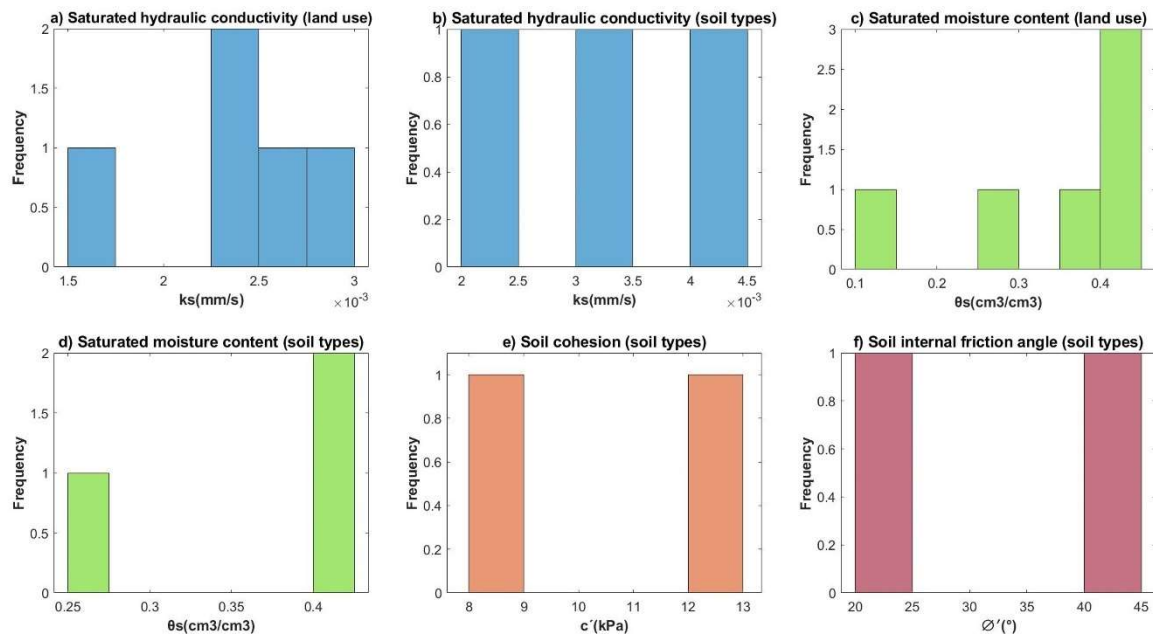


Figure 5.6 Hydrological and geotechnical input parameter value distributions.

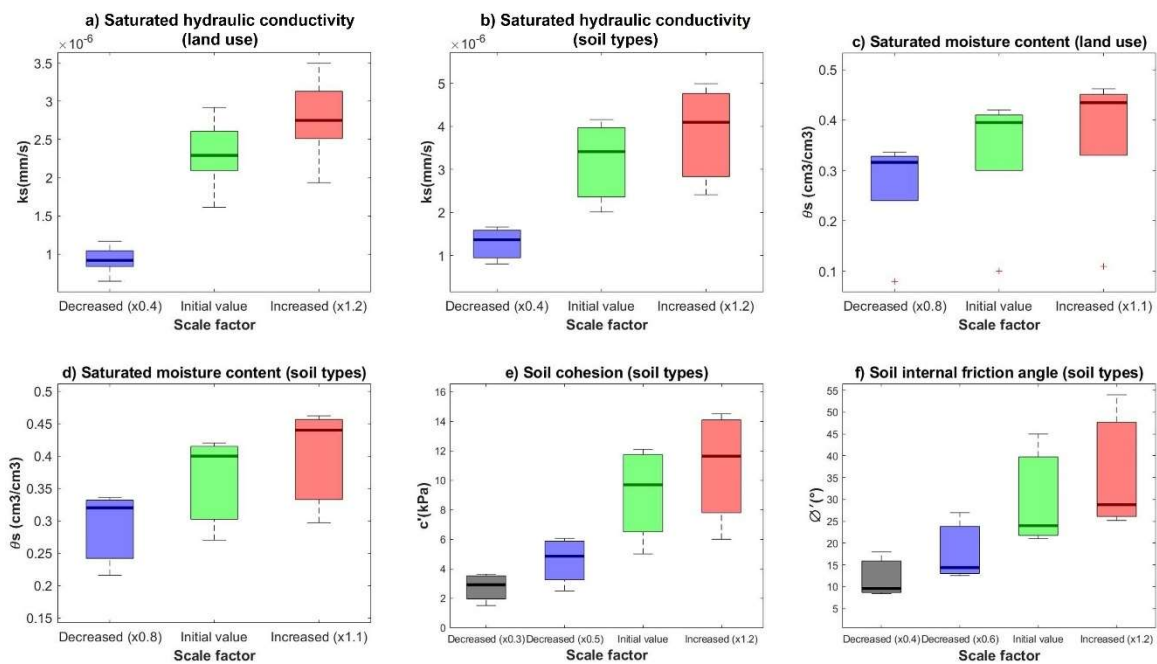


Figure 5.7 Hydrological and geotechnical input parameter value ranges.

### 5.3.3 Steps 3 & 4: Running parametric simulations and verifying catchment-scale hazard representation

The design of parametric simulation was performed according to the procedure established in section 3.2.5, Chapter 3. The parametric simulations were defined according to the combination of the hydrological and geotechnical input parameter value ranges established by the scale factors defined determined in section 5.3.2 for saturated hydraulic conductivity ( $k_s$ ), saturated moisture content ( $\theta_s$ ), for land use and soil types and soil cohesion ( $c'$ ) and soil internal friction angle ( $\phi'$ ) for soil types. The total ensemble of parameter set combinations gave 144 parametric simulations for running in the OpenLISEM hazard model. For the Maipo sub-catchment, the simulation time for the parametric simulations depended on the forcing rainfall defined in Figure 5.2 and the resolution of the input parameters. The duration of the rainfall event on February 25, 2017, was 480 min, and the spatial resolution of the input parameters for the Soufriere catchment corresponded to  $20 \times 20$  metres. The model outputs were computed with time steps of 20 seconds for the simulation time. The numerical settings for the slope stability and flow dynamics modelling for the parametric simulations were based on the values indicated in the OpenLISEM hazard model manual. Each simulation required approximately 4 h on a quad-core (i7) Windows PC with an i7 processor.

The parametric simulations were verified according to the hazard metrics defined in section 3.2.6, Chapter 3. The aim is to screen out the non-behavioural simulations that resulted in unrealistic hazard representations. For the Maipo sub-catchment, a non-behavioural simulation was defined as the hazard representation that does not follow the spatial attributes of the observed hazards in the hazard inventory elaborated in section 5.3.1.

### 5.3.4 Steps 5 & 6: Sub-catchment scale verification of parameter-sets and simulations

For the Maipo sub-catchment, the modelling workflow steps for model verification were adapted according to the observations available for the catchment. In section 5.3.1, it was described the availability of debris flows observations for the 25 February rainfall event. Therefore, the spatial similarity method was adapted to assess the area difference between the total debris flow runout area ( $A_D$ ) resulting from the parametric simulations and the debris flow area estimated from the hazard inventory. The spatial similarity method is described as follows:

#### Spatial similarity

The spatial similarity for the Maipo sub-catchment was addressed by computing the area difference  $\Delta A_D$  (Equation 5.1) between the total debris flow runout areas ( $A_D$ ) resulting from parametric simulations and the total debris flow areas identified from the hazard inventory. The aim is to rank parametric simulations with the best spatial similarity to the observed debris flows. For the Maipo sub-catchment, three criteria were established to identify the parametric simulation with the best spatial similarity. The first corresponds to an area difference of  $\Delta A_T \geq 50 \text{ ha}$ . This difference was considered with no approximation of the total debris flow inventory area. The second corresponds to an area difference  $\Delta A_T \geq -1 \text{ and } \leq 50 \text{ ha}$ . This difference was considered to be proximate to the total debris inventory

area, and the third corresponded to an area difference  $\Delta A_T < -1 \text{ ha}$ . This difference was not considered when approximating the total debris flow inventory area. The area difference  $\Delta A_D$  is expressed as follows:

$$A_T = A_{SIM} - A_{INV} \quad \text{Equation 5.1}$$

Where  $\Delta_D$  corresponds to the area difference,  $A_{SIM}$  is the total simulated debris flow area ( $ha$ ), and  $A_{INV}$  is the total debris flow inventory area ( $ha$ ). Behavioural simulations with area differences  $\Delta A_D \geq -1$  and  $\leq 50 \text{ ha}$  were ranked from the lowest to the highest difference. From the ranked behavioural simulations, the area distribution was compared to assess the similarity between the simulated debris flow runout areas ( $A_D$ ) and observed debris flow areas from the inventory.

### Accuracy assessment

The accuracy assessment was performed by estimating the Jaccard Index (Equation 5.2). The accuracy metric was estimated according to the spatial overlapping method described in Chapter 2, section 2.3.2.2. The Jaccard Index correspond to a similarity coefficient that determines the similarity between two sets with a score ranging from 0 to 1. A score close to 1 indicates a higher similarity between the two sets (Hagen-Zanker and Martens 2008). This metric is commonly used to assess the spatial agreement between debris flow deposition and runout areas (Mead et al. 2021). The Jaccard Index is described as follows:

$$\frac{TP}{TP + FN + FP} \quad \text{Equation 5.2}$$

Where TP correspond to the True Positive values that represent the overlap between the simulated and observed debris flow areas. FN correspond to the False Negative values that represent the debris flow inventory areas minus the TP values and the FP corresponds to the False Positive values that represent the simulated debris flow areas minus the TP values. A tolerance area of 0.5 meters was apply to the debris flow inventory polygons to reduce the mismatch between the spatial overlap of simulated debris flows and debris flow inventory polygons.

### Simulation selection criteria

The simulation selection criteria were determined according to the spatial similarity and the accuracy assessment results. From these results, two criteria were determined to select the parametric simulation with the parameter set that provided the best similitude between the simulated debris flow areas and debris flow inventory areas. The first criteria correspond to behavioural simulations with area difference  $\Delta A_D \geq -1$  and  $\leq 50 \text{ ha}$ . The second criteria correspond to the area distribution fit between the simulated debris flow runout areas and the observed debris flow areas. The parametric simulation that meets these requirements will be selected as the behavioural simulation whose parameter-set provides the best representation of the debris flows observed for the 25 February 2017 rainfall event in the Maipo sub-catchment.



### 5.3.5 Steps 7 & 8: Sensitivity Analysis (SA) and sensitivity to land use and soil type variations

The sensitivity analysis (SA) was performed according to the method described in section 4.2.4, Chapter 4. Regional Sensitivity Analysis (RSA) was applied to assess the sensitivity of the parameter-set corresponding to the selected behavioural simulation. Parameter set confirmation was performed on the selected behavioural simulation according to the criteria established in section 5.3.4. The goal is to identify the hydrological and geotechnical factor values in accordance with the land use categories and soil types that influenced the occurrence of landslides, debris flows and net erosion rates according to the rainfall event. This was performed by identifying the total debris flow runout areas ( $A_D$ ) for every land use category and soil type unit. Categories and units with a high number of debris flow runout areas ( $A_D$ ) were established as sensitive land use categories and soil types units in the influence debris flows. From the identification of the sensitive units, the hydrological and geotechnical parameter values were identified for each land use category and soil type unit from the parameter-set corresponding to the selected behavioural simulation.

### 5.3.6 Step 9: Explore land use and climate change scenarios

#### Hazard magnitude evolution

The magnitude of hazard evolution was assessed through a map series report established according to the total time step corresponding to the simulation, which is a function of the total duration of the rainfall event. The duration of the February 25 rainfall event corresponds to 8 h, which is equivalent to 480 min. The determination of the time step for the simulation is a function of the resolution of the input data, which has a size of 20 × 20 metres. Therefore, the number of time steps corresponds to 1440, resulting from the total rainfall duration in seconds divided by the data resolution. The map series report was established for every 60-time steps, giving a total number of map series for the simulation of 24 maps. The hazard representations for every map series were estimated according to the hazard metrics established in section 3.2.6, Chapter 3.

#### Response to land use and climate change scenarios

The responsiveness to land use and rainfall change was assessed using the same matrix proposed for the Soufriere catchment in section 4.2.6, Chapter 4, which incorporates the responses of the land use categories and different rainfall patterns (Table D.3). The land use change matrix was adapted to the land use and rainfall corresponding to the Maipo sub-catchment. Within the land use change matrix, the categories corresponding to the *native forest were changed to scrub forest*. The preceding was proposed assuming the scenario in which the loss of native forest due to hillslope deforestation due to the growing pressure of urbanisation and the loss of natural land cover by increasing wildfires during the summer period increases the magnitude of landslides, debris flows, and hillslope erosion (Garreaud et al. 2017; Moreiras et al. 2021). On the other hand, the categories of the *scrub forest were changed to a native forest*, assuming a scenario in which the increase of native forest on hillslopes with less land cover increases the slope stability and reduces the impacts and magnitude of landslides, debris flows, and hillslope erosion (Sidle and Ochiai 2006). A change in land use categories implies a change in the

values of the hydrological parameters corresponding to these categories. The hydrological parameter values corresponded to the confirmed parameter-set values identified according to each land use unit and soil type.

The responsiveness of the catchment to the proposed land use change was assessed with respect to the February 25, 2017, rainfall event and rainfall events of 10-year return period intensity–duration–frequency curves (IDFs) obtained from the technical report of UNESCO (2013) (Pizarro et al. 2007) for the metropolitan region of Santiago. The selected rainfall events correspond to a 12-hour rainfall with a total volume of 34.2 mm, a 6-hour rainfall with a total volume of 16.2 mm and a 4-hour rainfall with a total volume of 12.8 mm (Appendix D.2 ). Therefore, eight scenarios were proposed to assess the response of land use change to the selected rainfall events within the Maipo sub-catchment. The responses to different hazard patterns were assessed according to the hazard metrics established in section 3.2.6, Chapter 3. The rate of change between the hazard representations resulting from the selected behavioural simulation in section 5.4.1 was compared with respect to the hazard representations resulting from the eight proposed scenarios to assess the rate of change in the magnitude of each hazard.

## 5.4 Results

### 5.4.1 Behavioural simulation selection

The response of the Maipo sub-catchment to 144 parametric simulations resulted in 40 behavioural simulations with representations of total landslide surface area ( $A_L$ ), total debris flow runout area ( $A_D$ ), and total net erosion ( $Net_E$ ). These hazard representations were registered from simulations 1 to 36 and 38, 39, 42, and 45. From simulations 46–144, no landslide representation was observed. The behavioural simulation was selected from simulations that resulted in a landslide, debris flow and net erosion rate representation. According to the spatial similarity method, five simulations were within the area difference  $\Delta A_D \geq -1$  and  $\leq 50$  ha (Table 5.1). The lowest area difference between the total debris flow runout area and debris flow inventory area was observed in simulations 30 and 4. However, despite having the lowest area difference  $A_D$ , the area distribution of the debris flow flooded areas did not follow the same distribution pattern as the debris flow inventory. The most approximate distribution pattern was observed in simulations 27, 25, and 21 (Figure D.6). According to the area difference  $A_D$ , these simulations obtained differences  $\geq 30$  and  $\leq 44.5$  ha. In these simulations, an overprediction of debris flow runout areas was observed between 0 and 3 ha and between 3 and 6 ha. This overprediction was observed within the same area distribution in the debris flow inventory areas, indicating that the simulated debris flow from those simulations was similar to the observed debris flows.

Regarding the accuracy metrics, the Jaccard Index showed the highest values for simulations 27 and 21 (Table 5.2). In this case, simulation 27 achieved an accuracy score of 0.33 and simulation 21 achieved a score of 0.32. These values indicate an improvement in the accuracy scores after application of the tolerance area for debris flow inventory polygons. The accuracy score was highly influenced by the difference in resolution of the image in which the inventory polygons were identified, and the

resolution of the debris flow simulated areas. This affected the overlapping between the simulated and observed areas. This affects the overlap between the simulated and observed areas. Regarding the area difference ( $A_D$ ), the area distribution between the simulated and observed debris flow runout areas and the accuracy metric score. Behavioural simulation 27 (Table 5.2) was selected as the simulation with the parameter set that provided the best similarity between the simulated and observed debris flows. From the selected simulation, it was identified a total simulated debris flow runout area ( $A_D$ ) of 59.7 ha, a total landslide area ( $A_L$ ) of 58 ha and net erosion rate ( $Net_E$ ) of  $-2452.9$  ( $ton.m^{-2}$ ) which mostly corresponds to deposition rates.

Table 5.2 Behavioural simulations ranking and accuracy scores.

Simulations	Simulated			Observed	Verification	
	Landslide surface area $A_L$ (ha)	Net erosion $Net_E$ ( $ton.m^{-2}$ )	Debris flow runout area $A_D$ (ha)	Total area (ha)	$\Delta A_T$	Jaccard Index
<b>SIM30</b>	2.8	-3230.7	52.8	51.3	1.6	0.22
<b>SIM27</b>	<b>57.2</b>	<b>-2451.9</b>	<b>59.6</b>	<b>51.3</b>	<b>8.4</b>	<b>0.33</b>
<b>SIM4</b>	153.4	-2180.4	67.2	51.3	16.0	0.06
<b>SIM25</b>	60.2	-3487.7	61.7	51.3	10.4	0.28
<b>SIM21</b>	<b>60.4</b>	<b>-4991.2</b>	<b>73.8</b>	<b>51.3</b>	<b>22.5</b>	<b>0.32</b>

#### 5.4.2 Sensitivity Analysis (SA)

A Regional Sensitivity Analysis (RSA) was performed to identify the most influential input parameters for land use categories and soil types in the Maipo sub-catchment for the selected behavioural simulation. According to the maximum distance (K-S statistics) derived from the cumulative distribution function curves (CDFs), the sensitivity indices were computed for the total number of parameters. Figure 5.8 illustrates the sensitivity indices estimated using the bootstrap method with 95% confidence. The results indicated that the most influential parameters were saturated moisture content ( $\theta_{s2}$ ) for soil types, saturated hydraulic conductivity ( $k_{s1}$ ) for land use, and soil internal friction angle ( $\phi'$ ) and soil cohesion ( $c'$ ) for soil types. These results indicate that these parameters are the most influential within the parameter-set of behavioural simulation 27, showing that they significantly influenced the magnitude of the total landslide surface area ( $A_L$ ), total debris flow runout area ( $A_D$ ), and total net erosion ( $Net_E$ ). The less influential parameters corresponded to the saturated moisture content ( $\theta_{s1}$ ) for land use and the saturated hydraulic conductivity ( $k_{s2}$ ) for soil types.

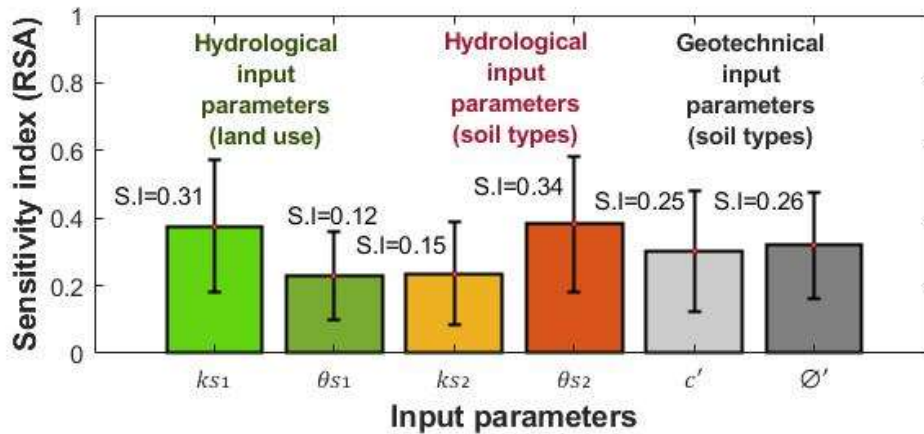


Figure 5.8 Sensitivity indices (S.I) for each input parameter. The bars correspond to the sensitivity indices mean value estimated with bootstrapping while the vertical lines at the top bar represent the confidence intervals for each input.

### 5.4.3 Hazard magnitudes evolution

Figure 5.9 illustrates the evolution of the total landslide surface area ( $A_L$ ), total debris flow runout area ( $A_D$ ), and total net erosion ( $Net_E$ ) magnitudes according to the duration of the February 25 rainfall event. The most significant landslide magnitudes ( $A_L$ ) were registered within the first two hours of rainfall in which a total landslide area ( $A_L$ ) of 36.16 ha was identified (Figure 5.9b). Similarly, the total debris flow runout area ( $A_D$ ) also reached a considerable magnitude within the first two hours of rainfall, registering a total cumulative area of 58.04 ha (Figure 5.9b). However, it was observed that from the total cumulative area, the biggest magnitudes were registered within the period in which the landslides occurred, identifying a total area of 46.6 ha for the same period. The observed results indicated that the magnitude of the landslide influenced the debris flow magnitude. This influence was given by the hillslope runoff generated that reached the  $1.9 (m^3 \cdot s^{-1})$  accumulated during the first two hours of rainfall (Figure 5.9a). However, the hillslope runoff generated during this period did not reach its peak discharge after four hours of rainfall. The influence of entrainment rates increased the sediment material within the flow, according to the landslide volume material generated within the first two hours. The foregoing was observed in the accumulated deposition rates that reached the  $4183.3 (ton \cdot m^{-2})$  of deposited material and the accumulated erosion rates that registered  $2582.2 (ton \cdot m^{-2})$  of eroded material between the two and three hours after the landslides and debris flow occurred (Figure 5.9c).

The total net erosion ( $Net_E$ ) obtained from the erosion and deposition rates for the period between the two and three hours of rainfall resulted in  $-1601.1 (ton \cdot m^{-2})$  of accumulated deposited sediment, indicating the predominance of deposition during that period (Figure 5.9c). From the net erosion results, it was observed that the predominance of deposition was due to the debris flow magnitude registered for three hours. This indicates that after the landslide occurred, the magnitude of the debris flow was still influenced by the landslide material volume. This influence was given by the flow generated between the two and three hours of rainfall that increased to the  $4.7 (m^3 \cdot s^{-1})$ . In the case of the Maipo sub-

catchment, it was observed that hillslope runoff determined the interaction mechanism between landslides and debris flows and their impacts on net erosion rates. It was identified that after four hours of rainfall, when no landslides were simulated, debris flow and net erosion magnitude were reduced.

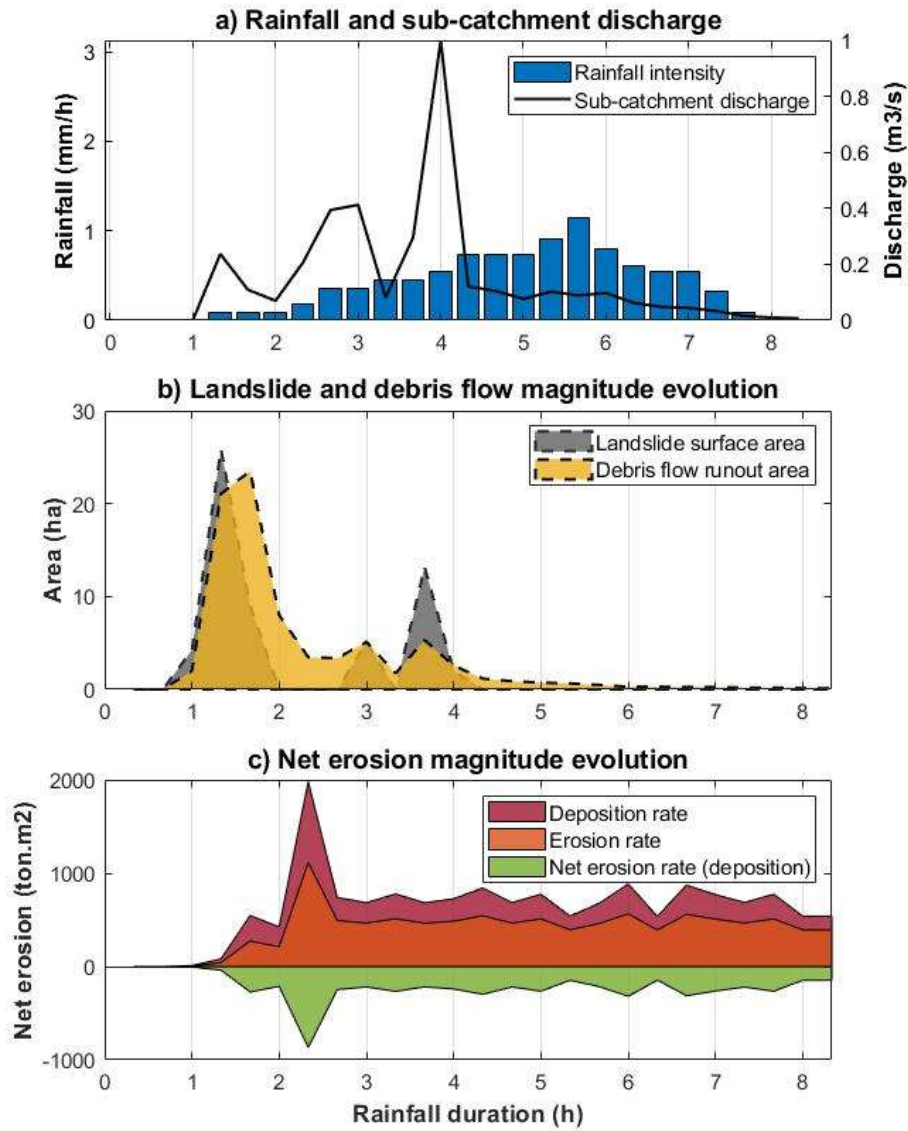


Figure 5.9 Hazard magnitude evolution. (a) Rainfall duration and discharge, (b) landslide and debris flow magnitude evolution, (c) net erosion rates.

#### 5.4.4 Sensitivity to land use and soil type variation

Figure 5.10 shows the distribution of hydrological and geotechnical parameters values for the sensitive land use units and soil types that influenced debris flow within the Maipo sub-catchment. The parameter value distribution for saturated hydraulic conductivity ( $k_{s1}$ ) for land units (Figure 5.10a) indicated that the highest values were distributed in grasslands, scrub forests, and native forests. The lowest values were found in bare soil, mixed farming, and urban settlements. However, according to the Regional Sensitivity Analysis (RSA) results, this parameter was one of the less influential factors in the occurrence of debris flows. Figure 5.10b shows the parameter distribution corresponding to the saturated moisture content ( $\theta_{s1}$ ) for land use. From the RSA results, this parameter is one of the most sensitive to the occurrence of debris flows. The highest values for this parameter were equally distributed among units such as native forests, scrub forests, grasslands, and bare soils (Figure 5.11a). The lowest values were observed in mixed farming and urban settlements. The largest total debris flow runout areas were registered in the scrub forest category, indicating that the value for this unit highly influenced the magnitude of debris flows.

Regarding the value distribution for saturated hydraulic conductivity ( $k_{s2}$ ) for soil types (Figure 5.10), the highest values were observed in residual and colluvial soils, and volcanic soils (Figure 5.11b). In contrast, the lowest values were observed in soils from the fluvial terraces. According to the RSA results, this parameter exhibited the highest sensitivity. For this parameter, the highest total debris flow runout areas were observed within the unit of volcanic soils, indicating that the value distribution for this unit impacted debris flow occurrence. The value distribution for saturated moisture content ( $\theta_{s2}$ ) for soil types (Figure 5.10d) indicated the highest values in units, such as volcanic soil and soils from fluvial terraces. The lowest values were observed in residual and colluvial soils (Figure 5.11b). The RSA results indicated that this parameter was less sensitive to the influence of debris flows and saturated hydraulic conductivity on land use.

In relation to the parameter value distribution for soil cohesion ( $c'$ ) for soil types (Figure 5.10e), the highest values were equally distributed in the soil types of residuals, colluvial soils, and soils from fluvial terraces. The lowest values were observed in the volcanic soils. In the case of soil internal friction values ( $\phi'$ ) (Figure 5.10f), the highest values were distributed in volcanic soils and the lowest in residual and colluvial soils and soils from fluvial terraces. According to the RSA results, these two parameters were the most sensitive to the occurrence of debris flows, especially in volcanic soils where the highest debris flow flooded areas were registered. It was observed that for the parameter set of simulation 27, the parameter value combination of saturated moisture content ( $\theta_{s1}$ ) for land use, saturated hydraulic conductivity ( $k_{s2}$ ) for soil types, soil cohesion ( $c'$ ) and soil internal friction values ( $\phi'$ ) influence the occurrence and distribution of debris flow within the Maipo-sub catchment. Therefore, the value distribution for these units is considered to be highly sensitive to the spatial representation of debris flows.

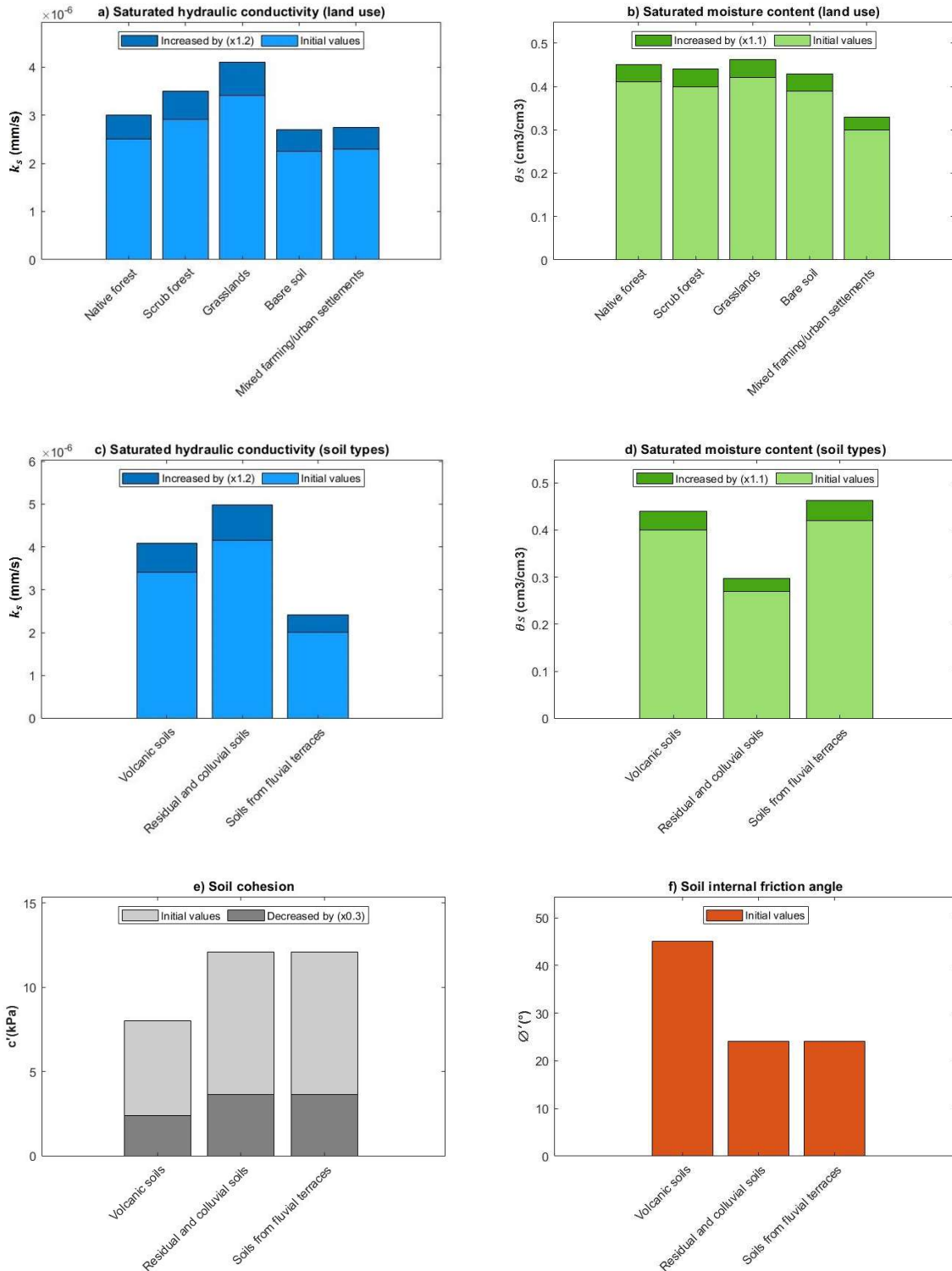
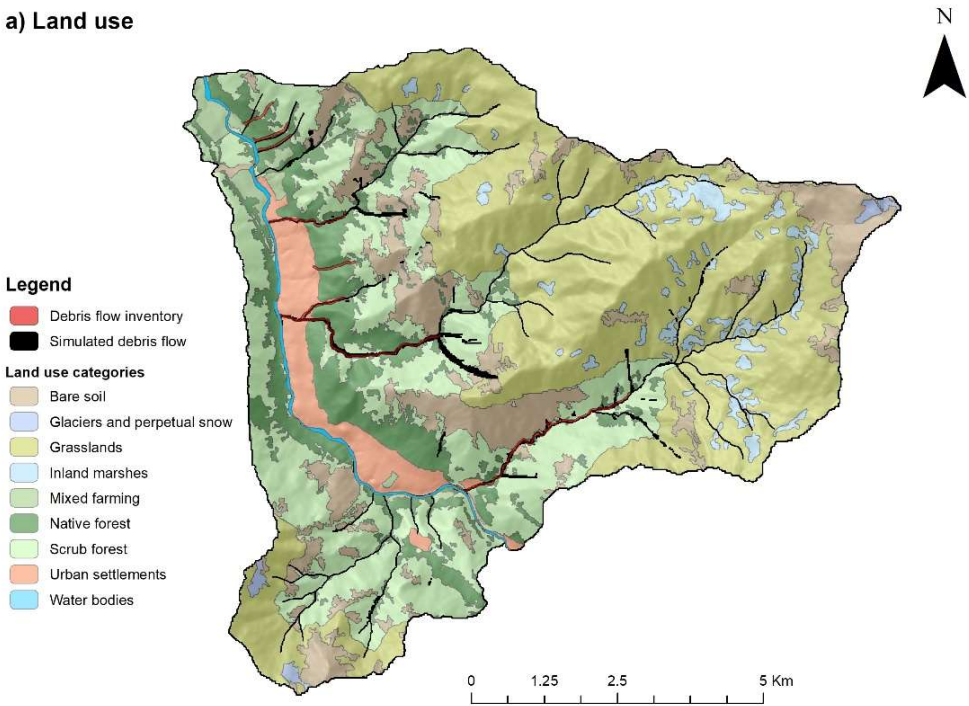


Figure 5.10 Parameter values for soil types. (a) Saturated hydraulic conductivity (land use), (b) Saturated moisture content (land use), (c) Saturated hydraulic conductivity (soil types), (d) Saturated moisture content (soil types), (e) Soil cohesion (soil types), (f) Soil internal friction angle (soil types).

a) Land use



b) Soil types

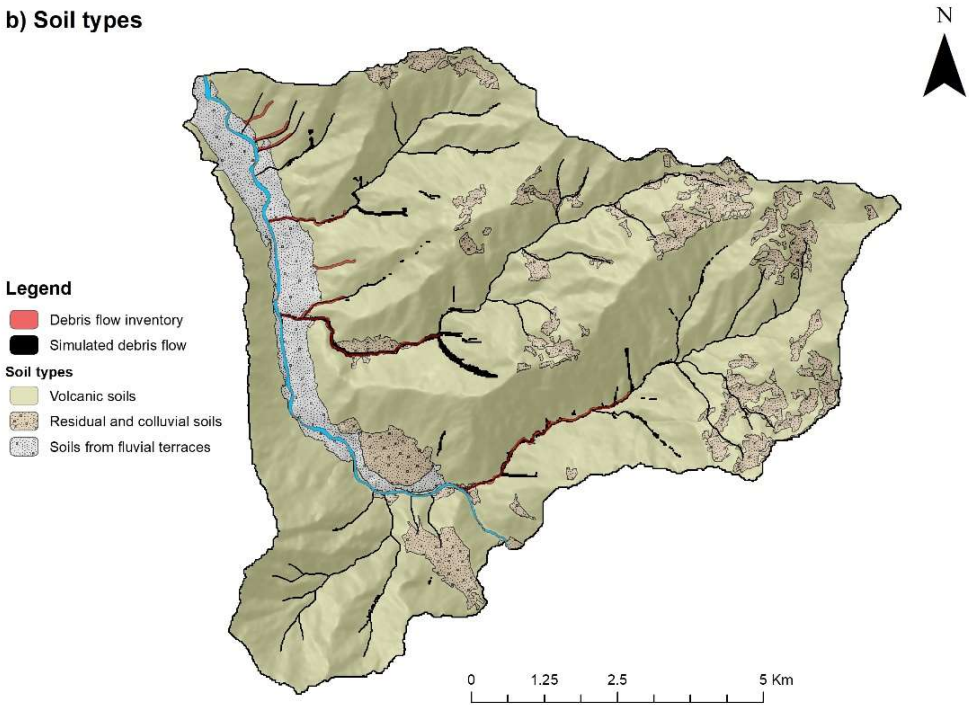


Figure 5.11 (a) Land use and (b) soil types of the Maipo sub-catchment.



### 5.4.5 Responsiveness of the Maipo sub-catchment to land use and rainfall change

Figure 5.12 illustrates the percentage of change in total landslide surface area ( $A_L$ ), total debris flow runout area ( $A_D$ ), and total net erosion ( $Net_E$ ) magnitudes according to the responsiveness to land use and rainfall change scenarios. The hazard magnitudes estimated from the selected behavioural simulation in section 5.4.1. Under the current land use for the Maipo sub-catchment, there was an increase in the landslide, debris flow, and net erosion rate magnitudes for a 12-hour rainfall event and a decrease for 6- and 4-hour rainfall events (Figure 5.12). For the February 25, 2017, rainfall event (8-hour rainfall), an increase of +5.2% in landslides, a +16.7% in debris flows, and a +5.9% increase in net erosion rates for a rainfall of 12-hour (Figure 5.12). On the other hand, for a 6-hour rainfall event, it was identified a decrease of -23.6% in landslides, -30.1% in debris flows, and -47.7% in net erosion rates (Figure 5.12). Similarly, the same decreasing pattern was observed for a 4-hour rainfall event, in which the landslides decreased by -12.4%, the debris flow by -16.8%, and the net erosion rates decreased by -23.7% (Figure 5.12). It was identified that the spatial distribution of landslide and debris flows observed for the 12, 6, and 4-hour rainfall events under the current land use followed the same spatial location regarding the observed hazards during the 25 February 2017 rainfall event.

Land use scenarios in which the scrub forest was changed to a native forest. Responsiveness to the February 25 rainfall event (8-hour rainfall) and to 12, 6 and 4-hour rainfall events indicated a decrease in the hazard magnitude with respect to the current land use. For example, in the case of the February 25 rainfall event, the landslide magnitude decreased by -1.8%, the debris flow by -1.3 and the net erosion rates by -4.8% (Figure 5.12). Similarly, for the 12-hour rainfall event, it was observed a decrease of -6.3% in landslides, -11.8% in debris flows, and -1.1% in net erosion rates (Figure 5.12). The same decrease was observed for the 6 and 4-hour rainfall events. For the first one, there was a decrease of -9.2% in landslides, -32.2% in debris flows and -26.7% in net erosion rates (Figure 5.12). For the second scenario, a decrease of -9% in landslides, -14.2% in debris flows, and -6.7% in net erosion rates was observed (Figure 5.12). Under this land use scenario, the spatial location of landslides and debris flows followed the same location pattern observed according to the simulated hazards for the current land use. The response of this land use scenario to the February 25 rainfall event (8-hour rainfall) and the 12-, 6-, and 4-hour rainfall events indicated a decrease in landslides, debris flows, and net erosion rate magnitudes for the set rainfall events. In this scenario, the hazard magnitude decreases with respect to current land use, validating the hypothesis that an increase in native forest over scrub forest decreases the magnitude and frequency of rainfall-triggered landslides, debris flows, and hillslope erosion hazards.

For the scenario in which the native forest was changed to scrub forest. The response to the February 25, 2017, rainfall event indicated an increase of +3.6% in landslide magnitude, +4.8% in debris flows, and +2.3% in net erosion rates concerning the simulated hazard under the current land use (Figure 5.12). For the 12-hour rainfall event, the landslide magnitude increased by +2.9%, the debris flows by +4.4%, and the net erosion rates increased by +3.9% (Figure 5.12). However, for the 6- and 4-hour rainfall events, an increase in the hazard magnitude was also observed for this land use scenario. For the case of h 6-hour rainfall event, the landslide magnitude increased by +7.4%, the debris flow was +5.5%, and the net erosion rate was +0.59% (Figure 5.12). Concerning the 4-hour rainfall event, it was

observed an increase of +10% in the landslide magnitude, +4.6% in debris flows, and +11.3% in net erosion rates (Figure 5.12).

For this land use scenario, the spatial location of landslides and debris flows followed the same location pattern observed for the current land use and for the scrub forest compared to the native forest scenario. The only difference was that the hazard magnitude increased for landslides, debris flows, and net erosion rates. On the other hand, as was observed for the previous land use scenarios, the response to the February 25 rainfall event (8-hour rainfall) and the 12-, 6-, and 4-hour rainfall events indicated a decrease in landslides, debris flows, and net erosion rate magnitudes for each rainfall event Figure 5.12). According to the hazard magnitude observed for this scenario, it was validated the hypothesis that the decrease in native forest due to hillslope urbanisation and wildfires increased the magnitude and frequency of rainfall-triggered landslides, debris flows, and hillslope erosion hazards in areas in which scrub forest is more predominant.

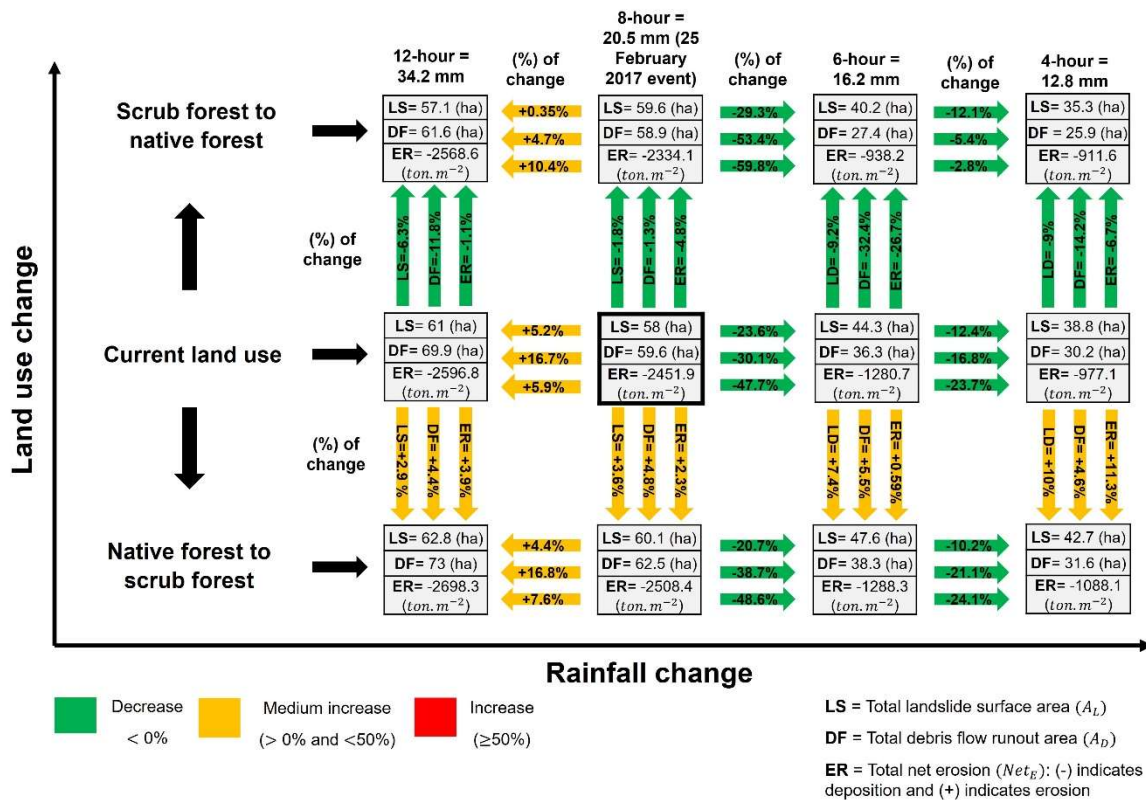


Figure 5.12 Multi-hazard response of the Maipo sub-catchment to land use and rainfall change.

## 5.5 Discussion

### 5.5.1 Applicability of the modelling workflow for the Maipo sub-catchment

The response of the Maipo sub-catchment to the parametric simulations identified 40 behavioural simulations with representations of rainfall-triggered landslides, debris flows and hillslope erosion rates. The application of the spatial similarity method identified behavioural simulations 21 and 27 as the most proximate to the debris flows observed for the 25 February 2017 rainfall event. The identification of these simulations reflected the usability of the full extent of the modelling workflow applied for the Maipo sub-catchment. For example, when applying the first stage for experimental design. The run of parametric simulations identified the regions of the input parameter ranges that introduced the largest sources of uncertainty in the representation of the three hazards. This was reflected in the hazard magnitude that was expressed in total landslide surface area ( $A_L$ ), total debris flow runout area ( $A_D$ ), and total net erosion ( $Net_E$ ). The first stage of the modelling workflow demonstrated managing these uncertainties for the Maipo sub-catchment, especially by considering the limitation related to the lack of information and data available. Several methods have been proposed to explore parameters-sets in catchments with limited data information, studies such as Merz et al. (2020); Lane et al. (2021) and Herrera et al. (2022) have highlighted the necessity to develop methodologies to identify the necessary parameters to discretize the catchment domain. This an important stage for complex models, such as the OpenLISEM hazard model that requires a large number of input parameters to model hillslope hydrological hazard interactions.

When comparing to the stage one of modelling workflow applied in Chapter 3, the magnitude of the simulated hazards for the Maipo sub-catchment followed the same magnitude pattern observed for the Soufriere catchment. This magnitude pattern was expressed in the hazard magnitude estimated according to the hazard metrics proposed to verify the parametric simulations. For both cases, it was observed that the major uncertainties were registered in parametric simulations that reduced soil cohesion by (x0.3) (see Table D.2), reduce soil internal friction angle by (x0.4) (see Table D.2) and increase saturated moisture content by (x1.1) (see Table D.1). According to Khatami et al. (2019), the uncertainty in input parameters are addressed by searching multiple acceptable parameter range values. The application of multiplication factors to explore parameter ranges for hydrological and geotechnical input factors estimated for different catchment environments shows the effectiveness of the modelling workflow to identify the sensitive regions of the estimated input parameters.

The stage two of modelling workflow for model verification also demonstrated its effectiveness. The application of the spatial similarity method according to the debris flow inventory indicated that is possible to define spatial attributes for debris flows to assess the similarity between the simulated and observed hazards. Moreover, the application of the Jaccard index and the definition of tolerance areas also showed the efficiency of the proposed spatial overlapping method to estimate the model accuracy. According to these methods, it was possible to select behavioural simulation 27 as the most proximate to the observed debris flows.

### 5.5.2 Representation of hillslope hydrological multi-hazard interactions

For the case of the 25 February 2017 rainfall event, the interaction between rainfall-triggered landslides, debris flows hillslope erosion in the Maipo sub-catchment was influenced by the hillslope runoff and flash floods generated during the first 2 hours of the rainfall event. According to Figure 5.9a, the magnitude evolution of the simulated hazards depended on the rainfall intensity and the hillslope runoff at the moment these hazards occur. For example, within the first two hours of rainfall, the hillslope runoff generated reached  $1.9 (m^3 \cdot s^{-1})$  and the rainfall intensity was less than  $0.5 (mm \cdot h^{-1})$ . These results indicated that for Mediterranean catchments such as the Maipo sub-catchment. Short and less intense rainfall can generate the necessary hillslope runoff and flash floods to influence the interactions of rainfall-triggered landslides, debris flows and hillslope erosion. Recent studies for the central Andes, such as Carretier et al. (2018) and Lobo and Bonilla (2019) have evidenced that short rainfall periods in semi-arid catchments increase the sediment yield. This increase has been evidenced during the last 10 years, especially during El Niño events periods (Garreaud et al. 2017). However, this increase in sediment yields does not account for the influence of sediment material from landslides and debris flows (Moreiras et al. 2021). For example, for the Maipo sub-catchment, is possible to confirm that shallow landslides are the primary hazard that influences the magnitude of debris flows and hillslope erosion rates.

Figure 5.9c, shows how the magnitude of hillslope erosion rates decreased after the period in which landslides occurred, indicating the influence of landslides on debris flow magnitude increases the net erosion rates, especially in the deposition. According to Pudasaini and Fischer (2020), these influences are governed by entrainment rates, which are determined by the amount of hillslope runoff generated during the rainfall event. According to Michaelides and Martin (2012), rainfall in Mediterranean environments is characterised by short, spatially variable, high-intensity storm events that generate surface infiltration - excess runoff from sparsely vegetated slopes. The combination of short duration, high intensity storms and sparse vegetation increases the susceptibility to generate hillslope runoff and flash floods (Yeh and Tsai 2018). During these intense storm events, excess runoff accumulates rapidly, leading to increased water flow and erosion potential. Debris-covered slopes, especially after landslides, exacerbate this effect as landslides can mobilize loose material and contribute to debris flow, sediment transport, and hillslope erosion (Moreiras et al. 2021). To understand these interactions, it is necessary to identify the catchment physical characteristics that influence them. The modelling workflow for model verification identified the sensitive input parameters influencing these relationships. According to the Regional Sensitivity Analysis (RSA) performed, saturated moisture content ( $\theta_{s2}$ ) for soil types and saturated hydraulic conductivity ( $k_{s1}$ ) for land use were the most sensitive input parameters. The spatial distribution of these sensitive input parameters values was observed for soil types such as volcanic soils and native and scrub forests for land use. The parameter-set confirmation corroborated the sensitivity of these units in which most of the simulated landslides and debris flow were spatially distributed.

### 5.5.3 Responsiveness to land use and rainfall change scenarios

The change of native forest to scrub forest was identified as the main scenario that influenced the increase in the magnitudes of the three hazards. These model findings are in accord with observations presented by Vergara et al. (2020) and Moreiras et al. (2021), which identified how the changes in land use, precisely due to deforestation by wildfires, logging and the growing pressure of human activities, have increased the magnitude of debris flows in the central Andes. For the case of the Maipo sub-catchment, assessing this scenario is in line with the tendency observed for the Andean catchments of the Metropolitan area of Santiago de Chile. According to Henríquez-Dole et al. (2018), the projections in land use to 2050 for the Maipo sub-catchment indicate an increase in farmland areas. As was observed for the Soufriere catchment, the scenario where the natural tropical forest was changed to mixed farming and forest stated an increase in the magnitude of the landslides, debris flows and net erosion rates with Hurricane Tomas rainfall and the 24, 10 and 5-hour rainfall events. The same tendency might be observed for the Maipo sub-catchment. However, the differences in climate, geological and land use settings might influence the increase of these hazards differently.

First, the potential impact of land use on hillslope hydrological hazard interactions depends on the land use dynamics of each catchment. In the case of the Soufriere catchment, these dynamics are driven by human and economic activities (Walters 2016). In the Maipo sub-catchment, on the other hand, land use dynamics have been influenced by both the effects of climate change in recent years and anthropogenic factors (Garreaud et al. 2017; Moreiras et al. 2021). For example, in terms of land uses to which native forest has been converted by anthropogenic actions, official figures show that between 1995 and 2016, most of it was replaced by grassland and scrubland (47%) or forest plantations (40%), followed by conversion to agricultural land (6%), with the remainder converted to agriculture (6%) (Miranda et al. 2017). In addition, the combined effects of drought and wildfire in the region have led to long-term changes in the physical characteristics of the catchment and in hydrological and stability processes (Martínez-Retureta et al. 2020). These effects may be reflected in reductions in vegetation cover and impacts on soil moisture and infiltration capacity (Balocchi et al. 2023). The above is consistent with the land use scenarios simulated for the Maipo sub-catchment, where the change from native forest to shrubland shows an increase in the magnitude of hillslope hydrological hazards, leading to significant and interrelated impacts on landslides, debris flows and hillslope erosion. Therefore, the identification of the most sensitive hydrological and geotechnical parameters for land use and soil types for the Maipo sub-catchment was essential to assess these effects.

The assessment of the land use and rainfall change scenarios also indicated the reduction of the hazard magnitudes when the scrub forest is changed to native forests. The response of the land use scenarios to the 25 February 2017 rainfall event (8 hours) and the events of 12, 6 and 4 hours indicated that the simulated hazard followed the same spatial distribution for each rainfall event. The only difference is in the change of magnitude for each hazard. The same spatial pattern was observed for the Soufriere catchment, in which the hazard magnitudes for the proposed scenarios followed the same location, but the hazard magnitude changed according to the rainfall events. These results indicate that the

application of the full extent of the modelling workflow for the Maipo sub-catchment is effective to assess the potential effects of land use and rainfall change on hillslope hydrological hazards interactions.

## 5.6 Conclusions

In this chapter, the application of the complete modelling workflow for the Maipo sub-catchment, addressed answer research question 3 of this thesis (RQ3: *How do hillslope hydrological multi-hazards and their interactions respond to changes in land use and rainfall characteristics?*). This chapter shows how the full extent of the modelling workflow developed in this thesis can be applied in two catchments with different climatic and environmental settings. For the case of the Maipo sub-catchment, the application of the modelling workflow has demonstrated that is possible to assess hillslope hydrological hazard interactions and their response to different land use and rainfall change scenarios in a catchment with limited data and information. The application of the stage one of the modelling workflow for model parameterisation allowed the setting of parametric simulations to identify the behavioural simulations whose parameter-set provided the best representation of the debris flows observed for the 25 February 2017 rainfall event.

The hazard magnitude evolution identified that landslides are the primary hazard that influences the magnitude of debris flows and their impacts on hillslope erosion rates. For the case of the 25 February 2017 rainfall event, it was observed that during the first 2 hours of rainfall most of the hazards interact influencing in their magnitudes. The hazard interactions depend on the rainfall intensity, hillslope runoff and flash flood generated at the moment these hazards occur. The generation of these conditions within the catchment determine the feedback mechanisms that make these hazard produce cascading, concurrent, and compounding interactions.

The selection of the behavioural simulation 27 allowed the identification of the sensitive land use categories and soil types units that influenced the occurrence of rainfall-triggered landslides, debris flows and hillslope erosion hazards. The incorporation of sensitivity analysis in the modelling workflow for model verification was an essential step to identify the most influential input parameter values for land use categories and soil type units. The parameter-set confirmation identified land use categories such as native forest, and scrub forest and volcanic soils for soil types as the most sensitive. The land use change scenario in which the native forest was changed to scrub forest indicated an increase in the hazard magnitude. These results support the assumption that the decrease in native forest as consequence extensive drought periods, wildfires and anthropogenic activities impacts the magnitude of hillslope hydrological hazards in a context of land use and climate change.

---

---

## **Chapter 6 Summary and conclusions**

---

---

## 6.1 Research summary

The effects of land use and climate change are increasing the frequency and impacts of hillslope hydrological hazards in mountainous regions highly susceptible to these hazards. Physics-based multi-hazard models, representing rainfall-triggered landslides, debris flows, and hillslope erosion hazards at catchment scales, are necessary for assessing the interactions and impacts of these hazards for different land use and climate change scenarios and to support sustainable and resilient planning policies to reduce the impacts of these hazards and mitigate the effects. However, modelling methodologies must address challenges of parameterisation, equifinality and uncertainties associated with such complex spatially distributed models. This thesis has contributed by introducing a systematic modelling workflow that addresses the parameterisation and uncertainties in complex multi-hazard models – improving the modelling of these hazards for catchments with data scarcity. The OpenLISEM hazard model has been applied using this new workflow to investigate impacts of land use and climate change in two catchments prone to hillslope hydrological multi-hazards.

### 6.1.1 A modelling workflow to assess hillslope hydrological hazard interactions for land use and rainfall change

This thesis introduces a new modelling workflow to enable physics-based distributed modelling of multi-hazards in data-limited regions. The workflow draws on current best practice for environmental modelling and the application of conventional single-hazard models. It addresses the challenges of parameterisation, equifinality and uncertainty associated with complex physics-based distributed models and compounded by data limitations in many disaster-prone regions. Two case study catchments with contrasting climatic, environmental, and multi-hazard characteristics were selected for workflow testing and application. Both were representative of disaster-prone socio-economically vulnerable regions where data and resources for hazard assessment and risk management are limited. The modelling workflow starts by identifying statistical distributions of parameter values, this is an important step because allows the exploring of the quality of the input data by identifying the parameter ranges that might introduce uncertainty.

The sampling of parameter range values to perform parametric simulations in the stage one of the modelling workflow allows the exploring of the uncertainties by verifying at the catchment scale the behavioural simulations that resulted in the spatial representation of rainfall-triggered landslides, debris flows, and the hillslope erosion hazards observed for Hurricane Tomas. The application of the hazard metrics to estimate the total landslide surface area ( $A_L$ ), total debris flow runout area ( $A_D$ ) and the total net erosion ( $Net_E$ ) demonstrated to be an effective procedure to identify the behavioural simulations that resulted in extreme hazard representations. Landslide surface areas over  $\geq 100$  ha were observed in parametric simulations were the parameter range values for geotechnical input factors such as soil cohesion were reduced by (x0.3) (see value ranges in Table B.5) and soil internal friction angle were reduced by (x0.4) (see value ranges in Table B.5). For the case of the Maipo sub-catchment, the application of the first stage of the modelling workflow demonstrates its effectiveness if identifying the



parametric simulations with more proximity to the debris flows observed for the 24 February 2017 rainfall event allowing the identification of the parameters that most influenced the hazard representation. The elaboration of the first stage of the modelling workflow applied in Chapter 3, was effective for two catchments, both representative of disaster-prone socio-economically vulnerable regions where data and resources for hazard assessment and risk management are limited.

The new modelling workflow continues with the stage 2 for model verification and parameter-set selection to identify the behavioural simulations not only give a representative magnitude of the hazards at the catchment scale, but are verified in terms of their spatial scale, locations, and distributions within the catchment. This is an important step because it is considered the parameter set that can be used to assess future land use and climate change scenarios. The modelling workflow for model verification identified the effectiveness of the verification procedure allowing identifying, for example, the sensitive land use and soil type units that influenced the occurrence of rainfall-triggered landslides debris flows and hillslope erosion hazards. Identifying these units was important to address research question 2 (RQ2), especially because set the basis to simulate land use and climate change scenarios.

Having applied the new modelling workflow, this thesis quantifies how rainfall-triggered landslide, debris flow and hillslope erosion hazard magnitudes and interactions can change under potential land use and rainfall scenarios in the two case study catchments. These catchments exhibit contrasting climatic and environmental characteristics and hazard profiles. The application of the stage three of the modelling workflow was important to address research question 3 (RQ3) in Chapter 4 and Chapter 5. Applying the modelling workflow in the Soufriere catchment and the Maipo sub-catchment showed its effectiveness by allowing the assessment of the Hurricane Tomas rainfall event and the 25 February 2017 event in these two catchments allowing the possibility to explore the effects of those rainfall events and their potential effects on different land use and rainfall scenarios.

### **6.1.2 Identification parameter variations and uncertainties in multi-hazard assessment**

The application of the area difference method to assess the similarity in landslide and debris flow runout areas and sizes distribution in the stage three of the modelling workflow for model verification is an important step to identify the approximations between simulated and an observed hazard. This is an important procedure for multi-hazard modelling. Identifying the behavioural simulations that best reproduce an observation is essential to identifying the parameter-sets that influences the spatial representation of rainfall-triggered landslides, debris flows and hillslope erosion hazards for catchments with different environmental and climatic settings. The application of the equifinality approach to identify the simulation more proximate to the landslides registered for Hurricane Tomas and the debris flow registered for February 25, 2017, rainfall event allowed the understanding of the effects of uncertainty in the model results. This is essential for model verification in which not consideration of the effect of uncertainty in model results could result in unrealistic hazard representations that are not proximate to an observed hazard. This could constrain the parameter-set selection in order to identify the best representative parameters that influence hillslope hydrological hazard interaction for soil types and land use for specific catchments. Addressing the model verification considering uncertainty provides insight

into how, for example, landslides are distributed across the catchment. This allows the identification of the spatial distribution of the parameter values for soil types and land use that influence the magnitude and location of these hazards. This was important to address research question 1 (RQ1) in Chapter 1. The parameter-set confirmation for soil types and land use is essential to understanding how the values of hydrological and geotechnical parameters are distributed within the catchment. Identifying behavioural parameter-sets for land use and soil types for both study sites allowed the analysis to assess multi-hazards interactions for land use and climate change scenarios. This suggests that the applicability of the stage two of the modelling workflow is effective in determining the parameters-set values for different soil types and land use for catchment located in data scarce environments.

### 6.1.3 Single hazard vs multi-hazard for the Soufriere catchment and Maipo sub-catchment

The selection of the parameter-set for the Soufriere catchment and Maipo sub-catchment in stage two of the modelling workflow applied in Chapter 4 and Chapter 5 contributed to identifying the physical characteristics of both catchments that drove the representation and interaction of hillslope hydrological hazards according to the rainfall event selected for each study site. These catchments exhibit two different climatic and environmental settings that render different multi-hazard forming environments where rainfall-triggered landslides and debris flows are the most dominant hazards. Figure 6.1 illustrates the hazard representation for the modelled rainfall-triggered landslides, debris flows, and hillslope erosion obtained from the selected parameter-set for the Soufriere catchment. Alternatively, Figure 6.2 illustrates the same modelled hazards for the Maipo sub-catchment. From these results, it was possible to represent the landslides and debris flow registered during Hurricane Tomas and the debris flows registered for February 25, 2017, considering the uncertainties introduced in the representation of these hazards. Commonly, these hazards are assessed using a single-hazard approach limiting the quantifying of the interaction of one hazard on another, especially in terms of the effects on hazard magnitude. The advantage of assessing both events using a multi-hazard approach is the quantification of the magnitude resulting from the cascading, concurrent and compounding interactions between these three hazards. The application of the OpenLISEM hazard model achieved this purpose for both study sites by representing individual hazards as well as their interconnectedness in terms of magnitude. This was demonstrated according to the hazard metrics estimated for each hazard: for example, in the case of the Soufriere catchment, the total debris flow runout area ( $A_D$ ) and the total net erosion ( $Net_E$ ) dramatically increased in parametric simulations where the total landslide surface area ( $A_L$ ) was areas  $\geq 100$  ha. The same tendency was observed in the Maipo sub-catchment, for example, for total landslide surface area ( $A_L$ ) areas  $\geq 100$  ha, the total debris flow runout areas ( $A_D$ ) exceeded the 100 ha and the total net erosion ( $Net_E$ ) exceeded the  $-1000$  ( $ton.m^{-2}$ ). These results demonstrated that the occurrence of rainfall-triggered landslides was the primary hazard influencing cascading interactions that impacted the magnitude of debris flows and hillslope erosion rates in zones of the catchment where these interactions were produced in both study sites.

Figure 6.1a and Figure 6.2b shows the cascading interactions zones identified for both study sites as represented by landslide surface areas, debris flow runout areas, and erosion and deposition areas

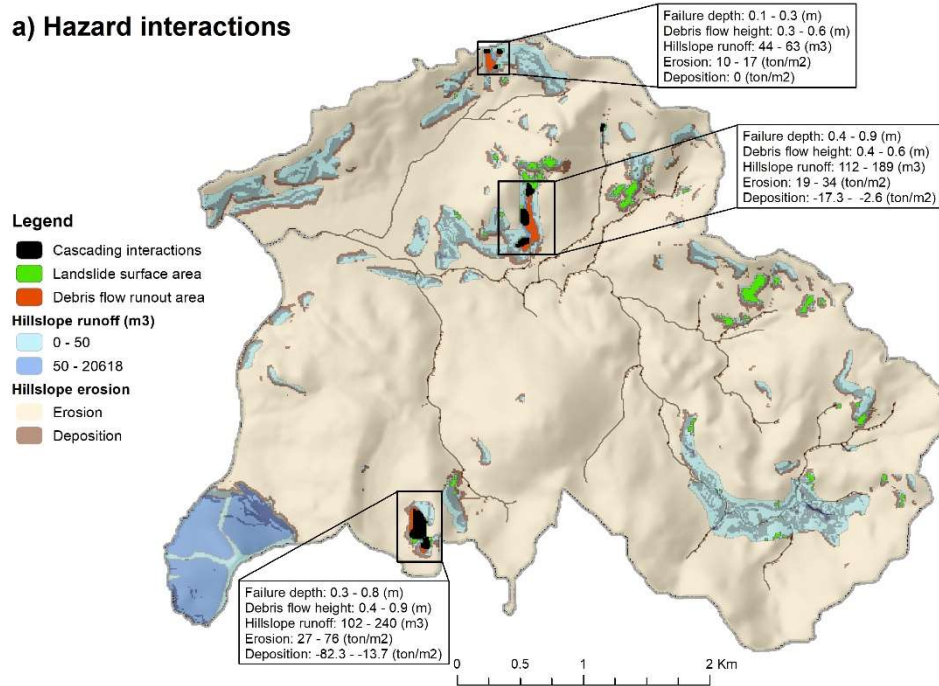
resulting from the behavioural simulations selected for each catchment. For both catchments, hillslope runoff was the main hydrological process influencing the cascading interaction of landslides with debris flow and hillslope erosion. According to the identified cascading interaction zones, the accumulated hillslope runoff was between 10 to 79 m<sup>3</sup> for the Soufriere catchment and 79 to 264 m<sup>3</sup> for the Maipo sub-catchment. This suggests that the magnitude of the generated hillslope runoff is an important factor in determining the cascading interactions given by the entrainment rates of landslide volume material and eroded bed material. Hillslope runoff magnitude influences the flow properties (rheology and viscosity) that make shallow landslides transition into debris flows, thus impacting debris flow depth and velocity. The resulting magnitude of the debris flow significantly impact the rates of erosion and deposition within the catchment, especially in ravines and outlets. As identified in Figure 6.1 and Figure 6.2a, the rates of hillslope erosion in the interaction zones are higher in comparison to those areas of the catchment in which hillslope erosion is only affected by hillslope runoff. Therefore, the advantage of the OpenLISEM hazard model is the spatial representation of hydrological processes, such as infiltration, hillslope runoff, and flash floods. This makes it possible to identify within the interaction zone which are the dominant processes that make these hazards interact.

The assessment of these hazards using a multi-hazard approach instead of a single-hazard approach in the Soufriere catchment and Maipo sub-catchment showed the advantage of representing the impacts of hazard interactions on the individual magnitude of each hazard. By mapping all the hillslope hydrological hazards simulated by the OpenLISEM hazard model it is possible to identify locations in which these hazards are predicted to interact. Figure 6.1 and Figure 6.2a illustrates the spatial distribution of the simulated landslides, debris flows and hillslope erosion for both study sites resulting from the selected parameter-set indicating that within these catchments, these hazards can occur independently, but their interaction will be determined by the hydrological and stability processes and spatial proximity of one hazard to another that can produce cascading, concurrent or compounding interactions. The application of the OpenLISEM hazard model at both study sites has effectively proven the representation of these hazards individually but considering the impacts of these interactions in their resulting magnitudes. This is an important aspect of assessing multi-hazard interactions for different climatic and environmental settings, as the identification and mapping of different interconnected hazards improves preparedness for the potential impacts of these hazards. These results suggests that the individual assessment of these hazards using single hazard models could potentially underestimate the impact of interacting hazards, constraining the estimation of the risk for regions highly exposed to multiple hazards, as the type of interactions amplifies the overall hazard in comparison to independent hazards. For example, single debris flow runout models directly include landslide failure volumes to assess their influence in debris flow magnitude and erosion. However, this is constrained by uncertainty in estimating landslide volumes using different statistical methods and landslide inventories. In addition, physically-based erosion models do not incorporate the effects of landslides and debris flow in the estimation of erosion and deposition rates. In addition, landslide hazard model is limited to single slopes limiting their application to catchment scales.

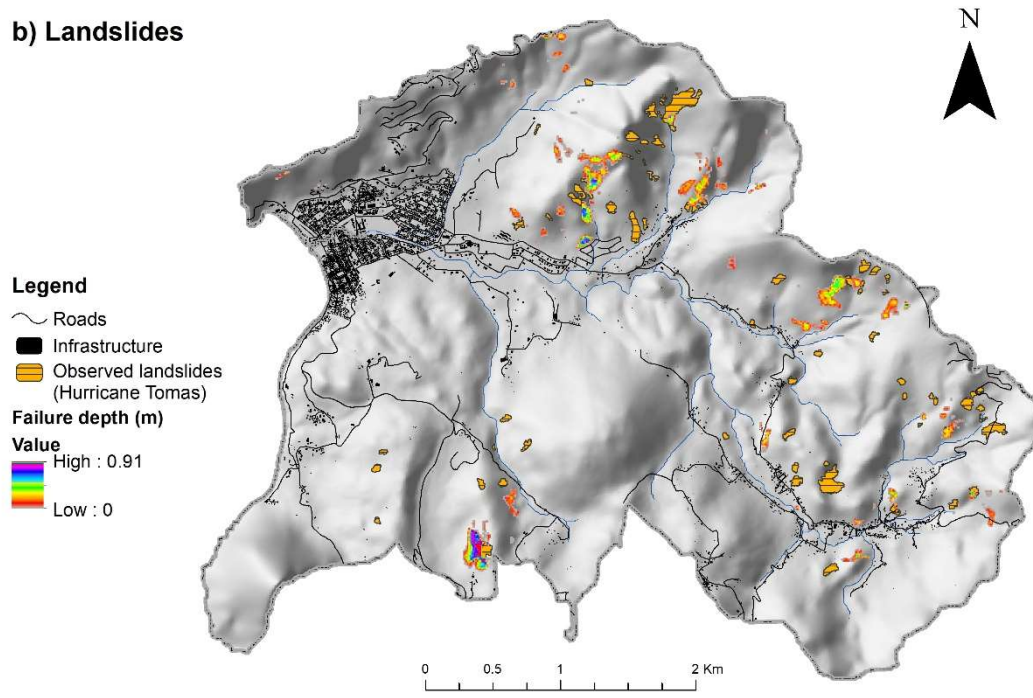
The results obtained for both study sites demonstrate the applicability of stage two of the modelling workflow. The selection of behavioural simulations to account for potential issues of equifinality and uncertainty contributed to selecting the parametric simulation with less uncertainty in the results for the Soufriere catchment and Maipo sub-catchment. Most of these results are difficult to achieve in some of the current multi-hazard models due to model complexities (e.g., number of input parameters for hydrological and stability processes representations and data quality) and the lack of guidelines to manage these model complexities and uncertainties.

The integration of these processes is essential for identifying the interrelationships that influence the interactions of hillslope hydrological hazards. However, more process integration in multi-hazard models requires more parameters for hazard representations. This is an important consideration when applying multi-hazard models in contrasting climatic and lithological catchments, where the difference in available data introduces sources of uncertainty in the setting of model input parameter values. Therefore, the application of multi-hazard models for two different study sites must be conducted by following guidelines that manage parameterisation (stage one), verification, and uncertainty (stage two). In this thesis, the following guidelines were important to address research question 2 (RQ2) by selecting the behavioural simulations whose parameter set properly represents the observed hazards for the selected rainfall events for both study sites considering the impacts of uncertainty in the input parameters. The foregoing is crucial to simulate multi-hazard interactions, especially to understand the real impact of the influence of one hazard on another and recognize the non-independence between these hazards. In summary, the assessment of multi-hazard interactions must be conducted following what is called “good practices.” This manages the complexity of multi-hazard models through parameterisation procedures and reduces uncertainties in the model outputs. This is an ethical procedure, as most of the model output is used by researchers and decision makers to implement policies and measures to reduce and manage the potential impacts of these hazards as a consequence of climate and land use change.

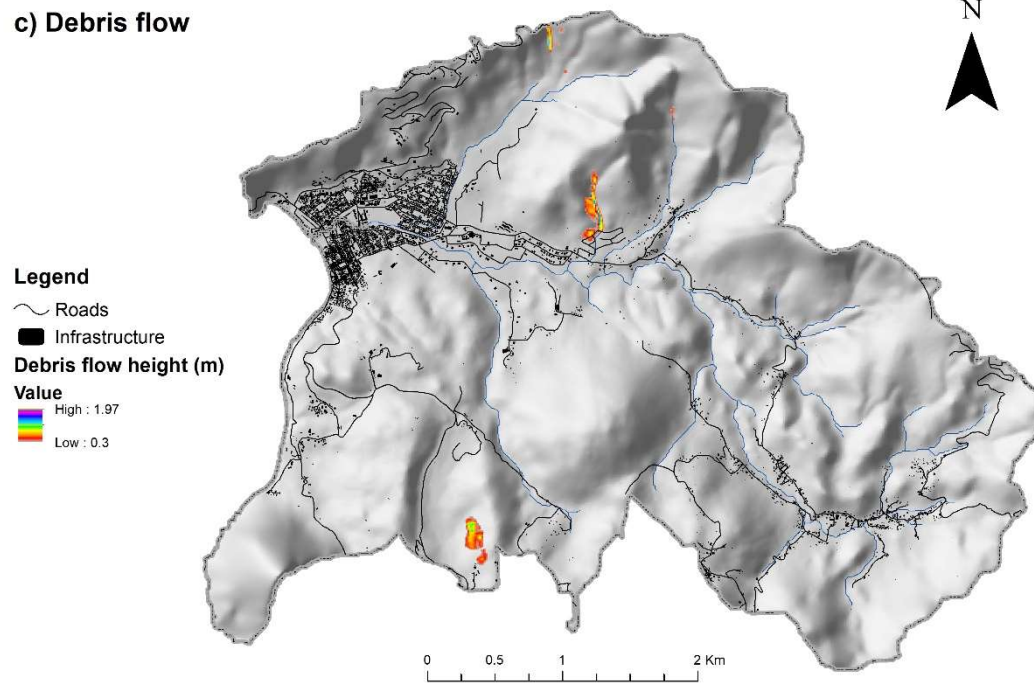
a) Hazard interactions



b) Landslides



## c) Debris flow



## d) Hillslope erosion

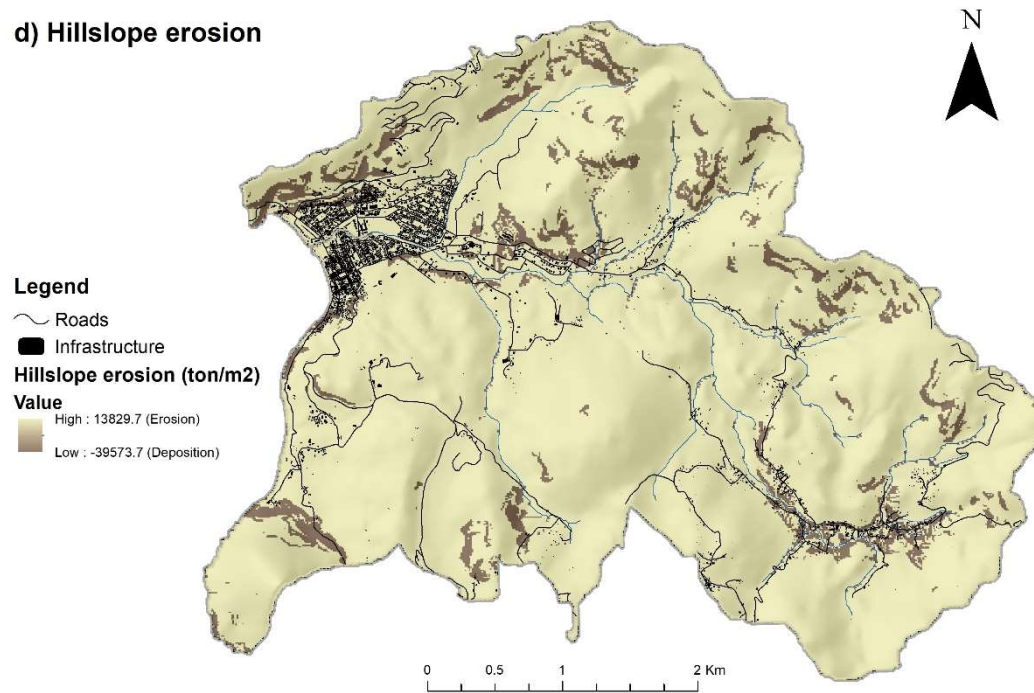
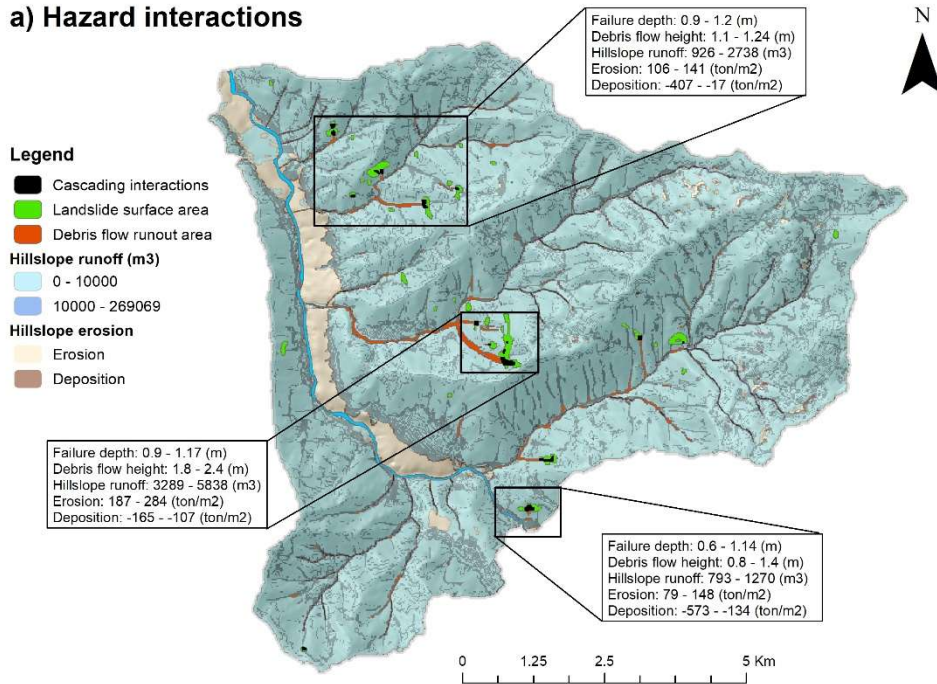
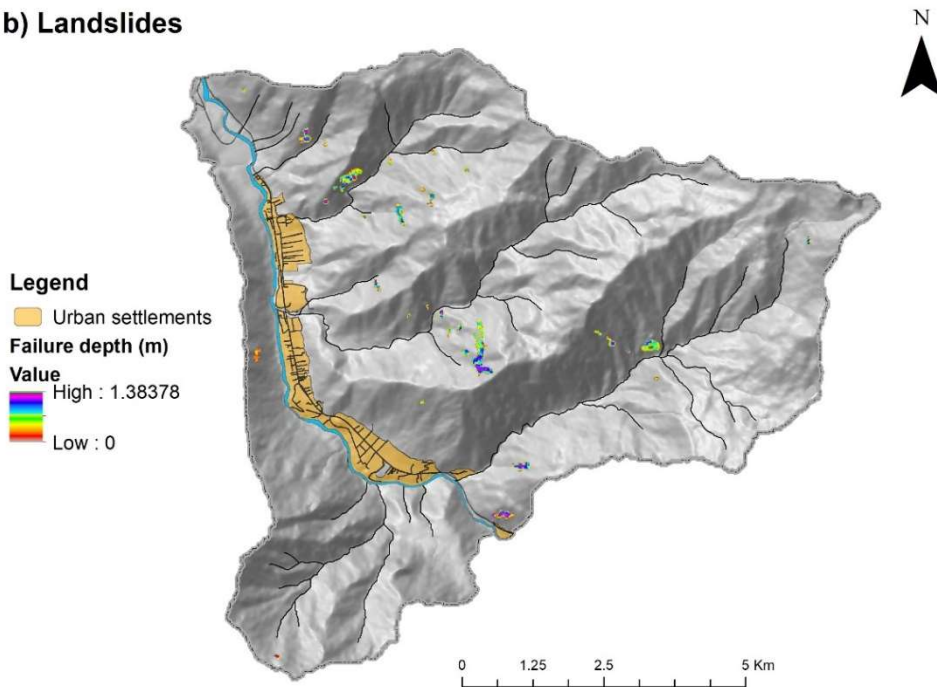


Figure 6.1 Hillslope hydrological hazard simulated as a multi-hazard event for the Soufriere catchment (Hurricane Tomas): (a) All hazards with location of cascading interactions indicated, (b) Landslides, (c) Debris flows, (d) Hillslope erosion hazards abstracted from the multi-hazard modelling result to indicate their extent more clearly.

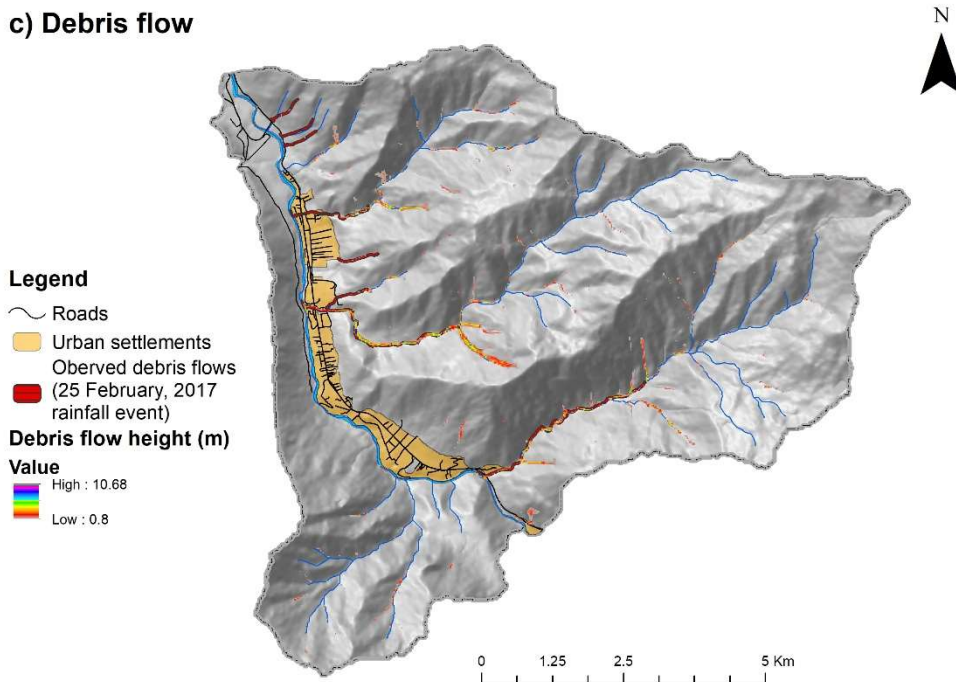
**a) Hazard interactions**



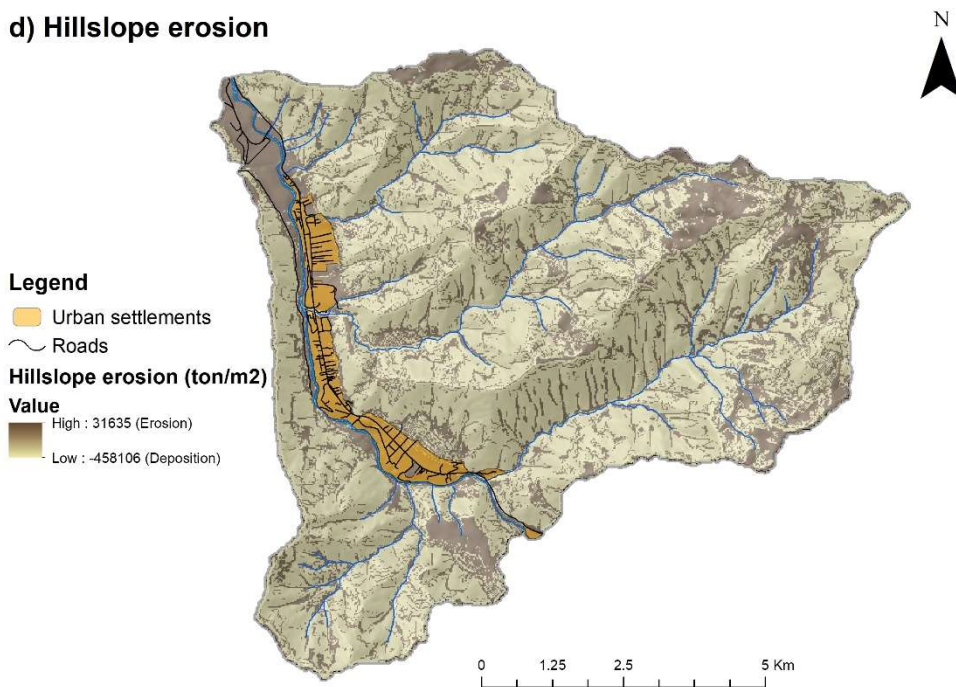
**b) Landslides**



**c) Debris flow**



**d) Hillslope erosion**



*Figure 6.2 Hillslope hydrological hazard representations for the Maipo sub-catchment (25 February 2017 rainfall event): (a) cascading interactions, (b) Landslides, (c) Debris flows, (d) Hillslope erosion.*



### 6.1.4 An end-to-end methodology to explore climate and land use scenarios for different catchment environments

The application of the full extent of the modelling workflow for the Soufriere catchment and the Maipo sub-catchment in Chapter 4 and Chapter 5 demonstrated its applicability to assess climate and land use scenarios in both study sites. Specifically, the application of stages one and two were important steps for the identification and selection of parameter sets, as well as the assessment of the most sensitive input parameters through the application of Regional Sensitivity Analysis (RSA) to the selected parameter sets. The incorporation of Sensitivity Analysis (SA) in stage two of the modelling workflow allowed the identification of the land use and soil type input parameters that had most influenced on the occurrence of the observed hazards for both catchments. This is an essential stage when it comes to exploring climate and land use scenarios. Identifying influential land use categories and soil type units indicates, for example, the sensitivity of a catchment's physical characteristics to hillslope deforestation, agriculture, or urbanization. These anthropogenic processes have significant impacts on hillslope hydrological and geotechnical properties such as saturation hydraulic conductivity, slope gradient, and soil moisture. The assessment of the most influential input parameters for the selected parameter-sets allowed the identification of the saturated hydraulic conductivity ( $k_{s1}$ ) for land use as the most influential parameter for the Soufriere catchment and the saturated moisture content ( $\theta_{s2}$ ) for soil types in the Maipo sub-catchment. This means that the spatial variation in these values has a significant impact on model outputs. However, for spatially distributed models, such as the OpenLISEM hazard model, it is necessary to identify how these influential values vary spatially. The identification of the spatial distribution of the simulated hazards (landslide surface areas and debris flow runout areas) for each land use category and soil type unit helped to identify the influential values for each category and unit. This was an important step in setting land use scenarios to identify the values for the most sensitive land use categories.

The OpenLISEM hazard model allowed for the assessment of the impact of land use change on multi-hazard occurrence. The setting of hydrological and geotechnical input parameter values for land use categories and soil type units is of great advantage to exploring how the spatial distribution of the most influential values impacts the hillslope hydrological hazard interactions. In the case of the Soufriere catchment, the exploring of land use scenarios was set by changing the saturated hydraulic conductivity ( $k_{s1}$ ) value of the natural tropical forests by the value of the mixed farming and forests. This allowed the exploration of the hypothesis that the expansion of farmlands to the detriment of natural tropical forests increases the magnitude of hillslope hydrological according to the 27-h, 24-h, 10-h, and 5-h rainfall events selected for the catchment. The assessment of these hazards is a significant step forward in providing insights into how they might respond to future land use and rainfall scenarios. For example, it was identified that the decrease of natural tropical forests to the detriment of farmlands areas increases the magnitude of these hazards up to +256.7% for landslides surface area ( $A_L$ ), +1457.8% for debris flows runout areas ( $A_D$ ), and +371% for net erosion rates ( $Net_E$ ), to rainfall events such as Hurricane Tomas. Moreover, the increase in natural tropical forests has significantly decreased the magnitude of these hazards. For example, for the same Hurricane Tomas rainfall event the magnitude of landslide

surface areas ( $A_L$ ) decreased to -16%, the debris flow runout area ( $A_D$ ) to +13.1% and the total net erosion rates ( $Net_E$ ) to -4%. For the Maipo sub-catchment, the exploration of the hypothesis that the increase of scrub forest to the detriment of natural forest increases the magnitude of hillslope hydrological hazards according to the 12-h, 8-h, 6-h, and 4-h rainfall events showed that for the 8-h rainfall event of February 25, 2017, the landslide surface area ( $A_L$ ), increased up to +3.6%, debris flow runout areas ( $A_D$ ) up to +4.8%, and total net erosion rates ( $Net_E$ ) up to +2.3%. Alternatively, the increase of natural forest decreased the magnitude of the landslides surface area ( $A_L$ ) to -1.8%, debris flows runout areas ( $A_D$ ) to +1.3% and total net erosion rates ( $Net_E$ ) to -4.8%. The application of the full extent of the modelling workflow was essential to address research question 3 (RQ3) of this thesis by exploring how hydrological hazard interaction respond to changes in climate and land use in both study sites. The foregoing demonstrates the applicability of the modelling workflow in catchments with different lithological and climatic settings as well as with different land use dynamics.

## 6.2 Overall thesis conclusions

This thesis provides a modelling workflow that addresses the parameterisation of complex multi-hazard models, such as the OpenLISEM hazard model, the management of uncertainty in input data and model outputs given by data-scarce contexts, model verification, the sensitivity of input parameters in hazard representations, and model application to explore climate and land use change scenarios for different catchment environments. It develops the necessary steps for each stage of the modelling workflow to assess the quality of the input data and identify suitable parameter-sets that best represent hillslope hydrological hazard interactions according to land use categories and soil type units of each catchment environment and the uncertainties associated with them. Most importantly, it demonstrated its applicability to different climatic and environmental catchment settings, allowing the identification of impacts associated with these hazards, such as the quantification of rainfall-triggered landslides, debris flows, and hillslope erosion hazard magnitudes. The application of the full extent of the modelling workflow allows the assessment of hillslope hydrological hazard interactions for different land use and climate change scenarios. This allows the assessment of the potential effects of rainfall and land use change on hillslope hydrological hazards according to land use and climatic settings for different catchments. This information is useful for decision-makers because it provides necessary guidelines to mitigate and reduce the impacts of these hazards on vulnerable populations and infrastructure exposed to the impacts of rainfall-triggered landslides, debris flows, and hillslope erosion hazards.

### 6.2.1 Direction for future works

The modelling workflow proposed in this thesis contributes to improving the confidence of multi-hazard modelling for data-scarce catchments located in different climatic and environmental settings. There is now an opportunity to apply the modelling workflow developed in this thesis to improve multi-hazard modelling considering the uncertainties that arise in the modelling process, especially to assess multi-hazard interactions for different climate and land use change scenarios. The following section provides an outlook on the contribution of the modelling workflow in the good practice to conduct multi-hazard

assessments, especially to assess the potential impacts of climate and land use change on the occurrence and magnitude of these hazards.

### **6.2.2 A modelling workflow methodology to improve confidence in multi-hazard modelling**

The approach to address the modelling workflow described in Chapter 2 contributes not only to address the uncertainties that arise in multi-hazard modelling but also to the user to perform an end-to-end methodology for an "ex-ante" assessment to apply physically-based distributed multi-hazard models that require a large number of input parameters to represent complex climatic-environmental systems. In particular, for the assessment of multi-hazard interactions, the application of multi-hazard models depends on the quality of their input parameters (van den Bout 2020; Williams et al. 2020). However, uncertainty is inherent in the input parameters because of the complexities in estimating them (e.g., data and information available for topography, hydrology, and geotechnical characteristics for different regions). Therefore, hazard representations and policy recommendations to mitigate them are constrained by the uncertainty introduced in their representation (Uusitalo et al. 2015; Fan et al. 2021). Moreover, assessing their impacts on different land use and rainfall change scenarios critically depends on the quality of these outputs. Hence, methodologies that guide these uncertainties are required (Merz et al. 2020).

According to Almeida et al. (2017) and Beven et al. (2018), addressing uncertainties for hazard modelling constitute a "good practice" to conduct natural hazard assessments that might have significant influence on decisions. In the case of multi-hazard modelling, the incorporation of methodologies that address uncertainties improves the understanding of these hazards, for example, the interaction of rainfall-triggered landslides, debris flows and hillslope erosion hazards and their potential impacts on the population and infrastructure. Notably, for multi-hazard assessment, understanding the relationships between catchment physical and climatic factors that influence the interactions of hillslope hydrological hazards is the starting point for identifying how different catchment environments can respond to the impacts of climate and land use change. This is a crucial stage in modelling multi-hazard interactions, especially for users who seek different purposes in assessing these hazards. For example, for engineers and hydrologists, stage one of the modelling workflow can identify catchment hydrological and geotechnical properties by exploring input parameter range values (e.g., saturated hydraulic conductivity, saturated moisture content, soil cohesion, and soil internal friction angle) for different soil types for the assessment of catchment stability conditions or hydrological behaviour for different rainfall events. This is a contribution, especially to the characterisation of the soil hydrological and geotechnical properties in catchments, where limited access to information to identify these physical factors prevents the application of physically-based distributed models be avoided due to the uncertainties introduced by the absence of information (McMillan et al. 2018; Bicocchi et al. 2019). The first stage of the modelling workflow allows exploration of the hydrological and geotechnical input parameter value ranges that might introduce sources of uncertainty on the hazard that is intended to model. Furthermore, screens the value distribution to set the parameterisation of the catchment hydrological and geotechnical values for different land use categories and soil type units.

Following the second stage of the modelling workflow for model verification and sensitivity analysis determines the necessary steps to select the behavioural simulation with the best approximation to an observed hazard. The spatial similarity using an equifinality approach contributes to the user in establishing the criteria to define the best spatial patterns with more proximity to an observation. In the case of rainfall-triggered landslides and debris flows, when comparing the area difference between the simulated and observed hazards, it is possible to assess the effects of uncertainty by comparing the hazard magnitudes (sizes) and spatial distributions. These spatial patterns provide the user with an understanding of how the uncertainties in the input parameters are propagated in the model outputs (Ardizzone et al. 2002; Mead et al. 2021). The integration of the spatial overlapping method to assess model accuracy considers these uncertainties. For example, the overlap between the simulated and observed landslides allows us to identify how the quality of the input data approximates the observation. Sensitivity analysis contributes to determining the most sensitive input parameters that influence the spatial representation of hillslope hydrological hazards. Identifying these input parameters is an essential step for model parameterisation, particularly for identifying land use categories and soil type properties that are more sensitive within the catchment in representing these hazards. This is an important stage for users seeking to explore the impact of climate and land use change on the occurrence of hillslope hydrological hazards from the perspective of understanding the interrelationships between catchment physical properties and climatic factors that influence the occurrence of hazard interactions, or decision and policy making regarding disaster risk reduction management (DRR) and land use planning.

### **6.2.3 Improving the understanding of multi-hazards and their interactions: Future outlook**

In practice, applying climate and land use scenarios provides insights into how catchments with different climatic and environmental settings will respond to the effects of land use dynamics and rainfall extremes (Wang et al. 2008; van Vliet et al. 2016). The assessment of these hazard scenarios allows for identifying the sensitivity of different catchment environments to the potential impacts of climate and land use change. This is useful information, as land use dynamics, such as agriculture, urbanization, and deforestation, significantly impact the hydrological and geotechnical processes on hillslopes (Sidle et al. 1985; Sidle and Ochiai 2006). In addition, changes in rainfall intensity and duration are significantly impacting the magnitude and frequency of these hazards in different regions of the world, especially in countries highly exposed to the impacts of climate change (Gariano and Guzzetti 2016; Alvioli et al. 2018). The application of the full extent of the modelling workflow contributes to providing the assessment of hillslope hydrological hazards for these scenarios. The quantification of the magnitude of rainfall-triggered landslides, debris flows, and hillslope erosion rates through the application of the hazard metrics allow an understanding of the catchment response to the impacts of land use and rainfall change. Moreover, contributes to determining which land use dynamics and rainfall duration might have the greatest impact on the catchment on hillslope hydrological hazard magnitudes. For example, determine if the changes in land use due to anthropogenic processes (e.g., intensive agriculture, urban expansion) or by the direct effects of climate change such as reduction of land cover by long drought periods or wildfire impacts the magnitude of hillslope hydrological hazards (Johnston et al. 2021). The

modelling workflow for land use and rainfall change identifies these dynamics by also considering the effects of rainfall. This useful information provides more effective disaster risk reduction policies and adaptation strategies for the effects of land use climate change (Cremen et al. 2022).

Although the modelling workflow developed and applied in this thesis demonstrated its applicability to managing parameterisation and uncertainties of multi-hazard models to explore climate and land use scenarios in data-scarce regions. There are some limitations that need to be considered when applying the full extent of the modelling workflow. These are related to the complexity to obtain and gather data for different catchment environments, especially when the model is applied over large catchments. For example, characterising soil types and identifying their spatial distribution over a catchment requires high-quality databases for geology, geomorphology, and topography as well as the availability of GIS software (van Westen et al. 2008). Moreover, estimating the hydrological and geotechnical properties of each soil type is a time-consuming process that requires an extensive literature review (Iwashita et al. 2012; Biccocchi et al. 2019). On the other hand, using high-resolution data over large catchments is expensive to obtain and increases the simulation time for models such as the OpenLISEM hazard model (van den Bout 2020). This makes the application of stage one of the modelling workflow to explore parametric simulations to be more extensive regarding data gathering and assembly and simulation times depending on data resolution and the rainfall duration. Therefore, the implementation of more highly efficient computational systems can improve the simulation times to run parametric simulations. However, this is still a disadvantage for countries that do not count on the necessary resources to implement highly efficient systems to simulate the impacts of hillslope hydrological hazards for different land use scenarios (van Westen et al. 2021).

Another limitation is the development of open databases to estimate hydrological and geotechnical input parameters, particularly for data-scarce regions. Several contributions have been made to developing databases for physically based modelling. The work of Iwashita et al. (2012); Fan et al. (2016); Tofani et al. (2017) and Biccocchi et al. (2019) have contributed in characterising the geotechnical and hydrological properties for different soil types improving the estimation of parameters for physically-based models. However, it is still challenging to define the catchment's physical characteristics, especially over large catchments. This becomes more challenging when estimating spatially distributed values, for example, for saturated hydraulic conductivity, soil cohesion, or soil internal friction angle, for which their value estimation relies on laboratory testing (Koo et al. 2020). Therefore, one of the key areas for improvement in multi-hazard modelling is the development of open databases with spatial information related to catchment physical characteristics, containing, for example, probability density functions (PDFs) related to parameters such as soil cohesion for different soil types. This can be used to estimate parameter values for different catchments in which the soil types are similar in terms of these characteristics. On the other hand, despite the growing availability of global datasets related to soil moisture, soil depth, Digital Elevation Models (DEMs), and land use/cover (LUC). There is still a need to pre-process these data containing different spatial resolutions to be adapted to the scale and resolution required for the selected catchment (Burton et al. 1998; van den Bout 2020). This also

introduces sources of uncertainty that affect the model's outputs. Therefore, guidelines are also required for spatial data processing for multi-hazard modelling.

In addition, the improvement of hazard inventory datasets is also required. The lack of record of the frequency of rainfall-triggered landslides, debris flows, and the amount rates of erosion and deposition is also a limitation to applying multi-hazard models in different regions as limits the verification of the model results (Blahut et al. 2010; Guzzetti et al. 2012). For example, in data-scarce regions, accessing high-resolution images such as RapidEye or LiDAR sensors is too expensive to identify the spatial distribution of landslides and debris flows at the moment when these hazards occurs, limiting their estimation using open-source coarse-resolution data (van Westen et al. 2008; Pellicani et al. 2013). Another improvement required is the availability of updated land use accounting for the latest changes in urbanization, agriculture and deforestation driven by anthropogenic processes or climate change. This is essential to explore land use scenarios according to the latest tendencies in land use dynamics for different catchments (van Westen et al. 2021). Moreover, the availability of high-resolution rainfall records is essential to explore the impacts of climate change on different regions (van den Bout 2020). For example, for the Maipo sub-catchment, the availability of the CAMELS-CL platform (Alvarez-Garreton et al. 2018), has contributed to providing rainfall records from 30 years allowing to identify the amounts of rainfall that triggered multiple hazards in the past.

According to the aforementioned requirements, improving multi-hazard modelling is a challenging task. However, the modelling workflow proposed in this thesis contributes to setting the basis for improving multi-hazard modelling by using complex models in data-scarce regions, managing uncertainty to provide a more comprehensive understanding of the physical and climatic relationships that influence multi-hazard interactions for different catchment environments. The workflow also generates reliable outputs to develop early warning systems and provide information to different stakeholders, such as governments, planners, and engineers, who can make decisions to support strategies and policies to reduce the impacts of these hazards, especially in regions highly exposed to the impacts of land use and climate change.

### **6.3 Concluding remarks**

The modelling workflow developed and applied in this thesis is relevant for improving multi-hazard modelling for catchments with different data scarcity levels. The full extent of the proposed modelling workflow addresses the gaps in the parameterisation of multi-hazard models, the management of uncertainties due to model complexities, and data quality due to the lack of information to represent all catchment physical variables required to model multi-hazard interactions. In practice, this modelling workflow sets guidelines to perform better practices in multi-hazard modelling. The assessment of the impacts of rainfall-triggered landslides, debris flows, and hillslope erosion hazards depends on addressing the uncertainty introduced in physically based multi-hazard models. This not only improves their modelling for different catchment settings but also sets the basis to address the gap related to the data quality and lack of information to generate the necessary inputs to model multi-hazard interactions. This is an improvement not only to properly model landslides, debris flows, and hillslope erosion hazards but also to improve the forecasting of these hazards for different land use and climate change scenarios, allowing the assessment of the impacts of these hazards on the population and infrastructure. The foregoing is relevant for supporting disaster risk reduction policies and improve the risk assessment and reduce the impact of these hazards accounting for their interactions.

## References

- Akinyemi, F. O. (2021). Vegetation trends, drought severity and land use-land cover change during the growing season in semi-arid contexts. *Remote Sensing*, 13(5), 1–20. <https://doi.org/10.3390/rs13050836>
- Aksoy, H., & Kavvas, M. L. (2005). A review of hillslope and watershed scale erosion and sediment transport models. *Catena*, 64(2–3), 247–271. <https://doi.org/10.1016/j.catena.2005.08.008>
- Alcántara-Ayala, I. (2002). Geomorphology , Natural Hazards , Vulnerability and Prevention of Natural Disasters in Developing Countries. *Geomorphology*, 47(September 2016), 107–124. [https://doi.org/10.1016/S0169-555X\(02\)00083-1](https://doi.org/10.1016/S0169-555X(02)00083-1)
- Aleotti, P. (2004). A warning system for rainfall-induced shallow failures. *Engineering Geology*, 73(3–4), 247–265. <https://doi.org/10.1016/j.enggeo.2004.01.007>
- Aleotti, P., & Chowdhury, R. (1999). Landslide hazard assessment: summary review and new perspectives. *Bulletin of Engineering Geology and the Environment*, 58(1), 21–44. <https://doi.org/10.1007/s100640050066>
- Almeida, S., Holcombe, E. A., Pianosi, F., & Wagener, T. (2017). Dealing with deep uncertainties in landslide modelling for disaster risk reduction under climate change. *Natural Hazards and Earth System Sciences*, 17(2), 225–241. <https://doi.org/10.5194/NHESS-17-225-2017>
- Alvarez-Garreton, C., Mendoza, P., Boisier, J. P., Addor, N., Galleguillos, M., Zambrano-Bigiarini, M., ... Ayala, A. (2018). The CAMELS-CL dataset: Catchment attributes and meteorology for large sample studies-Chile dataset. *Hydrology and Earth System Sciences*, 22(11), 5817–5846. <https://doi.org/10.5194/hess-22-5817-2018>
- Alvarez, M. (2006). *Factibilidad de utilización de técnicas geofísicas en estudios de fenómenos de remoción en masa. Caso: Deslizamiento de San José de Maipo*. Universidad de Chile.
- Alvioli, M., Melillo, M., Guzzetti, F., Rossi, M., Palazzi, E., von Hardenberg, J., ... Peruccacci, S. (2018). Implications of climate change on landslide hazard in Central Italy. *Science of the Total Environment*, 630, 1528–1543. <https://doi.org/10.1016/j.scitotenv.2018.02.315>
- Anache, J. A. A., Flanagan, D. C., Srivastava, A., & Wendland, E. C. (2018). Land use and climate change impacts on runoff and soil erosion at the hillslope scale in the Brazilian Cerrado. *Science of the Total Environment*, 622–623, 140–151. <https://doi.org/10.1016/j.scitotenv.2017.11.257>
- Anderson, M. G., Holcombe, E. A., Blake, J. R., Ghesquire, F., Holm-Nielsen, N., & Fisseha, T. (2011). Reducing landslide risk in communities: Evidence from the Eastern Caribbean. *Applied Geography*, 31(2), 590–599. <https://doi.org/10.1016/J.APGEOG.2010.11.001>
- Anderson, M. G., Holcombe, E. A., & Renaud, J. P. (2007). Assessing slope stability in unplanned settlements in developing countries. *J Environ Manage*, 85(1), 101–111. <https://doi.org/10.1016/j.jenvman.2006.08.005>
- Anderson, M., Holcombe, E. A., Flory, R., & Renaud, J. P. (2008). Implementing low-cost landslide risk reduction: A pilot study in unplanned housing areas of the Caribbean. *Natural Hazards*, 47(3), 297–315. <https://doi.org/10.1007/S11069-008-9220-Z/FIGURES/13>
- APSL. (2010). *Hurricane Tomas damage assessment report*.
- Ardizzone, F., Cardinali, M., Carrara, A., Guzzetti, F., & Reichenbach, P. (2002). Impact of mapping errors on the reliability of landslide hazard maps. *Natural Hazards and Earth System Sciences*, 2(1–2), 3–14. <https://doi.org/10.5194/NHESS-2-3-2002>
- Arnone, E., Noto, L. V., Lepore, C., & Bras, R. L. (2011). Physically-based and distributed approach to analyze rainfall-triggered landslides at watershed scale. *Geomorphology*, 133(3–4), 121–131. <https://doi.org/10.1016/J.GEOMORPH.2011.03.019>
- Aumann, C. A. (2007). A methodology for developing simulation models of complex systems. *Ecological Modelling*, 202(3–4), 385–396. <https://doi.org/10.1016/j.ecolmodel.2006.11.005>



- Ávila, F. F., Alvalá, R. C., Mendes, R. M., & Amore, D. J. (2020). The influence of land use/land cover variability and rainfall intensity in triggering landslides: a back-analysis study via physically based models. *Natural Hazards*, (0123456789). <https://doi.org/10.1007/s11069-020-04324-x>
- Baartman, J. E. M., Temme, A. J. A. M., Veldkamp, T., Jetten, V. G., & Schoorl, J. M. (2013). Exploring the role of rainfall variability and extreme events in long-term landscape development. *Catena*, 109, 25–38. <https://doi.org/10.1016/j.catena.2013.05.003>
- Balocchi, F., Galleguillos, M., Rivera, D., Stehr, A., Arumi, J. L., Pizarro, R., ... Ramírez de Arellano, P. (2023). Forest hydrology in Chile: Past, present, and future. *Journal of Hydrology*, 616, 128681. <https://doi.org/10.1016/j.jhydrol.2022.128681>
- Batista, P. V. G., Davies, J., Silva, M. L. N., & Quinton, J. N. (2019). On the evaluation of soil erosion models: Are we doing enough? *Earth-Science Reviews*, 197. <https://doi.org/10.1016/J.EARSCIREV.2019.102898>
- Batjes, N. H., Ribeiro, E., & Van Oostrum, A. (2020). Standardised soil profile data to support global mapping and modelling (WoSIS snapshot 2019). *Earth System Science Data*, 12(1), 299–320. <https://doi.org/10.5194/essd-12-299-2020>
- Baum, R. L., Savage, W. Z., & Godt, J. W. (2008). TRIGRS - A Fortran Program for Transient Rainfall Infiltration and Grid-Based Regional Slope-Stability Analysis, Version 2.0. *Open-File Report*. <https://doi.org/10.3133/OFR20081159>
- Baumann, V., Bonadonna, C., Cuomo, S., & Moscariello, M. (2020). Modelling of erosion processes associated with rainfall-triggered lahars following the 2011 Cordon Caulle eruption (Chile). *Journal of Volcanology and Geothermal Research*, 390, 106727. <https://doi.org/10.1016/j.jvolgeores.2019.106727>
- Beevers, L., Popescu, I., Pregolato, M., Liu, Y., & Wright, N. (2022). Identifying hotspots of hydro-hazards under global change: A worldwide review. *Frontiers in Water*, 4. <https://doi.org/10.3389/frwa.2022.879536>
- Bégin, C., Brooks, G., Larson, R. A., Dragičević, S., Ramos Scharrón, C. E., & Côté, I. M. (2014). Increased sediment loads over coral reefs in Saint Lucia in relation to land use change in contributing watersheds. *Ocean and Coastal Management*, 95, 35–45. <https://doi.org/10.1016/j.ocecoaman.2014.03.018>
- Beguiría, S., W. J. Van Asch, T., Malet, J. P., & Gröndahl, S. (2009). A GIS-based numerical model for simulating the kinematics of mud and debris flows over complex terrain. *Natural Hazards and Earth System Science*, 9(6), 1897–1909. <https://doi.org/10.5194/nhess-9-1897-2009>
- Beguiría, Santiago. (2006). Validation and evaluation of predictive models in hazard assessment and risk management. *Natural Hazards*, 37(3), 315–329. <https://doi.org/10.1007/s11069-005-5182-6>
- Benavidez-Silva, C., Jensen, M., & Pliscoff, P. (2021). Future scenarios for land use in Chile: Identifying drivers of change and impacts over protected area system. *Land*, 10(4), 1–21. <https://doi.org/10.3390/land10040408>
- Beven, K. (2000). Uniqueness of place and process representations in hydrological modelling. *Hydrology and Earth System Sciences*, 4(2), 203–213. <https://doi.org/10.5194/HESS-4-203-2000>
- Beven, K. (2006). A manifesto for the equifinality thesis. *Journal of Hydrology*, 320(1–2), 18–36. <https://doi.org/10.1016/J.JHYDROL.2005.07.007>
- Beven, K. (2021). Issues in generating stochastic observables for hydrological models. *Hydrological Processes*, 35(6), 1–12. <https://doi.org/10.1002/hyp.14203>
- Beven, K., Almeida, S., Aspinall, W. P., Bates, P. D., Blazkova, S., Borgomeo, E., ... Wilkins, K. L. (2018). Epistemic uncertainties and natural hazard risk assessment - Part 1: A review of different natural hazard areas. *Natural Hazards and Earth System Sciences*, 18(10), 2741–2768. <https://doi.org/10.5194/nhess-18-2741-2018>
- Beven, K., Aspinall, W. P., Bates, P. D., Borgomeo, E., Goda, K., Hall, J. W., ... Watson, M. (2018). Epistemic uncertainties and natural hazard risk assessment - Part 2: What should constitute good

- practice? *Natural Hazards and Earth System Sciences*, 18(10), 2769–2783. <https://doi.org/10.5194/nhess-18-2769-2018>
- Beven, K., & O'connell, P. (1982). *On the role of physically-based distributed modelling in hydrology*.
- Beven, K. (2001). How far can we go in distributed hydrological modelling? *Hydrology and Earth System Sciences*, 5(1), 1–12. <https://doi.org/10.5194/hess-5-1-2001>
- Beven, K. (2019). Validation and Equifinality. In *Computer Simulation Validation. Simulation Foundations, Methods and Applications* (pp. 791–809). [https://doi.org/10.1007/978-3-319-70766-2\\_32](https://doi.org/10.1007/978-3-319-70766-2_32)
- Beven, K., & Binley, A. (1992). The future of distributed models: Model calibration and uncertainty prediction. *Hydrological Processes*, 6(3), 279–298. <https://doi.org/10.1002/HYP.3360060305>
- Beven, K., & Freer, J. (2001). Equifinality, data assimilation, and uncertainty estimation in mechanistic modelling of complex environmental systems using the GLUE methodology. *Journal of Hydrology*, 249(1–4), 11–29. [https://doi.org/10.1016/S0022-1694\(01\)00421-8](https://doi.org/10.1016/S0022-1694(01)00421-8)
- Biocchi, G., Tofani, V., D'Ambrosio, M., Tacconi-Stefanelli, C., Vannocci, P., Casagli, N., ... Catani, F. (2019). Geotechnical and hydrological characterization of hillslope deposits for regional landslide prediction modeling. *Bulletin of Engineering Geology and the Environment*, 78(7), 4875–4891. <https://doi.org/10.1007/s10064-018-01449-z>
- Blahut, J., van Westen, C. J., & Sterlacchini, S. (2010). Analysis of landslide inventories for accurate prediction of debris-flow source areas. *Geomorphology*, 119(1–2), 36–51.
- Bogaard, T., & Greco, R. (2014, October 24). Preface “hillslope hydrological modelling for landslides prediction.” *Hydrology and Earth System Sciences*, Vol. 18, pp. 4185–4188. <https://doi.org/10.5194/hess-18-4185-2014>
- Bogaard, T., & Greco, R. (2016). Landslide hydrology: from hydrology to pore pressure. *Wiley Interdisciplinary Reviews: Water*, 3(3), 439–459. <https://doi.org/10.1002/WAT2.1126>
- Bordoni, M., Meisina, C., Valentino, R., Lu, N., Bittelli, M., & Chersich, S. (2015). Hydrological factors affecting rainfall-induced shallow landslides: From the field monitoring to a simplified slope stability analysis. *Engineering Geology*, 193, 19–37. <https://doi.org/10.1016/j.enggeo.2015.04.006>
- Borrelli, P., Robinson, D. A., Panagos, P., Lugato, E., Yang, J. E., Alewell, C., ... Ballabio, C. (2020). Land use and climate change impacts on global soil erosion by water (2015-2070). *Proceedings of the National Academy of Sciences of the United States of America*, 117(36), 21994–22001. [https://doi.org/10.1073/PNAS.2001403117/SUPPL\\_FILE/PNAS.2001403117.SAPP.PDF](https://doi.org/10.1073/PNAS.2001403117/SUPPL_FILE/PNAS.2001403117.SAPP.PDF)
- Bozzolan, E., Holcombe, E. A., Pianosi, F., Marchesini, I., Alvioli, M., & Wagener, T. (2023). A mechanistic approach to include climate change and unplanned urban sprawl in landslide susceptibility maps. *Science of the Total Environment*, 858. <https://doi.org/10.1016/J.SCITOTENV.2022.159412>
- Bozzolan, E., Holcombe, E., Pianosi, F., & Wagener, T. (2020). Including informal housing in slope stability analysis-an application to a data-scarce location in the humid tropics. *Natural Hazards and Earth System Sciences*, 20(11), 3161–3177. <https://doi.org/10.5194/nhess-20-3161-2020>
- Bravo-Zapata, M. F., Muñoz, E., Lapeña-Mañero, P., Montenegro-Cooper, J. M., & King, R. W. (2022). Analysis of the Influence of Geomechanical Parameters and Geometry on Slope Stability in Granitic Residual Soils. *Applied Sciences*, 12(11), 5574. <https://doi.org/10.3390/app12115574>
- Briggs, W., & Ruppert, D. (2005). *Assessing the Skill of Yes/No Predictions*. 61(3), 799–807. <https://doi.org/10.1111/j.1541-0420.2005.00347.x>
- Brown, B. G., Gilleland, E., & Ebert, E. E. (2012). Forecasts of Spatial Fields. *Forecast Verification*, 95–117. <https://doi.org/10.1002/9781119960003.ch6>
- Brunner, P., Doherty, J., & Simmons, C. T. (2012). Uncertainty assessment and implications for data acquisition in support of integrated hydrologic models. *Water Resources Research*, 48(7), 1–18. <https://doi.org/10.1029/2011WR011342>

- Burton, A., Arkell, T. J., & Bathurst, J. C. (1998). Field variability of landslide model parameters. *Environmental Geology*, 35(2–3), 100–114. <https://doi.org/10.1007/s002540050297>
- Caloiero, T. (2018). Hydrological Hazard: Analysis and Prevention. *Geosciences*, 8(11), 389. <https://doi.org/10.3390/geosciences8110389>
- Carrara, A., Cardinali, M., Detti, R., Guzzetti, F., Pasqui, V., & Reichenbach, P. (1991). GIS techniques and statistical models in evaluating landslide hazard. *Earth Surface Processes and Landforms*, 16(5), 427–445. <https://doi.org/10.1002/esp.3290160505>
- Carretier, S., Tolorza, V., Regard, V., Aguilar, G., Bermúdez, M. A., Martinod, J., ... Riquelme, R. (2018). Review of erosion dynamics along the major N-S climatic gradient in Chile and perspectives. *Geomorphology*, 300, 45–68. <https://doi.org/10.1016/J.GEOMORPH.2017.10.016>
- Casanova, M., Salazar, O., Seguel, O., & Luzio, W. (2013). The Soils of Chile. In *Springer*. <https://doi.org/10.1007/978-94-007-5949-7>
- Cascini, L., Cuomo, S., Pastor, M., & Sacco, C. (2013). Modelling the post-failure stage of rainfall-induced landslides of the flow type. *Canadian Geotechnical Journal*, 50(9), 924–934. <https://doi.org/10.1139/cgj-2012-0375>
- Cascini, L., Cuomo, S., & Sala, M. D. (2011). Geomorphology Spatial and temporal occurrence of rainfall-induced shallow landslides of flow type : A case of Sarno-Quindici , Italy. *Geomorphology*, 126(1–2), 148–158. <https://doi.org/10.1016/j.geomorph.2010.10.038>
- Chen, H. X., & Zhang, L. M. (2015). EDDA 1.0: Integrated simulation of debris flow erosion, deposition and property changes. *Geoscientific Model Development*, 8(3), 829–844. <https://doi.org/10.5194/gmd-8-829-2015>
- Chung, C. J. F., & Fabbri, A. G. (2003). Validation of spatial prediction models for landslide hazard mapping. *Natural Hazards*, 30(3), 451–472. <https://doi.org/10.1023/B:NHAZ.0000007172.62651.2b>
- Ciabatta, L., Camici, S., Brocca, L., Ponziani, F., Stelluti, M., Berni, N., & Moramarco, T. (2016). Assessing the impact of climate-change scenarios on landslide occurrence in Umbria Region, Italy. *Journal of Hydrology*, 541, 285–295. <https://doi.org/10.1016/J.JHYDROL.2016.02.007>
- CIGIDEN. (2022). *Centro de Investigación para Gestión Integrada del Riesgo de Desastres*. Santiago, Chile.
- Claessens, L., Heuvelink, G. B. M., Schoorl, J. M., & Veldkamp, a. (2005). DEM resolution effects on shallow landslide hazard and soil redistribution modelling. *Earth Surface Processes and Landforms*, 30(4), 461–477. <https://doi.org/10.1002/esp.1155>
- Coe, J., & Godt, J. (2012). Review of approaches for assessing the impact of climate change on landslide hazards. *11th International and 2nd North American Symposium on Landslides and Engineered Slopes*, (January), 371–377.
- CONAF. (2013). *Corporación Nacional Forestal*. Santiago, Chile.
- Corominas, J., & Moya, J. (2008). A review of assessing landslide frequency for hazard zoning purposes. *Engineering Geology*, 102(3–4), 193–213. <https://doi.org/10.1016/j.enggeo.2008.03.018>
- Corominas, J., van Westen, C. J., Frattini, P., Cascini, L., Malet, J. P., Fotopoulou, S., ... Smith, J. T. (2014). Recommendations for the quantitative analysis of landslide risk. *Bulletin of Engineering Geology and the Environment*, 73(2), 209–263. <https://doi.org/10.1007/s10064-013-0538-8>
- Corominas, J. (2011). The angle of reach as a mobility index for small and large landslides. <https://doi.org/10.1139/T96-005>, 33(2), 260–271. <https://doi.org/10.1139/T96-005>
- Cox, C. A., Sarangi, A., & Madramootoo, C. A. (2006). Effect of land management on runoff and soil losses from two small watersheds in St Lucia. *Land Degradation & Development*, 17(1), 55–72. <https://doi.org/10.1002/LDR.694>
- Cremon, G., Galasso, C., & McCloskey, J. (2022). Modelling and quantifying tomorrow's risks from natural hazards. *Science of the Total Environment*, 817.

- <https://doi.org/10.1016/J.SCITOTENV.2021.152552>
- Crosetto, M., Tarantola, S., & Saltelli, A. (2000). Sensitivity and uncertainty analysis in spatial modelling based on GIS. *Agriculture, Ecosystems and Environment*, 81(1), 71–79. [https://doi.org/10.1016/S0167-8809\(00\)00169-9](https://doi.org/10.1016/S0167-8809(00)00169-9)
- Crossley, J. F., Polcher, J., Cox, P. M., Gedney, N., & Planton, S. (2000). Uncertainties linked to land-surface processes in climate change simulations. *Climate Dynamics*, 16(12), 949–961. <https://doi.org/10.1007/s003820000092>
- Crosta, G., & Frattini, P. (2003). Distributed modelling of shallow landslides triggered by intense rainfall. *Natural Hazards and Earth System Sciences*, 3, 81–93.
- Crozier, M. J. (2010). Deciphering the effect of climate change on landslide activity: A review. *Geomorphology*, 124(3–4), 260–267. <https://doi.org/10.1016/j.geomorph.2010.04.009>
- Cruden, D. M., & Varnes, D. (1996). Landslides types and processes. In *Landslides: investigation and mitigation, Transport Research Board Special Report*. Retrieved from <http://onlinepubs.trb.org/Onlinepubs/sr/sr247/sr247-003.pdf>
- Cullmann, J., Krause, T., & Saile, P. (2011). Parameterising hydrological models - Comparing optimisation and robust parameter estimation. *Journal of Hydrology*, 404(3–4), 323–331. <https://doi.org/10.1016/J.JHYDROL.2011.05.003>
- Cuomo, S., & Della Sala, M. (2015). Large-area analysis of soil erosion and landslides induced by rainfall: A case of unsaturated shallow deposits. *Journal of Mountain Science*, 12(4), 783–796. <https://doi.org/10.1007/s11629-014-3242-7>
- Cuomo, S., Della Sala, M., & Novità, A. (2015). Physically based modelling of soil erosion induced by rainfall in small mountain basins. *Geomorphology*, 243, 106–115. <https://doi.org/10.1016/J.GEOMORPH.2015.04.019>
- Cuomo, S., Di Perna, A., & Martinelli, M. (2021). Modelling the spatio-temporal evolution of a rainfall-induced retrogressive landslide in an unsaturated slope. *Engineering Geology*, 294(September), 106371. <https://doi.org/10.1016/j.enggeo.2021.106371>
- Cutter, S. L. (2018). Compound, Cascading, or Complex Disasters: What's in a Name?. *Environment: Science and Policy for Sustainable Development* 60(6), 16–25. <https://doi.org/10.1080/00139157.2018.1517518>
- Dai, F. C., Lee, C. F., & Ngai, Y. Y. (2002). Landslide risk assessment and management: an overview. *Engineering Geology*, 64(1), 65–87. [https://doi.org/10.1016/S0013-7952\(01\)00093-X](https://doi.org/10.1016/S0013-7952(01)00093-X)
- Dai, F. C., Lee, C. F., & Zhang, X. H. (2001). GIS-based geo-environmental evaluation for urban land-use planning: A case study. *Engineering Geology*, 61(4), 257–271. [https://doi.org/10.1016/S0013-7952\(01\)00028-X](https://doi.org/10.1016/S0013-7952(01)00028-X)
- De Angeli, S., Malamud, B. D., Rossi, L., Taylor, F. E., Trasforini, E., & Rudari, R. (2022). A multi-hazard framework for spatial-temporal impact analysis. *International Journal of Disaster Risk Reduction*, 73, 102829. <https://doi.org/10.1016/j.ijdrr.2022.102829>
- de Brito, M. M. (2021). Compound and cascading drought impacts do not happen by chance: A proposal to quantify their relationships. *Science of the Total Environment*, 778. <https://doi.org/10.1016/J.SCITOTENV.2021.146236>
- De Haas, T., Braat, L., Leuven, J. R. F. W., Lokhorst, I. R., & Kleinhans, M. G. (2015). Effects of debris flow composition on runout, depositional mechanisms, and deposit morphology in laboratory experiments. *Journal of Geophysical Research: Earth Surface*, 120(9), 1949–1972. <https://doi.org/10.1002/2015JF003525>
- De Roo, A. P. J., & Offermans, R. J. E. (1995). LISEM: a physically-based hydrological and soil erosion model for basin-scale water and sediment management. *Modelling and Management of Sustainable Basin-Scale Water Resource Systems*, (231), 399–407.
- De Roo, A. P. J., Offermans, R. J. E., & Cremers, N. H. D. T. (1996). Lisem: a Single-Event, Physically Based Hydrological and Soil Erosion Model for Drainage Basins. II: Sensitivity Analysis, Validation

- and Application. *Hydrological Processes*, 10(8), 1119–1126. [https://doi.org/10.1002/\(SICI\)1099-1085\(199608\)10:8<1119::AID-HYP416>3.0.CO;2-V](https://doi.org/10.1002/(SICI)1099-1085(199608)10:8<1119::AID-HYP416>3.0.CO;2-V)
- De Roo, A. P. J., Wesseling, C. G., Cremers, N. H. D. T., Offermans, R. J. E., Ritsema, C. J., & Van Oostindie, K. (1994). LISEM: a new physical-based hydrological and soil erosion model in a GIS-environment, theory and implementation. *Variability in Stream Erosion and Sediment Transport, Proc. Symposium, Canberra, 1994*, (224), 439–448. Retrieved from [http://hydrologie.org/redbooks/a224/iahs\\_224\\_0439.pdf](http://hydrologie.org/redbooks/a224/iahs_224_0439.pdf)
- de Ruiter, M. C., Couasnon, A., van den Homberg, M. J. C., Daniell, J. E., Gill, J. C., & Ward, P. J. (2020). Why We Can No Longer Ignore Consecutive Disasters. *Earth's Future*, 8(3). <https://doi.org/10.1029/2019EF001425>
- De Sy, V., Schoorl, J. M., Keesstra, S. D., Jones, K. E., & Claessens, L. (2013). Landslide model performance in a high resolution small-scale landscape. *Geomorphology*, 190, 73–81. <https://doi.org/10.1016/j.geomorph.2013.02.012>
- Delmonaco, G., Margottini, C., & Spizzichino, D. (2006). *Report on new methodology for multi-risk assessment and the harmonisation of different natural risk maps*. Roma, Italy.
- Demaria, E. M. C., Maurer, E. P., Thrasher, B., Vicuña, S., & Meza, F. J. (2013). Climate change impacts on an alpine watershed in Chile: Do new model projections change the story? *Journal of Hydrology*, 502, 128–138. <https://doi.org/10.1016/J.JHYDROL.2013.08.027>
- DGA. (2017). *Dirección General de Aguas*. Santiago, Chile.
- Douglas-Smith, D., Iwanaga, T., Croke, B. F. W., & Jakeman, A. J. (2020). Certain trends in uncertainty and sensitivity analysis: An overview of software tools and techniques. *Environmental Modelling and Software*, 124. <https://doi.org/10.1016/J.ENVSOFT.2019.104588>
- Dragičević, S., Lai, T., & Balram, S. (2015). GIS-based multicriteria evaluation with multiscale analysis to characterize urban landslide susceptibility in data-scarce environments. *Habitat International*, 45, 114–125. <https://doi.org/10.1016/j.habitatint.2014.06.031>
- Đukić, V., & Radić, Z. (2016). Sensitivity Analysis of a Physically Based Distributed Model. *Water Resour Manage*, 30, 1669–1684. <https://doi.org/10.1007/s11269-016-1243-8>
- ECLAC. (2011). *Macro socio-economic and environmental assessment of the damage and losses caused by Hurricane Tomas: A geo-environmental disaster*.
- Ellison, W. D. (1948). Soil detachment by water in erosion processes. In *Eos, Transactions American Geophysical Union* (Vol. 29). <https://doi.org/10.1029/TR029i004p00499>
- Fan, L., Lehmann, P., McArdeil, B., & Or, D. (2017). Linking rainfall-induced landslides with debris flows runout patterns towards catchment scale hazard assessment. *Geomorphology*, 280, 1–15. <https://doi.org/10.1016/j.geomorph.2016.10.007>
- Fan, L., Lehmann, P., & Or, D. (2016). Effects of soil spatial variability at the hillslope and catchment scales on characteristics of rainfall-induced landslides. *Water Resources Research*, 52(3), 1781–1799. <https://doi.org/10.1002/2015WR017758>
- Fan, Y. R., Yu, L., Shi, X., & Duan, Q. Y. (2021). Tracing Uncertainty Contributors in the Multi-Hazard Risk Analysis for Compound Extremes. *Earth's Future*, 9(12). <https://doi.org/10.1029/2021EF002280>
- Farrell, D. A., & Larson, W. E. (1972). Modeling the pore structure of porous media. *Water Resources Research*, 8(3), 699–706. <https://doi.org/10.1029/WR008i003p00699>
- Fawcett, K. R., Anderson, M. G., Bates, P. D., Jordan, J.-P., & Bathurst, J. C. (1995). The Importance of Internal Validation in the Assessment of Physically Based Distributed Models. *Geographers*, 20(2), 248–265. Retrieved from <https://about.jstor.org/terms>
- Fell, R., Corominas, J., Bonnard, C., Cascini, L., Leroi, E., & Savage, W. (2008). Guidelines for landslide susceptibility, hazard and risk zoning for land use planning. *Engineering Geology*, 102(3–4), 85–98. <https://doi.org/10.1016/j.enggeo.2008.03.022>

- Feyen, L., Vázquez, R., Christiaens, K., Sels, O., & Feyen, J. (2000). Application of a distributed physically-based hydrological model to a medium size catchment. *Hydrology and Earth System Sciences*, 4(1), 47–63. <https://doi.org/10.5194/hess-4-47-2000>
- Fisher, P. F. (1986). Models of uncertainty in spatial data. *Geographical Information Systems: Principles, Techniques, Management and Applications*, 191–205.
- Flato, G. M. (2011). Earth system models: An overview. *Wiley Interdisciplinary Reviews: Climate Change*, 2(6), 783–800. <https://doi.org/10.1002/wcc.148>
- Foley, J. A., DeFries, R., Asner, G. P., Barford, C., Bonan, G., Carpenter, S. R., ... Snyder, P. K. (2005). Global consequences of land use. *Science*, 309(5734), 570–574. <https://doi.org/10.1126/SCIENCE.1111772>
- Formetta, G., Capparelli, G., & Versace, P. (2016). Evaluating performance of simplified physically based models for shallow landslide susceptibility. *Hydrol. Earth Syst. Sci*, 20, 4585–4603. <https://doi.org/10.5194/hess-20-4585-2016>
- Francos, A., Elorza, F. J., Bouraoui, F., Bidoglio, G., & Galbiati, L. (2003). Sensitivity analysis of distributed environmental simulation models: understanding the model behaviour in hydrological studies at the catchment scale. *Reliability Engineering & System Safety*, 79(2), 205–218. [https://doi.org/10.1016/S0951-8320\(02\)00231-4](https://doi.org/10.1016/S0951-8320(02)00231-4)
- Fraser, A. M., Chester, M. V, & Underwood, B. S. (2022). Wildfire risk, post-fire debris flows, and transportation infrastructure vulnerability. *Sustainable and Resilient Infrastructure*, 7(3), 188–200. <https://doi.org/10.1080/23789689.2020.1737785>
- Frattini, P., Crosta, G., & Carrara, A. (2010). Techniques for evaluating the performance of landslide susceptibility models. *Engineering Geology*, 111(1–4), 62–72. <https://doi.org/10.1016/j.enggeo.2009.12.004>
- Froude, M. J., & Petley, D. N. (2018). Global fatal landslide occurrence from 2004 to 2016. *Hazards Earth Syst. Sci*, 18, 2161–2181. <https://doi.org/10.5194/nhess-18-2161-2018>
- Fuchs, M., Torizin, J., & Kühn, F. (2014). The effect of DEM resolution on the computation of the factor of safety using an infinite slope model. *Geomorphology*, 224, 16–26. <https://doi.org/10.1016/j.geomorph.2014.07.015>
- Gabet, E. J., & Mudd, S. M. (2006). The mobilization of debris flows from shallow landslides. *Geomorphology*, 74(1–4), 207–218. <https://doi.org/10.1016/J.GEOMORPH.2005.08.013>
- Galli, M., Ardizzone, F., Cardinali, M., Guzzetti, F., & Reichenbach, P. (2008). Comparing landslide inventory maps. *Geomorphology*, 94(3–4), 268–289. <https://doi.org/10.1016/j.geomorph.2006.09.023>
- Gallina, V., Torresan, S., Critto, A., Sperotto, A., Glade, T., & Marcomini, A. (2016). A review of multi-risk methodologies for natural hazards: Consequences and challenges for a climate change impact assessment. *Journal of Environmental Management*, 168, 123–132. <https://doi.org/10.1016/J.JENVMAN.2015.11.011>
- Gao, J. (1993). Identification of topographic settings conducive to landsliding from dem in Nelson county, Virginia, U.S.A. *Earth Surface Processes and Landforms*, 18(7), 579–591. <https://doi.org/10.1002/esp.3290180702>
- Gao, L., Zhang, L. M., Chen, H. X., Fei, K., & Hong, Y. (2021). Topography and geology effects on travel distances of natural terrain landslides: Evidence from a large multi-temporal landslide inventory in Hong Kong. *Engineering Geology*, 292, 106266. <https://doi.org/10.1016/J.ENGCEO.2021.106266>
- García-Gutiérrez, C., Pachepsky, Y., & Ángel Martín, M. (2018). Technical note: Saturated hydraulic conductivity and textural heterogeneity of soils. *Hydrology and Earth System Sciences*, 22(7), 3923–3932. <https://doi.org/10.5194/HESS-22-3923-2018>
- García, M., Pastén, C., Sepúlveda, S., & Montalva, G. (2018). Dynamic numerical investigation of a stepped-planar rockslide in the Central Andes, Chile. *Engineering Geology*, 237(February), 64–75. <https://doi.org/10.1016/j.enggeo.2018.02.001>

- Gariano, S. L., & Guzzetti, F. (2016, November 1). Landslides in a changing climate. *Earth-Science Reviews*, Vol. 162, pp. 227–252. <https://doi.org/10.1016/j.earscirev.2016.08.011>
- Garland, G. G., & Olivier, M. J. (1993). Predicting landslides from rainfall in a humid, sub-tropical region. *Geomorphology*, 8(2–3), 165–173. [https://doi.org/10.1016/0169-555X\(93\)90035-Z](https://doi.org/10.1016/0169-555X(93)90035-Z)
- Garreaud, R. D., Alvarez-Garretón, C., Barichivich, J., Boisier, J. P., Christie, D., Galleguillos, M., ... Zambrano-Bigiarini, M. (2017). The 2010-2015 megadrought in central Chile: impacts on regional hydroclimate and vegetation. *Hydrol. Earth Syst. Sci*, 21, 6307–6327. <https://doi.org/10.5194/hess-21-6307-2017>
- Gentile, R., Cremen, G., Galasso, C., Jenkins, L. T., Manandhar, V., Menteşe, E. Y., ... McCloskey, J. (2022). Scoring, selecting, and developing physical impact models for multi-hazard risk assessment. *International Journal of Disaster Risk Reduction*, 82. <https://doi.org/10.1016/J.IJDRR.2022.103365>
- Giertz, S., Junge, B., & Diekkrüger, B. (2005). Assessing the effects of land use change on soil physical properties and hydrological processes in the sub-humid tropical environment of West Africa. *Physics and Chemistry of the Earth, Parts A/B/C*, 30(8–10), 485–496. <https://doi.org/10.1016/J.PCE.2005.07.003>
- Gill, J. C., & Malamud, B. D. (2014). Reviewing and visualizing the interactions of natural hazards. *Reviews of Geophysics*, 52(4), 680–722. <https://doi.org/10.1002/2013RG000445>
- Gill, J. C., & Malamud, B. D. (2016). Hazard interactions and interaction networks (cascades) within multi-hazard methodologies. *Earth System Dynamics*, 7(3), 659–679. <https://doi.org/10.5194/esd-7-659-2016>
- Gill, J. C., & Malamud, B. D. (2017). Anthropogenic processes, natural hazards, and interactions in a multi-hazard framework. *Earth-Science Reviews*, 166, 246–269. <https://doi.org/10.1016/J.EARSCIREV.2017.01.002>
- Gill, J. C., Malamud, B. D., Barillas, E. M., & Noriega, A. G. (2020). Construction of regional multi-hazard interaction frameworks, with an application to Guatemala. *Natural Hazards and Earth System Sciences*, 20(1), 149–180. <https://doi.org/10.5194/nhess-20-149-2020>
- Giorgi, F., & Lionello, P. (2008). Climate change projections for the Mediterranean region. *Global and Planetary Change*, 63(2–3), 90–104. <https://doi.org/10.1016/j.gloplacha.2007.09.005>
- Glade, T., & Crozier, M. J. (2010). Landslide geomorphology in a changing environment. *Geomorphology*, 120(1–2), 1–2. <https://doi.org/10.1016/j.geomorph.2009.09.018>
- Godt, J. W., Baum, R. L., Savage, W. Z., Salciarini, D., Schulz, W. H., & Harp, E. L. (2008). Transient deterministic shallow landslide modeling: Requirements for susceptibility and hazard assessments in a GIS framework. *Engineering Geology*, 102(3–4), 214–226. <https://doi.org/10.1016/J.ENGGEOL.2008.03.019>
- González-Díez, a., Fernández-Maroto, G., Doughty, M. W., Díaz de Terán, J. R., Bruschi, V., Cardenal, J., ... Delgado, J. (2013). Development of a methodological approach for the accurate measurement of slope changes due to landslides, using digital photogrammetry. *Landslides*, 11(4), 615–628. <https://doi.org/10.1007/s10346-013-0413-5>
- González, M. B., Rodríguez-Oroz, D., Alcalá-Reygosa, J., & Campos, N. (2020). Geomorphological mapping and landforms characterization of a high valley environment in the Chilean Andes. *Journal of South American Earth Sciences*, 104, 102918. <https://doi.org/10.1016/j.jsames.2020.102918>
- Gonzalez, P. (2010). *Geología y geomorfología del complejo de remoción en masa La Engorda, Chile Central*. Universidad de Chile.
- Goossens, D., & Buck, B. (2011). Gross erosion, net erosion and gross deposition of dust by wind: Field data from 17 desert surfaces. *Earth Surface Processes and Landforms*, 36(5), 610–623. <https://doi.org/10.1002/esp.2080>
- Gorgoglione, A., Castro, A., Chreties, C., & Etcheverry, L. (2020). Overcoming data scarcity in earth

- science. *Data*, 5(1), 2–6. <https://doi.org/10.3390/data5010005>
- Govers, G., Wallings, D. E., Yair, A., & Berkowicz, S. (1990). Empirical relationships for the transport capacity of overland flow. *Transport*, (189), 45–64. Retrieved from [https://iahs.info/uploads/dms/iahs\\_189\\_0045.pdf](https://iahs.info/uploads/dms/iahs_189_0045.pdf)
- Green, W., & Ampt, G. A. (1911). Studies on Soil Physics. *The Journal of Agricultural Science*, 4(1), 1–24. <https://doi.org/10.1017/S0021859600001441>
- GUERRA, A. J. T., FULLEN, M. A., JORGE, M. do C. O., BEZERRA, J. F. R., & SHOKR, M. S. (2017). Slope Processes, Mass Movement and Soil Erosion: A Review. *Pedosphere*, 27(1), 27–41. [https://doi.org/10.1016/S1002-0160\(17\)60294-7](https://doi.org/10.1016/S1002-0160(17)60294-7)
- Guinot, V., & Gourbesville, P. (2003). Calibration of physically based models: back to basics? *Journal of Hydroinformatics*, 5(4), 233–244. <https://doi.org/10.2166/HYDRO.2003.0020>
- Guns, M., & Vanacker, V. (2013). Forest cover change trajectories and their impact on landslide occurrence in the tropical Andes. *Environmental Earth Sciences*, 70(7), 2941–2952. <https://doi.org/10.1007/s12665-013-2352-9>
- Guthrie, R. H., & Evans, S. G. (2005). The role of magnitude-frequency relations in regional landslide risk analysis. In *Landslide Risk Management* (pp. 385–390). <https://doi.org/10.1201/9781439833711-19>
- Guthrie, Richard H., Deadman, P. J., Cabrera, A. R., & Evans, S. G. (2008). Exploring the magnitude–frequency distribution: a cellular automata model for landslides. *Landslides*, 5(1), 151–159. <https://doi.org/10.1007/s10346-007-0104-1>
- Guzzetti, F., Ardizzone, F., Cardinali, M., Rossi, M., & Valigi, D. (2009). Landslide volumes and landslide mobilization rates in Umbria, central Italy. *Earth and Planetary Science Letters*, 279(3–4), 222–229. <https://doi.org/10.1016/j.epsl.2009.01.005>
- Guzzetti, F., Carrara, A., Cardinali, M., & Reichenbach, P. (1999). Landslide hazard evaluation: a review of current techniques and their application in a multi-scale study, Central Italy. *Geomorphology*, 31(1–4), 181–216. [https://doi.org/10.1016/S0169-555X\(99\)00078-1](https://doi.org/10.1016/S0169-555X(99)00078-1)
- Guzzetti, F., Mondini, A. C., Cardinali, M., Fiorucci, F., Santangelo, M., & Chang, K. T. (2012). Landslide inventory maps: New tools for an old problem. *Earth-Science Reviews*, 112(1–2), 42–66. <https://doi.org/10.1016/j.earscirev.2012.02.001>
- Guzzetti, F., Peruccacci, S., Rossi, M., & Stark, C. P. (2007). The rainfall intensity–duration control of shallow landslides and debris flows: an update. *Landslides*, 5(1), 3–17. <https://doi.org/10.1007/s10346-007-0112-1>
- Guzzetti, F., Reichenbach, P., Ardizzone, F., Cardinali, M., & Galli, M. (2006). Estimating the quality of landslide susceptibility models. *Geomorphology*, 81(1–2), 166–184. <https://doi.org/10.1016/j.geomorph.2006.04.007>
- Guzzetti, F., Cardinali, M., & Reichenbach, P. (1996). The influence of structural setting and lithology on landslide type and pattern. *Environmental and Engineering Geoscience*, 2(4), 531–555. <https://doi.org/10.2113/gseegeosci.ii.4.531>
- Guzzetti, F., Malamud, B. D., Turcotte, D. L., & Reichenbach, P. (2002). Power-law correlations of landslide areas in central Italy. *Earth and Planetary Science Letters*, 195(3–4), 169–183. [https://doi.org/10.1016/S0012-821X\(01\)00589-1](https://doi.org/10.1016/S0012-821X(01)00589-1)
- Hagen-Zanker, A., & Martens, P. (2008). Map Comparison Methods for Comprehensive Assessment of Geosimulation Models. *LNCS*, 5072, 194–209.
- He, X., Hong, Y., Vergara, H., Zhang, K., Kirstetter, P.-E., Gourley, J. J., ... Liu, C. (2016). Development of a coupled hydrological-geotechnical framework for rainfall-induced landslides prediction. *Journal of Hydrology*. <https://doi.org/10.1016/j.jhydrol.2016.10.016>
- Henríquez-Dole, L., Usón, T. J., Vicuña, S., Henríquez, C., Gironás, J., & Meza, F. (2018). Integrating strategic land use planning in the construction of future land use scenarios and its performance: The Maipo River Basin, Chile. *Land Use Policy*, 78, 353–366.



- <https://doi.org/10.1016/J.LANDUSEPOL.2018.06.045>
- Herrera, P. A., Angel Marazuela, M., Hofmann, T., & Paulo Herrera, C. A. (2022). Parameter estimation and uncertainty analysis in hydrological modeling. *Wiley Interdisciplinary Reviews: Water*, 9(1), e1569. <https://doi.org/10.1002/WAT2.1569>
- Hessel, R. (2005). Effects of grid cell size and time step length on simulation results of the Limburg soil erosion model (LISEM). *Hydrological Processes*, 19(15), 3037–3049. <https://doi.org/10.1002/hyp.5815>
- Hessel, R., & Jetten, V. (2007). Suitability of transport equations in modelling soil erosion for a small Loess Plateau catchment. *Engineering Geology*, 91(1), 56–71. <https://doi.org/10.1016/J.ENGGEOL.2006.12.013>
- Hillier, J. K., Matthews, T., Wilby, R. L., & Murphy, C. (2020). Multi-hazard dependencies can increase or decrease risk. *Nature Climate Change*, 10(7), 595–598. <https://doi.org/10.1038/s41558-020-0832-y>
- Hino, M., Odaka, Y., Nadaoka, K., & Sato, A. (1988). Effect of initial soil moisture content on the vertical infiltration process — A guide to the problem of runoff-ratio and loss. *Journal of Hydrology*, 102(1–4), 267–284. [https://doi.org/10.1016/0022-1694\(88\)90102-3](https://doi.org/10.1016/0022-1694(88)90102-3)
- Hirschberg, J., Fatichi, S., Bennett, G. L., McArdell, B. W., Peleg, N., Lane, S. N., ... Molnar, P. (2021). Climate Change Impacts on Sediment Yield and Debris-Flow Activity in an Alpine Catchment. *Journal of Geophysical Research: Earth Surface*, 126(1), e2020JF005739. <https://doi.org/10.1029/2020JF005739>
- Hofmann, M. (2005). *On the Complexity of Parameter Calibration in Simulation Models*. 2(4), 217–226.
- Holcombe, E. A. (2006). Modelling Landslide Risk on Highway Cut Slopes in Developing Countries. *PhD Thesis, University of Bristol, Bristol, UK*.
- Huggel, C., Khabarov, N., Korup, O., & Obersteiner, M. (2012). Physical impacts of climate change on landslide occurrence and related adaptation. In *Landslides* (pp. 121–133). <https://doi.org/10.1017/CBO9780511740367.012>
- Hungr, O., Evans, S. G., Bovis, M. J., & Hutchinson, J. N. (2001). A review of the classification of landslides of the flow type. *Environmental and Engineering Geoscience*, 7(3), 221–238. <https://doi.org/10.2113/gseegeosci.7.3.221>
- Hungr, O., Leroueil, S., & Picarelli, L. (2014). The Varnes classification of landslide types, an update. *Landslides*, 11(2), 167–194. <https://doi.org/10.1007/s10346-013-0436-y>
- Hurst, M. D., Ellis, M. A., Royse, K. R., Lee, K. A., & Freeborough, K. (2013). Controls on the magnitude-frequency scaling of an inventory of secular landslides. *Earth Surface Dynamics*, 1(1), 67–78. <https://doi.org/10.5194/ESURF-1-67-2013>
- Hutter, K., Svendsen, B., & Rickenmann, D. (1994). Debris flow modeling: A review. *Continuum Mechanics and Thermodynamics*, 8(1), 1–35. <https://doi.org/10.1007/BF01175749>
- IDE Chile. (2021). *Infraestructura de Datos Geoespaciales de Chile*. Santiago, Chile.
- Iverson, R. M. (1997). The physics of debris flows. *Reviews of Geophysics*, 35(3), 245–296. <https://doi.org/10.1029/97RG00426>
- Iverson, R. M., & Ouyang, C. (2015). Entrainment of bed material by Earth-surface mass flows: Review and reformulation of depth-integrated theory. *Reviews of Geophysics*, 53(1), 27–58. <https://doi.org/10.1002/2013RG000447>
- Iverson, R. M., Reid, M. E., & LaHusen, R. G. (2002). Debris-Flow Mobilization From Landslides. In *Annual Review of Earth and Planetary Sciences* (Vol. 25). <https://doi.org/10.1146/annurev.earth.25.1.85>
- Iwashita, F., Friedel, M. J., Ribeiro, G. F., & Fraser, S. J. (2012). Intelligent estimation of spatially distributed soil physical properties. *Geoderma*, 170, 1–10. <https://doi.org/10.1016/J.GEODERMA.2011.11.002>

- Jetten, V., Govers, G., & Hessel, R. (2003). Erosion models: quality of spatial predictions. *Hydrological Processes*, 17(5), 887–900. <https://doi.org/10.1002/hyp.1168>
- Johnston, E. C., Davenport, F. V., Wang, L., Caers, J. K., Muthukrishnan, S., Burke, M., & Diffenbaugh, N. S. (2021). Quantifying the Effect of Precipitation on Landslide Hazard in Urbanized and Non-Urbanized Areas. *Geophysical Research Letters*, 48(16), e2021GL094038. <https://doi.org/10.1029/2021GL094038>
- Julien, P. Y., & Simons, D. B. (1985). Sediment Transport Capacity of Overland Flow. *Transactions of the ASAE*, 28(3), 755–762. <https://doi.org/10.13031/2013.32333>
- Kappes, M., Keiler, M., von Elverfeldt, K., & Glade, T. (2012, November). Challenges of analyzing multi-hazard risk: A review. *Natural Hazards*, Vol. 64, pp. 1925–1958. <https://doi.org/10.1007/s11069-012-0294-2>
- Kappes, M. S., Keiler, M., & Glade, T. (2010). From Single- to Multi-Hazard Risk Analyses: a concept addressing emerging challenges. *Mountain Risks: Bringing Science to Society*, (November), 351–356.
- Kelman, I., Gaillard, J. C., Lewis, J., & Mercer, J. (2016). Learning from the history of disaster vulnerability and resilience research and practice for climate change. *Natural Hazards*, 82(1), 129–143. <https://doi.org/10.1007/s11069-016-2294-0>
- Khatami, S., Peel, M. C., Peterson, T. J., & Western, A. W. (2019). Equifinality and Flux Mapping: A New Approach to Model Evaluation and Process Representation Under Uncertainty. *Water Resources Research*, 55(11), 8922–8941. <https://doi.org/10.1029/2018WR023750>
- Kiani-Harchegani, M., Talebi, A., Asgari, E., & Rodrigo-Comino, J. (2022). Topographical features and soil erosion processes. In *Computers in Earth and Environmental Sciences* (pp. 117–126). <https://doi.org/10.1016/B978-0-323-89861-4.00034-8>
- Kim, M. S., Onda, Y., Uchida, T., & Kim, J. K. (2016). Effects of soil depth and subsurface flow along the subsurface topography on shallow landslide predictions at the site of a small granitic hillslope. *Geomorphology*, 271, 40–54. <https://doi.org/10.1016/j.geomorph.2016.07.031>
- Kirkby, M. (1988). Hillslope runoff processes and models. *Journal of Hydrology*, 100(1–3), 315–339. [https://doi.org/10.1016/0022-1694\(88\)90190-4](https://doi.org/10.1016/0022-1694(88)90190-4)
- Koo, H., Iwanaga, T., Croke, B. F. W., Jakeman, A. J., Yang, J., Wang, H. H., ... Chen, M. (2020). Position paper: Sensitivity analysis of spatially distributed environmental models- a pragmatic framework for the exploration of uncertainty sources. *Environmental Modelling and Software*, 134. <https://doi.org/10.1016/J.ENVSOF.2020.104857>
- Korup, O. (2009). Linking landslides, hillslope erosion, and landscape evolution. *Earth Surface Processes and Landforms*, 34(9), 1315–1317. <https://doi.org/10.1002/esp.1830>
- Korup, O. (2012). Landslides in the Earth system. In *Landslides* (pp. 10–23). <https://doi.org/10.1017/CBO9780511740367.003>
- Korup, O., Clague, J. J., Hermanns, R. L., Hewitt, K., Strom, A. L., & Weidinger, J. T. (2007). Giant landslides, topography, and erosion. *Earth and Planetary Science Letters*, 261(3–4), 578–589. <https://doi.org/10.1016/J.EPSL.2007.07.025>
- Kremmydas, D., Athanasiadis, I. N., & Rozakis, S. (2018). A review of Agent Based Modeling for agricultural policy evaluation. *Agricultural Systems*, 164, 95–106. <https://doi.org/10.1016/J.AGSY.2018.03.010>
- Kuriakose, S. L., van Beek, L. P. H., & van Westen, C. J. (2009). Parameterizing a physically based shallow landslide model in a data poor region. *Earth Surface Processes and Landforms*, 34(6), 867–881. <https://doi.org/10.1002/esp.1794>
- Labrière, N., Locatelli, B., Laumonier, Y., Freycon, V., & Bernoux, M. (2015). Soil erosion in the humid tropics: A systematic quantitative review. *Agriculture, Ecosystems & Environment*, 203, 127–139. <https://doi.org/10.1016/J.AGEE.2015.01.027>
- Landis, J. R., & Koch, G. G. (1977). The Measurement of Observer Agreement for Categorical Data.

- Biometrics*, 33(1), 159. <https://doi.org/10.2307/2529310>
- Lane, R. A., Freer, J. E., Coxon, G., & Wagener, T. (2021). Incorporating Uncertainty Into Multiscale Parameter Regionalization to Evaluate the Performance of Nationally Consistent Parameter Fields for a Hydrological Model. *Water Resources Research*, 57(10). <https://doi.org/10.1029/2020WR028393>
- Lanni, C., Borga, M., Rigon, R., & Tarolli, P. (2012). Modelling shallow landslide susceptibility by means of a subsurface flow path connectivity index and estimates of soil depth spatial distribution. *Hydrology and Earth System Sciences*, 16(11), 3959–3971. <https://doi.org/10.5194/HESS-16-3959-2012>
- Lanni, Cristiano, McDonnell, J., Hopp, L., & Rigon, R. (2013). Simulated effect of soil depth and bedrock topography on near-surface hydrologic response and slope stability. *Earth Surface Processes and Landforms*, 38(2), 146–159. <https://doi.org/10.1002/esp.3267>
- Lari, S., Frattini, P., & Crosta, G. (2014). A probabilistic approach for landslide hazard analysis. *Engineering Geology*, 182(PA), 3–14. <https://doi.org/10.1016/j.enggeo.2014.07.015>
- Larsen, I. J., Montgomery, D. R., & Korup, O. (2010). Landslide erosion controlled by hillslope material. *Nature Geoscience*, 3(4), 247–251. <https://doi.org/10.1038/ngeo776>
- Larsen, M. C., & Simon, A. (1993). A Rainfall Intensity-Duration Threshold for Landslides in a Humid-Tropical Environment, Puerto Rico. *Geografiska Annaler: Series A, Physical Geography*, 75(1–2), 13–23. <https://doi.org/10.1080/04353676.1993.11880379>
- Leavesley, G. H., Markstrom, S. L., Restrepo, P. J., & Viger, R. J. (2002). A modular approach to addressing model design, scale, and parameter estimation issues in distributed hydrological modelling. *Hydrological Processes*, 16(2), 173–187. <https://doi.org/10.1002/hyp.344>
- Lee, E., & Kim, S. (2021). Characterization of soil moisture response patterns and hillslope hydrological processes through a self-organizing map. *Hydrology and Earth System Sciences*, 25(11), 5733–5748. <https://doi.org/10.5194/hess-25-5733-2021>
- Lee, G., Kim, W., Oh, H., Youn, B. D., & Kim, N. H. (2019). Review of statistical model calibration and validation—from the perspective of uncertainty structures. *Structural and Multidisciplinary Optimization*, 60(4), 1619–1644. <https://doi.org/10.1007/s00158-019-02270-2>
- Lee, S., Chu, M. L., & Schmidt, A. R. (2020). Effective Green-Ampt Parameters for Two-Layered Soils. *Journal of Hydrologic Engineering*, 25(4). [https://doi.org/10.1061/\(ASCE\)HE.1943-5584.0001897](https://doi.org/10.1061/(ASCE)HE.1943-5584.0001897)
- Leonard, M., Westra, S., Phatak, A., Lambert, M., van den Hurk, B., McInnes, K., ... Stafford-Smith, M. (2014). A compound event framework for understanding extreme impacts. *Wiley Interdisciplinary Reviews: Climate Change*, 5(1), 113–128. <https://doi.org/10.1002/WCC.252>
- Li, G., Zheng, T., Fu, Y., Li, B., & Zhang, T. (2017). Soil detachment and transport under the combined action of rainfall and runoff energy on shallow overland flow. *Journal of Mountain Science*, 14(7), 1373–1383. <https://doi.org/10.1007/s11629-016-3938-y>
- Li, Z., & Fang, H. (2016, December 1). Impacts of climate change on water erosion: A review. *Earth-Science Reviews*, Vol. 163, pp. 94–117. <https://doi.org/10.1016/j.earscirev.2016.10.004>
- Lilburne, L., & Tarantola, S. (2009). Sensitivity analysis of spatial models. *International Journal of Geographical Information Science*, 23(2), 151–168. <https://doi.org/10.1080/13658810802094995>
- Lionello, P., Abrantes, F., Gacic, M., Planton, S., Trigo, R., & Ulbrich, U. (2014). The climate of the Mediterranean region: research progress and climate change impacts. *Regional Environmental Change*, 14(5), 1679–1684. <https://doi.org/10.1007/s10113-014-0666-0>
- Liu, B., Siu, Y. L., & Mitchell, G. (2016). Hazard interaction analysis for multi-hazard risk assessment: A systematic classification based on hazard-forming environment. *Natural Hazards and Earth System Sciences*, 16(2), 629–642. <https://doi.org/10.5194/nhess-16-629-2016>
- Liu, C., Frazier, P., & Kumar, L. (2007). Comparative assessment of the measures of thematic classification accuracy. *Remote Sensing of Environment*, 107(4), 606–616. <https://doi.org/10.1016/J.RSE.2006.10.010>

- Liu, Q. ., Chen, L., Li, J. ., & Singh, V. . (2004). Two-dimensional kinematic wave model of overland-flow. *Journal of Hydrology*, 291(1–2), 28–41. <https://doi.org/10.1016/J.JHYDROL.2003.12.023>
- Liu, W., & He, S. (2020). Comprehensive modelling of runoff-generated debris flow from formation to propagation in a catchment. *Landslides*, 17(7), 1529–1544. <https://doi.org/10.1007/s10346-020-01383-w>
- Liu, W., He, S., Chen, Z., Yan, S., & Deng, Y. (2021). Effect of viscosity changes on the motion of debris flow by considering entrainment. *Journal of Hydraulic Research*, 59(1), 120–135. <https://doi.org/10.1080/00221686.2020.1744746>
- Liu, W., Yang, Z., & He, S. (2020). Modeling the landslide-generated debris flow from formation to propagation and run-out by considering the effect of vegetation. *Landslides*, (July). <https://doi.org/10.1007/s10346-020-01478-4>
- Lobo, G. P., & Bonilla, C. A. (2019). Predicting soil loss and sediment characteristics at the plot and field scales: Model description and first verifications. *Catena*, 172, 113–124. <https://doi.org/10.1016/j.catena.2018.08.017>
- Lombardo, L., Tanyas, H., Huser, R., Guzzetti, F., & Castro-Camilo, D. (2021). Landslide size matters: A new data-driven, spatial prototype. *Engineering Geology*, 293, 106288. <https://doi.org/10.1016/J.ENGGEOL.2021.106288>
- Lu, N., & Godt, J. W. (2013). Hillslope Hydrology and Stability. In *Cambridge* (Vol. 58). <https://doi.org/10.1017/CBO9781139108164>
- Luterbacher, J., Xoplaki, E., Casty, C., Wanner, H., Pauling, A., Küttel, M., ... Ladurie, E. L. R. (2006). Chapter 1 Mediterranean climate variability over the last centuries: A review. In *Developments in Earth and Environmental Sciences* (Vol. 4, pp. 27–148). [https://doi.org/10.1016/S1571-9197\(06\)80004-2](https://doi.org/10.1016/S1571-9197(06)80004-2)
- Luzio, W. (2010). Suelos de Chile. *Universidad de Chile*, p. 352.
- Mahat, V., Silins, U., & Anderson, A. (2016). Effects of wildfire on the catchment hydrology in southwest Alberta. *CATENA*, 147, 51–60. <https://doi.org/10.1016/J.CATENA.2016.06.040>
- Malamud, B. D., Turcotte, D. L., Guzzetti, F., & Reichenbach, P. (2004). Landslide inventories and their statistical properties. *Earth Surface Processes and Landforms*, 29(6), 687–711. <https://doi.org/10.1002/esp.1064>
- Malet, J.-P., Van Asch, T. W. J., Van Beek, R., & Maquaire, O. (2005). Forecasting the behaviour of complex landslides with a spatially distributed hydrological model. *Natural Hazards and Earth System Sciences*, 5.
- Malone, R. W., Yagow, G., Baffaut, C., Gitau, M. W., Qi, Z., Amatya, D. M., ... Malone, R. (2015). Parameterization guidelines and considerations for hydrologic models. *Transactions of the ASABE*, 58(6), 1681–1703. <https://doi.org/10.13031/TRANS.58.10709>
- Marhaento, H., Booij, M. J., & Hoekstra, A. Y. (2018). Hydrological response to future land-use change and climate change in a tropical catchment. *Hydrological Sciences Journal*, 63(9), 1368–1385. <https://doi.org/10.1080/02626667.2018.1511054>
- Marhaento, H., Booij, M. J., Rientjes, T. H. M., & Hoekstra, A. Y. (2017). Attribution of changes in the water balance of a tropical catchment to land use change using the SWAT model. *Hydrological Processes*, 31(11), 2029–2040. <https://doi.org/10.1002/hyp.11167>
- Marín, M., Contreras, J. P., & Olea, P. (2017). *Efectos geológicos del sistema frontal en la zona central del pas, el 25 y 26 de febrero de 2017. Region metropolitana, comuna de San José de Maipo*. Santiago, Chile.
- Marshall, E., & Randhir, T. (2008). Effect of climate change on watershed system: a regional analysis. *Climatic Change*, 89(3–4), 263–280. <https://doi.org/10.1007/s10584-007-9389-2>
- Martelloni, G., Segoni, S., Fanti, R., & Catani, F. (2011). Rainfall thresholds for the forecasting of landslide occurrence at regional scale. *Landslides*, 9(4), 485–495. <https://doi.org/10.1007/s10346-011-0308-2>

- Martínez-Retureta, R., Aguayo, M., Stehr, A., Sauvage, S., Echeverría, C., & Sánchez-Pérez, J.-M. (2020). Effect of Land Use/Cover Change on the Hydrological Response of a Southern Center Basin of Chile. *Water*, *12*(1), 302. <https://doi.org/10.3390/w12010302>
- Marzocchi, W., Garcia-Aristizabal, A., Gasparini, P., Mastellone, M. L., & Di Ruocco, A. (2012). Basic principles of multi-risk assessment: a case study in Italy. *Natural Hazards*, *62*(2), 551–573. <https://doi.org/10.1007/s11069-012-0092-x>
- Masi, E. B., Segoni, S., & Tofani, V. (2021). Root Reinforcement in Slope Stability Models: A Review. *Geosciences*, *11*(5), 212. <https://doi.org/10.3390/geosciences11050212>
- Mateos, R. M., López-Vinielles, J., Poyiadji, E., Tsagkas, D., Sheehy, M., Hadjicharalambous, K., ... Herrera, G. (2020). Integration of landslide hazard into urban planning across Europe. *Landscape and Urban Planning*, *196*, 103740. <https://doi.org/10.1016/j.landurbplan.2019.103740>
- Matott, L. S., Babendreier, J. E., & Purucker, S. T. (2009). Evaluating uncertainty in integrated environmental models: A review of concepts and tools. *Water Resources Research*, *45*(6), 6421. <https://doi.org/10.1029/2008WR007301>
- McMillan, H. K., Westerberg, I. K., & Krueger, T. (2018). Hydrological data uncertainty and its implications. *Wiley Interdisciplinary Reviews: Water*, *5*(6). <https://doi.org/10.1002/WAT2.1319>
- McNamee, M., Pagnon Eriksson, C., Wahlqvist, J., & Johansson, N. (2022). A methodology for assessing wildfire hazard in Sweden – The first step towards a multi-hazard assessment method. *International Journal of Disaster Risk Reduction*, *83*, 103415. <https://doi.org/10.1016/J.IJDRR.2022.103415>
- Mead, S. R., Procter, J., & Kereszturi, G. (2021). Quantifying location error to define uncertainty in volcanic mass flow hazard simulations. *Natural Hazards and Earth System Sciences*, *21*(8), 2447–2460. <https://doi.org/10.5194/nhess-21-2447-2021>
- Meng, Xianmeng, Zhu, Y., Yin, M., & Liu, D. (2021). The impact of land use and rainfall patterns on the soil loss of the hillslope. *Scientific Reports 2021 11:1*, *11*(1), 1–10. <https://doi.org/10.1038/s41598-021-95819-5>
- Meng, Xiannan, & Wang, Y. (2016). Modelling and numerical simulation of two-phase debris flows. *Acta Geotechnica*, *11*(5), 1027–1045. <https://doi.org/10.1007/s11440-015-0418-4>
- Mergili, M., Fellin, W., Moreiras, S., & Stötter, J. (2012). Simulation of debris flows in the Central Andes based on Open Source GIS: Possibilities, limitations, and parameter sensitivity. *Natural Hazards*, *61*(3), 1051–1081. <https://doi.org/10.1007/s11069-011-9965-7>
- Mergili, M., Fischer, J., Krenn, J., & Pudasaini, S. (2017). R.avaflow v1, an advanced open-source computational framework for the propagation and interaction of two-phase mass flows. *Geoscientific Model Development*, *10*(2), 553–569. <https://doi.org/10.5194/gmd-10-553-2017>
- Mergili, M., Marchesini, I., Alvioli, M., Metz, M., Schneider-Muntau, B., Rossi, M., & Guzzetti, F. (2014). A strategy for GIS-based 3-D slope stability modelling over large areas. *Geosci. Model Dev*, *7*, 2969–2982. <https://doi.org/10.5194/gmd-7-2969-2014>
- Mergili, M., Marchesini, I., Rossi, M., Guzzetti, F., & Fellin, W. (2014). Spatially distributed three-dimensional slope stability modelling in a raster GIS. *Geomorphology*, *206*, 178–195. <https://doi.org/10.1016/j.geomorph.2013.10.008>
- Merritt, W.S., Letcher, R. A., & Jakeman, A. J. (2003). A review of erosion and sediment transport models. *Environmental Modelling & Software*, *18*(8–9), 761–799. [https://doi.org/10.1016/S1364-8152\(03\)00078-1](https://doi.org/10.1016/S1364-8152(03)00078-1)
- Merritt, W. S., Alila, Y., Barton, M., Taylor, B., Cohen, S., & Neilsen, D. (2006). Hydrologic response to scenarios of climate change in sub watersheds of the Okanagan basin, British Columbia. *Journal of Hydrology*, *326*(1–4), 79–108. <https://doi.org/10.1016/J.JHYDROL.2005.10.025>
- Merz, R., Tarasova, L., & Basso, S. (2020). Parameter's Controls of Distributed Catchment Models—How Much Information is in Conventional Catchment Descriptors? *Water Resources Research*, *56*(2), e2019WR026008. <https://doi.org/10.1029/2019WR026008>

- Michaelides, K., & Martin, G. J. (2012). Sediment transport by runoff on debris-mantled dryland hillslopes. *Journal of Geophysical Research: Earth Surface*, 117(F3), n/a-n/a. <https://doi.org/10.1029/2012JF002415>
- Michel, J., Dario, C., Marc-Henri, D., Thierry, O., Ivanna Marina, P., & Benjamin, R. (2020). A review of methods used to estimate initial landslide failure surface depths and volumes. *Engineering Geology*, 267, 105478. <https://doi.org/10.1016/j.enggeo.2020.105478>
- Miller, D. J., & Burnett, K. M. (2007). Effects of forest cover, topography, and sampling extent on the measured density of shallow, translational landslides. *Water Resources Research*, 43(3), 1–23. <https://doi.org/10.1029/2005WR004807>
- Ming, X., Liang, Q., Dawson, R., Xia, X., & Hou, J. (2022). A quantitative multi-hazard risk assessment framework for compound flooding considering hazard inter-dependencies and interactions. *Journal of Hydrology*, 607, 127477. <https://doi.org/10.1016/J.JHYDROL.2022.127477>
- Miranda, A., Altamirano, A., Cayuela, L., Lara, A., & González, M. (2017). Native forest loss in the Chilean biodiversity hotspot: revealing the evidence. *Regional Environmental Change*, 17(1), 285–297. <https://doi.org/10.1007/s10113-016-1010-7>
- Montgomery, D. R., & Dietrich, W. E. (1994). A physically based model for the topographical control on shallow landsliding. *Water Resources Research*, 30(4), 1153–1171. <https://doi.org/10.1029/93WR02979>
- Moreiras, S., & Sepúlveda, S. (2022). Landslides in Arid and Semi-Arid Environments. In *Treatise on Geomorphology* (pp. 322–337). <https://doi.org/10.1016/B978-0-12-818234-5.00105-X>
- Moreiras, S., Sepúlveda, S., Correas-González, M., Lauro, C., Vergara, I., Jeanneret, P., ... Lara, M. (2021). Debris Flows Occurrence in the Semiarid Central Andes under Climate Change Scenario. *Geosciences 2021, Vol. 11, Page 43, 11(2)*, 43. <https://doi.org/10.3390/GEOSCIENCES11020043>
- Muntohar, A. S., & Liao, H. J. (2010). Rainfall infiltration: Infinite slope model for landslides triggering by rainstorm. *Natural Hazards*, 54(3), 967–984. <https://doi.org/10.1007/s11069-010-9518-5>
- Murgia, I., Giadrossich, F., Mao, Z., Cohen, D., Capra, G. F., & Schwarz, M. (2022). Modeling shallow landslides and root reinforcement: A review. *Ecological Engineering*, 181, 106671. <https://doi.org/10.1016/J.ECOLENG.2022.106671>
- Neal, J. (2022). Recent Innovations in Flood Hazard Modelling Over Large Data Sparse Regions. In *Springer Climate*. [https://doi.org/10.1007/978-3-030-86211-4\\_15](https://doi.org/10.1007/978-3-030-86211-4_15)
- Nepf, H. M., & Koch, E. W. K. (1999). Vertical secondary flows in submersed plant-like arrays. *Limnology and Oceanography*, 44(4), 1072–1080. <https://doi.org/10.4319/lo.1999.44.4.1072>
- Nguyen, V. B., Nguyen, Q. B., Zhang, Y. W., Lim, C. Y. H., & Khoo, B. C. (2016). Effect of particle size on erosion characteristics. *Wear*, 348–349, 126–137. <https://doi.org/10.1016/j.wear.2015.12.003>
- Nishiguchi, Y., & Uchida, T. (2022). Long-Runout-Landslide-Induced Debris Flow: The Role of Fine Sediment Deposition Processes in Debris Flow Propagation. *Journal of Geophysical Research: Earth Surface*, 127(2). <https://doi.org/10.1029/2021JF006452>
- Noacco, V., Sarrazin, F., Pianosi, F., & Wagener, T. (2019). Matlab/R workflows to assess critical choices in Global Sensitivity Analysis using the SAFE toolbox. *MethodsX*, 6, 2258–2280. <https://doi.org/10.1016/j.mex.2019.09.033>
- O'Brien, J. S., Julien, P. Y., & Fullerton, W. T. (1993). Two-Dimensional Water Flood and Mudflow Simulation. *Journal of Hydraulic Engineering*, 119(2), 244–261. [https://doi.org/10.1061/\(asce\)0733-9429\(1993\)119:2\(244\)](https://doi.org/10.1061/(asce)0733-9429(1993)119:2(244))
- Oberkampf, W. L. (2019). *Simulation Accuracy, Uncertainty, and Predictive Capability: A Physical Sciences Perspective*. [https://doi.org/10.1007/978-3-319-70766-2\\_3](https://doi.org/10.1007/978-3-319-70766-2_3)
- Oberkampf, W. L., & Barone, M. F. (2006). Measures of agreement between computation and experiment: Validation metrics. *Journal of Computational Physics*, 217(1), 5–36. <https://doi.org/10.1016/J.JCP.2006.03.037>

- Oreskes, N., Shrader-Frechette, K., & Belitz, K. (1994). Verification, validation, and confirmation of numerical models in the earth sciences. *Science*, 263(5147), 641–646. <https://doi.org/10.1126/science.263.5147.641>
- Panday, S., & Huyakorn, P. S. (2004). A fully coupled physically-based spatially-distributed model for evaluating surface/subsurface flow. *Advances in Water Resources*, 27(4), 361–382. <https://doi.org/10.1016/J.ADVWATRES.2004.02.016>
- Pardeshi, S. D., Autade, S. E., & Pardeshi, S. S. (2013). Landslide hazard assessment: recent trends and techniques. *SpringerPlus*, 2(1), 523. <https://doi.org/10.1186/2193-1801-2-523>
- Parise, M., & Cannon, S. H. (2012). Wildfire impacts on the processes that generate debris flows in burned watersheds. *Natural Hazards*, 61(1), 217–227. <https://doi.org/10.1007/s11069-011-9769-9>
- Pellicani, R., Van Westen, C. J., & Spilotro, G. (2013). Assessing landslide exposure in areas with limited landslide information. *Landslides*, 11(3), 463–480. <https://doi.org/10.1007/s10346-013-0386-4>
- Persichillo, M. G., Bordoni, M., & Meisina, C. (2017). The role of land use changes in the distribution of shallow landslides. *Science of The Total Environment*, 574, 924–937. <https://doi.org/10.1016/j.scitotenv.2016.09.125>
- Pescaroli, G., & Alexander, D. (2018). Understanding Compound, Interconnected, Interacting, and Cascading Risks: A Holistic Framework. *Risk Analysis*, 38(11), 2245–2257. <https://doi.org/10.1111/risa.13128>
- Pianosi, F., Beven, K., Freer, J., Hall, J. W., Rougier, J., Stephenson, D. B., & Wagener, T. (2016). Sensitivity analysis of environmental models: A systematic review with practical workflow. *Environmental Modelling and Software*, Vol. 79, pp. 214–232. <https://doi.org/10.1016/j.envsoft.2016.02.008>
- Pianosi, F., Iwema, J., Rosolem, R., & Wagener, T. (2016). A Multimethod Global Sensitivity Analysis Approach to Support the Calibration and Evaluation of Land Surface Models. In *Sensitivity Analysis in Earth Observation Modelling*. <https://doi.org/10.1016/B978-0-12-803011-0.00007-0>
- Pianosi, F., Sarrazin, F., & Wagener, T. (2015). A Matlab toolbox for Global Sensitivity Analysis. *Environmental Modelling & Software*, 70, 80–85. <https://doi.org/10.1016/J.ENVSOFT.2015.04.009>
- Pianosi, F., & Wagener, T. (2018). Distribution-based sensitivity analysis from a generic input-output sample. *Environmental Modelling and Software*, 108, 197–207. <https://doi.org/10.1016/j.envsoft.2018.07.019>
- Pizarro, R., Aravena, D., Macaya, K., Abarza, A., Cornejo, M., Labra, M., ... Roman, L. (2007). Curvas intensidad - duración - frecuencia para la zona centro sur de Chile. In *Nuevos sistemas de comunicación e información*. UNESCO Office Montevideo and Regional Bureau for Science in Latin America and the Caribbean, Universidad de Talca (Chile).
- Pogson, M., & Smith, P. (2015). Effect of spatial data resolution on uncertainty. *Environmental Modelling & Software*, 63, 87–96. <https://doi.org/10.1016/J.ENVSOFT.2014.09.021>
- Prancevic, J. P., Lamb, M. P., McARDell, B. W., Rickli, C., & Kirchner, J. W. (2020). Decreasing Landslide Erosion on Steeper Slopes in Soil-Mantled Landscapes. *Geophysical Research Letters*, 47(10). <https://doi.org/10.1029/2020GL087505>
- Pudasaini, S. P. (2012). A general two-phase debris flow model. *Journal of Geophysical Research: Earth Surface*, 117(3), n/a-n/a. <https://doi.org/10.1029/2011JF002186>
- Pudasaini, S. P. (2019). A fully analytical model for virtual mass force in mixture flows. *International Journal of Multiphase Flow*, 113, 142–152. <https://doi.org/10.1016/j.ijmultiphaseflow.2019.01.005>
- Pudasaini, S. P., & Fischer, J. T. (2020). A mechanical erosion model for two-phase mass flows. *International Journal of Multiphase Flow*, 132. <https://doi.org/10.1016/j.ijmultiphaseflow.2020.103416>
- Pudasaini, S. P., & Krautblatter, M. (2021). The mechanics of landslide mobility with erosion. *Nature Communications*, 12(1), 6793. <https://doi.org/10.1038/s41467-021-26959-5>

- Rahardjo, H., Kim, Y., & Satyanaga, A. (2019). Role of unsaturated soil mechanics in geotechnical engineering. *International Journal of Geo-Engineering*, *10*(1), 8. <https://doi.org/10.1186/s40703-019-0104-8>
- Raymond, C., Horton, R. M., Zscheischler, J., Martius, O., AghaKouchak, A., Balch, J., ... White, K. (2020). Understanding and managing connected extreme events. *Nature Climate Change* *2020* *10*:7, *10*(7), 611–621. <https://doi.org/10.1038/s41558-020-0790-4>
- Reading, A. J. (1991). Stability of tropical residual soils from Dominica, West Indies. *Engineering Geology*, *31*(1), 27–44. [https://doi.org/10.1016/0013-7952\(91\)90055-P](https://doi.org/10.1016/0013-7952(91)90055-P)
- Reed, K. A., Wehner, M. F., & Zarzycki, C. M. (2022). Attribution of 2020 hurricane season extreme rainfall to human-induced climate change. *Nature Communications*, *13*(1), 1905. <https://doi.org/10.1038/s41467-022-29379-1>
- Refsgaard, J. C., (1997). Parameterisation, calibration and validation of distributed hydrological models. *Journal of Hydrology*, *198*(1–4), 69–97. [https://doi.org/10.1016/S0022-1694\(96\)03329-X](https://doi.org/10.1016/S0022-1694(96)03329-X)
- Refsgaard, J. C., & Storm, B. (1996). Construction, Calibration And Validation of Hydrological Models. In *Distributed Hydrologic Modeling*, (pp. 41–54). [https://doi.org/10.1007/978-94-009-0257-2\\_3](https://doi.org/10.1007/978-94-009-0257-2_3)
- Refsgaard, J. C., van der Sluijs, J., Højberg, A., & Vanrolleghem, P. (2007). Uncertainty in the environmental modelling process - A framework and guidance. *Environmental Modelling and Software*, *22*(11), 1543–1556. <https://doi.org/10.1016/J.ENVSOFT.2007.02.004>
- Reichenbach, P., Busca, C., Mondini, A. C., & Rossi, M. (2014). The Influence of Land Use Change on Landslide Susceptibility Zonation: The Briga Catchment Test Site (Messina, Italy). *Environmental Management*, *54*(6), 1372–1384. <https://doi.org/10.1007/s00267-014-0357-0>
- Reichenbach, P., Rossi, M., Malamud, B. D., Mihir, M., & Guzzetti, F. (2018). A review of statistically-based landslide susceptibility models. *Earth-Science Reviews*, *180*(November 2017), 60–91. <https://doi.org/10.1016/j.earscirev.2018.03.001>
- Reid, M. E., Christian, S. B., Brien, D. L., & Henderson, S. T. (2015). *Scoops3D-Software to Analyze Three-Dimensional Slope Stability Throughout a Digital Landscape Chapter 1 of Section A, Modeling Methods Book 14, Landslide and Debris-Flow Assessment*. <https://doi.org/https://doi.org/10.3133/tm14A1>
- Ruiz Sinoga, J. D., Romero Diaz, A., Ferre Bueno, E., & Martínez Murillo, J. F. (2010). The role of soil surface conditions in regulating runoff and erosion processes on a metamorphic hillslope (Southern Spain): Soil surface conditions, runoff and erosion in Southern Spain. *CATENA*, *80*(2), 131–139. <https://doi.org/10.1016/J.CATENA.2009.09.007>
- Rus, K., Kilar, V., & Koren, D. (2018). Resilience assessment of complex urban systems to natural disasters: A new literature review. *International Journal of Disaster Risk Reduction*, *31*, 311–330. <https://doi.org/10.1016/J.IJDRR.2018.05.015>
- Sadegh, M., Mofakhari, H., Gupta, H. V., Ragno, E., Mazdiyasi, O., Sanders, B., ... AghaKouchak, A. (2018). Multihazard Scenarios for Analysis of Compound Extreme Events. *Geophysical Research Letters*, *45*(11), 5470–5480. <https://doi.org/10.1029/2018GL077317>
- Saito, H., Nakayama, D., & Matsuyama, H. (2010). Relationship between the initiation of a shallow landslide and rainfall intensity-duration thresholds in Japan. *Geomorphology*, *118*(1–2), 167–175. <https://doi.org/10.1016/j.geomorph.2009.12.016>
- Salciarini, D., Godt, J. W., Savage, W. Z., Conversini, P., Baum, R. L., & Michael, J. A. (2006). Modeling regional initiation of rainfall-induced shallow landslides in the eastern Umbria Region of central Italy. *Landslides*, *3*(3), 181–194. <https://doi.org/10.1007/s10346-006-0037-0>
- Salvatici, T., Tofani, V., Rossi, G., D'Ambrosio, M., Tacconi Stefanelli, C., Benedetta Masi, E., ... Casagli, N. (2018). Application of a physically based model to forecast shallow landslides at a regional scale. *Natural Hazards and Earth System Sciences*, *18*(7), 1919–1935. <https://doi.org/10.5194/NHESS-18-1919-2018>
- Santangelo, M., Marchesini, I., Bucci, F., Cardinali, M., Fiorucci, F., & Guzzetti, F. (2015). An approach



- to reduce mapping errors in the production of landslide inventory maps. *Natural Hazards and Earth System Sciences*, 15(9), 2111–2126. <https://doi.org/10.5194/NHESS-15-2111-2015>
- Sarrazin, F., Pianosi, F., & Wagener, T. (2016). Global Sensitivity Analysis of environmental models: Convergence and validation. *Environmental Modelling & Software*, 79, 135–152. <https://doi.org/10.1016/J.ENVSOF.2016.02.005>
- Sassa, K., & Wang, G. hui. (2007). Mechanism of landslide-triggered debris flows: Liquefaction phenomena due to the undrained loading of torrent deposits. In *Debris-flow Hazards and Related Phenomena* (pp. 81–104). [https://doi.org/10.1007/3-540-27129-5\\_5](https://doi.org/10.1007/3-540-27129-5_5)
- Schmaltz, E. M., Steger, S., & Glade, T. (2017). The influence of forest cover on landslide occurrence explored with spatio-temporal information. *Geomorphology*, 290(December 2016), 250–264. <https://doi.org/10.1016/j.geomorph.2017.04.024>
- Schmidt, J., Matcham, I., Reese, S., King, A., Bell, R., Henderson, R., ... Bell, R. (2011). *Quantitative multi-risk analysis for natural hazards: a framework for multi-risk modelling*. 58, 1169–1192. <https://doi.org/10.1007/s11069-011-9721-z>
- Schulz, J. J., Cayuela, L., Echeverria, C., Salas, J., & Rey Benayas, J. M. (2010). Monitoring land cover change of the dryland forest landscape of Central Chile (1975–2008). *Applied Geography*, 30(3), 436–447. <https://doi.org/10.1016/j.apgeog.2009.12.003>
- Selby, M. J. (1993). *Hillslope Materials and Processes* (2nd Edn.; O. U. Press, Ed.). Oxford.
- Sepúlveda, S. A., & Petley, D. N. (2015). Regional trends and controlling factors of fatal landslides in Latin America and the Caribbean. *Natural Hazards and Earth System Sciences*, 15(8), 1821–1833. <https://doi.org/10.5194/nhe-15-1821-2015>
- Sepúlveda, S. A., Petley, D., Brain, M., & Tunstall, N. (2016). The effect of dynamic loading on the shear strength of pyroclastic Ash Deposits and implications for landslide hazard: The case of Pudahuel Ignimbrite, Chile. *Engineering Geology*, 205, 54–61. <https://doi.org/10.1016/J.ENGEO.2016.02.005>
- Sepúlveda, S. A., Rebolledo, S., & Vargas, G. (2006). Recent catastrophic debris flows in Chile: Geological hazard, climatic relationships and human response. *Quaternary International*, 158(1), 83–95. <https://doi.org/10.1016/j.quaint.2006.05.031>
- SERNAGEOMIN. (2017). *Servicio Nacional de Geología y Minería*. Santiago, Chile.
- Shano, L., Raghuvanshi, T. K., & Meten, M. (2020, December 1). Landslide susceptibility evaluation and hazard zonation techniques – a review. *Geoenvironmental Disasters*, Vol. 7, pp. 1–19. <https://doi.org/10.1186/s40677-020-00152-0>
- Sharma, S., Talchabhadel, R., Nepal, S., Ghimire, G. R., Rakhal, B., Panthi, J., ... Kumar, S. (2022). Increasing risk of cascading hazards in the central Himalayas. *Natural Hazards*. <https://doi.org/10.1007/s11069-022-05462-0>
- Sheikh, V., van Loon, E., Hessel, R., & Jetten, V. (2010). Sensitivity of LISEM predicted catchment discharge to initial soil moisture content of soil profile. *Journal of Hydrology*, 393(3–4), 174–185. <https://doi.org/10.1016/j.jhydrol.2010.08.016>
- Shen, P., Zhang, M. L., Chen, H., & Fan, R. (2018). EDDA 2.0: integrated simulation of debris flow initiation and dynamics considering two initiation mechanisms. *Geosci. Model Dev*, 11, 2841–2856. <https://doi.org/10.5194/gmd-11-2841-2018>
- Shen, Ping, Zhang, L., Wong, H. F., Peng, D., Zhou, S., Zhang, S., & Chen, C. (2020). Debris flow enlargement from entrainment: A case study for comparison of three entrainment models. *Engineering Geology*, 270, 105581. <https://doi.org/10.1016/j.enggeo.2020.105581>
- Shepherd, C. J., Vardanega, P. J., Holcombe, E. A., Hen-Jones, R., & De Luca, F. (2019). Minding the geotechnical data gap: appraisal of the variability of key soil parameters for slope stability modelling in Saint Lucia. *Bulletin of Engineering Geology and the Environment*, 78(7), 4851–4864. <https://doi.org/10.1007/s10064-018-01451-5>
- Shou, K. J., & Chen, J. (2021). On the rainfall induced deep-seated and shallow landslide hazard in

- Taiwan. *Engineering Geology*, 288(December 2020), 106156. <https://doi.org/10.1016/j.enggeo.2021.106156>
- Sidle, R. C., Greco, R., & Bogaard, T. (2019). Overview of Landslide Hydrology. *Water* 2019, Vol. 11, Page 148, 11(1), 148. <https://doi.org/10.3390/W11010148>
- Sidle, R. C., & Ochiai, H. (2006). *Landslides: Processes, Prediction, and Land Use*. <https://doi.org/10.1029/WM018>
- Sidle, R. C., Pearce, A. J., & O'Loughlin, C. L. (1985). *Hillslope Stability and Land Use*. <https://doi.org/10.1029/WM011>
- Sillero-Medina, J. A., Pérez-González, M. E., Martínez-Murillo, J. F., & Ruiz-Sinoga, J. D. (2020). Factors affecting eco-geomorphological dynamics in two contrasting Mediterranean environments. *Geomorphology*, 352, 106996. <https://doi.org/10.1016/J.GEOMORPH.2019.106996>
- Siriwardena, L., Finlayson, B. L., & McMahon, T. A. (2006). The impact of land use change on catchment hydrology in large catchments: The Comet River, Central Queensland, Australia. *Journal of Hydrology*, 326(1–4), 199–214. <https://doi.org/10.1016/J.JHYDROL.2005.10.030>
- Sivakumar, B., & Singh, V. P. (2012). Hydrologic system complexity and nonlinear dynamic concepts for a catchment classification framework. *Hydrology and Earth System Sciences*, 16(11), 4119–4131. <https://doi.org/10.5194/hess-16-4119-2012>
- Song, X., Zhang, J., Zhan, C., Xuan, Y., Ye, M., & Xu, C. (2015). Global sensitivity analysis in hydrological modeling: Review of concepts, methods, theoretical framework, and applications. *Journal of Hydrology*, 523, 739–757. <https://doi.org/10.1016/J.JHYDROL.2015.02.013>
- Soto, M., Sarricolea, P., Sepúlveda, S., Rodolfi, G., Cabello, M., & Maerker, M. (2017). Assessment of hydro-geomorphological hazard potentials in the Chilean semiarid coastal range and its impacts on La Serena city, Coquimbo Region. *Natural Hazards*, 88(1), 431–452. <https://doi.org/10.1007/s11069-017-2873-8>
- Spear, R. C., & Hornberger, G. M. (1980). Eutrophication in peel inlet-II. Identification of critical uncertainties via generalized sensitivity analysis. *Water Research*, 14(1), 43–49. [https://doi.org/10.1016/0043-1354\(80\)90040-8](https://doi.org/10.1016/0043-1354(80)90040-8)
- Stancanelli, L. M., Peres, D. J., Cancelliere, A., & Foti, E. (2017). A combined triggering-propagation modeling approach for the assessment of rainfall induced debris flow susceptibility. *Journal of Hydrology*, 550, 130–143. <https://doi.org/10.1016/J.JHYDROL.2017.04.038>
- Starkloff, T., Stolte, J., Hessel, R., Ritsema, C., & Jetten, V. (2018). Integrated, spatial distributed modelling of surface runoff and soil erosion during winter and spring. *Catena*. <https://doi.org/10.1016/j.catena.2018.04.001>
- Sterlacchini, S., Ballabio, C., Blahut, J., Masetti, M., & Sorichetta, A. (2011). Spatial agreement of predicted patterns in landslide susceptibility maps. *Geomorphology*, 125(1), 51–61. <https://doi.org/10.1016/J.GEOMORPH.2010.09.004>
- Stoffel, M., Mendlik, T., Schneuwly-Bollschweiler, M., & Gobiet, A. (2014). Possible impacts of climate change on debris-flow activity in the Swiss Alps. *Climatic Change*, 122(1–2), 141–155. <https://doi.org/10.1007/s10584-013-0993-z>
- Summerell, G. K., Vaze, J., Tuteja, N. K., Grayson, R. B., Beale, G., & Dowling, T. I. (2005). Delineating the major landforms of catchments using an objective hydrological terrain analysis method. *Water Resources Research*, 41(12), 1–12. <https://doi.org/10.1029/2005WR004013>
- Takahashi, T. (1978). Mechanical Characteristics of Debris Flow. *Journal of the Hydraulics Division*, 104(8), 1153–1169. <https://doi.org/10.1061/JYCEAJ.0005046>
- Takken, I., Beuselinck, L., Nachtergaele, J., Govers, G., Poesen, J., & Degraer, G. (1999). Spatial evaluation of a physically-based distributed erosion model (LISEM). *Catena*, 37(3–4), 431–447. [https://doi.org/10.1016/S0341-8162\(99\)00031-4](https://doi.org/10.1016/S0341-8162(99)00031-4)
- Tang, H., McGuire, L. A., Rengers, F. K., Kean, J. W., Staley, D. M., & Smith, J. B. (2019). Evolution of Debris-Flow Initiation Mechanisms and Sediment Sources During a Sequence of Postwildfire

- Rainstorms. *Journal of Geophysical Research: Earth Surface*, 124(6), 1572–1595. <https://doi.org/10.1029/2018JF004837>
- Tanyaş, H., van Westen, C. J., Allstadt, K. E., & Jibson, R. . (2019). Factors controlling landslide frequency–area distributions. *Earth Surface Processes and Landforms*, 44(4), 900–917. <https://doi.org/10.1002/esp.4543>
- Taylor, F. E., Malamud, B. D., Witt, A., & Guzzetti, F. (2018). Landslide shape, ellipticity and length-to-width ratios. *Earth Surface Processes and Landforms*, 43(15), 3164–3189. <https://doi.org/10.1002/ESP.4479>
- Terlien, M. T. J., Van Westen, C. J., & van Asch, T. W. J. (1995). *Deterministic Modelling in Gis-Based Landslide Hazard Assessment*. [https://doi.org/10.1007/978-94-015-8404-3\\_4](https://doi.org/10.1007/978-94-015-8404-3_4)
- Terzi, S., Torresan, S., Schneiderbauer, S., Critto, A., Zebisch, M., & Marcomini, A. (2019, February 15). Multi-risk assessment in mountain regions: A review of modelling approaches for climate change adaptation. *Journal of Environmental Management*, Vol. 232, pp. 759–771. <https://doi.org/10.1016/j.jenvman.2018.11.100>
- Tilloy, A., Malamud, B. D., Winter, H., & Joly-Laugel, A. (2019, September 1). A review of quantification methodologies for multi-hazard interrelationships. *Earth-Science Reviews*, Vol. 196, p. 102881. <https://doi.org/10.1016/j.earscirev.2019.102881>
- Tofani, V., Bicocchi, G., Rossi, G., Segoni, S., D'Ambrosio, M., Casagli, N., & Catani, F. (2017). *Soil characterization for shallow landslides modeling: a case study in the Northern Apennines (Central Italy)*. <https://doi.org/10.1007/s10346-017-0809-8>
- Tolson, B. A., & Shoemaker, C. A. (2008). Efficient prediction uncertainty approximation in the calibration of environmental simulation models. *Water Resources Research*, 44(4). <https://doi.org/10.1029/2007WR005869>
- Townsend, F. C. (1985). Geotechnical characteristics of residual soils. *Journal of Geotechnical Engineering*, 111(1), 77–94. [https://doi.org/10.1061/\(ASCE\)0733-9410\(1985\)111:1\(77\)](https://doi.org/10.1061/(ASCE)0733-9410(1985)111:1(77))
- Turkington, T., Remaître, A., Ettema, J., Hussin, H., & van Westen, C. (2016). Assessing debris flow activity in a changing climate. *Climatic Change*, 137(1–2), 293–305. <https://doi.org/10.1007/s10584-016-1657-6>
- UNDDR. (2020). *Hazard, Definition & Classification Review. Technical Report*. Geneva, Switzerland.
- Usovicz, B., & Lipiec, J. (2021). Spatial variability of saturated hydraulic conductivity and its links with other soil properties at the regional scale. *Scientific Reports 2021 11:1*, 11(1), 1–12. <https://doi.org/10.1038/s41598-021-86862-3>
- Uusitalo, L., Lehtikainen, A., Helle, I., & Myrberg, K. (2015). An overview of methods to evaluate uncertainty of deterministic models in decision support. *Environmental Modelling & Software*, 63, 24–31. <https://doi.org/10.1016/J.ENVSOF.2014.09.017>
- van Beek, L. P. H., & Van Asch, T. W. J. (2004). Regional assessment of the effects of land-use change on landslide hazard by means of physically based modelling. *Natural Hazards*, 31(1), 289–304. <https://doi.org/10.1023/B:NHAZ.0000020267.39691.39>
- van Beek, R., Cammeraat, E., Andreu, V., Mickovski, S. B., & Dorren, L. (2008). Hillslope Processes: Mass Wasting, Slope Stability and Erosion. In *Slope Stability and Erosion Control: Ecotechnological Solutions* (pp. 17–64). [https://doi.org/10.1007/978-1-4020-6676-4\\_3](https://doi.org/10.1007/978-1-4020-6676-4_3)
- van den Bout, B. (2020). *Integrated physically-based multi-hazard modelling* (University of Twente). <https://doi.org/10.3990/1.9789036550482>
- van den Bout, B., Jetten, V., De Roo, A., van Westen, C. J., & Ritsema, C. (2018). *OpenLISEM Multi-Hazard Land Surface Process Model*. Retrieved from <https://blog.utwente.nl/lisem/>
- van den Bout, B., & Jetten, V. G. (2018). The validity of flow approximations when simulating catchment-integrated flash floods. *Journal of Hydrology*, 556, 674–688. <https://doi.org/10.1016/j.jhydrol.2017.11.033>

- van den Bout, B., Lombardo, L., Chiyang, M., van Westen, C. J., & Jetten, V. (2021). Physically-based catchment-scale prediction of slope failure volume and geometry. *Engineering Geology*, *284*, 105942. <https://doi.org/10.1016/j.enggeo.2020.105942>
- van den Bout, B., Lombardo, L., van Westen, C. J., & Jetten, V. G. (2018). Integration of two-phase solid fluid equations in a catchment model for flashfloods, debris flows and shallow slope failures. *Environmental Modelling and Software*, *105*, 1–16. <https://doi.org/10.1016/j.envsoft.2018.03.017>
- van Den Bout, B., Van Asch, T., Hu, W., Tang, C. X., Mavrouli, O., Jetten, V. G., & van Westen, C. J. (2021). Towards a model for structured mass movements: the OpenLISEM hazard model 2.0a. *Geosci. Model Dev*, *14*, 1841–1864. <https://doi.org/10.5194/gmd-14-1841-2021>
- van Oost, K., Govers, G., Cerdan, O., Thauré, D., Van Rompaey, A., Steegen, A., ... Poesen, J. (2005). Spatially distributed data for erosion model calibration and validation: The Ganspoel and Kinderveld datasets. *Catena*, *61*(2-3 SPEC. ISS.), 105–121. <https://doi.org/10.1016/j.catena.2005.03.001>
- van Vliet, J., Bregt, A. K., Brown, D. G., van Delden, H., Heckbert, S., & Verburg, P. H. (2016). A review of current calibration and validation practices in land-change modeling. *Environmental Modelling & Software*, *82*, 174–182. <https://doi.org/10.1016/J.ENVSOFT.2016.04.017>
- van Westen, C. J., Castellanos, E., & Kuriakose, S. L. (2008). Spatial data for landslide susceptibility, hazard, and vulnerability assessment: An overview. *Engineering Geology*, *102*(3–4), 112–131. <https://doi.org/10.1016/j.enggeo.2008.03.010>
- van Westen, C. J., & Terlien, M. T. J. (1996). An approach towards deterministic landslide hazard analysis in GIS. A case study from Manizales (Colombia). *Earth Surface Processes and Landforms*, *21*(9), 853–868. [https://doi.org/10.1002/\(SICI\)1096-9837\(199609\)21:9<853::AID-ESP676>3.0.CO;2-C](https://doi.org/10.1002/(SICI)1096-9837(199609)21:9<853::AID-ESP676>3.0.CO;2-C)
- van Westen, C. J., van Asch, T. W. J., & Soeters, R. (2006). Landslide hazard and risk zonation - Why is it still so difficult? *Bulletin of Engineering Geology and the Environment*, *65*(2), 167–184. <https://doi.org/10.1007/s10064-005-0023-0>
- van Westen, C. J., Van den Bout, B., & Arevalo Fonseca, F. A. (2021). Challenges in analyzing landslide risk dynamics for risk reduction planning. *13th International Symposium on Landslides (ISL2020)*, 31. Retrieved from <https://www.issmge.org/publications/online-library>
- van Westen, C.J., Kappes, M. S., Luna, B. Q., Frigerio, S., Glade, T., & Malet, J. P. (2014). Medium-scale multi-hazard risk assessment of gravitational processes. In *Advances in Natural and Technological Hazards Research* (Vol. 34). [https://doi.org/10.1007/978-94-007-6769-0\\_7](https://doi.org/10.1007/978-94-007-6769-0_7)
- Vanacker, V., Vanderschaeghe, M., Govers, G., Willems, E., Poesen, J., Deckers, J., & De Bievre, B. (2003). Linking hydrological, infinite slope stability and land-use change models through GIS for assessing the impact of deforestation on slope stability in high Andean watersheds. *Geomorphology*, *52*(3–4), 299–315. [https://doi.org/10.1016/S0169-555X\(02\)00263-5](https://doi.org/10.1016/S0169-555X(02)00263-5)
- Varnes, D. (1978). Slope Movement Types and Processes. *Transportation Research Board Special Report*, (176), 11–33. [https://doi.org/10.1007/978-94-007-6769-0\\_7](https://doi.org/10.1007/978-94-007-6769-0_7) In Special report 176: Landslides: Analysis and Control, Transportation Research Board, Washington, D.C.
- Vázquez, F., Feyen, L., Feyen, J., & Refsgaard, J. (2002). Effect of grid size on effective parameters and model performance of the MIKE-SHE code. *Hydrological Processes*, *16*(2), 355–372. <https://doi.org/10.1002/HYP.334>
- Vereecken, H., Huisman, J. A., Hendricks Franssen, H. J., Brüggemann, N., Bogaen, H. R., Kollet, S., ... Vanderborght, J. (2015). Soil hydrology: Recent methodological advances, challenges, and perspectives. *Water Resources Research*, *51*(4), 2616–2633. <https://doi.org/10.1002/2014WR016852>
- Vergara, I., Garreaud, R., Moreiras, S., Araneo, D., & Beigt, D. (2022). Exploring the association between landslides and fluvial suspended sediment in a semi-arid basin in central Chile. *Geomorphology*, *402*, 108129. <https://doi.org/10.1016/J.GEOMORPH.2022.108129>
- Vergara, I., M. Moreiras, S., Araneo, D., & Garreaud, R. (2020). Geo-climatic hazards in the eastern

- subtropical Andes: Distribution, climate drivers and trends. *Natural Hazards and Earth System Sciences*, 20(5), 1353–1367. <https://doi.org/10.5194/nhess-20-1353-2020>
- Visser-Quinn, A., Beevers, L., Collet, L., Formetta, G., Smith, K., Wanders, N., ... Kumar, R. (2019). Spatio-temporal analysis of compound hydro-hazard extremes across the UK. *Advances in Water Resources*, 130, 77–90. <https://doi.org/10.1016/J.ADVWATRES.2019.05.019>
- von Ruetten, J., Lehmann, P., & Or, D. (2013). Rainfall-triggered shallow landslides at catchment scale: Threshold mechanics-based modeling for abruptness and localization. *Water Resources Research*, 49(10), 6266–6285. <https://doi.org/10.1002/WRCR.20418>
- von Ruetten, J., Lehmann, P., & Or, D. (2016). Linking rainfall-induced landslides with predictions of debris flow runout distances. *Landslides*, 13(5), 1097–1107. <https://doi.org/10.1007/s10346-015-0621-2>
- Wagener, T., Boyle, D. P., Lees, M. J., Wheeler, H. S., Gupta, H. V., & Sorooshian, S. (2001). A framework for development and application of hydrological models. *Hydrology and Earth System Sciences*, 5(1), 13–26. <https://doi.org/10.5194/HESS-5-13-2001>
- Wagener, T., & Pianosi, F. (2019). What has Global Sensitivity Analysis ever done for us? A systematic review to support scientific advancement and to inform policy-making in earth system modelling. *Earth-Science Reviews*, 194, 1–18. <https://doi.org/10.1016/J.EARSCIREV.2019.04.006>
- Wagener, T., & Wheeler, H. S. (2006). Parameter estimation and regionalization for continuous rainfall-runoff models including uncertainty. *Journal of Hydrology*, 320(1–2), 132–154. <https://doi.org/10.1016/j.jhydrol.2005.07.015>
- Walker, W. E., Harremoës, P., Rotmans, J., van der Sluijs, J. P., van Asselt, M. B. A., Janssen, P., & Kraayer von Krauss, M. P. (2003). Defining Uncertainty: A Conceptual Basis for Uncertainty Management in Model-Based Decision Support. *Integrated Assessment*, 4(1), 5–17. <https://doi.org/10.1076/iaij.4.1.5.16466>
- Walters, B. B. (2016). Migration, land use and forest change in St. Lucia, West Indies. *Land Use Policy*, 51, 290–300. <https://doi.org/10.1016/j.landusepol.2015.11.025>
- Wang, J., He, Z., & Weng, W. (2020). A review of the research into the relations between hazards in multi-hazard risk analysis. *Natural Hazards*, 104(3), 2003–2026. <https://doi.org/10.1007/s11069-020-04259-3>
- Wang, S., Flanagan, D. C., & Engel, B. A. (2019). Estimating sediment transport capacity for overland flow. *Journal of Hydrology*, 578, 123985. <https://doi.org/10.1016/j.jhydrol.2019.123985>
- Wang, S., Kang, S., Zhang, L., & Li, F. (2008). Modelling hydrological response to different land-use and climate change scenarios in the Zamu River basin of northwest China. *Hydrological Processes*, 22(14), 2502–2510. <https://doi.org/10.1002/HYP.6846>
- Ward, P. J., Daniell, J., Duncan, M., Dunne, A., Hananel, C., Hochrainer-Stigler, S., ... De Ruiter, M. C. (2022). Invited perspectives: A research agenda towards disaster risk management pathways in multi-(hazard-)risk assessment. *Natural Hazards and Earth System Sciences*, 22(4), 1487–1497. <https://doi.org/10.5194/nhess-22-1487-2022>
- Wei, L., Yang, M., Li, Z., Shao, J., Li, L., Chen, P., ... Zhao, R. (2022). Experimental Investigation of Relationship between Infiltration Rate and Soil Moisture under Rainfall Conditions. *Water*, 14(9). <https://doi.org/10.3390/w14091347>
- Wheatcroft, E. (2019). Interpreting the skill score form of forecast performance metrics. *International Journal of Forecasting*, 35(2), 573–579. <https://doi.org/10.1016/J.IJFORECAST.2018.11.010>
- White, L. W., Vieux, B., Armand, D., & LeDimet, F. X. (2003). Estimation of optimal parameters for a surface hydrology model. *Advances in Water Resources*, 26(3), 337–348. [https://doi.org/10.1016/S0309-1708\(02\)00189-6](https://doi.org/10.1016/S0309-1708(02)00189-6)
- Wilkinson, P. L., Anderson, M. G., & Lloyd, D. M. (2002). An integrated hydrological model for rain-induced landslide prediction. *Earth Surface Processes and Landforms*, 27(12), 1285–1297. <https://doi.org/10.1002/esp.409>

- Williams, T. G., Guikema, S. D., Brown, D. G., & Agrawal, A. (2020). Assessing model equifinality for robust policy analysis in complex socio-environmental systems. *Environmental Modelling and Software*, *134*. <https://doi.org/10.1016/J.ENVSOFT.2020.104831>
- Wohl, E., Barros, A., Brunzell, N., Chappell, N. A., Coe, M., Giambelluca, T., ... Ogden, F. (2012). The hydrology of the humid tropics. *Nature Climate Change*, *2*(9), 655–662. <https://doi.org/10.1038/nclimate1556>
- Wooldridge, S., Kalma, J., & Kuczera, G. (2001). Parameterisation of a simple semi-distributed model for assessing the impact of land-use on hydrologic response. *Journal of Hydrology*, *254*(1–4), 16–32. [https://doi.org/10.1016/S0022-1694\(01\)00489-9](https://doi.org/10.1016/S0022-1694(01)00489-9)
- Wu, Y. M., Lan, H. X., Gao, X., Li, L. P., & Yang, Z. H. (2015). A simplified physically based coupled rainfall threshold model for triggering landslides. *Engineering Geology*, *195*, 63–69. <https://doi.org/10.1016/j.enggeo.2015.05.022>
- Wu, Y., Zhang, X., & Shen, L. (2011). The impact of urbanization policy on land use change: A scenario analysis. *Cities*, *28*(2), 147–159. <https://doi.org/10.1016/j.cities.2010.11.002>
- Xiao, H., Liu, G., Liu, P., Zheng, F., Zhang, J., & Hu, F. (2017). Sediment transport capacity of concentrated flows on steep loessial slope with erodible beds. *Scientific Reports*, *7*(1), 2350. <https://doi.org/10.1038/s41598-017-02565-8>
- Xiaolong, D., Li, L., & Tan, Y. (2017). Validation of spatial prediction models for landslide susceptibility mapping by considering structural similarity. *ISPRS International Journal of Geo-Information*, *6*(4). <https://doi.org/10.3390/ijgi6040103>
- Yaalon, D. H. (1997). Soils in the Mediterranean region: what makes them different? *CATENA*, *28*(3–4), 157–169. [https://doi.org/10.1016/S0341-8162\(96\)00035-5](https://doi.org/10.1016/S0341-8162(96)00035-5)
- Yang, R., Xiao, P., & Qi, S. (2019). Analysis of Slope Stability in Unsaturated Expansive Soil: A Case Study. *Frontiers in Earth Science*, *7*(November), 1–11. <https://doi.org/10.3389/feart.2019.00292>
- Yeh, H.-F., & Tsai, Y.-J. (2018). Effect of Variations in Long-Duration Rainfall Intensity on Unsaturated Slope Stability. *Water*, *10*(4), 479. <https://doi.org/10.3390/w10040479>
- Yen, H., Wang, X., Fontane, D. G., Harmel, R. D., & Arabi, M. (2014). A framework for propagation of uncertainty contributed by parameterization, input data, model structure, and calibration/validation data in watershed modeling. *Environmental Modelling & Software*, *54*, 211–221. <https://doi.org/10.1016/J.ENVSOFT.2014.01.004>
- Yildiz, A., Zhao, H., & Kowalski, J. (2023). Computationally-feasible uncertainty quantification in model-based landslide risk assessment. *Frontiers in Earth Science*, *10*(February), 1–15. <https://doi.org/10.3389/feart.2022.1032438>
- Zhang, G.-H., Wang, L.-L., Tang, K.-M., Luo, R.-T., & Zhang, X. C. (2011). Effects of sediment size on transport capacity of overland flow on steep slopes. *Hydrological Sciences Journal*, *56*(7), 1289–1299. <https://doi.org/10.1080/02626667.2011.609172>
- Zhang, J., Qiu, H., Tang, B., Yang, D., Liu, Y., Liu, Z., ... Zhu, Y. (2022). Accelerating Effect of Vegetation on the Instability of Rainfall-Induced Shallow Landslides. *Remote Sensing 2022, Vol. 14, Page 5743*, *14*(22), 5743. <https://doi.org/10.3390/RS14225743>
- Zhang, K., Wang, S., Bao, H., & Zhao, X. (2019). Characteristics and influencing factors of rainfall-induced landslide and debris flow hazards in Shaanxi Province, China. *Hazards Earth Syst. Sci*, *19*, 93–105. <https://doi.org/10.5194/nhess-19-93-2019>
- Zhang, L. L., Zhang, J., Zhang, L. M., & Tang, W. H. (2011). Stability analysis of rainfall-induced slope failure: a review. *Proceedings of the Institution of Civil Engineers - Geotechnical Engineering*, *164*(5), 299–316. <https://doi.org/10.1680/geng.2011.164.5.299>
- Zhang, L. M., Zhang, S., & Huang, R. Q. (2014). Multi-hazard scenarios and consequences in Beichuan, China: The first five years after the 2008 Wenchuan earthquake. *Engineering Geology*, *180*, 4–20. <https://doi.org/10.1016/J.ENGGE.2014.03.020>
- Zhang, W., Ji, J., Gao, Y., Li, X., & Zhang, C. (2020). Spatial variability effect of internal friction angle

- on the post-failure behavior of landslides using a random and non-Newtonian fluid based SPH method. *Geoscience Frontiers*, 11(4), 1107–1121. <https://doi.org/10.1016/J.GSF.2020.02.003>
- Zhang, X., Drake, N. A., & Wainwright, J. (2013). Spatial Modelling and Scaling Issues. In *Environmental Modelling: Finding Simplicity in Complexity: Second Edition* (pp. 69–90). <https://doi.org/10.1002/9781118351475.ch5>
- Zieher, T., Rutzinger, M., Schneider-Muntau, B., Perzl, F., Leidinger, D., Formayer, H., & Geitner, C. (2017). Sensitivity analysis and calibration of a dynamic physically based slope stability model. *Hazards Earth Syst. Sci*, 17, 971–992. <https://doi.org/10.5194/nhess-17-971-2017>
- Zittis, G., Hadjinicolaou, P., Klangidou, M., Proestos, Y., & Lelieveld, J. (2019). A multi-model, multi-scenario, and multi-domain analysis of regional climate projections for the Mediterranean. *Regional Environmental Change*, 19(8), 2621–2635. <https://doi.org/10.1007/s10113-019-01565-w>
- Zscheischler, J., Westra, S., van den Hurk, B. J. J. M., Seneviratne, S. I., Ward, P. J., Pitman, A., ... Zhang, X. (2018). Future climate risk from compound events. *Nature Climate Change*, 8(6), 469–477. <https://doi.org/10.1038/s41558-018-0156-3>

## Appendix A- Supporting information for Chapter 2

### A.1 The OpenLISEM modelling approach

#### Slope stability and slope failure

The method for estimating slope stability is based on the infinite-slope approach. This method calculates both the local downslope and local resisting forces. The OpenLISEM hazard model assumes that the slope consists of two layers, a bedrock material with high cohesion that is considered as a boundary condition for calculations and a top layer of loose material (Van den Bout et al. 2021) (Figure A.1). On slopes, the soil above the potential shear plane is subject to a demanding force  $F_d$ , which includes the downslope component of the own weight of the soil ( $W$ ) and any additional loads acting on it (Figure A.1). Movement is resisted by a reaction force of the mobilised shear strength  $\sigma'_n$ . The mobilised shearing resistance is finite and can be considered as the force capacity  $F_c$  of the soil to resist failure. Failure occurs as soon as the demand  $F_d$  exceeds the capacity  $F_c$ . Within this approach, the slope stability can be expressed as the ratio between the capacity  $F_c$  and the demand  $F_d$ . This ratio is known as the factor of safety, FoS (Equation A.1).

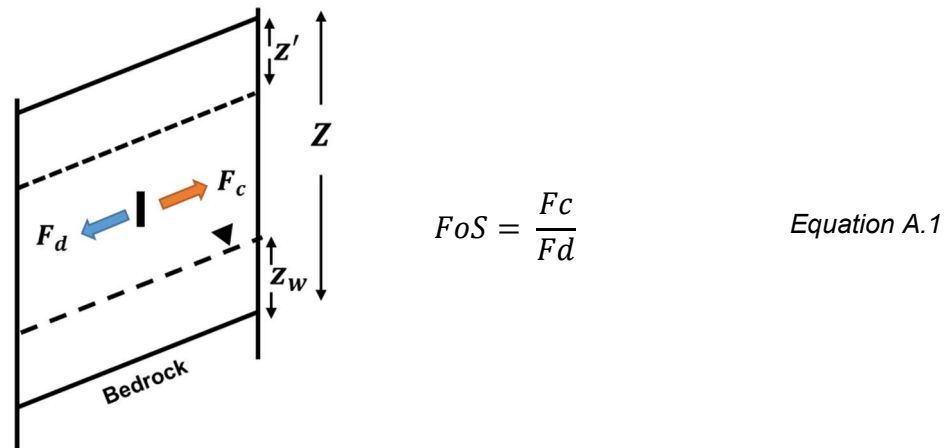


Figure A.1: Diagram of forces for infinite slope approach

Soil initial moisture content plays an essential role in hillslope hydrology as it regulates the partitioning of rainfall into infiltration and surface runoff in unsaturated soil, affecting slope stability (Sheikh et al. 2010). In the OpenLISEM hazard model, instead of considering the moisture content distribution within the soil pores, it is assumed that moisture is distributed at the bottom of the soil layer (Van den Bout et al. 2018). This water distribution is named “pseudo-groundwater,” which starts rising when the wetting front reaches the pseudo-groundwater level and stops when the soil pores are filled with water. When the pseudo-groundwater level start increasing the moisture varies linearly according to the equation proposed by (Van Beek, 2002).

$$Z_w = \frac{\theta_i - \theta_r}{\theta_s - \theta_r} * Z \quad \text{Equation A.2}$$



Where  $\theta_i$  ( $cm^3.cm^{-3}$ ) is the initial moisture content,  $\theta_r$  ( $cm^3.cm^{-3}$ ) the residual soil moisture,  $\theta_s$  ( $cm^3.cm^{-3}$ ) the porosity, and  $Z$  the soil depth (m). The mechanism in which the wetting front reaches the pseudo-groundwater level is given by the Green and Ampt (1911) infiltration model in Equation A.3.

$$z' = -k_s * \left( \psi * \frac{\theta_s - \theta_i}{F} + 1 \right) \quad \text{Equation A.3}$$

Where  $z'$  is wetting front depth (mm),  $-k_s$  is the saturated hydraulic conductivity ( $mm.h^{-1}$ ),  $\psi$  is the matric suction at the wetting front,  $\theta_s$  is the soil porosity ( $cm^3.cm^{-3}$ ),  $\theta_i$  is the initial moisture content ( $cm^3.cm^{-3}$ ) and  $F$  is the cumulative infiltrated water (m). The increase of the soil weight (force demand  $Fd$ ) is given by the shear stress  $\tau = W \sin\beta \cos\beta$ , where  $W$  is the sum of all weights acting on the slope.  $W$  is given by Equation A.4.

$$W = [(Z - Z_w) * \gamma + Z_w * \gamma_{sat}] \quad \text{Equation A.4}$$

However, the landslide triggering mechanism is the wetting front infiltration  $z'$ , then the wetting front depth is added to the sum of all weights, so  $W$  is now given by Equation A.5.

$$W = [(Z - z_w - z') * \gamma + z' * \gamma_{sat} + z_w * \gamma_{sat}] \quad \text{Equation A.5}$$

In this context, the force demand  $Fd$  is now given by Equation A.6.

$$\tau = [(Z - z_w - z') * \gamma + z' * \gamma_{sat} + z_w * \gamma_{sat}] \sin\beta \cos\beta \quad \text{Equation A.6}$$

The force capacity  $Fc$  can be described by the Mohr-Coulomb failure criterion:  $\tau_f = c' + \sigma' \tan\phi$ . If the weight of the soil ( $W$ ), is the only load acting at the potential shear plane, the total normal stress  $\sigma$  is given by:  $\sigma = W * \cos^2\beta$ . When part of the load is influenced by the water present in the soil pores, the frictional components of the shear resistance depend on the effective normal stress,  $\sigma' = \sigma - u$ , which is the total normal stress reduced with the pore pressure. Under the assumption that the groundwater levels are unconfined, the effective stress is affected by the buoyancy of the particles below the groundwater level, so the pore water pressure is expressed by the relation:  $u = z_w * \gamma'$ .

According to the above mentioned, the total normal stresses are given by:  $\sigma' = [(Z - z_w - z') * \gamma + z' * \gamma_{sat} + z_w * \gamma'] \cos^2\beta$ , where  $Z$  is the soil depth (m),  $z_w$  (m) represents the groundwater height above the shear surface,  $z'$  is the wetting front depth (m),  $\gamma$  is the unit weight of soil ( $kN.m^{-3}$ ),  $\gamma_{sat}$  is the saturated unit weight ( $kN.m^{-3}$ ), and  $\gamma'$  is the buoyant unit weight ( $kN.m^{-3}$ ). Once all weights on the slope are known, the relationship between the  $Fd$  and  $Fc$  is now given by the Factor of Safety, FoS, in Equation A.7.

$$FoS = \frac{Fc}{Fd} = \frac{c' + [(Z - z_w - z') * \gamma + z' * \gamma_{sat} + z_w * \gamma'] \cos^2\beta \tan\phi}{[(Z - z_w - z') * \gamma + z' * \gamma_{sat} + z_w * \gamma_{sat}] \sin\beta \cos\beta} \quad \text{Equation A.7}$$

Once the slope stability is estimated the slope failure is calculated according to the iterative slope failure method (Van den Bout et al. 2018). This method was developed to calculate the progressive slope

failure within a raster element determined to be unstable (Van den Bout et al. 2021). The raster element corresponds to the FoS derived from Equation A.7 estimated over a Digital Elevation Model (DEM). The iterative method assumes that slope stability could be achieved by decreasing the elevations of the DEM (removing failure depths) of the pixels estimated as unstable ( $FoS \leq 1$ ). From this assumption, all unstable pixels with  $FoS \leq 1$  will be removed by establishing an angle of the elevation differences between the stable and unstable raster cells. This angle is based on the height difference of the elevation model (DEM), which is given by Equation A.8.

$$\beta = \text{atan}\left(\frac{\max(h_{x-1} - h_x, h_x - h_{x+1})}{dx}\right) \quad \text{Equation A.8}$$

Where  $h_x$  is the elevation of the unstable cell (m),  $h_{x-1}$  is the elevation of the previous cell (m),  $h_{x+1}$  is the elevation of the next cell (m), and  $dx$  is the cell size (m). From this assumption, all unstable pixels with  $FoS \leq 1$  will be removed by using Equation A.9 until find the depth of the remaining soil required for stability.

$$FoS = \frac{F_c}{F_d} = \frac{c' + [(Z - z_w - z') * \gamma + (z' * \gamma_{sat}) + (z_w * \gamma')]}{[(Z - z_w - z') * \gamma + (z' * \gamma_{sat}) + (z_w * \gamma_{sat})]} \frac{\cos\left(\text{atan}\left(\frac{h - h_0}{dx}\right)\right)^2 \tan \phi'}{\sin\left(\text{atan}\left(\frac{h - h_0}{dx}\right)\right) \cos\left(\text{atan}\left(\frac{h - h_0}{dx}\right)\right)} \quad \text{Equation A.9}$$

### Debris flow modelling

In the OpenLISEM hazard model, the debris flow modelling approach consists of a set of two-phase equations derived from Pudasaini (2012), including mass, momentum and energy conservation. These equations are highly flexible in simulating the interaction of water and solids. The fluid phase ( $S_{x,f}$ ) (Equation A.13) and ( $S_{y,f}$ ) (Equation A.14) consists of a fluid volume fraction  $\alpha_f$  ( $m^3$ ) derived from the Saint-Venant equations for shallow water that include gravitational forces, pressure, Newtonian viscous effects, friction caused by the solid phase and drag forces. This equation includes the fluid density ( $\rho_f$ ) ( $kg.m^{-3}$ ), the fluid velocity ( $u_f$ ) ( $m.s^{-1}$ ), the fluid pressure at the basal surface ( $P_b$ ) ( $kg.m^{-1}.s^{-2}$ ) with  $b$  the basal surface (m), the density ration between fluid and solid phase ( $\gamma$ ) (-), and the vertical shearing of the fluid velocity ( $X$ ) ( $m.s^{-1}$ ) and drag coefficient  $C_{DG}$  (-). Within the OpenLISEM hazard model the frictional force for fluid phase was replaced with the Darcy-Weisbach equation for water flow friction (Van den Bout et al. 2018). Moreover, additional forces defined by Pudasaini (2012) are included within the momentum equations, these are the  $N_R$  which is the Reynolds number (-) and  $N_{RA}$  that corresponds to quasi-Reynolds number (-) these are used to scale turbulent and viscous forces. These are defined as follows:

$$N_R = \frac{\sqrt{gLH\rho_f}}{\alpha_f \eta} \quad \text{Equation A.10}$$

$$N_{RA} = \frac{\sqrt{gLH\rho_f}}{A\eta} \quad \text{Equation A.11}$$

Where  $L$  is the length scale of the flow (m),  $H$  is the height of the flow (m),  $A$  is the mobility of the interface (-) and  $\eta$  the viscosity ( $kg \cdot s^{-1}m^{-1}$ ) based on the empirical relation defined by O'Brien et al. (1993). The viscosity is described as follow:

$$\eta = \alpha e^{\beta \alpha_s} \quad \text{Equation A.12}$$

Where  $\alpha$  is the first viscosity parameter (-) and ( $\beta$ ) the second viscosity parameter (-).

The solid phase ( $S_{x,s}$ ) (Equation A.15) and ( $S_{y,s}$ ) (Equation A.16) consists of a solid volume fraction  $\alpha_s$  ( $m^3$ ), derived from the volume of soil resulting from the slope failure and entrained by the surface flow (Liu et al. 2020). However, the volume of sediment concentrated within the flow as a result of the sediment load by bed erosion is also included within the solid volume fraction (Pudasaini and Fischer 2020). Within the solid phase, are included gravitational forces, pressure and buoyancy, Mohr-Coulomb plasticity criteria that is based on the reaction of the surface to the weight of the flow material (Van Den Bout et al. 2021), and drag forces. These equations also include the solid density ( $\rho_s$ ) ( $kg \cdot m^{-3}$ ), the fluid velocity ( $u_s$ ) ( $m \cdot s^{-1}$ ), the pressure at the basal surface ( $P_b$ ) ( $kg \cdot m^{-1} \cdot s^{-2}$ ) with  $b$  the basal surface (m), the density ratio between fluid and solid phase ( $\gamma$ ) (-), and the vertical shearing of the fluid velocity ( $X$ ) ( $m \cdot s^{-1}$ ) and drag coefficient  $C_{DG}$  (-).

$$\begin{aligned} S_{x,f} = & \alpha_f \left\{ g \left( \frac{\partial b}{\partial x} \right) - \varepsilon \left[ \frac{1}{h} \frac{\partial}{\partial x} \left( \frac{h^2}{2} P_{bf} \right) + P_{bf} \frac{\partial b}{\partial x} - \frac{1}{\alpha_f N_R} \left( 2 \frac{\partial^2 u_f}{\partial x^2} + \frac{\partial^2 v_f}{\partial y \partial x} + \frac{\partial^2 u_f}{\partial y^2} - \frac{X u_f}{\varepsilon^2 h^2} \right) + \right. \right. \\ & \left. \left. \frac{1}{\alpha_f N_R} \left( 2 \frac{\partial}{\partial x} \left( \frac{\partial \alpha_s}{\partial x} (u_f - u_s) \right) + \frac{\partial}{\partial y} \left( \frac{\partial \alpha_s}{\partial x} (v_f - v_s) + \frac{\partial \alpha_s}{\partial y} (u_f - u_s) \right) \right) - \frac{\xi \alpha_s (v_f - v_s)}{\varepsilon^2 \alpha_f N_{RA} h^2} \right] \right\} - \\ & \frac{1}{\gamma} C_{DG} (u_f - u_s) |\vec{u}_f - \vec{u}_s|^{j-i} \end{aligned} \quad \text{Equation A.13}$$

$$\begin{aligned} S_{y,f} = & \alpha_f \left\{ g \left( \frac{\partial b}{\partial y} \right) - \varepsilon \left[ \frac{1}{h} \frac{\partial}{\partial y} \left( \frac{h^2}{2} P_{bf} \right) + P_{bf} \frac{\partial b}{\partial y} - \frac{1}{\alpha_f N_R} \left( 2 \frac{\partial^2 u_f}{\partial y^2} + \frac{\partial^2 v_f}{\partial y \partial x} + \frac{\partial^2 u_f}{\partial y^2} - \frac{X u_f}{\varepsilon^2 h^2} \right) + \right. \right. \\ & \left. \left. \frac{1}{\alpha_f N_R} \left( 2 \frac{\partial}{\partial x} \left( \frac{\partial \alpha_s}{\partial x} (u_f - u_s) \right) + \frac{\partial}{\partial y} \left( \frac{\partial \alpha_s}{\partial x} (v_f - v_s) + \frac{\partial \alpha_s}{\partial y} (u_f - u_s) \right) \right) - \frac{\xi \alpha_s (v_f - v_s)}{\varepsilon^2 \alpha_f N_{RA} h^2} \right] \right\} - \\ & \frac{1}{\gamma} C_{DG} (u_f - u_s) |\vec{u}_f - \vec{u}_s|^{j-i} \end{aligned} \quad \text{Equation A.14}$$

$$S_{x,s} = \alpha_s \left( g \left( \frac{\partial b}{\partial x} \right) - \frac{u_s}{|\vec{u}_s|} \tan(\partial P_{b_s}) - \varepsilon \alpha_s \gamma P_{bf} \left( \frac{\partial h}{\partial x} + \frac{\partial b}{\partial x} \right) + C_{DG} (u_f - u_s) |\vec{u}_f - \vec{u}_s|^{j-1} \right) \quad \text{Equation A.15}$$

$$S_{y,s} = \alpha_s \left( g \left( \frac{\partial b}{\partial y} \right) - \frac{u_s}{|\vec{u}_s|} \tan(\partial P_{b_s}) - \varepsilon \alpha_s \gamma P_{bf} \left( \frac{\partial h}{\partial y} + \frac{\partial b}{\partial y} \right) + C_{DG} (u_f - u_s) |\vec{u}_f - \vec{u}_s|^{j-1} \right) \quad \text{Equation A.16}$$

### Hillslope erosion modelling

In the OpenLISEM hazard model the erosion modelling is given under two approaches. The first one is according to sediment load in overland flow and channel flow using the transport capacity given by (Govers et al. 1990). The  $T_c$  is the maximum amount of sediment that the flow can transport ( $kg.m^{-3}$ ). From the transport capacity ( $T_c$ ) equation (Equation A.17), the sediment load in overland flow and channel flow will determine the detachment and deposition of the soil.

$$T_c = \rho_s c (\omega - \omega_{cr})^d \quad \text{Equation A.17}$$

Where  $\rho_s$  is the density of the sediment material ( $kg.m^{-3}$ ),  $\omega$  is the stream power ( $m.s^{-1}$ ) and  $\omega_{cr}$  the critical stream power ( $m.s^{-1}$ ),  $c$  and  $d$  are given by Equation A.18.

$$c = \frac{(D_{50} + 5)^{-0.6}}{0.32}, \quad d = \frac{(D_{50} + 5)^{0.25}}{300} \quad \text{Equation A.18}$$

With  $D_{50}$  the median grain diameter (m).

The sediment is loaded into the flow according to a set of sediment load equations for bed and suspended sediment load for overland and channel flow from Van Rijn (1984a) and Van Rijn (1984b). The user chooses the most suitable equation for sediment load. It was used Van Rijn (1984a and 1984b) bed and suspended load full equations. Once the sediment is loaded into the flow, the sediment concentration will determine the flow transport capacity ( $T_c$ ), in which for sediment concentrations  $C_v$  less than  $T_c$  ( $kg.m^{-3}$ ), flow detachment will take place (erosion), and for sediment concentrations,  $C_v$  larger than  $T_c$  ( $kg.m^{-3}$ ) deposition will take place. The sediment is transported and modelled in a 2-D kinematic wave and in a saint-venant equation for surface flow that was rewritten to 2-dimensions in Equation A.19

$$\frac{ds}{dt} + \frac{d(Q_x C)}{dx} + \frac{d(Q_y C)}{dy} = dep - det \quad \text{Equation A.19}$$

Where  $S$  is the sediment load ( $kg$ ),  $C$  is the sediment concentration ( $kg.m^{-3}$ ),  $Q$  is the discharge ( $m^3.s^{-1}$ ),  $dep$  is the deposition ( $kg.s^{-1}$ ) and  $det$  is the detachment ( $kg.s^{-1}$ ). The erosion within the OpenLISEM hazard model is given by the total amount of detached soil ( $kg.m^{-2}$ ) and the total amount of deposited soil ( $kg.m^{-2}$ ). These are the result of the transport capacity equation ( $T_c$ ). According to these results, the net erosion is computed by the total soil loss ( $kg.m^{-2}$ ), which is the total amount of detached soil minus the total amount of deposited soil. A positive result indicates erosion; this is more sediment that is leaving the surface than is deposited. A negative value indicates deposition, which is a more significant fraction of sediment that is deposited than is leaving the surface.

The second approach corresponds to the changes in the basal topography due to erosion and deposition ( $\partial b/\partial t$ ) based on the entrainment rates. These changes are included within the source terms of the fluid and solid phases of the two-phase debris flow equations. It was use the entrainment rate derived from Pudasaini and Fischer (2020), which is based on two competitive forces. The first corresponds to

the force exerted by the moving mixture on the erodible bed along the flow direction ( $\tau_{si}^m$ ), and the second corresponds to the resistance of the hillslope bed on the moving material opposite to the flow ( $-\tau_s^b$ ). The interface between these two opposite forces results in net shear stresses between the moving material and erodible basal layer resulting in a solid erosion rate ( $E_s$ ) (Equation A.20). The shear stress between the flow and the bed frictional resistance opposite to the flow direction is described by the Chezy-type friction coefficient  $C$ , resulting in a fluid erosion rate ( $E_f$ ) (Equation A.21) The sum of the solid ( $E_s$ ) and fluid ( $E_f$ ) erosion rates correspond to the entrainment rate (Equation A.22).

$$E_s + E_f \quad \text{Equation A.20}$$

$$E_s = \frac{\sqrt{(1 - \gamma^m)\rho_s^m \mu_s^m \alpha_s^m - (1 - y^b)\rho_s^b \mu_s^b \beta_s^b}}{\sqrt{v(\rho_s^m \lambda_{sl}^m \alpha_s^m - \rho_s^b \lambda_{sl}^b \alpha_s^b)}} \sqrt{g \cos \zeta h} \quad \text{Equation A.21}$$

$$E_s = \frac{[C_f^m \rho_f^m (\lambda_{fl}^m)^2 \alpha_f^m - C_f^b \rho_f^b (\lambda_f^b)^2 \alpha_f^b]}{H(C_f^m \rho_f^m \lambda_{fl}^m \alpha_f^m - C_f^b \lambda_f^b \alpha_f^b)} \quad \text{Equation A.22}$$

## Appendix B - Supporting information for Chapter 3

### B.1 Hurricane Tomas rainfall event intensity-duration estimation

The rainfall intensity-duration for the Hurricane Tomas rainfall event was estimated using a synthetic rainfall design from the total hurricane rainfall volume. The Hurricane Tomas rainfall event had approximately 27 hours in the Soufriere catchment. The total rainfall volume registered corresponded to 668 mm according to the station of Desraches located near the Soufriere catchment (ECLAC, 2011). From the total identified rainfall volume, the synthetic rainfall design was performed according to the maximum intensity peak registered during the Hurricane. The maximum peak was obtained from a cumulative rainfall curve corresponding to the station Anse-La Raye located north of the Soufriere catchment, which contains the cumulative percentage of the Hurricane rainfall for 27 hours (Figure B.1). The accumulated rainfall curve was identified from the volume of 668 mm for the rainfall duration for the Soufriere catchment.

The cumulative rainfall curve resulting from the Soufriere catchment was almost identical to the estimated for the Anse-La Raye station (Figure B.1). According to APSL Inc. (2011), the maximum intensity peak for Hurricane Tomas corresponded to 13% of the total rainfall. According to this, from the cumulative rainfall curve estimated for the Soufriere catchment, it was possible to identify that the maximum intensity peak corresponded to 86 ( $mm \cdot h^{-1}$ ). From the identified maximum intensity peak, the synthetic rainfall was designed to determine the rainfall intensity for the Hurricane Tomas rainfall duration.

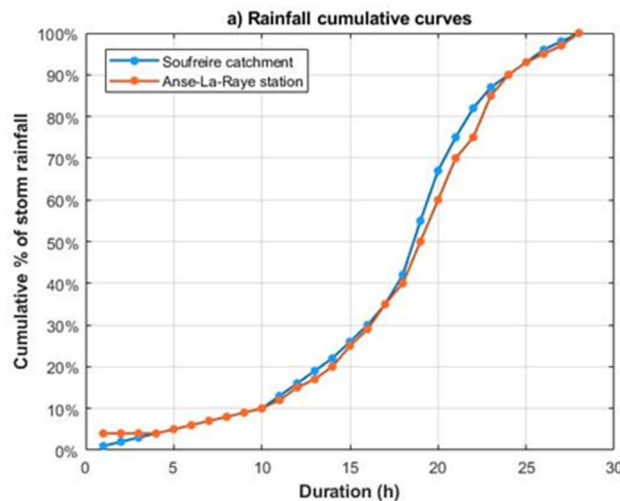


Figure B.1. Hurricane Tomas rainfall cumulative curves.

The designed rainfall intensity duration for the Hurricane Tomas rainfall event was discretized in time intervals of 10 minutes. The latter was performed because within the OpenLISEM model. The simulation time is the function of the rainfall duration in minutes. For this case, the total 27 hours duration of the Hurricane Tomas rainfall event was converted into 1620 minutes for the OpenLISEM hazard model.

## B.2 Landslide inventory rectification

The rectification of the landslide inventory from the British Geological Survey (2014) was performed by selecting spectral signature values from the RapidEye image corresponding to bare soil (Figure B.2a). According to Schmaltz et al. (2017), landslide activity can disturb vegetation cover, exposing soil at the surface. From the RapidEye image, spectral values  $\geq 130$  for no vegetated areas were selected to identify the areas with bare soil within the Soufriere catchment (Figure B.2b). However, the pixel selection included urban areas, exposed rocks and bare soil resulting from farming. In order to select the bare soil spectral values corresponding to the landslides and debris flows that occurred during Hurricane Tomas, the landslide inventory obtained from the British Geological Survey (2014) was used to identify the bare soil spectral values corresponding to the landslide inventory areas. Once the spectral values were identified, these were exported as a vector file to reshape the landslide and debris flow polygons contour according to the polygons estimated by the British Geological Survey (2014) (Figure B.2c). The result is a rectification of the contour corresponding to the polygons of landslides and debris flows. The update maintained the exact location and spatial distribution of the identified polygons from the British Geological Survey (2014) but gave the attributes of the recognised processes and reshaped the polygon contour to the RapidEye image pixel resolution (Figure B.2d).

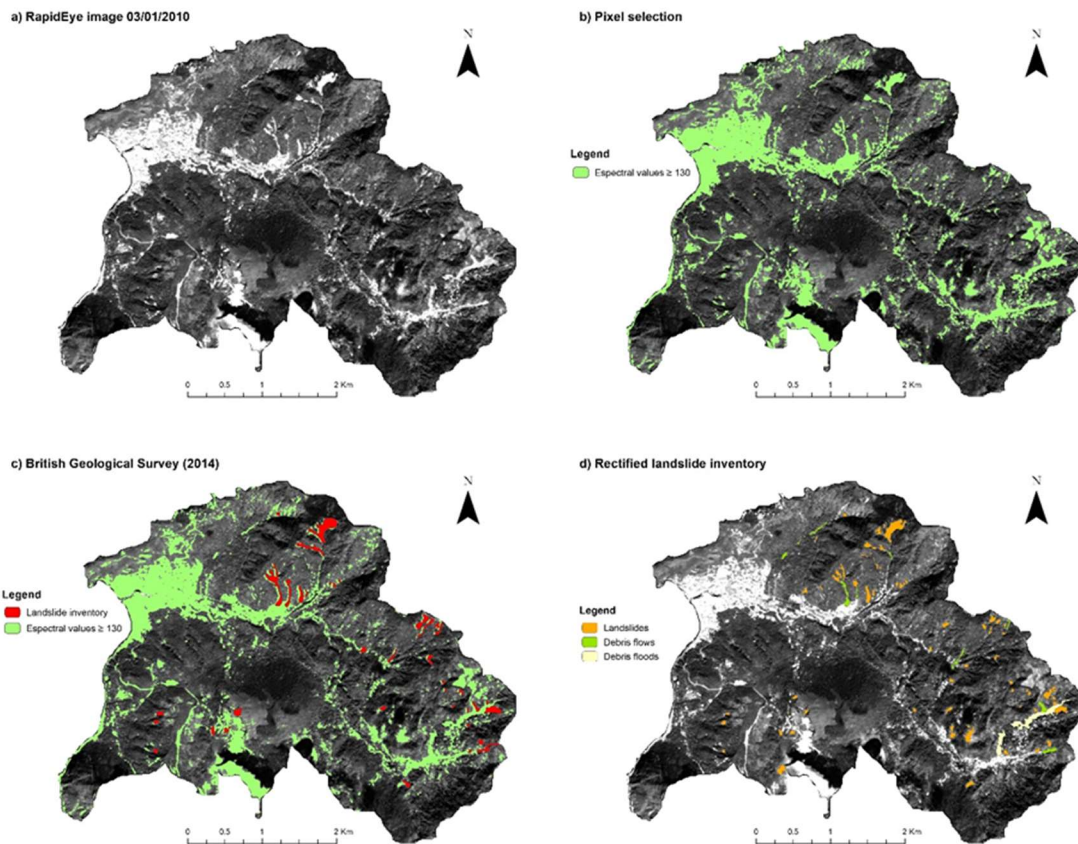


Figure B.2: Landslide inventory rectification process.

### B.3 Setting the OpenLISEM hazard model input parameters

Figure B.3 illustrates the spatial distribution of land use categories and soil types for the Soufriere catchment. The land use and soil types dataset are available in the CHARIM GeoNode platform: <http://charim-geonode.net/>.

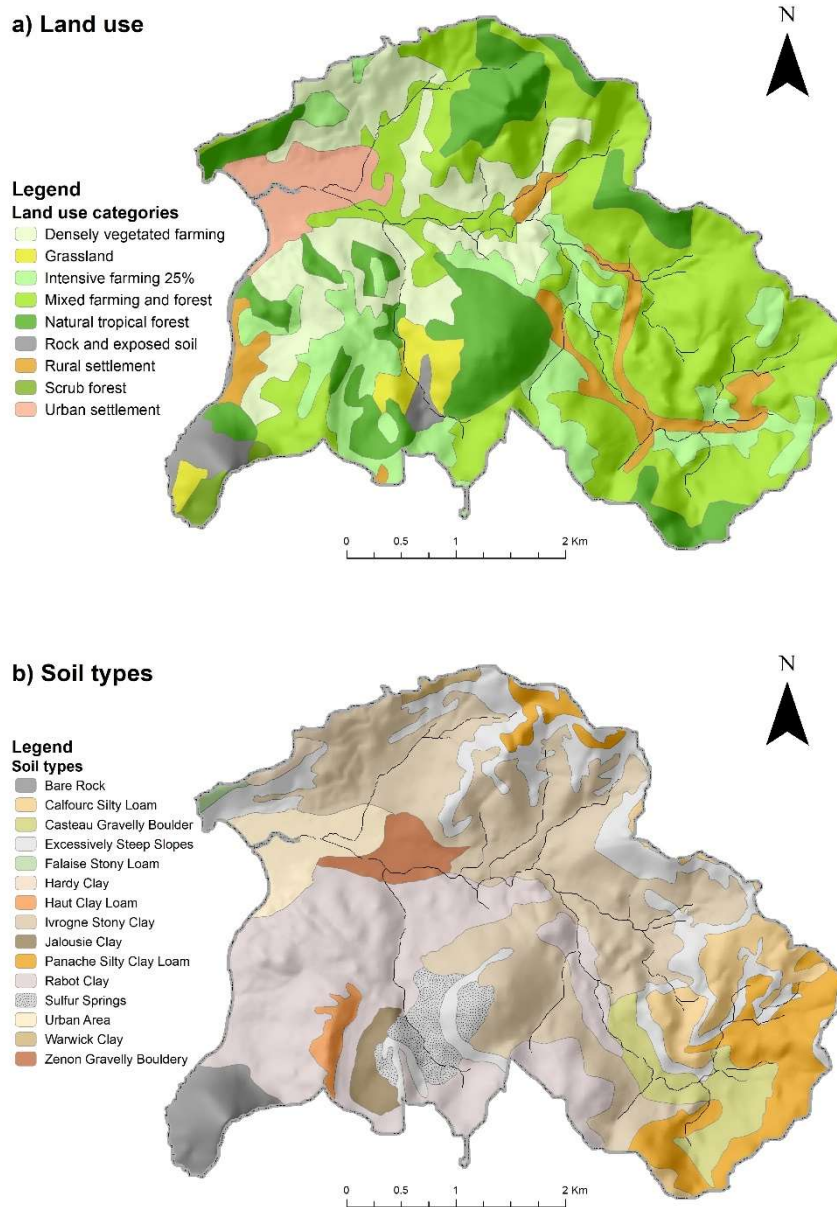


Figure B.3: (a) land use categories, (b) soil types units.

Figure B.4 shows the spatial distribution of soil depths for the Soufriere catchment. Figure B.4a shows soil depth 1 and Figure B.4b shows soil depth 2. These two layer are used as inputs for the OpenLISEM hazard model infiltration method based on the Green and Ampt (1911). These datasets are available at: <https://sourceforge.net/projects/lisem/files/Example%20Datasets/>.



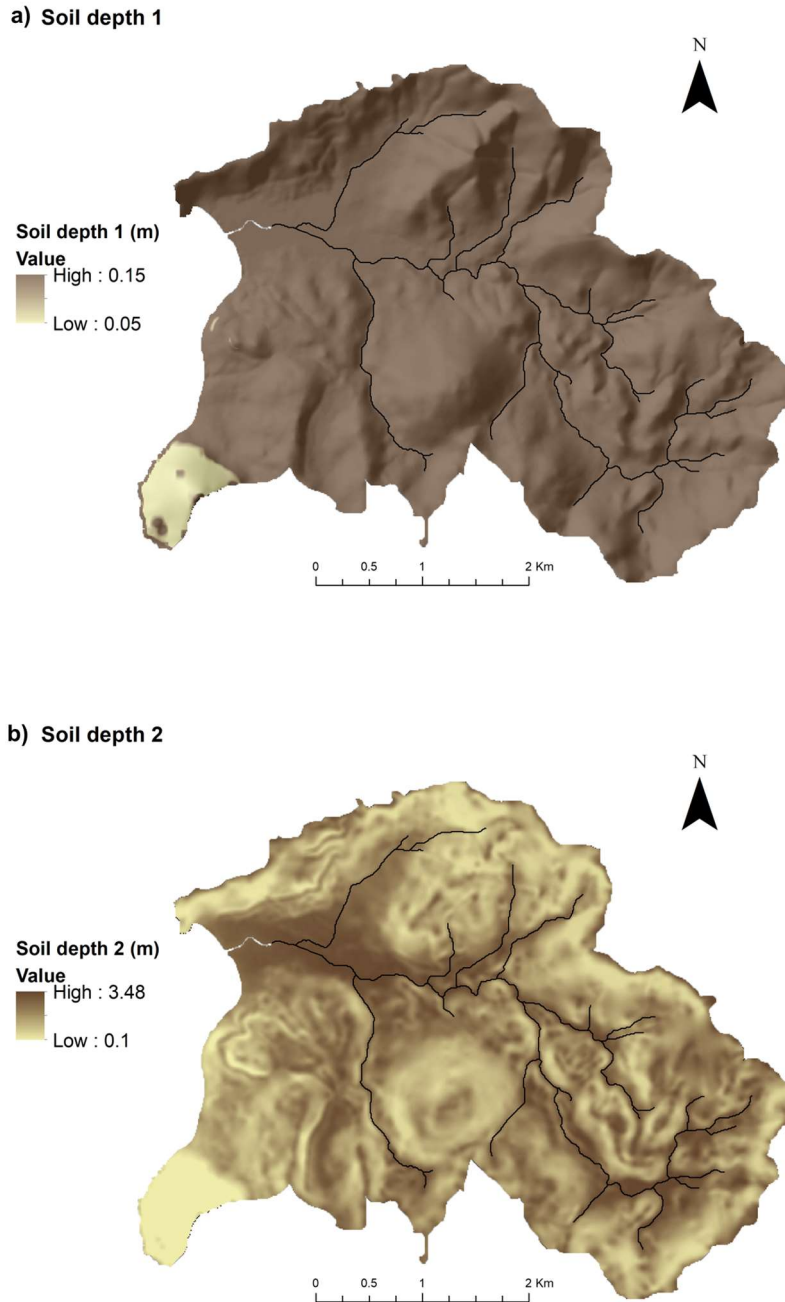


Figure B.4: (a) soil depth for soil layer 1, (b) soil depth for soil layer 2.

The parameter value for soil cohesion and soil internal friction angle was estimated from a geotechnical classification performed on the main soil groups within the Soufriere catchment. The soil groups were obtained from a classification performed on the soil types according to the Regional Research Laboratory (RRL) (1966), which identifies and describes the main soil types for Saint Lucia Island. Each soil type was classified within the main soil groups corresponding to the Soufriere catchment describing their composition and characteristics. According to the soil group classification, it was possible to establish a geotechnical classification for each soil group (Table B.1). The geotechnical classification was performed from the classified soil groups based on formation and weathering made by Shephard

et al. (2019). From this classification, it was possible to group the Soufriere catchment soil groups into A (Tropical residual soils), B (Agglomerate soils), and U (Unclassified) (Table B.1). For each geotechnical classification, the parameter values for soil cohesion and soil internal friction angle were estimated from probability functions PDFs obtained from an unpublished report that describes the geotechnical parameters for these geotechnical classifications (St. Lucia parameters PRISM) (Table B.1). The most frequent value determined the estimation of soil cohesion and internal friction angle values.

Table B.1. Soil geotechnical parameters.

Soil classification	Soil groups	Geotechnical classification	PDF $c'$ (kPa)	PDF $\Phi'$ (°)	$c'$ (kPa)	$\Phi'$ (°)
Calfourc Silty Loam	Latosols	A (Tropical residual soils)	LN(2.3, 0.5)	LN(3.2, 0.2)	8	24
Panache Silty Clay Loam						
Rabot Clay						
Warwick Clay						
Haut Clay Loam						
Hardy Clay	Smectoid Clay soils					
Ivrogne Stony Clay	Colluvial soils					
Urban area	Unclassified					
Sulfur springs						
Steep slopes						
Falaise Stony Loam	Lithosols	B (Agglomerate soils)	WBL(24.9, 1.5)	N(22.9, 8.7)	5	25
Casteau Gravelly Bouldery Silt Loam	Colluvial soils					
Zenon Gravelly Bouldery Loamy Sand	Alluvial soils					
Jalousie Clay						
Bare rock	Unclassified	U (Unclassified)	(-)	(-)	80	60

LN= Lognormal distribution; WBL= Weibull distribution; N= Normal distribution.

#### B.4 Parametric simulations

The user-defined parameters to set the behavioural simulations are based on the values indicated in the OpenLISEM manual (Table B.2). The setting of these parameters is described as follow:

**Slope stability:** These numerical settings correspond to the maximum factor of safety  $F_i$ , which is the cut-off value for the slope failure initiation and the resulting factor of safety  $F_r$ , which is the cut-off value to calculate how much failure depths should be removed from the unstable pixels. The  $F_r$  value influences the landslide simulation influencing the landslide size and depth.

**Flow dynamics:** These numerical settings correspond to viscosity parameters, these are based on the empirical relationship by O'Brien et al. (1993), the solid-fluid drag coefficient, the drag force power law based on the relation provided by Pudasaini (2012) a value of 1 indicates a drag force equation for flows with high solid concentrations. The entrainment coefficient indicates the rate at which the loose sediment material and landslide failure volumes are incorporated into the flow. The entrainment rate will increase the sediment mixture within the flow according to the flow depth and velocity allowing the transition between landslides and debris flows and influencing erosion-deposition rates. The volumetric sediment fraction indicates the minimal volume of sediment displayed as debris flow.

Table B.2. Slope stability and flow dynamics numerical settings.

Slope stability				Flow dynamics			
$F_i$	$F_r$	Viscosity		Solid-fluid drag	Drag force power law	Entrainment coefficient	Volumetric sediment fraction
		$\alpha$	$\beta$				
1.0	1.1	1	20	50	1	0.5	0.45

The following figure (Figure B.5) describe the total number of behavioural simulations derived from the Global Sensitivity Analysis (GSA) All-[factors]-At-a-Time (ATT) method. The number of behavioural simulations were set according to the parameter combination from the decreased, initial, and increased parameter values subject to variation within the OpenLISEM hazard model.

Slope hydrology												
		$k_s (mm.h^{-1})$ (x0.4)			$k_s (mm.h^{-1})$ Initial value			$k_s (mm.h^{-1})$ (x1.2)				
		$\theta_s (cm^3.cm^{-3})$			$\theta_s (cm^3.cm^{-3})$			$\theta_s (cm^3.cm^{-3})$				
Slope stability	$c' (kPa)$	$\phi' (^{\circ})$	(x0.8)	Initial value	(x1.1)	(x0.8)	Initial value	(x1.1)	(x0.8)	Initial value	(x1.1)	
	(x0.3)	(x0.4)		SIM1	SIM2	SIM3	SIM4	SIM5	SIM6	SIM7	SIM8	SIM9
		(x0.6)		SIM10	SIM11	SIM12	SIM13	SIM14	SIM15	SIM16	SIM17	SIM18
		Initial value		SIM19	SIM20	SIM21	SIM22	SIM23	SIM24	SIM25	SIM26	SIM27
		(x1.2)		SIM28	SIM29	SIM30	SIM31	SIM32	SIM33	SIM34	SIM35	SIM36
	(x0.5)	(x0.4)		SIM37	SIM38	SIM39	SIM40	SIM41	SIM42	SIM43	SIM44	SIM45
		(x0.6)		SIM46	SIM47	SIM48	SIM49	SIM50	SIM51	SIM52	SIM53	SIM54
		Initial value		SIM55	SIM56	SIM57	SIM58	SIM59	SIM60	SIM61	SIM62	SIM63
		(x1.2)		SIM64	SIM65	SIM66	SIM67	SIM68	SIM69	SIM70	SIM71	SIM72
	Initial value	(x0.4)		SIM73	SIM74	SIM75	SIM76	SIM77	SIM78	SIM79	SIM80	SIM81
		(x0.6)		SIM82	SIM83	SIM84	SIM85	SIM86	SIM87	SIM88	SIM89	SIM90
		Initial value		SIM91	SIM92	SIM93	SIM94	SIM95	SIM96	SIM97	SIM98	SIM99
		(x1.2)		SIM100	SIM101	SIM102	SIM103	SIM104	SIM105	SIM106	SIM107	SIM108
(x1.2)	(x0.4)		SIM109	SIM110	SIM111	SIM112	SIM113	SIM114	SIM115	SIM116	SIM117	
	(x0.6)		SIM118	SIM119	SIM120	SIM121	SIM122	SIM123	SIM124	SIM125	SIM126	
	Initial value		SIM127	SIM128	SIM129	SIM130	SIM131	SIM132	SIM133	SIM134	SIM135	
	(x1.2)		SIM136	SIM137	SIM138	SIM139	SIM140	SIM141	SIM142	SIM143	SIM144	

Figure B.5. Total of parametric simulations for the OpenLISEM model.

The following tables show the initial and the scaled input parameter values for hydrological and geotechnical values for land use categories and soil type units for the Soufriere catchment.

Table B.3. Hydrological input parameter for land use categories.

Land use categories	Saturated hydraulic conductivity ( $k_s$ ) ( $mm \cdot s^{-1}$ )			Saturated moisture content ( $\theta_s$ ) ( $cm^3 \cdot cm^{-3}$ )		
	Scale factors			Scale factors		
	(x0.4)	Initial value	(x1.2)	(x0.8)	Initial value	(x1.1)
Natural tropical forest	0.01759	0.04397	0.05277	0.50	0.63	0.69
Scrub forest	0.00748	0.01869	0.02243	0.42	0.53	0.58
Grassland	0.00611	0.01528	0.01833	0.49	0.61	0.67
Mixed farming and forest	0.00310	0.00775	0.00930	0.42	0.53	0.58
	0.00100	0.00250	0.00300	0.44	0.55	0.61
Intensive farming 25%	0.00011	0.00028	0.00033	0.24	0.30	0.33
	0.00533	0.01333	0.01600	0.40	0.50	0.55
	0.00244	0.00611	0.00733	0.32	0.40	0.44
	0.00100	0.00250	0.00300	0.40	0.50	0.55
Densely vegetated farming	0.00011	0.00028	0.00033	0.24	0.30	0.33
	0.00167	0.00417	0.00500	0.16	0.20	0.22
	0.00100	0.00250	0.00300	0.24	0.30	0.33
Rural settlement	0.00011	0.00028	0.00033	0.40	0.50	0.55
	0.00244	0.00611	0.00733	0.44	0.55	0.61
	0.00100	0.00250	0.00300	0.16	0.20	0.22
Urban Settlement	0.00011	0.00028	0.00033	0.24	0.30	0.33
	0.00167	0.00417	0.00500	0.44	0.55	0.61
	0.00100	0.00250	0.00300	0.24	0.30	0.33
Rock and exposed soil	0.00011	0.00028	0.00033	0.40	0.50	0.55
	0.00244	0.00611	0.00733	0.44	0.55	0.61

Table B.4. Hydrological input parameter for soil type units.

Soil type units	Saturated hydraulic conductivity ( $k_s$ ) ( $mm \cdot s^{-1}$ )			Saturated moisture content ( $\theta_s$ ) ( $cm^3 \cdot cm^{-3}$ )		
	Scale factors			Scale factors		
	(x0.4)	Initial value	(x1.2)	(x0.8)	Initial value	(x1.1)
Bare rock	0.00010	0.00024	0.00029	0.21	0.26	0.29
	0.00480	0.01200	0.01440	0.34	0.43	0.47
Calfourc Silty Loam	0.00469	0.01172	0.01407	0.34	0.42	0.46
	0.00150	0.00375	0.00450	0.40	0.50	0.55
Casteau Gravelly Boulder	0.00011	0.00027	0.00032	0.22	0.28	0.31
Excessively Steep Slopes	0.00010	0.00024	0.00029	0.21	0.26	0.29
Hardy Clay	0.00096	0.00240	0.00288	0.42	0.52	0.57
Haut Clay Loam	0.00157	0.00392	0.00470	0.38	0.48	0.53
	0.00096	0.00239	0.00287	0.42	0.52	0.57
Ivrogne Stony Clay	0.00100	0.00250	0.00300	0.44	0.55	0.61
	0.00098	0.00245	0.00294	0.42	0.53	0.58
	0.00090	0.00225	0.00270	0.39	0.49	0.54
Jalousie Clay	0.00088	0.00220	0.00264	0.38	0.48	0.53
				0.35	0.44	0.48
Panache Silty Clay Loam	0.00234	0.00586	0.00703	0.38	0.48	0.53
	0.00088	0.00220	0.00264	0.42	0.52	0.57
Rabot Clay	0.00096	0.00240	0.00288	0.38	0.48	0.53
	0.00090	0.00225	0.00270	0.44	0.55	0.61
	0.00100	0.00250	0.00300	0.39	0.49	0.54
Sulfur Springs	0.00214	0.00536	0.00643	0.35	0.44	0.48

Urban Area	0.00147	0.00367	0.00440	0.14	0.17	0.19
Warwick Clay	0.00088	0.00219	0.00263	0.38	0.48	0.53
	0.00090	0.00225	0.00270	0.39	0.49	0.54
Zenon Gravelly Bouldery	0.00010	0.00025	0.00030	0.22	0.27	0.30
Falaise Stony Loam	0.00806	0.02014	0.02417	0.35	0.44	0.48

Table B.5. Geotechnical input parameters for soil type units.

Soil type units	Soil cohesion ( $c'$ ) (kPa)				Internal friction angle ( $\phi'$ ) ( $^\circ$ )			
	Scale factors				Scale factors			
	(x0.3)	(x0.5)	Initial value	(x1.2)	(x0.4)	(x0.6)	Initial value	(x1.2)
Calfourc Silty Loam								
Panache Silty Clay Loam								
Rabot Clay								
Warwick Clay								
Haut Clay Loam								
Hardy Clay	2	4	8	10	10	14	24	29
Ivrogne Stony Clay								
Urban area								
Sulfur springs								
Steep slopes								
Falaise Stony Loam								
Casteau Gravelly Bouldery								
Silt Loam								
Zenon Gravelly Bouldery	2	3	5	6	10	15	25	30
Loamy Sand								
Jalousie Clay								
Bare rock	24	40	80	96	24	36	60	72

## Appendix C- Supporting information for Chapter 4

### C.1 Spatial similarity assessment

Figure C.1 illustrates the spatial similarity results performed to the total of parametric simulations. Red squares indicate the landslide magnitude ( $A_L$ ) and green squares indicates the area difference ( $\Delta A_L$ ).

Table C.1 illustrates the spatial similarity ranking performed to select the behavioural simulation with the best presentation of rainfall-triggered landslides, debris flows and hillslope erosion hazards.

		Slope hydrology																		
		$k_s (mm.h^{-1})$						$k_s (mm.h^{-1})$												
		$\theta_s (cm^3.cm^{-3})$						$\theta_s (cm^3.cm^{-3})$												
		$c' (kPa)$		$\phi' (^{\circ})$		$\theta_s (cm^3.cm^{-3})$		$\theta_s (cm^3.cm^{-3})$		$\theta_s (cm^3.cm^{-3})$		$\theta_s (cm^3.cm^{-3})$								
		(x0.8)	(x1.0)	(x1.1)	(x0.8)	(x1.0)	(x1.1)	(x0.8)	(x1.0)	(x1.1)	(x0.8)	(x1.0)	(x1.1)							
Slope stability	(x0.3)	(x0.4)	754.7	731.1	1139.3	1115.7	1275.3	1251.7	445.2	421.7	1039.3	1015.7	1259.4	1235.8	430.6	407.0	1044.7	1021.1	1273.6	1250.0
		(x0.6)	258.4	234.8	818.2	794.6	1055.7	1032.2	270.1	246.5	830.3	806.7	1053.8	1030.2	263.3	239.7	832.9	809.3	1054.4	1030.8
		(x1.0)	69.3	45.7	330.2	306.6	410.3	386.7	23.1	-0.5	287.6	264.0	410.0	386.4	23.2	-0.4	285.8	262.2	410.2	386.7
		(x1.2)	4.1	-19.5	74.0	50.4	115.0	91.5	1.7	-21.9	65.2	41.6	113.7	90.1	1.8	-21.8	66.6	43.0	112.8	89.2
	(x0.5)	(x0.4)	1.9	-21.7	7.3	-16.3	9.2	-14.4	1.4	-22.2	6.1	-17.5	9.6	-14.0	1.3	-22.3	6.3	-17.3	9.7	-13.9
		(x0.6)	0.0	-23.6	0.4	-23.2	1.1	-22.5	0.0	-23.6	0.1	-23.5	1.0	-22.6	0.0	-23.6	0.2	-23.4	1.1	-22.5
		(x1.0)	0.0	0.0	0.0	0.0	0.0	0.0	0.0	0.0	0.0	0.0	0.0	0.0	0.0	0.0	0.0	0.0	0.0	0.0
		(x1.2)	0.0	0.0	0.0	0.0	0.0	0.0	0.0	0.0	0.0	0.0	0.0	0.0	0.0	0.0	0.0	0.0	0.0	0.0
	(x1.0)	(x0.4)	0.0	0.0	0.0	0.0	0.0	0.0	0.0	0.0	0.0	0.0	0.0	0.0	0.0	0.0	0.0	0.0	0.0	0.0
		(x0.6)	0.0	0.0	0.0	0.0	0.0	0.0	0.0	0.0	0.0	0.0	0.0	0.0	0.0	0.0	0.0	0.0	0.0	0.0
		(x1.0)	0.0	0.0	0.0	0.0	0.0	0.0	0.0	0.0	0.0	0.0	0.0	0.0	0.0	0.0	0.0	0.0	0.0	0.0
		(x1.2)	0.0	0.0	0.0	0.0	0.0	0.0	0.0	0.0	0.0	0.0	0.0	0.0	0.0	0.0	0.0	0.0	0.0	0.0
(x1.2)	(x0.4)	0.0	0.0	0.0	0.0	0.0	0.0	0.0	0.0	0.0	0.0	0.0	0.0	0.0	0.0	0.0	0.0	0.0	0.0	
	(x0.6)	0.0	0.0	0.0	0.0	0.0	0.0	0.0	0.0	0.0	0.0	0.0	0.0	0.0	0.0	0.0	0.0	0.0	0.0	
	(x1.0)	0.0	0.0	0.0	0.0	0.0	0.0	0.0	0.0	0.0	0.0	0.0	0.0	0.0	0.0	0.0	0.0	0.0	0.0	
	(x1.2)	0.0	0.0	0.0	0.0	0.0	0.0	0.0	0.0	0.0	0.0	0.0	0.0	0.0	0.0	0.0	0.0	0.0	0.0	

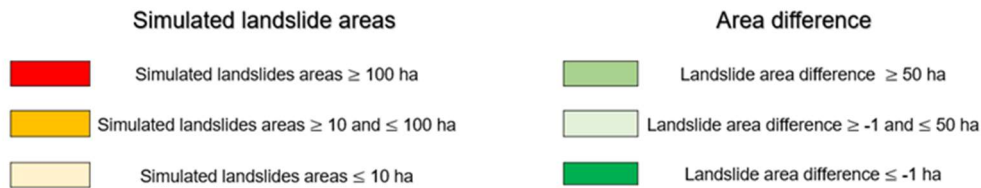


Figure C.1 Spatial similarity assessment parametric simulations.

Table C.1. Spatial similarity ranking.

Parametric simulations	Catchment discharge ( $m^3$ )	Landslide surface area $A_{SIM}$ (ha)	Landslide inventory area $A_{INV}$ (ha)	$\Delta A_L$	Debris flow runoff area (ha)	Debris flow inventory area (ha)	$\Delta A_D$	Net erosion ( $ton.m^{-2}$ )
<b>SIM22</b>	<b>76059.2</b>	<b>23.08</b>	<b>23.58</b>	<b>-0.5</b>	<b>3.77</b>	<b>6.02</b>	<b>-2.3</b>	<b>-240.35</b>
<b>SIM25</b>	<b>76059.2</b>	<b>23.22</b>	<b>23.58</b>	<b>-0.4</b>	<b>0.42</b>	<b>6.02</b>	<b>-5.6</b>	<b>-197.71</b>
<b>SIM32</b>	2678279.4	65.17	23.58	41.6	22.32	6.02	16.3	-1306.16
<b>SIM35</b>	2757857.9	66.59	23.58	43.0	24.19	6.02	17.2	-1193.95
<b>SIM19</b>	1646415.9	69.30	23.58	45.7	9.37	6.02	3.4	-792.06
<b>SIM29</b>	2950861.5	73.98	23.58	50.4	21.9	6.02	15.9	-1600.43

## C.2 Accuracy assessment

### Tolerance area

The Fuzzy membership function (Figure C.2) applies a linear transformation between a minimum and maximum threshold specified by the user. The values below the minimum threshold will be assigned as 0 with no membership and values above the maximum threshold will be assigned as 1 with membership (Mead et al. 2021)

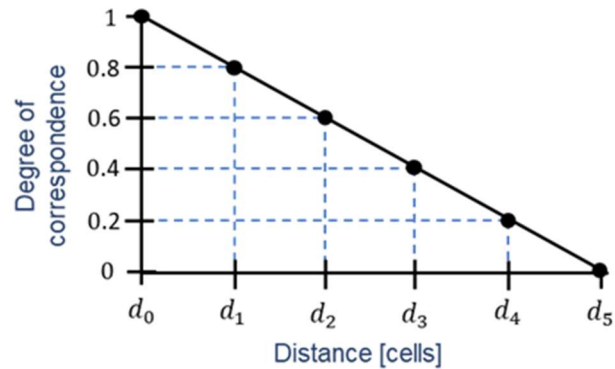


Figure C.2 Fuzzy membership function.

The fuzzy membership function was calculated according to two steps. The first step corresponded to the estimation of the Euclidean distance from the location of the landslide inventory polygons. The Euclidean distance was performed in ArcMap 10.6. where the maximum distance from the boundary of the landslide inventory polygons was obtained (Figure C.3a). After estimating the Euclidean distance, the Fuzzy membership was applied to the maximum distances where a raster with values from a scale from 0 to 1 was obtained (Figure C.3b). The Fuzzy membership function was applied in ArcMap 10.6. The values closer to 1 indicate a strong membership. To select the values with strong membership a threshold of 0.6 meters was applied to selecting the tolerance area for the landslide inventory polygons.

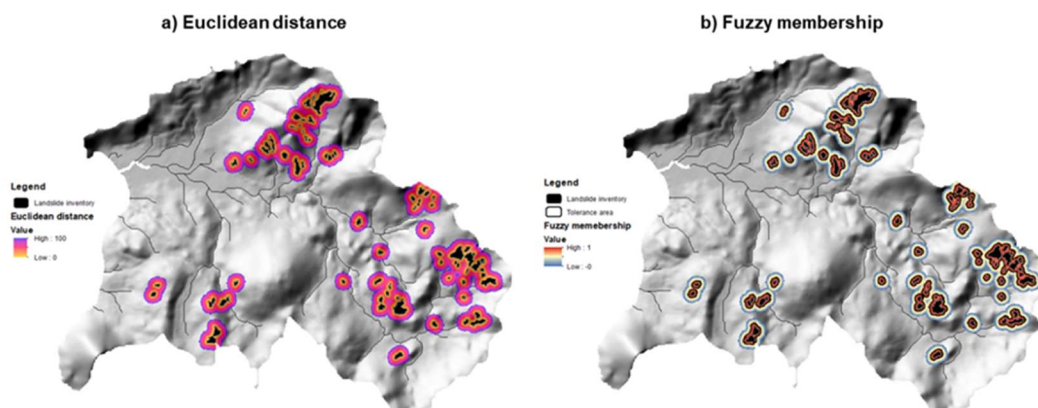


Figure C.3: (a) Euclidean distance for the landslide inventory polygons, (b) fuzzy membership distance.

After determining the tolerance area, the identification of the flat areas within the catchment was performed. The flat areas were estimated by selecting the slopes  $\geq 15^\circ$  within the catchment (Figure C.4). The aim is to remove from the catchment area the zones with no influence on landslide occurrence which can influence the estimation of the True Negative values (TN) and may impact the accuracy metrics estimation.

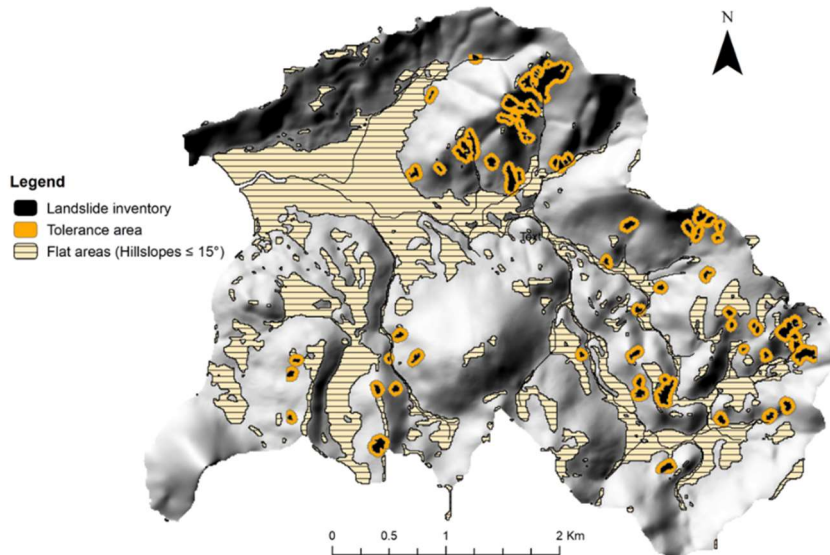


Figure C.4. Tolerance area and catchment flat areas identification.

### C.3 Response to land use and rainfall change scenarios

Table C.2 illustrates the land use change matrix elaborated to estimate the magnitude of landslides, debris flows and net erosion rates for the proposed land use and rainfall scenarios.

Table C.2. Template land use change matrix to explore the rate of change of hazard magnitudes for land use change scenarios.

Land use		Hurricane Tomas	Rainfall change [1:20]			
		27-hour = 662 mm	24-hour = 252 mm	10-hour = 200 mm	5-hour = 160 mm	
	<b>Hazard response (ha)</b>	<b>Baseline 1</b>	<b>Baseline 2</b>	<b>Baseline 3</b>	<b>Baseline 4</b>	
<b>Current Land use</b>	Landslides					
	Debris flows					
	Net erosion					
<b>Unit</b>	<b>Change</b>	<b>Hazard response (ha)</b>	<b>Scenario 1</b>	<b>Scenario 2</b>	<b>Scenario 3</b>	<b>Scenario 4</b>
		Landslides				



Natural tropical forest	Mixed farming and forest	Debris flows				
		Net erosion				
<b>Unit</b>	<b>Change</b>	<b>Hazard response (ha)</b>	<b>Scenario 5</b>	<b>Scenario 6</b>	<b>Scenario 7</b>	<b>Scenario 8</b>
Mixed farming and forest	Natural tropical forest	Landslides				
		Debris flows				
		Net erosion				

Figure C.5 shows the 24, 10 and 5-hour rainfall selected to assess hillslope hydrological hazard interactions according to the land use scenarios proposed. This rainfall was obtained from an intensity–duration–frequency relationship (IDFs) obtained from Klohn–Crippen (1995). Synthetic rainfall events were performed to recreate the selected events.

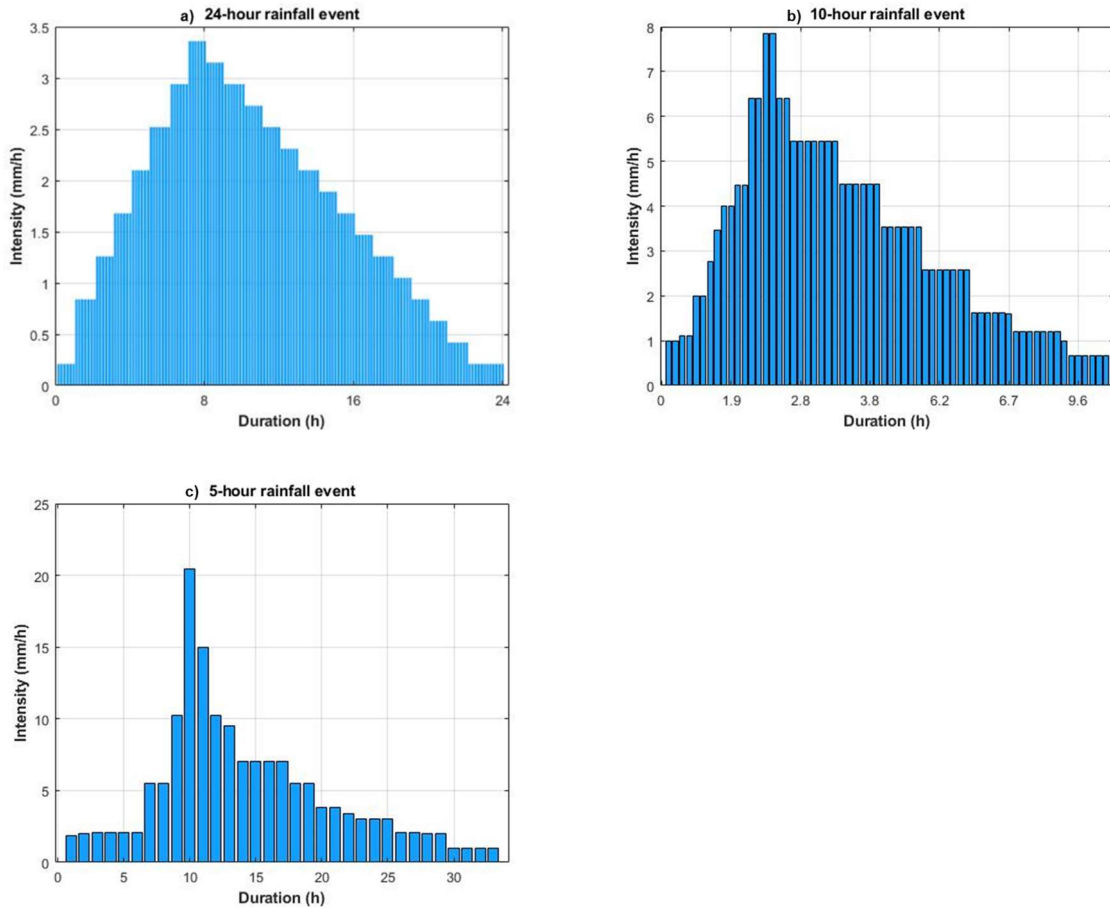


Figure C.5. 20-year return period synthetic rainfall intensity-duration: (a) 24-hour rainfall event, (b) 10-hour rainfall event and (c) 5-hour rainfall event.

## Appendix D- Supporting information for Chapter 5

### D.1 Setting the OpenLISEM hazard model input parameters

Figure D.1a shows the spatial distribution of the geological units obtained from CIGIDEN (2021) for the Maipo sub-catchment. Figure D.1b illustrates the soil types classified according to the geological units and identified according to literature review from Thiele and (González-Díez et al. 2013; González et al. 2020).

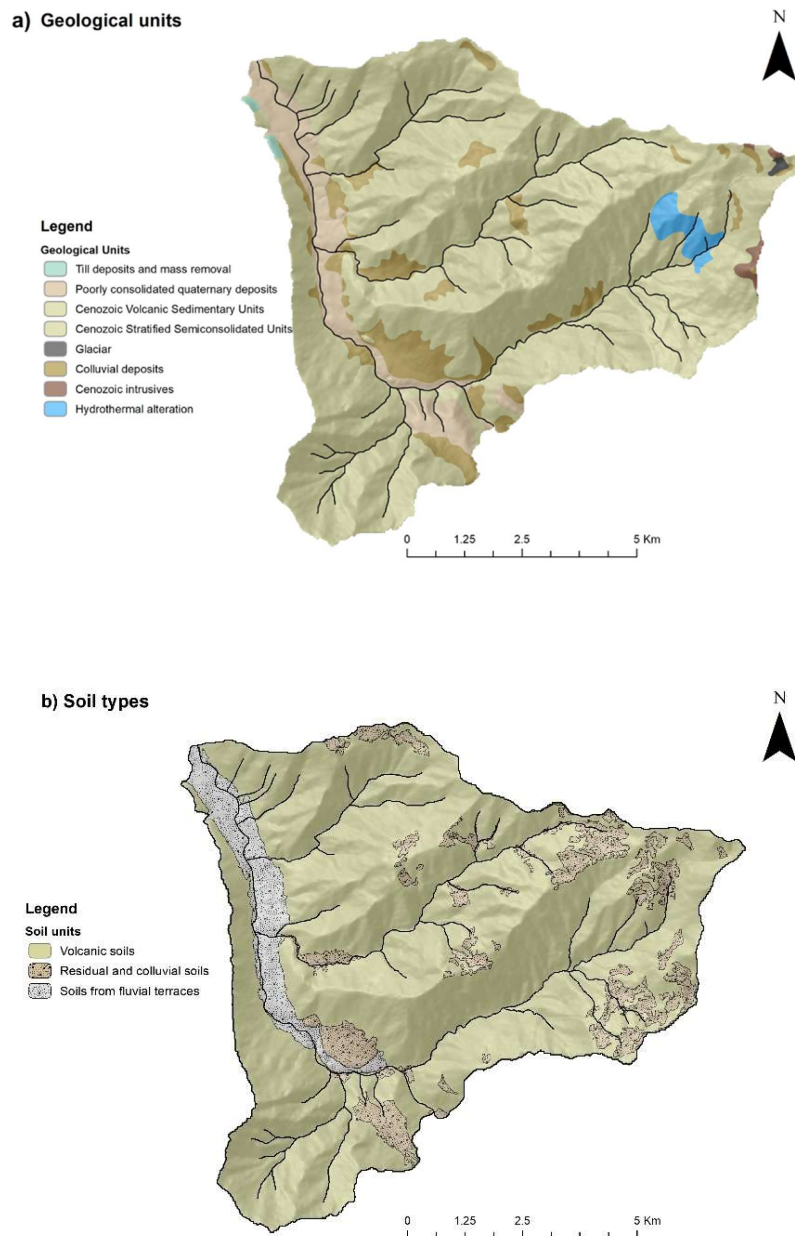


Figure D.1: (a) geological units, (b) soil types.

Figure D.2 illustrates the soil depth distribution for the Maipo sub-catchment. These datasets were obtained from <https://www.isric.org/explore/soilgrids>. Due to the chosen data resolution for the Maipo sub-catchment, the soil depth layers were also resampled to 20x20 metres resolution using bilinear interpolation with the *Resample* tool in ArcMap 10.6.

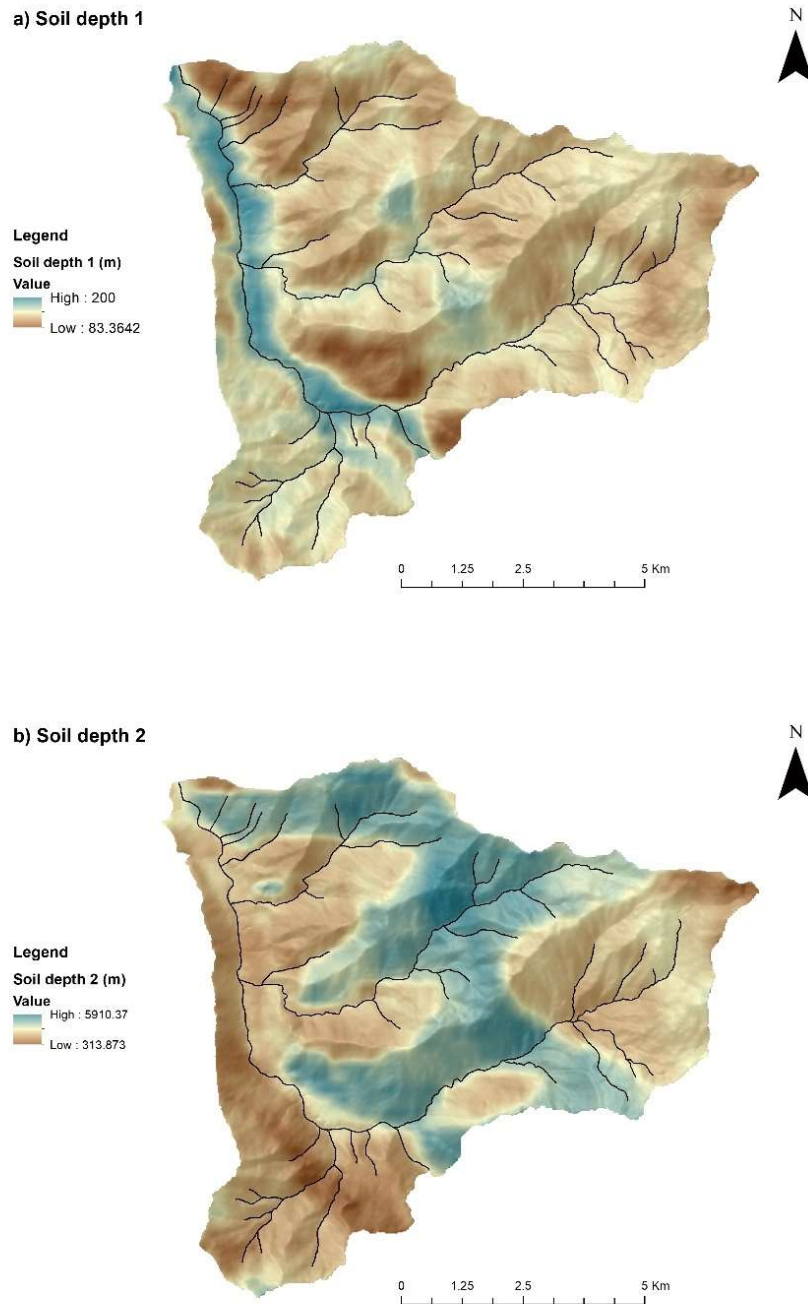


Figure D.2 Soil depth spatial distribution for the Maipo sub-catchment: (a) soil depth 1, (b) soil depth 2.

Figure D.3 illustrates the land use units for the Maipo sub-catchment obtained from CONAF (2013). The information is available at: <https://www.ide.cl/index.php/flora-y-fauna/item/1513-catastros-de-uso-de-suelo-y-vegetacion>

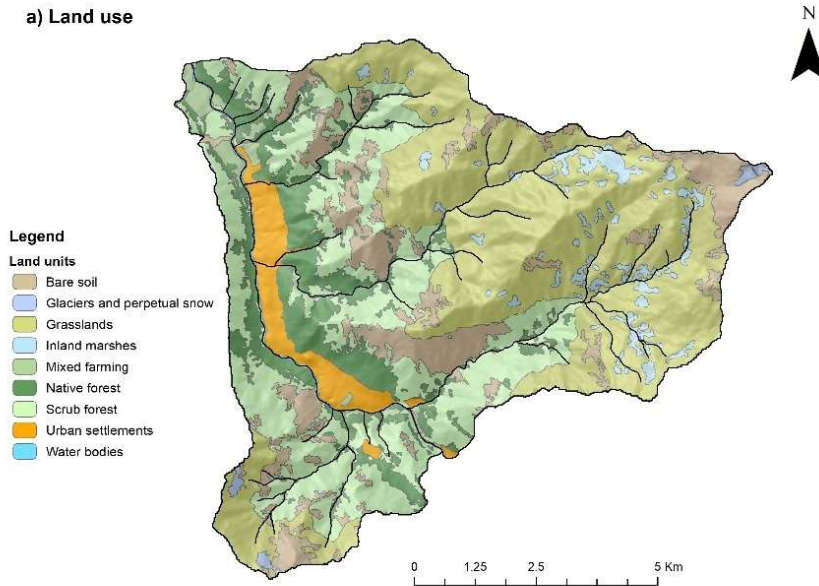


Figure D.3. Land use for the Maipo sub-catchment.

Table D.1 shows the hydrological input parameter values estimated for Maipo sub-catchment land use categories and soil type units.

Table D.1. Hydrological input parameter for land use categories and soil type units.

Land use categories	Saturated hydraulic conductivity ( $k_s$ ) ( $mm \cdot s^{-1}$ )			Saturated moisture content ( $\theta_s$ ) ( $cm^3 \cdot cm^{-3}$ )		
	Scale factors			Scale factors		
	(x0.4)	Initial value	(x1.2)	(x0.8)	Initial value	(x1.1)
Native forest	0.00100	0.00251	0.00301	0.328	0.41	0.451
Scrub forest	0.00117	0.00292	0.00350	0.32	0.4	0.44
Grasslands	0.00064	0.00161	0.00193	0.336	0.42	0.462
Bare soil	0.00090	0.00225	0.00270	0.312	0.39	0.429
Mixed farming/Urban settlements	0.00092	0.00229	0.00275	0.24	0.3	0.33
Glaciers and perpetual snows	0	0	0	0.08	0.1	0.11
Soil types	(x0.4)	(x1.0)	(x1.2)	(x0.8)	(x1.0)	(x1.1)
Volcanic residual soils/Volcanic soils	0.00136	0.00341	0.00409	0.32	0.4	0.44
Soils from fluvial terraces	0.00166	0.00416	0.00499	0.216	0.27	0.297
Soils from colluvial deposits	0.00080	0.00201	0.00241	0.336	0.42	0.462

Table D.2 shows the geotechnical input parameter values estimated for Maipo sub-catchment soil type units.

Table D.2. Geotechnical input parameters for soil type units.

Soil types	Soil cohesion ( $c'$ ) (kPa)				Internal friction angle ( $\phi'$ ) ( $^{\circ}$ )			
	Scale factors				Scale factors			
	(x0.3)	(x0.5)	Initial value	(x1.2)	(x0.4)	(x0.6)	Initial value	(x1.2)
Volcanic residual soils/Volcanic soils	2.4	4	8	9.6	18	27	45	54
Soils from fluvial terraces	3.63	6.05	12.1	14.52	9.6	14.4	24	28.8
Soils from colluvial deposits	3.63	6.05	12.1	14.52	9.6	14.4	24	28.8

## D.2 Response to land use and rainfall change scenarios

Table D.3 illustrates the land use change matrix elaborated to estimate the magnitude of rainfall-triggered landslides, debris flows and net erosion rates for the proposed land use and rainfall scenarios for the Maipo sub-catchment.

Table D.3. Template land use change matrix to explore the rate of change of hazard magnitudes for land use change scenarios.

Land use		Hurricane Tomas	Rainfall change [1:20]			
		12-hour = 34.2 mm	8-hour = 20.5 mm	6-hour = 16.2 mm	4-hour = 12.8 mm	
	<b>Hazard response (ha)</b>	<b>Baseline 1</b>	<b>Baseline 2</b>	<b>Baseline 3</b>	<b>Baseline 4</b>	
<b>Current Land use</b>		Landslides				
		Debris flows				
		Net erosion				
<b>Unit</b>	<b>Change</b>	<b>Hazard response (ha)</b>	<b>Scenario 1</b>	<b>Scenario 2</b>	<b>Scenario 3</b>	<b>Scenario 4</b>
Scrub forest	Native forest	Landslides				
		Debris flows				
		Net erosion				
<b>Unit</b>	<b>Change</b>	<b>Hazard response (ha)</b>	<b>Scenario 5</b>	<b>Scenario 6</b>	<b>Scenario 7</b>	<b>Scenario 8</b>
Native forest	Scrub forest	Landslides				
		Debris flows				
		Net erosion				

Figure D.4 shows the 12, 6 and 4-hour rainfall selected to assess hillslope hydrological hazard interactions according to the land use scenarios proposed for the Maipo sub-catchment. These correspond to a 10-year return period intensity–duration–frequency curves (IDFs) obtained from the technical report of UNESCO (2013) for the Metropolitan region of Santiago. The selected rainfall events correspond to a 12-hour rainfall with a total volume of 34.2 mm, a 6-hour rainfall with a total volume of 16.2 mm and a 4-hour rainfall with a total volume of 12.8 mm.

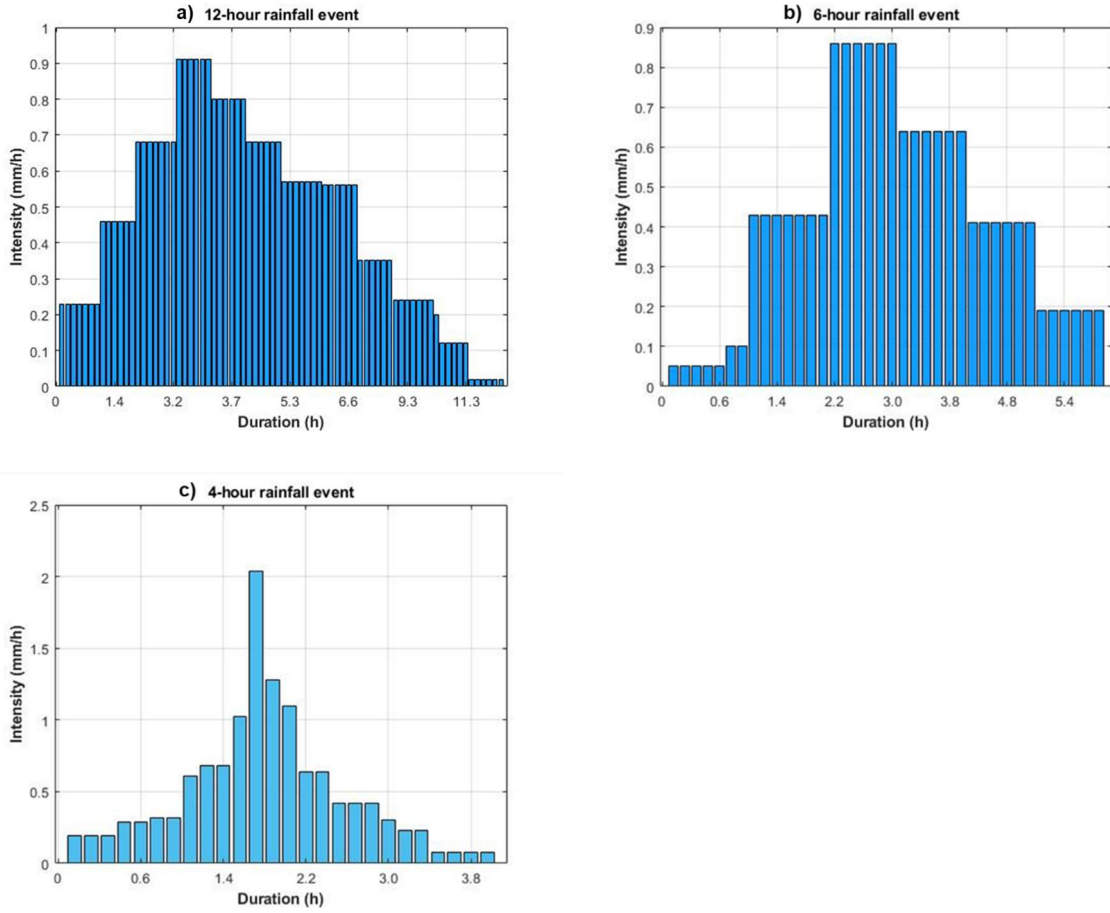


Figure D.4. 10-year return period synthetic rainfall intensity-duration: (a) 12-hour rainfall event, (b) 6-hour rainfall event and (c) 4-hour rainfall event.

### D.3 Parametric simulations

Figure D.5 illustrates the total landslide surface area ( $A_L$ ) resulted from 144 parametric simulations applied for the Maipo sub-catchment. Figure D.6 illustrates the total debris flow runout area ( $A_D$ ) and Figure D.7 illustrates the total net erosion ( $Net_E$ ). From these simulations, it was selected the behavioural simulation with the best representation of debris flows observed for the 25 February rainfall event.

**a) Total landslide surface area ( $A_L$ ) (ha)**

		Slope hydrology									
		$k_s$ (mm.h <sup>-1</sup> )			$k_s$ (mm.h <sup>-1</sup> )			$k_s$ (mm.h <sup>-1</sup> )			
		(x0.4)			(x1.0)			(x1.2)			
		$\theta_s$ (cm <sup>3</sup> .cm <sup>-3</sup> )			$\theta_s$ (cm <sup>3</sup> .cm <sup>-3</sup> )			$\theta_s$ (cm <sup>3</sup> .cm <sup>-3</sup> )			
Slope stability	$c'$ (kPa)	$\phi'$ (°)	(x0.8)	(x1.0)	(x1.1)	(x0.8)	(x1.0)	(x1.1)	(x0.8)	(x1.0)	(x1.1)
	(x0.3)	(x0.4)	113.04	998.64	1556.96	153.44	917.12	1552.72	94.40	953.04	1549.12
		(x0.6)	5.52	521.88	840.44	19.68	444.40	835.12	16.12	443.20	832.88
		(x1.0)	4.72	35.44	60.48	5.36	27.28	60.28	5.32	27.20	59.44
		(x1.2)	0.00	1.72	2.88	0.00	0.00	2.88	0.00	0.00	2.94
	(x0.5)	(x0.4)	0.00	0.00	0.00	0.00	0.00	0.00	0.00	0.00	0.00
		(x0.6)	0.00	0.00	0.00	0.00	0.00	0.00	0.00	0.00	0.00
		(x1.0)	0.00	0.00	0.00	0.00	0.00	0.00	0.00	0.00	0.00
		(x1.2)	0.00	0.00	0.00	0.00	0.00	0.00	0.00	0.00	0.00
	(x1.0)	(x0.4)	0.00	0.00	0.00	0.00	0.00	0.00	0.00	0.00	0.00
		(x0.6)	0.00	0.00	0.00	0.00	0.00	0.00	0.00	0.00	0.00
		(x1.0)	0.00	0.00	0.00	0.00	0.00	0.00	0.00	0.00	0.00
		(x1.2)	0.00	0.00	0.00	0.00	0.00	0.00	0.00	0.00	0.00
	(x1.2)	(x0.4)	0.00	0.00	0.00	0.00	0.00	0.00	0.00	0.00	0.00
(x0.6)		0.00	0.00	0.00	0.00	0.00	0.00	0.00	0.00	0.00	
(x1.0)		0.00	0.00	0.00	0.00	0.00	0.00	0.00	0.00	0.00	
(x1.2)		0.00	0.00	0.00	0.00	0.00	0.00	0.00	0.00	0.00	

**Simulations**

- N°4
- N°21
- N°25
- N°27
- N°30

Figure D.5. Hazard representation: (a) total landslide surface area.

**b) Total debris flow runout area ( $A_D$ ) (ha)**

		Slope hydrology									
		$k_s$ (mm.h <sup>-1</sup> )			$k_s$ (mm.h <sup>-1</sup> )			$k_s$ (mm.h <sup>-1</sup> )			
		(x0.4)			(x1.0)			(x1.2)			
		$\theta_s$ (cm <sup>3</sup> .cm <sup>-3</sup> )			$\theta_s$ (cm <sup>3</sup> .cm <sup>-3</sup> )			$\theta_s$ (cm <sup>3</sup> .cm <sup>-3</sup> )			
Slope stability	$c'$ (kPa)	$\phi'$ (°)	(x0.8)	(x1.0)	(x1.1)	(x0.8)	(x1.0)	(x1.1)	(x0.8)	(x1.0)	(x1.1)
	(x0.3)	(x0.4)	50.32	401.16	552.52	67.20	360.12	547.28	34.48	397.24	529.60
		(x0.6)	0.04	134.44	223.12	1.04	108.80	207.64	0.04	105.60	208.08
		(x1.0)	0.04	43.32	73.80	0.28	34.00	61.7	0.08	30.68	59.6
		(x1.2)	0.00	15.52	52.8	0.00	10.28	39.72	0.00	11.36	39.00
	(x0.5)	(x0.4)	0.00	14.84	32.52	0.00	9.60	26.12	0.00	9.92	28.00
		(x0.6)	0.00	14.84	32.52	0.00	9.60	26.12	0.00	9.92	28.00
		(x1.0)	0.00	14.84	32.52	0.00	9.60	26.12	0.00	9.92	28.00
		(x1.2)	0.00	14.84	32.52	0.00	9.60	26.12	0.00	9.92	28.00
	(x1.0)	(x0.4)	0.00	7.12	19.12	0.00	6.72	17.24	0.00	7.40	18.88
		(x0.6)	0.00	7.12	19.12	0.00	6.72	17.24	0.00	7.40	18.88
		(x1.0)	0.00	7.12	19.12	0.00	6.72	17.24	0.00	7.40	18.88
		(x1.2)	0.00	7.12	19.12	0.00	6.72	17.24	0.00	7.40	18.88
	(x1.2)	(x0.4)	0.00	6.64	14.52	0.00	6.32	11.88	0.00	6.00	11.80
(x0.6)		0.00	6.64	14.52	0.00	6.32	11.88	0.00	6.00	11.80	
(x1.0)		0.00	6.64	14.52	0.00	6.32	11.88	0.00	6.00	11.80	
(x1.2)		0.00	6.64	14.52	0.00	6.32	11.88	0.00	6.00	11.80	

**Simulations**

- N°4
- N°21
- N°25
- N°27
- N°30

Figure D.6. Hazard representation: (b) total debris flow runout area.

**c) Total net erosion ( $Net_E$ ) ( $ton.m^{-2}$ )**

		Slope hydrology								
		$k_s (mm.h^{-1})$			$k_s (mm.h^{-1})$			$k_s (mm.h^{-1})$		
		(x0.4)			(x1.0)			(x1.2)		
		$\theta_s (cm^3.cm^{-3})$			$\theta_s (cm^3.cm^{-3})$			$\theta_s (cm^3.cm^{-3})$		
$c' (kPa)$	$\phi' (^{\circ})$	(x0.8)	(x1.0)	(x1.1)	(x0.8)	(x1.0)	(x1.1)	(x0.8)	(x1.0)	(x1.1)
		(x0.3)	(x0.4)	-5697.80	-28964.42	-59867.37	-2180.39	-26835.14	-56071.34	-2700.03
(x0.6)	-11.84		-6339.78	-15518.07	-26.72	-7578.19	-14057.64	-10.87	-4184.47	-12236.65
(x1.0)	-20.50		-1942.24	-4991.15	-16.84	-945.43	-3487.67	-11.42	-2129.08	-5135.38
(x1.2)	-9.38		-1227.01	-3230.66	-9.72	-698.73	-2451.18	-11.61	-681.64	-2703.26
(x0.5)	(x0.4)	-10.29	-731.57	-2046.46	-10.47	-591.60	-1695.34	-13.40	-532.67	-1670.64
	(x0.6)	-10.29	-721.65	-1820.18	-10.47	-595.04	-1796.27	-13.40	-546.89	-1922.32
	(x1.0)	-10.29	-721.65	-1820.18	-10.47	-595.04	-1796.27	-13.40	-546.89	-1922.32
	(x1.2)	-10.29	-721.65	-1820.18	-10.47	-595.04	-1796.27	-13.40	-546.89	-1922.32
(x1.0)	(x0.4)	-12.43	-401.47	-1076.41	-11.76	-300.52	-1037.23	-13.17	-276.15	-1091.45
	(x0.6)	-12.43	-401.47	-1076.41	-11.76	-300.52	-1037.23	-13.17	-276.15	-1091.45
	(x1.0)	-12.43	-401.47	-1076.41	-11.76	-300.52	-1037.23	-13.17	-276.15	-1091.45
	(x1.2)	-12.43	-401.47	-1076.41	-11.76	-300.52	-1037.23	-13.17	-276.15	-1091.45
(x1.2)	(x0.4)	-14.78	-280.65	-847.32	-16.20	-248.87	-905.33	-15.97	-259.44	-952.46
	(x0.6)	-14.78	-280.65	-847.32	-16.20	-248.87	-905.33	-15.97	-259.44	-952.46
	(x1.0)	-14.78	-280.65	-847.32	-16.20	-248.87	-905.33	-15.97	-259.44	-952.46
	(x1.2)	-14.78	-280.65	-847.32	-16.20	-248.87	-905.33	-15.97	-259.44	-952.46

**Simulations**

- N°4
- N°21
- N°25
- N°27
- N°30

Figure D.7. Hazard representations: (c) total net erosion.



## Appendix E – Curriculum Vitae

Pablo Lopez Filun

[pablo.lopezfilun@bristol.ac.uk](mailto:pablo.lopezfilun@bristol.ac.uk)

---

Education	
<b>05/2018 – 11/2022</b>	<b>PhD in Civil Engineering</b> University of Bristol Bristol, United Kingdom Thesis: Integrated modelling of slope hydrology and stability hazards to explore the potential effects of land use and climate change on dynamic multi-hazard interactions. Supervisors: Dr. Liz Holcombe, Dr. Katerina Michaelides, Dr. Jeremy Phillips.
<b>03/2015 – 04/2017</b>	<b>MSc in Geography and Geomatics (First Class Honours)</b> Pontifical Catholic University of Chile Santiago, Chile
<b>04/2014 – 08/2014</b>	<b>Postgraduate Diploma (PgDip) in Geomatics</b> Pontifical Catholic University of Chile Santiago, Chile
<b>03/2006 – 03/2013</b>	<b>BSc in Geography</b> University of Concepcion Concepcion, Chile

---

Teaching experience	
<b>03/2021 – 07/2021</b>	<b>Lecturer in Hydrology</b> Institute of Geography Pontifical Catholic University of Chile Santiago, Chile (Remote)
<b>03/2015 – 12/2017</b>	<b>Teaching assistance</b> for postgraduate modules at Pontifical Catholic University of Chile, Santiago, Chile <ul style="list-style-type: none"><li>• Evolution and dynamics of coastal zones: Planning for coastal resilience</li><li>• Evaluation and management of natural hazards for sustainable cities</li></ul>
<b>04/2016 – 08/2017</b>	<b>Teaching assistance</b> for Postgraduate Diploma (PgDip) in Disaster Risk Reduction: Prevention and Management.

---

Work experience	
<b>03/2015 – 04/2017</b>	<b>Geospatial Analyst</b> Institute of Geography Pontifical Catholic University of Chile Santiago, Chile  Project: FONDECYT Project N°1151367 (2015-2019) "Coastal evolution, morpho-dynamics and factors of change of the coastline on a coast of tectonic influence: guidelines for integrated management of the coast."  <b>Geohazard consultant</b> Centre for Environmental Sciences EULA-Chile Concepcion, Chile
<b>07/2015 – 12/2017</b>	<ul style="list-style-type: none"><li>• Principal consultant in the assessment of landslide susceptibility for the Municipality of San Pedro de la Paz. Biobio Region, Chile.</li><li>• Principal consultant in the assessment of landslide susceptibility for the Municipality of Panguipulli. Araucania Region, Chile.</li></ul>

- Consultant in the assessment of landslide susceptibility for the City Council of Puerto Montt. Los Lagos Region, Chile

#### **GIS and Geohazard Consultant (Part-time)**

##### **Ecumene Geography and Environment LTDA**

- 05/2017 – 12/2017**
- Consultant in the preparation of landslide inventory maps for susceptibility assessment for the mining company Los Pelambres, Coquimbo region, Chile.
  - Consultant in the preparation of landslide inventory maps for susceptibility assessment for the mining company La Coipa, Atacama region, Chile

**04/2016 – 08/2016** **Institute of Geography - Pontifical Catholic University of Chile**

- GIS analyst in the study of coastline change and coastal erosion for the City Council of Santo Domingo, Central Chile.

**05/2015 – 12/2015** **Terramar Territorial Studies**

- Consultant geographer in the development of physical environment baselines for environmental assessment projects

#### **Publications**

##### **Peer reviewed journals publications:**

**López P**, Qüense J, Henríquez C, Martínez C. 2021. Applicability of spatial prediction models for landslide susceptibility in land-use zoning instruments: a guideline in a coastal settlement in South-Central Chile. *Geocarto Int.*:1–20. doi:10.1080/10106049.2021.1939440.

Martínez C, Sepúlveda-Zúñiga E, Villagrán M, Rojas O, Gómez M, **López P**, Rojas C. 2021. Coastal Evolution in a Wetland Affected by Large Tsunamigenic Earthquakes in South-Central Chile: Criteria for Integrated Coastal Management. *Water* 2021, Vol 13, Page 1467. 13(11):1467. doi:10.3390/W13111467.

Martínez C, **López P**, Rojas C, Qüense J, Hidalgo R, Arenas F. 2020. A sustainability index for anthropized and urbanized coasts: The case of Concón Bay, central Chile. *Appl Geogr.* 116. doi:10.1016/j.apgeog.2020.102166.

Aránguiz R, Martínez C, Rojas O, Hoffmann C, **López P**. 2020. The generation of new tsunami risk areas due to an intentionally biased reconstruction process: Case study of Illico after the 2010 Chile tsunami. *Int J Disaster Risk Reduct.* 50:101727. doi:10.1016/j.ijdr.2020.101727.

**López P**. 2015. Análisis de umbrales de precipitación de procesos de remoción en masa, en laderas urbanizadas de la costa de Chile centro-sur. *Cuad Geogr Rev Colomb Geogr.* 24(2):93–112. doi:10.15446/rcdg.v24n2.50212.

#### **Conference presentations**

##### **Oral presentation**

López, P., Holcombe, L., Michaelides, K., and Phillips, J.: Parameter exploration for hydrological hazard interactions in a data-scarce catchment., EGU General Assembly 2022, Vienna, Austria, 23–27 May 2022, EGU22-5815, <https://doi.org/10.5194/egusphere-egu22-5815>, 2022.

##### **Awards**

- Award academic excellence Pontifical Catholic University of Chile (2017)
- ANID (Chile) Master scholarship (2016 - 2017)
- ANID (Chile) PhD scholarship (2018 – 2022)

##### **Skills**

- Programming languages: R (Expert), MATLAB (Intermediate), Python (Beginner)
- GIS software: ArcMap (Expert), QGIS (Expert), PCRaster (python) (Expert)
- Database management: MySQL (Intermediate), PostGIS (Intermediate)
- Languages: Spanish (native), English (fluent)